General Disclaimer

One or more of the Following Statements may affect this Document

- This document has been reproduced from the best copy furnished by the organizational source. It is being released in the interest of making available as much information as possible.

- This document may contain data, which exceeds the sheet parameters. It was furnished in this condition by the organizational source and is the best copy available.

- This document may contain tone-on-tone or color graphs, charts and/or pictures, which have been reproduced in black and white.

- This document is paginated as submitted by the original source.

- Portions of this document are not fully legible due to the historical nature of some of the material. However, it is the best reproduction available from the original submission.

NASA CR 72512
AGC 9400-15

FINAL REPORT

LARGE HYDROGEN-OXYGEN ABLATIVE CHAMBER TEST PROGRAM

by

R. J. Kovach
J. A. Mellish
R. W. Michel

Prepared for

National Aeronautics and Space Administration

Contract NAS 3-11214

AEROJET-GENERAL CORPORATION

SACRAMENTO, CALIFORNIA

NOTICE

This report was prepared as an account of Government sponsored work. Neither the United States, nor the National Aeronautics and Space Administration (NASA), nor any person acting on behalf of NASA:

A.) Makes any warranty or representation, expressed or implied, with respect to the accuracy, completeness, or usefulness of the information contained in this report, or that the use of any information, apparatus, method or process disclosed in this report may not infringe privately owned rights, or

B.) Assumes any liabilities with respect to the use of, or for damages resulting from the use of any information, apparatus, method or process disclosed in this report.

As used above, "person acting on behalf of NASA" includes any employees or contractor of NASA, or employee of such contractor, to the extent that such employee or contractor of NASA, or employee of such contractor prepares, disseminates, or provides access to, any information pursuant to his employment or contract with NASA, or his employment with such contractor.

Requests for copies of this report should be referred to:

National Aeronautics and Space Administration
Office of Scientific and Technical Information
Attention: AFSS-A
Washington, D. C. 20546

NASA CR-72512

AGC 9400-15

TECHNOLOGY REPORT

LARGE HYDROGEN-OXYGEN ABLATIVE CHAMBER TEST PROGRAM FINAL REPORT

Prepared for

NATIONAL AERONAUTICS AND SPACE ADMINISTRATION

14 March 1969

CONTRACT NAS 3-11214

Prepared by:

AEROJET-GENERAL CORPORATION
LIQUID ROCKET OPERATIONS
SACRAMENTO, CALIFORNIA

AUTHORS: R. J. Kovach
J. A. Mellish
R. W. Michel

APPROVED: J. C. Moise
Manager
M-1 Program

Technical Management:

NASA LEWIS RESEARCH CENTER
CLEVELAND, OHIO

TECHNICAL MANAGER: W. A. Tomazic

APPROVED: W. A. Tomazic
M-1 Project Manager
NASA Lewis Research Center

ABSTRACT

A large-scale, silica phenolic, ablative-lined combustion chamber with a coaxial element injector having baffles, was tested to ascertain duration capability using the propellant combination of liquid hydrogen/liquid oxygen. The degradation of the liner was evaluated at nominal chamber pressures of 1040 psia and 570 psia at various over-all thrust chamber mixture ratios and a nominal hydrogen injection temperature of approximately 110°R. The average throat regression rates of the liner wall in-line with the baffles were approximately 0.0023 in./sec (1040 psia chamber pressure) and 0.001 in./sec (570 psia chamber pressure) at a nominal over-all thrust chamber mixture ratio of 5.5. These average regression rates became approximately 0.004 in./sec (1040 psia chamber pressure) and 0.00275 in./sec (570 psia chamber pressure) between the baffles where the total fuel film coolant was less than in the in-line locations at the same 5.5 over-all thrust chamber mixture ratio.

TABLE OF CONTENTS

TABLE OF CONTENTS (cont.)

APPENDIXES (cont.)

LIST OF TABLES

LIST OF TABLES (cont.)

LIST OF FIGURES

LIST OF FIGURES (cont.)

LIST OF FIGURES (cont.)

LIST OF FIGURES (cont.)

LIST OF FIGURES (cont)

I. SUMMARY

The Large Hydrogen-Oxygen Ablative Chamber Test Program was conducted for the purpose of determining the duration capability of ablative chamber liners under the following operational conditions.

Thrust (sea level)	930,000 lb and 465,000 lb
Chamber Pressure (face)	1040 ± 40 psia and 520 ± 20 psia
Throat Diameter (nominal)	30.0 in.
Mixture Ratio (over-all)	4.8 to 5.7
Hydrogen Injection Temperature	95 ± 5°R

The actual operating conditions obtained were as follows:

Chamber Pressure (face)	1040 psia to 1065 psia and 540 psia to 585 psia
Mixture Ratio (over-all)	4.0 to 6.0
Hydrogen Injection Temperature	82°R and 126°R

Unsteady flow in the facility fuel system was encountered during two tests at 520 psia chamber pressure. As a result, low chamber pressure testing was limited to a minimal pressure level of 550 psia and the succeeding tests actually were run at a chamber pressure of 570 psia. The stability tests were also conducted at this chamber pressure level.

When temperature was decreased, instability occurred at fuel injection temperatures between 74°R and 76°R, but stable operation was regained at approximately 110°R. Normal thrust chamber operation was stable.

The ablative liners tested were made of silica-reinforced (tape-wrapped) phenolic (WBC-2230). The injector used was made of 3248 coaxial elements and 3-1/2-in. long copper baffles. Uncooled ablative baffles also were tested and proved to be satisfactory.

Three liners (S/N's 001, 002B, and 002C) were used in the 18 tests conducted. Two of the tests made with S/N 002C liner were combined duration-stability tests.

Maximum regression(1) of the liner occurred at the throat between the baffles while very little regression was noted at the 2:1 expansion nozzle exit. Char depths averaged 0.15 in. to 0.40 in. throughout the liner. The

(1) Regression as used throughout this report is defined as the erosion or loss of ablative material. Degradation as used throughout this report is defined as the sum of the regression and the ablative liner char depth.

regression and char depth analyses, along with supporting data, are presented as Appendix A of this report.

The total test duration accumulated with liner S/N 001 was 144 sec at a chamber pressure exceeding 90%. This included 54 sec of testing at 1040 psia chamber pressure during the M-1 engine development program.(2)(3) The average regression rates at the throat of the liner were approximately 0.0023 in./sec in-line with the baffles and 0.004 in./sec between the baffles at a chamber pressure of 1040 psia and a nominal over-all mixture ratio of 5.5. In the five tests conducted with this liner (excluding the previous program testing), the average over-all steady-state thrust chamber mixture ratio was varied between approximately 5.1 and 5.5.

The total test duration accumulated with liner S/N 002B was 265 sec at a chamber pressure exceeding 90% (570 psia level). The average regression rates at the throat of the liner were approximately 0.001 in./sec in-line with the baffles and 0.00275 in./sec between the baffles at a nominal over-all mixture ratio 5.5. In the seven tests conducted with this liner, the average over-all thrust chamber mixture ratio was varied between 4.2 and 5.96.

The total test duration accumulated with liner S/N 002C was 250 sec at a chamber pressure exceeding 90% (570 psia level). Regression rates were the same as for the S/N 002B liner. In the six tests conducted with this liner, the average over-all thrust chamber mixture ratio was varied between 4.9 and 5.75.

Ablative baffles were fabricated from silica phenolic and satisfactorily tested. These baffles replaced two of the six copper inner baffles and four of the outer ones. No supplementary cooling was provided and heavy erosion was experienced, but these ablative baffles performed well. There was no apparent difference in erosion characteristics when test results from the 570 psia and 1040 psia chamber pressure levels were compared.

Measured injector performance was consistent with previously obtained data.(4) No distinct difference in specific impulse efficiencies was noted between the 570 psia and 1040 psia chamber pressure levels. A specific impulse efficiency (not including nozzle geometry losses) of 96% was obtained for the 2:1 expansion ratio nozzle at a nominal over-all mixture ratio of 5.5.

Several low-cost ablative samples were tested at the 2:1 expansion nozzle exit, but none of these samples performed as well as the silica phenolics. The low-cost ablative material data are presented as Appendix B of this report.

(2) Contract NAS 3-2555

(3) Barsotti, R. J., et al., Development of Liquid Oxygen/Liquid Hydrogen Thrust Chamber for the M-1 Engine, NASA CR-54813, 15 May 1968

(4) Contract NAS 3-2555

II. INTRODUCTION

All of the development testing of the ablative chambers for the Large Hydrogen-Oxygen Ablative Chamber Test Program delineated herein was conducted at the Aerojet-General Corporation Sacramento Facility (Sacramento, California) during the period from December 1967 through September 1968 for the NASA/Lewis Research Center, Cleveland, Ohio, under Contract NAS 3-11214.

The basic objective of the program was to determine the duration capability of silica-phenolic ablative chamber liners at two different thrust chamber pressure levels (570 psia and 1040 psia).

Additional program objectives included:

- Obtaining profile degradation data at both of the designated chamber pressure levels.
- Evaluating the performance of low-cost ablatives attached to the nozzle exit.
- Obtaining performance and stability data at the 570 psia thrust chamber pressure level.

The thrust chamber hardware used in this program was designed, fabricated, and tested previously in the M-1 engine program (Contract NAS 3-2555). Necessary associated hardware tooling and special test equipment also were utilized. Ablative liners S/N's 002B and 002C, along with the ablative baffles were fabricated as part of this program.

III. TECHNICAL DISCUSSION

A. DESCRIPTION OF HARDWARE AND FABRICATION CONSIDERATIONS

1. Ablative Liner

The ablative liner was constructed by wrapping phenolic-impregnated silica cloth, in tape form (WBC-2230), to the surface of a mandrel having the same contour as the chamber. Then, the laminate was subjected to hydroclave curing, after which the liner was contour-machined at the throat. The liner was match-machined on the outside to provide a line-to-line fit with the steel outer shell (see Figure No. 1). The laminate was wrapped 55-degrees off of the axis of thrust in the chamber section of the liner and 40-degrees in the nozzle section (see sheet 2 of Figure No. 1). Table I lists the physical and mechanical properties as well as the wrapping technique used for all three of the liners tested.

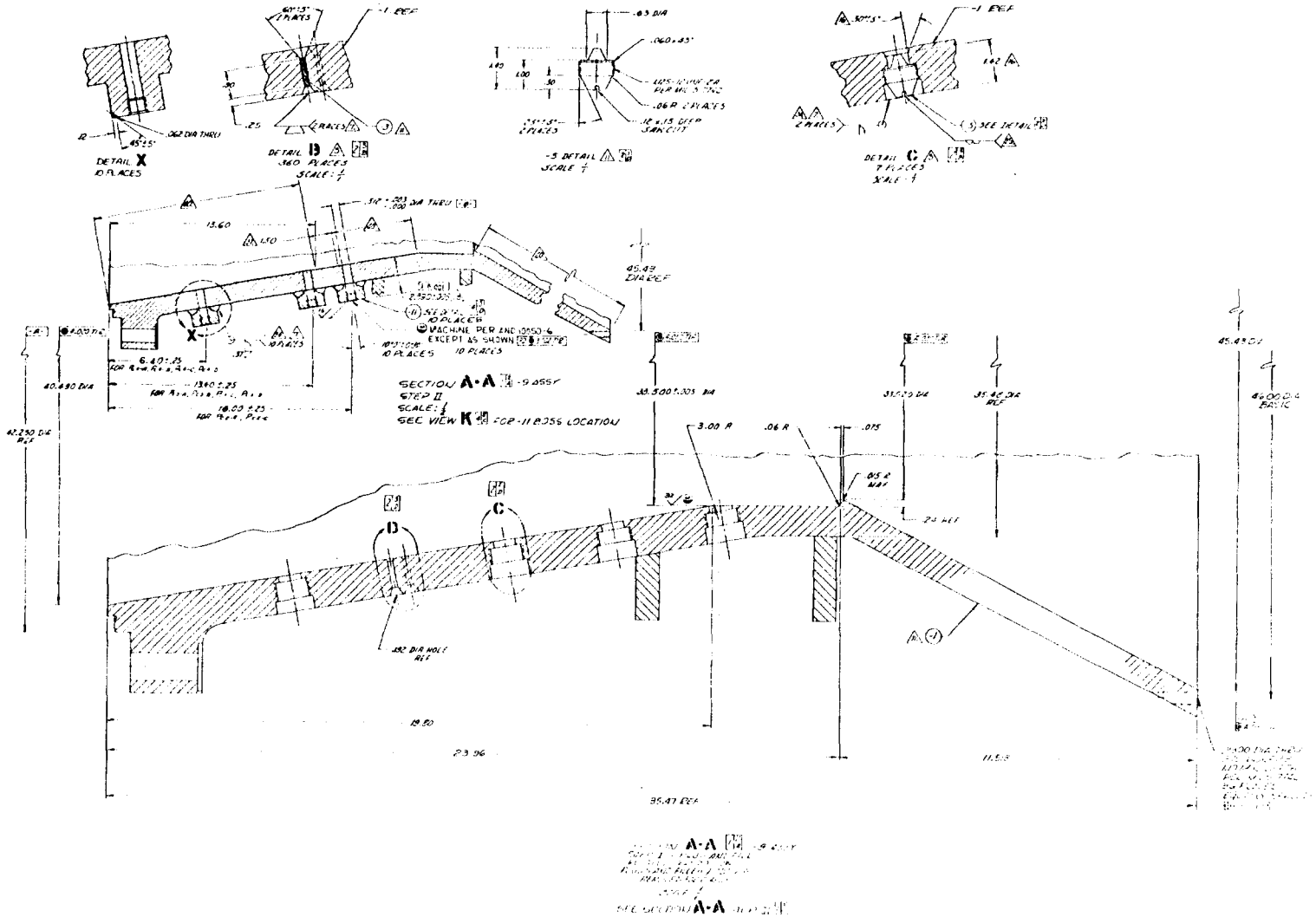

Figure 1. Line-to-Line Fit of Liner to Steel Outer Shell

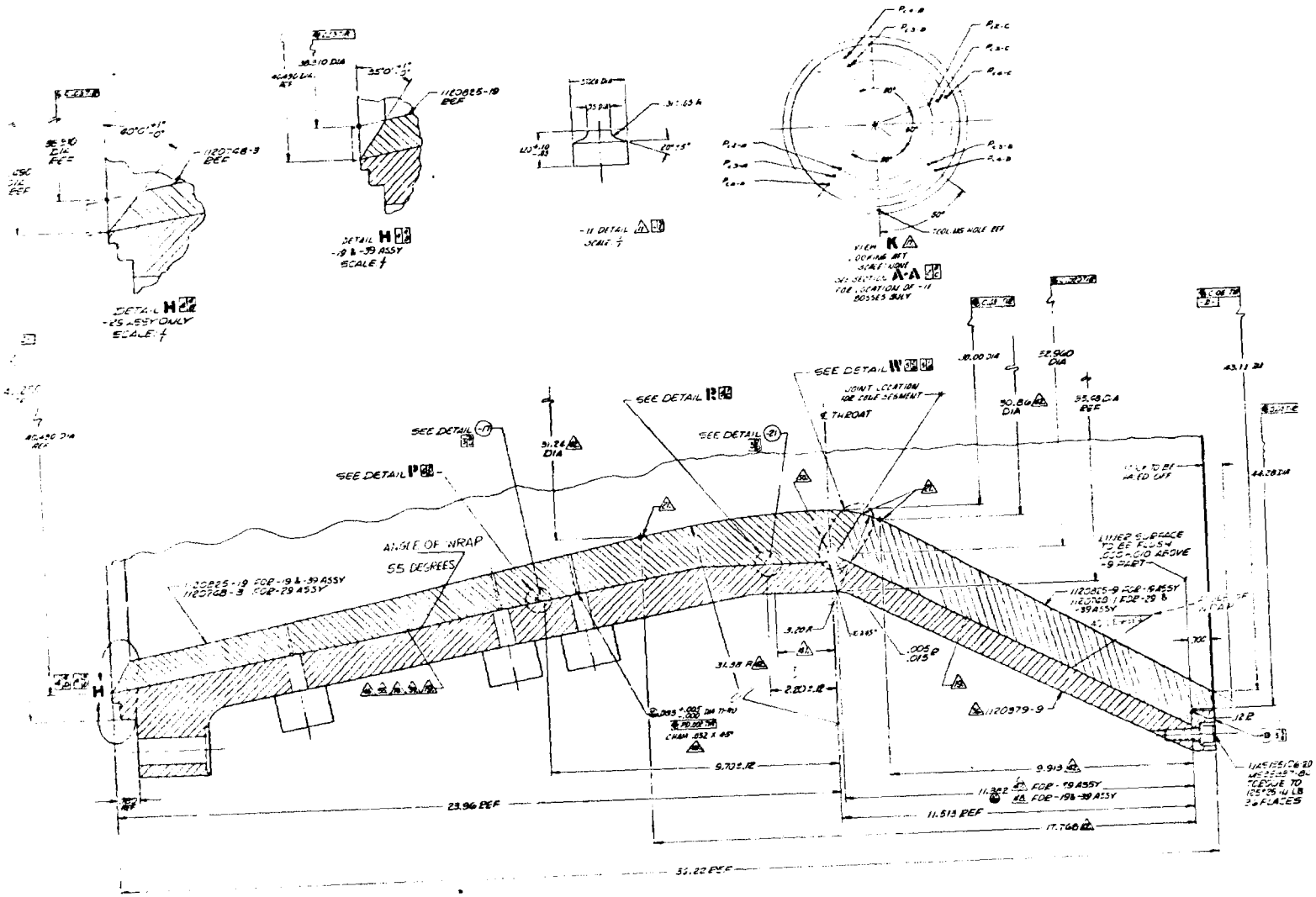

Figure 1. Line-to-Line Fit of Liner to Steel Outer Shell

TABLE I

COMPARISON OF FABRICATION TECHNIQUES FOR
ABLATIVE CHAMBER LINERS

Wrapping Process	Liner S/N 001	002B	002C
Tape Wrapping Temperature, °F	230-240	230-240	148-208
Tape Wrapping Pressure, psig	230-240	250-294	224-392
Tape Wrapping Speed, rpm	0.5	0.5	1.25
Tape Wrapping Span Time, hours	36	49	17

Uncured Material Properties

	Requirement	Test		
Resin Solids, %	24-28	27.5	27.58	27.98
Resin Flow, %	6-10	6.8	6.72	8.48
Volatiles, %		3.8	3.82	3.7

Cured Laminate Properties

	Requirement	Test		
Interlaminar Shear, psi	1000 min.	2,539	2,500	2,380
Acetone Extraction, %	1 max.	0.21	0.21	0.23
Specific Gravity	1.72	1.73	1.73	1.74
Volatile Content, %	3 max.	2.30	2.30	2.90
Tensile Strength, psi		12,808	12,800	12,658

2. Injector

The injector (S/N 012)(5) contained 3248 coaxial elements with the oxidizer being injected in the center and the fuel injected annularly around the oxidizer. This injector also incorporated 3-1/2-in. long bolt-on copper baffles consisting of a thin base plate mated to the injector face, an intermediate base containing convection coolant holes, and a tip which had a combination of convection coolant and film cooling holes. Baffle film cooling was limited to the corners and none was supplied through the injector face. Figure No. 2 is a view of the injector face and baffle pattern.

A row of orifices, drilled through the porous face, was located around the injector periphery and provided the chamber wall film cooling. Approximately 3.7% of the total fuel flow rate was used for chamber wall

(5) Barsotti, R. J., et al, op. cit.

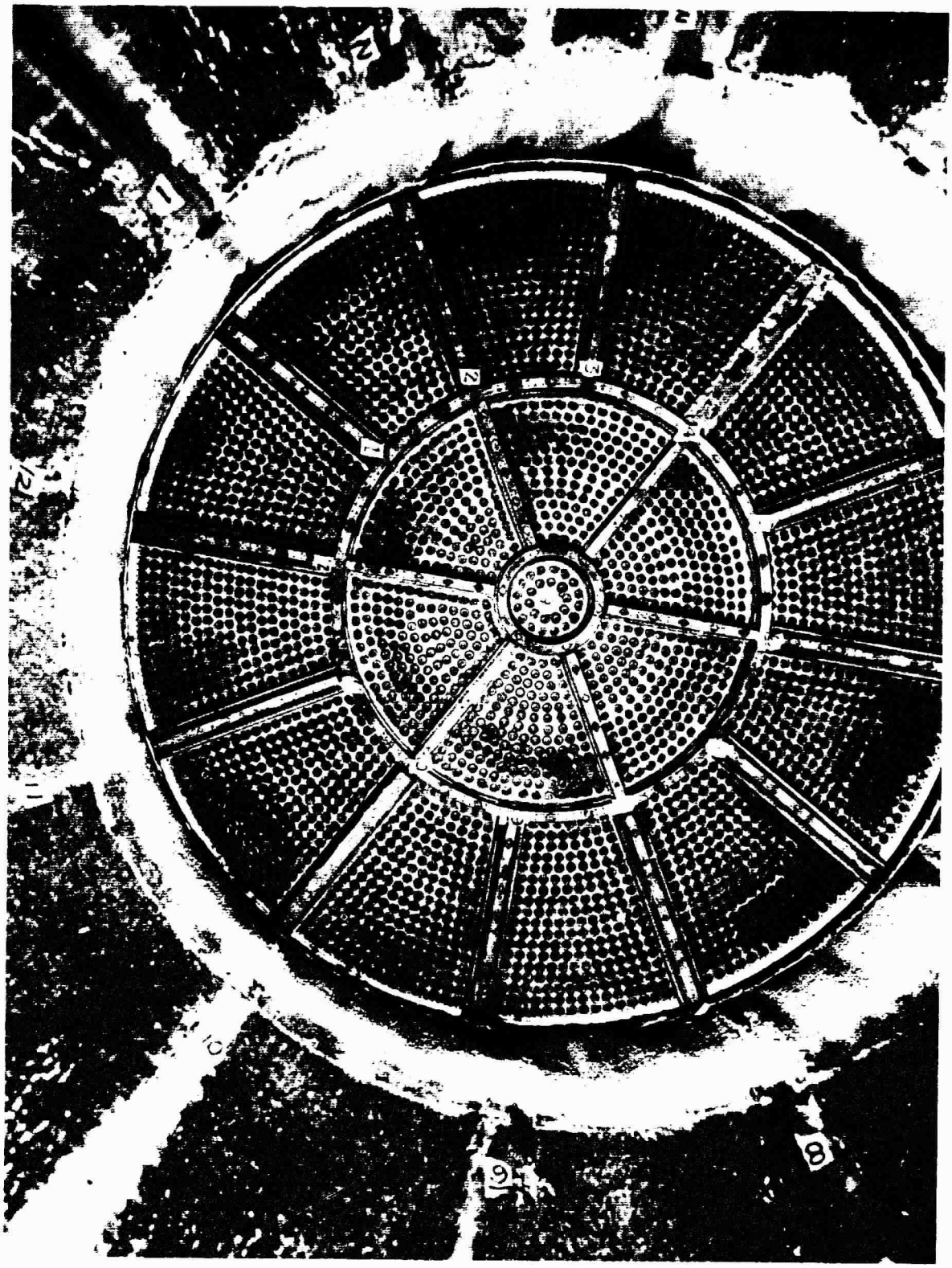

Figure 2. Injector S/N 012 Showing Face and Baffle Pattern

film cooling at both the 1040 psia and 570 psia chamber pressure levels. Total fuel element flow rate was 89.8% of the thrust chamber fuel flow rate with a baffle fuel film cooling flow rate of 7.9% at both chamber pressure levels. The remaining 2.6% of the fuel flowed through the rigimesh injector face.

3. Fuel Torus

Previous test experience with this hardware indicated possible fuel torus ablative liner expulsion when it operated at unstable conditions. Twice during stability tests of this injector without baffles, there was expulsion of the fuel torus liner when instability was induced. Therefore, a bolt-on copper liner extending from the injector face to 3.5-in. downstream was incorporated. This copper section appear undamaged under all operational conditions.

4. Ablative Baffles

Uncooled outer and inner ablative baffles were fabricated and tested in place of the cooled copper baffles. The ablative baffle consisted of a flat steel plate with steel webs welded perpendicularly to this plate (see Figure No. 3). Phenolic-impregnated silica cloth (WBC-2230) was intermittently wrapped parallel to these webs as well as around the ends of these webs to lessen the possibility of delamination from the open ends. Then, the assembly was compression-molded and final-machined. Figure No. 4 is a typical installation view of an ablative inner baffle. Note that the base-bolt access holes are shown as being unplugged, but dowel-pin type inserts were used to plug them before firing.

5. Low-Cost Ablative Materials

Several ablative materials that are less expensive than the silica phenolic used in the liners were tested at the 570 psia chamber pressure level to permit qualitative analysis as well as a comparison of char and regression properties. Samples were attached to the nozzle exit ring and subjected to the exhaust conditions at the 2:1 expansion ratio.

Four general groups of materials were tested. Silica-reinforced phenolics, asbestos-reinforced phenolics, cellulose-reinforced phenolics, and compounded materials. Low-cost ablative material data are included in Appendix B of this report.

B. DEGRADATION EVALUATION METHOD

1. Diametral Measurements

Sufficient diametral dimensions were taken before the first test of each liner and after each subsequent test to determine the ablative erosion at the throat as well as the convergent and divergent portions of the ablative liner.

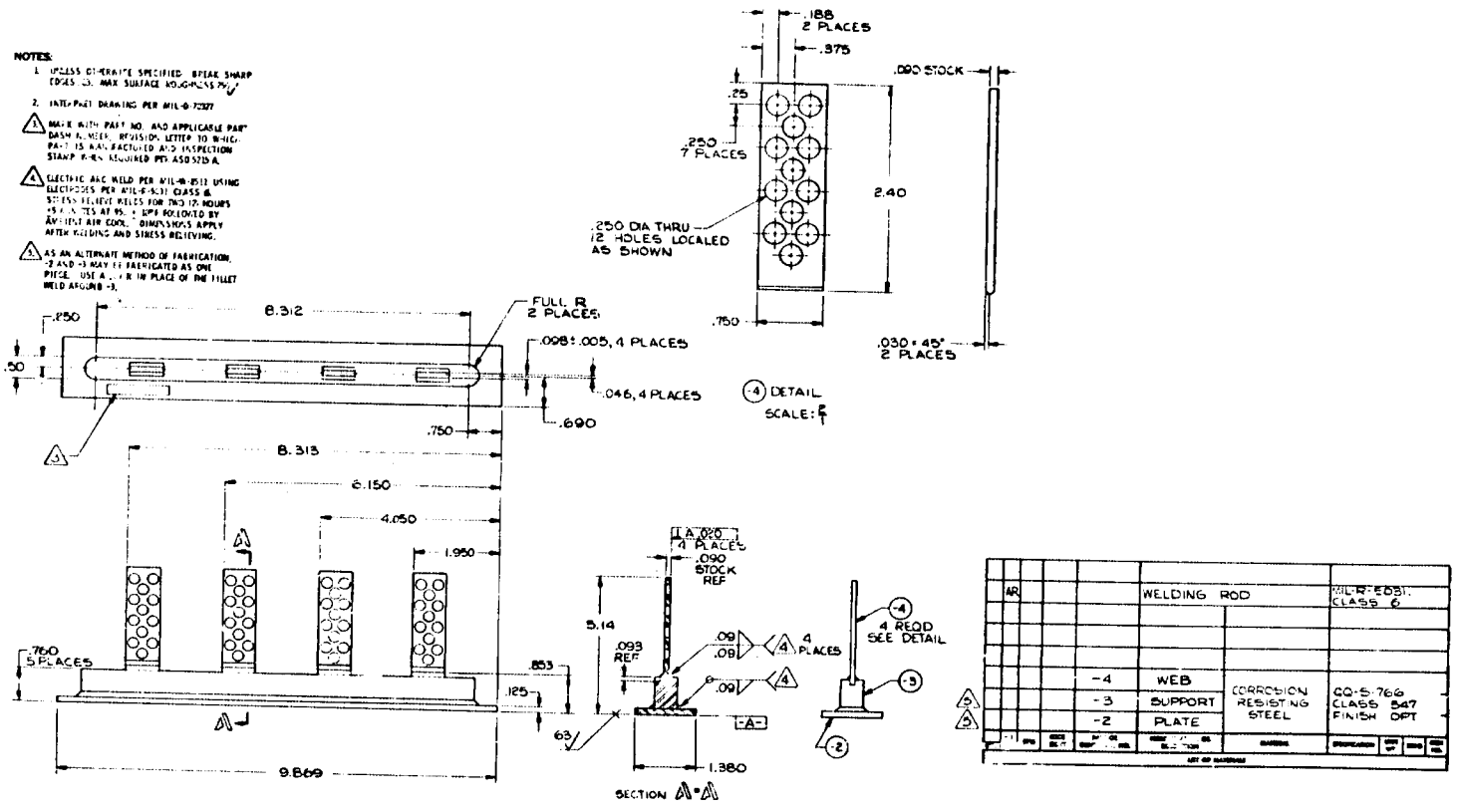

Figure 3. Ablative Baffle Base Plate Assembly

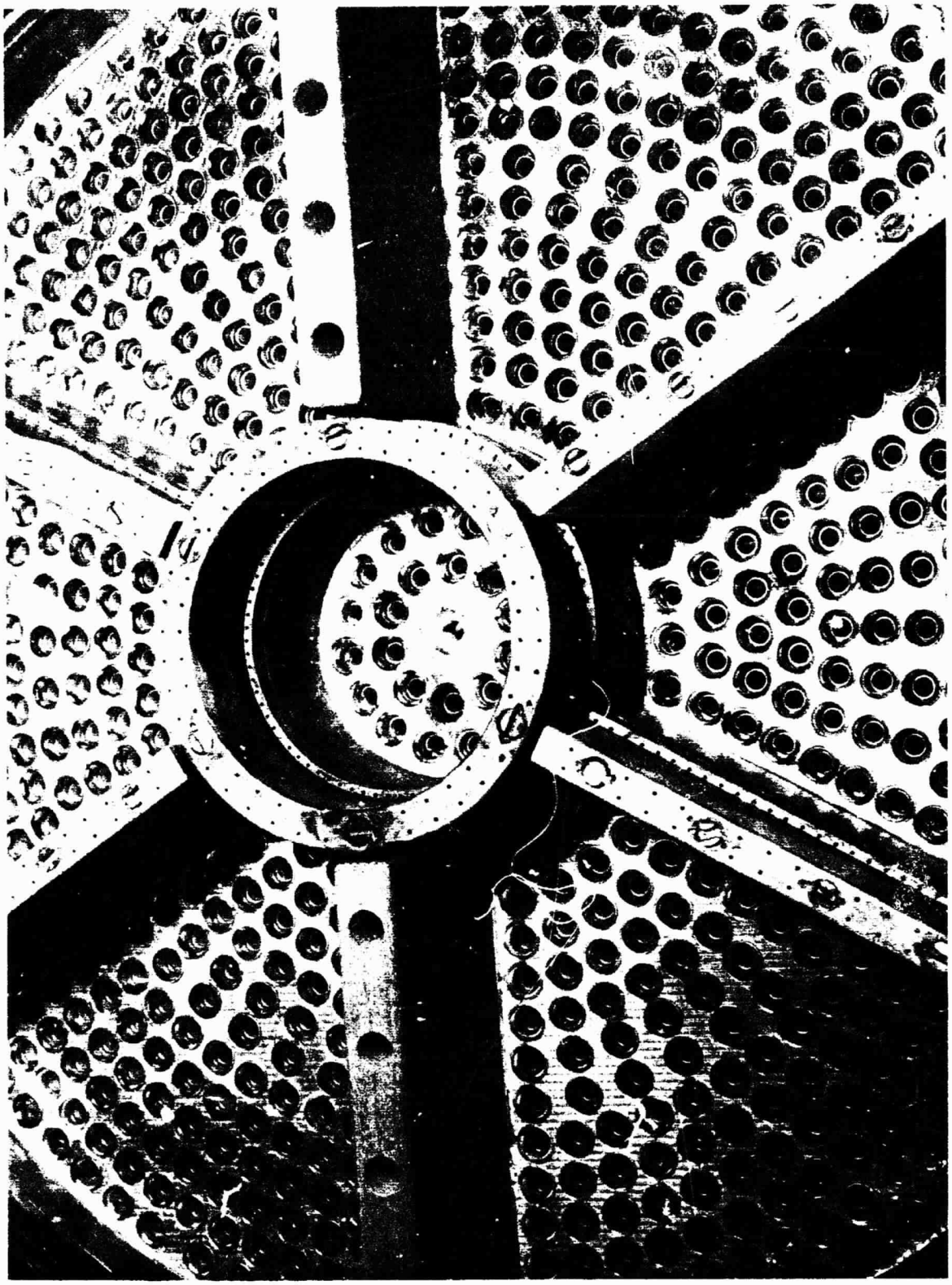

Figure 4. Typical Installation of an Ablative Inner Baffle

Measurements were taken at 12 locations around the periphery of the chamber and nozzle. Six measurements were taken in-line with the baffles and six measurements were taken equi-distant between the baffles. These 12 measurements were taken at the following five axial stations:

- 14-in. from the injector face measured along the chamber profile
- 25-in. from the injector face measured along the chamber profile
- at the throat
- 8-in. downstream from the throat measured along the nozzle profile
- 1/4-in. from the nozzle exit

A special piece of test equipment was used for taking these measurements. This measuring device was mounted on a rod which was inserted into the center of the injector face. Both the rod and device were marked so that measurements could be taken at exactly the same locations after each test.

2. Char Depth Measurements

Four char depth measurements were taken at each of the above indicated five axial stations after each test. Three of these measurements were taken at equally-spaced locations between baffles and one measurement was taken in-line with a baffle. These char depth measurements were taken by tapping through the liner with a flat-tipped drill until virgin material was reached, at which time the measurement was taken.

3. Core Samples

Four core samples were taken of each liner to determine the elemental composition of the char. These samples were from three, equally-spaced locations between the baffles and one in-line with a baffle at the 25-in. axial station. Each sample was analyzed for composition at two different depths where the char layer thickness and required sample size were compatible. The samples were analyzed for carbon, hydrogen, nitrogen, and oxygen. Also, X-ray diffraction and spectrographic analyses were utilized to ascertain metallic content.

C. TEST RESULTS

1. Ablative Liner Degradation Evaluation

The three ablative liners were used in 18 duration tests. Five of these tests were with S/N 001 liner at the 1040 psia chamber pressure

level, seven tests were made with S/N 002B liner, and six tests with the S/N 002C liner at the 570 psia chamber pressure level. Two of the six tests with liner S/N 002C were combined duration-stability tests.

a. Regression and Char Depth

The regression and char depth as well as an analysis of these data are included as Appendix A. The test data are plotted on Figures No. 5 and No. 6 as a function of the over-all thrust mixture ratio. It can be seen from these plots that for an over-all thrust chamber mixture ratio of 5.5, the average regression rates at the throat are approximately 0.0023-in./sec pressure of 1040 psia. At 570 psia chamber presssure, the average regression rates are 0.001-in./sec in-line with the baffles and 0.00275-in./sec between the baffles. Higher regression rates occurred between the baffles where the boundary layer mixture ratio was higher than in-line with the baffles because the additional baffle fuel film cooling lowered the in-line boundary layer mixture ratio. Figure No. 7 is a typical local view of the throat profile with the locations in-line with the baffles designated by the numbers on the figure. The liner shown is S/N 002B after an accumulated steady-state duration of 265 sec.

The one data point on Figure No. 5 in-line with the baffles which does not seem to be consistent with the rest of the data was obtained after Test 1198-D01-0C-001 for liner S/N 001. This liner had previously accumulated 54 sec duration of testing at 1040 psia chamber pressure in the M-1 engine program (Contract NAS 3-2555). The data obtained with this liner after Test -001 appear to be erroneous; however, the reason for this error is not apparent. A discussion of the validity of some of the other data points also is included in Appendix A.

It is suggested from Figures No. 5 and No. 6 that the regression rates are a function of the boundary layer conditions; therefore, the data were correlated as a function of the wall temperature (boundary layer recovery temperature). Figures No. 8 and No. 9 are plots of the throat regression rates as a function of the wall temperature for the 1040 psia and 570 psia thrust chamber pressures, respectively. It can be noted from these figures that the regression data for both the in-line and between the baffle locations reasonably fit one curve for each of the chamber pressures as a function of the wall temperature. It also can be noted that the regression rates at 1040 psia chamber pressure are approximately twice those at 570 psia chamber pressure at wall temperatures below approximately 3600°R. These higher regression rates at higher pressure can be attributed to the increased shear forces and higher heat flux. The fusion temperature of silica phenolic is approximately 3600°R and the plots show that the regression rate increases exponentially beyond this point as can be expected.

Regression analyses similar to that discussed above for the throat were conducted for both the two downstream stations on the nozzle and two stations upstream of the throat. Results are reported in Appendix A.

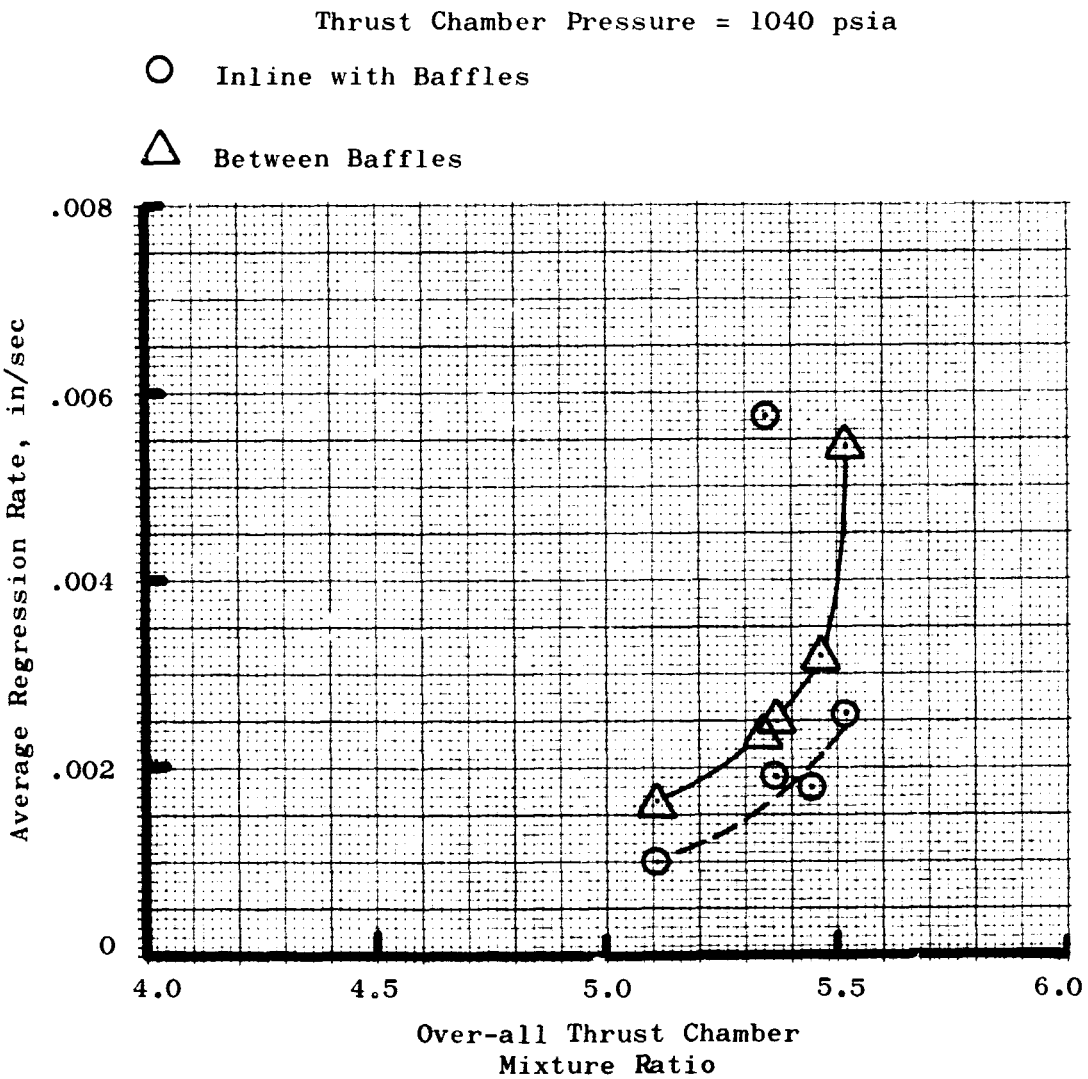

Figure 5. Average Regression Rate at the Throat vs Over-all Thrust Chamber Mixture Ratio (P_c = 1040 psia)

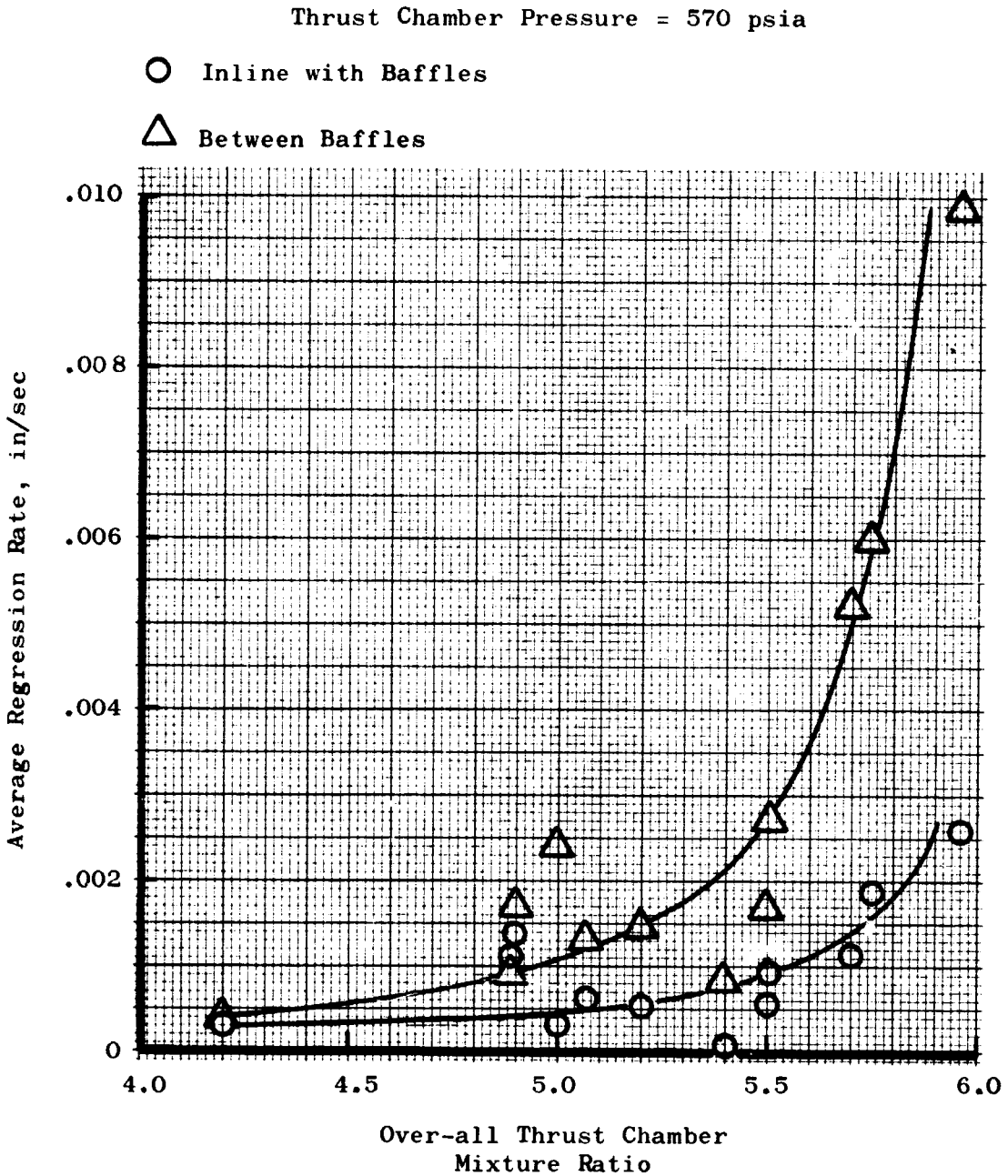

Figure 6. Average Regression Rate at the Throat vs Over-all Thrust Chamber Mixture Ratio (P_c = 570 psia)

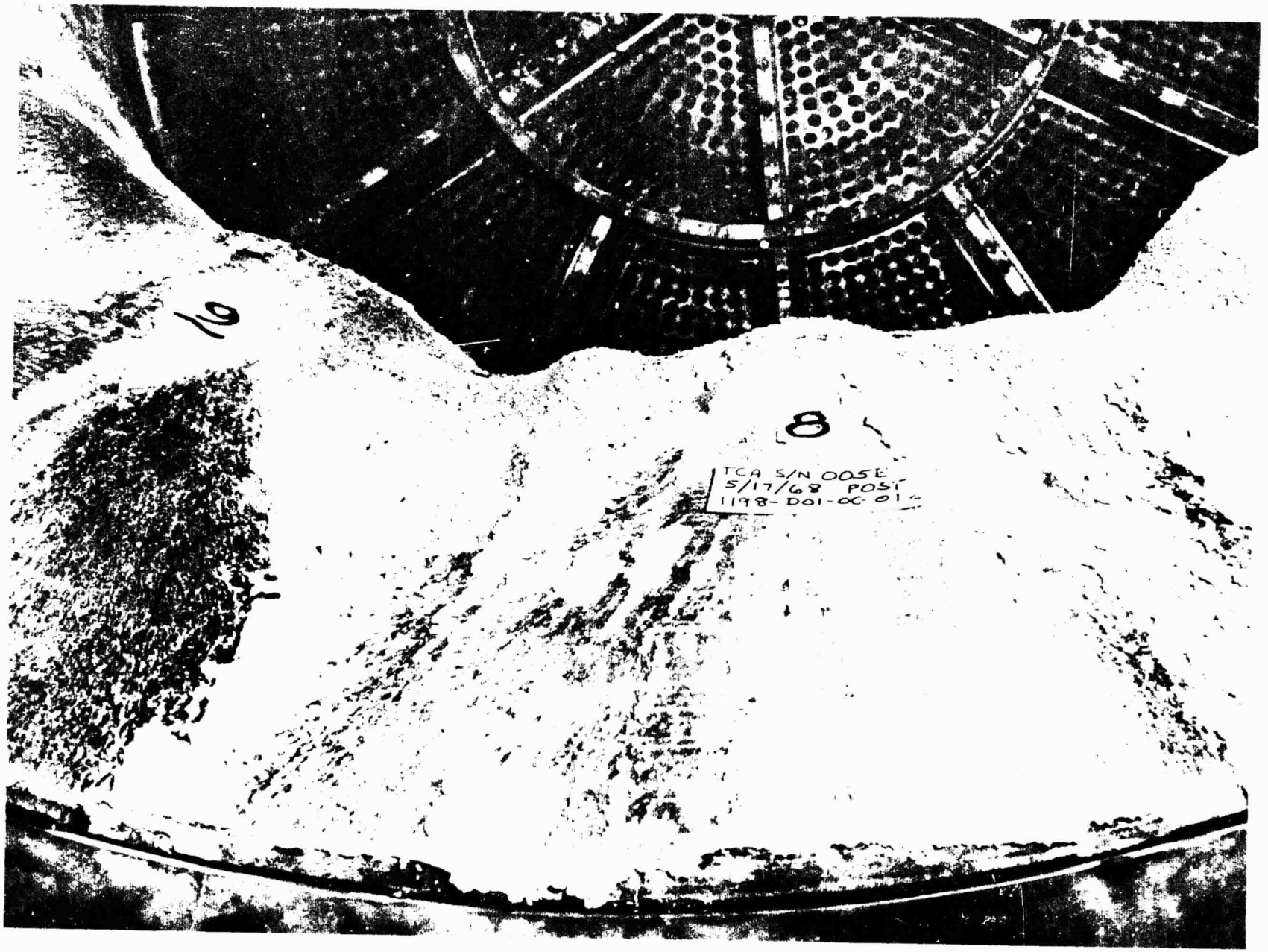

Figure 7. Throat Profile of S/N 002B Liner After 265 sec of Accumulated Steady-State Testing

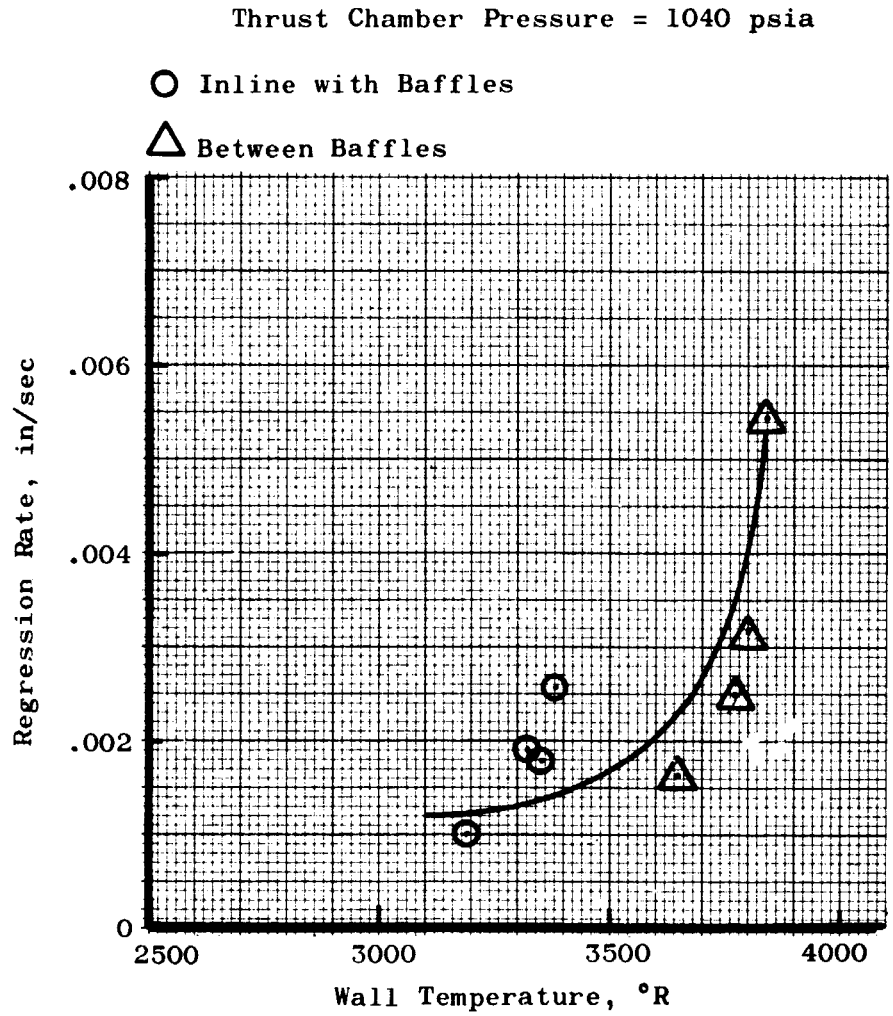

Figure 8. Regression Rate at the Throat vs Theoretical Static Boundary Layer Temperature (P_c = 1040 psia)

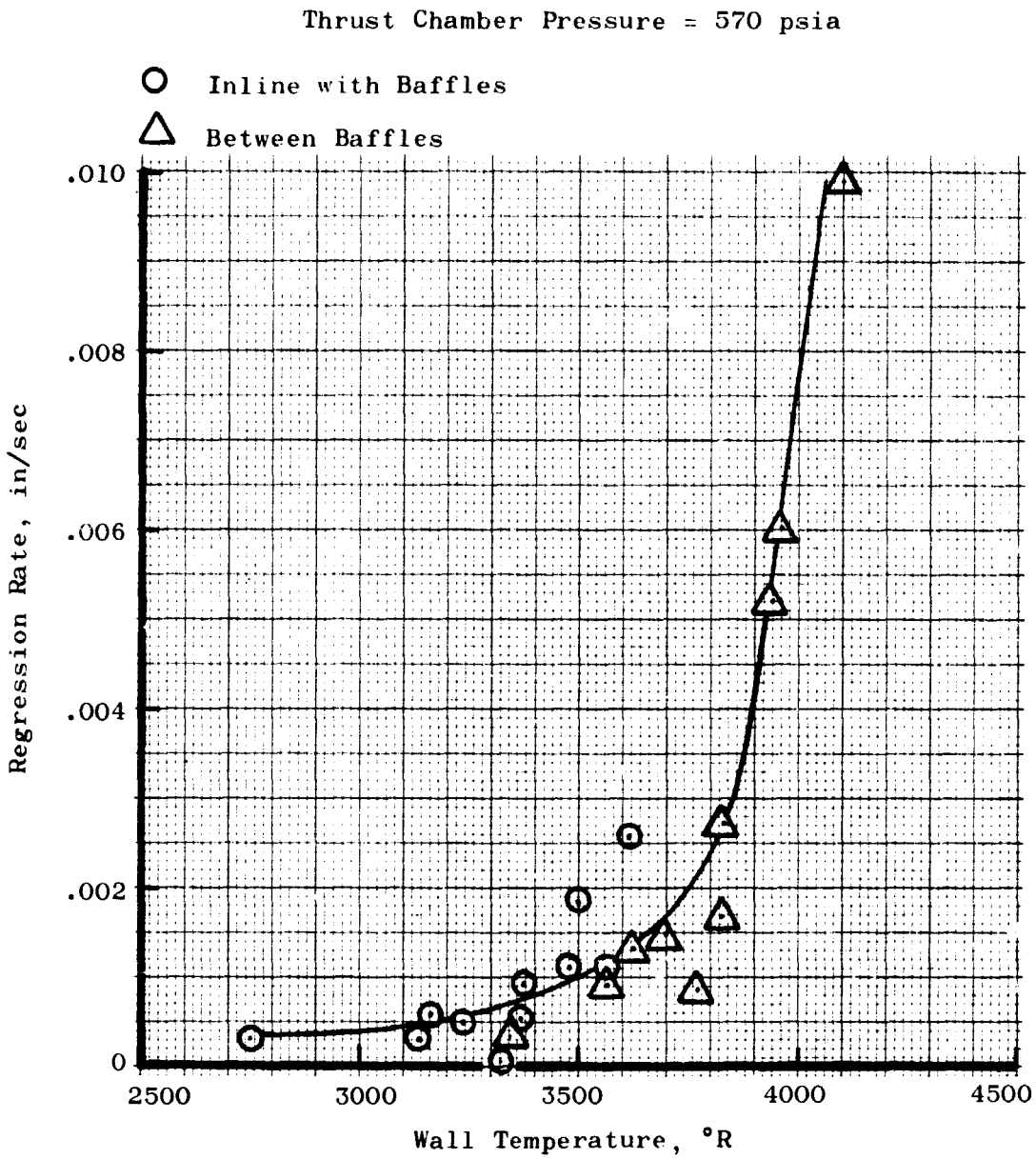

Figure 9. Regression Rate at the Throat vs Theoretical Static Boundary Layer Temperature (P_c = 570 psia)

The regression rates obtained in the nozzle were small because the heat flux is substantially reduced as a result of the lower heat transfer coefficient. Regression rates 14-in. from the injector face were small (0.001-in./sec or less), but those 25-in. from the injector face approached the values shown for the throat.

Examination of the char data obtained shows that the char depths in-line with the baffles and between the baffles were approximately the same. Char depths at 570 psia chamber pressure were greater than at 1040 psia chamber pressure because of the reduced regression rates at the lower pressure level. The variations of the char depth with axial distance from the injector face is shown on Figure No. 10. The actual test data fall between the bands shown on this figure. Greater depths of char occurred with lower mixture ratios.

Damage to liner S/N 001 in the form of gouged cavities occurred during Test No. 1198-D01-0C-003 (see Figure No. 11). The maximum depth of the cavity was approximately 0.2-in. Repeat testing resulted in a maximum depth increases to approximately 0.7-in. (see Figure No. 12). The succeeding test yielded no increase in the cavity depth.

This same type of damage occurred during the first stability test (Test No. 1198-D01-0C-018) with S/N 002C liner (see Figure No. 13), but the succeeding test filled the cavities with froth(6) (see Figure No. 14). No apparent difficulties in liner performance were noted as a result of these gouged activities, except for a decreasing amount of virgin material remaining at the damaged locations.

The last test in the program, Test No. 1198-D01-0C-020, which also was a combined stability-duration test, resulted in expulsion of the nozzle liner. The amount of material remaining at the throat prior to this test was very marginal for a repeat test of 45 sec duration. Severe damage to the nozzle steel shell was experienced (see Figure No. 15), but repair could be readily accomplished by welding another nozzle shell onto it. The expulsion of the nozzle liner invalidated the throat regression readings for this test.

b. Core Sample Comparison

The char residues from each liner were analyzed for elemental and metal content. These residue content data are provided as Appendix C. The analysis consisted of determining the carbon, hydrogen, nitrogen, and oxygen content as well as the amount of any metals present by means of X-ray diffraction and emission spectrographic techniques.

(6) During testing, the ablative material reached temperatures at which it became molten, causing it to lose the fabric reinforcement. The flow of this molten material created build-ups of non-reinforced, reformed silica, and it was these build-ups that are defined as "froth."

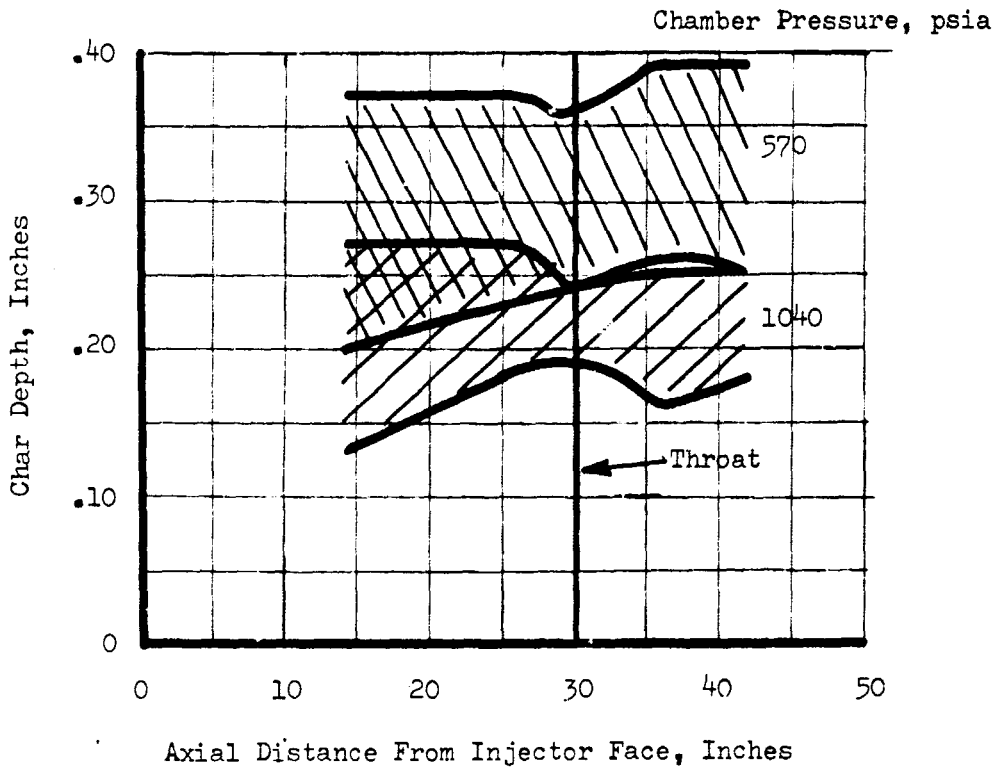

Figure 10. Char Depth vs Axial Distance for the Injector Face

Figure 11. Damage to Liner S/N 001

Figure 12. Increased Gouging Damage to Liner S/N 001

Figure 13. Damage to S/N 002C Liner Following First Stability Test

Figure 14. S/N 002C Liner Cavities Filled with "Froth"

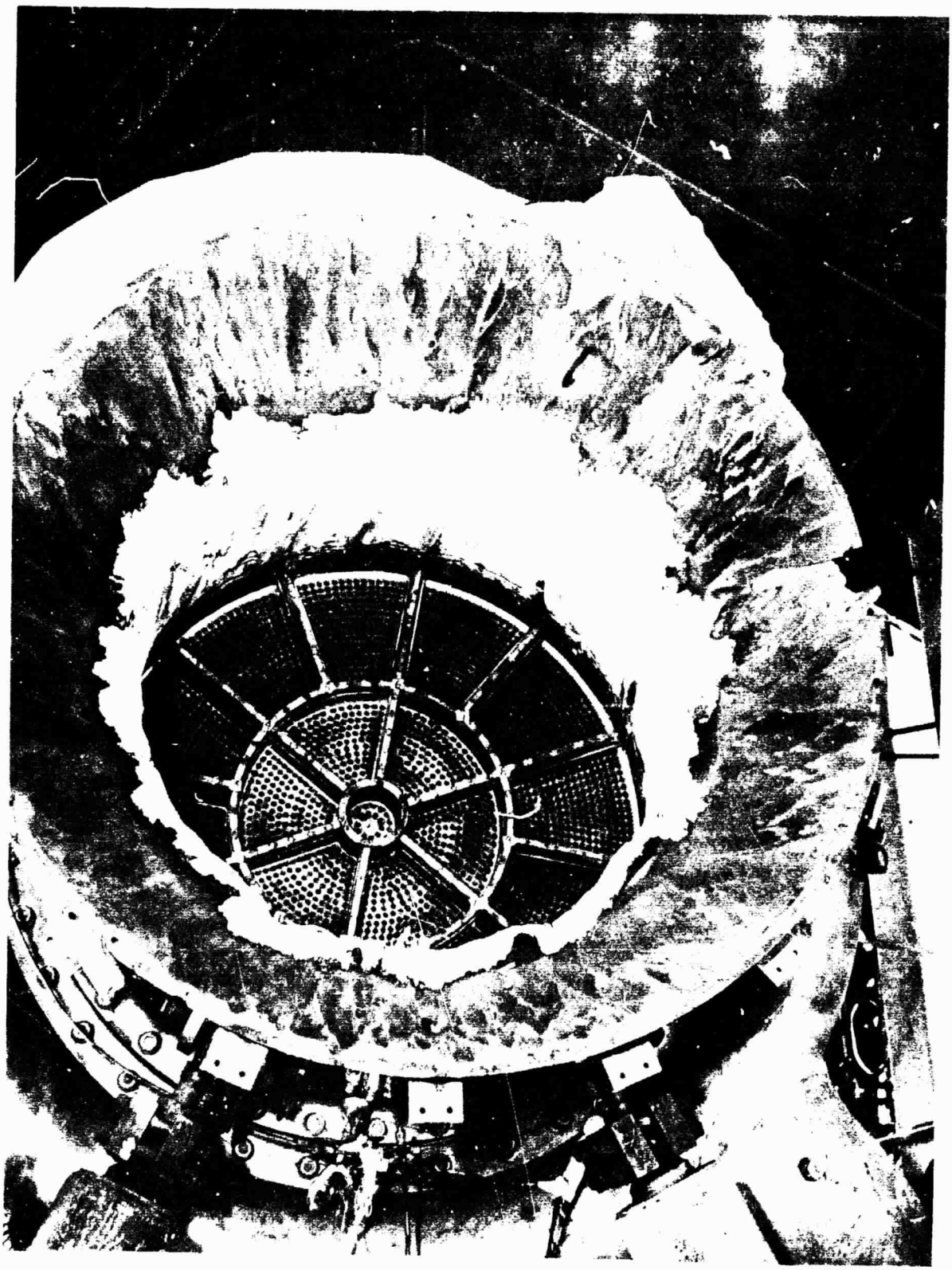

Figure 15. Damage to Nozzle Steel Shell Following Test No. 1198-D01-0C-020

X-ray diffraction revealed the presence of silicone carbide in specific samples. Apparently the heat of formation of the silica-reinforcement and char residue composite had been reached. In most tests, an amorphous substance was found which indicated the existence of virgin material.

Emission spectrographic analyses indicated that the major constituents were silica, alumina, and titanium oxide, all of which were present in the reinforcement.

There was no difference in the residue composition noted among the liners analyzed.

c. Appraisal of Sectioned Liners

The chamber and nozzle liners were removed from the metal shells and inspected via visual observations as well as the recording of char depths and degradation measurements. These observations and measurements of all the liners tested are included as Appendix D.

Liner damage was similar after each series of tests. The degree of char penetration and regression was dependent upon the test mixture ratios and chamber pressures. Generally, heavy streaking and silica flow between the baffles was noted. Most of the frothing observed commenced at approximately 14-in. aft of the injector face. The char depth remained constant with advancing regression when the mixture ratio remained constant.

Maintaining the sealed liner-to-liner interfaces before a test was of primary concern throughout the test program. Ablative silicone adhesive/sealant was applied as required to the fuel torus liner-chamber liner joint as well as to the chamber liner-nozzle liner joint immediately aft of the throat. Sufficient sealing was maintained to prevent hot gas leakage under the nozzle liner. This reduced the possibility of liner separation, which is the mode of failure that is particularly suspected of causing nozzle liner expulsion.

Sectioning of the liners revealed large amounts of virgin material remaining in-line with the baffles. Char-through was experienced in areas between the baffles only.

d. Theoretical Analysis of Ablative Chamber Thermal Behavior

The objective of this analysis, which is included as Appendix E, was to theoretically predict thermal behavior in terms of temperature responses as well as the erosion and char rates of the ablative liner at various axial and circumferential locations.

2. Ablative Baffle Evaluation

The ablative baffles performed as well as could be expected in view of the lack of any supplementary cooling being provided. Heavy erosion occurred after each test, but testing was continued in most cases. There were no apparent degradation differences between an inner baffle after 132 sec of steady-state and an outer baffle after 120 sec (see Figures No. 16 and No. 17) or at 1040 psia and 570 psia chamber pressure levels. No additional damage to the baffles was noted as the result of unstable operation.

Improved baffle performance might have been achieved if the angle of laminate was similar to the liner lay-up instead of being parallel to the axis of thrust. However, schedule requirements precluded the use of this fabrication method.

Three types of baffle contours were tested: parallel-sided, taper-sided from midway to a 3/4-in. wide trailing edge, and fully-taper-sided from baffle base to a 5/8-in. wide trailing edge. In general, the tapered baffles appeared to degrade at slightly lower rates but still eroded badly with a few tests.

The ablative baffles were installed opposite of each other for a balancing effect upon throat regression. Table II is a summary of the ablative baffle testing.

TABLE II

HISTORY OF ABLATIVE BAFFLE TESTING

Specimen No.	Location	Installed Test No.	Accumulated Duration, sec
1	Inner at 4	4*, 5*, 6, 7, 8, 9	171.69
2	Inner at 10	6, 7, 8, 9	132.18
3	Inner at 4	10, 11, 12	132.44
4	Inner at 10	10, 11, 12	132.44
5**	Outer at 4	13, 14, 15, 16, 17, 18	165.26
6**	Outer at 5	13, 14	44.20
7	Outer at 10	13, 14	44.20
8**	Outer at 11	13, 14	44.20
9***	Outer at 10	15, 16, 17, 18, 19	162.62

Notes: *1040 psia thrust chamber pressure tests
**Half-taper
***Full-taper

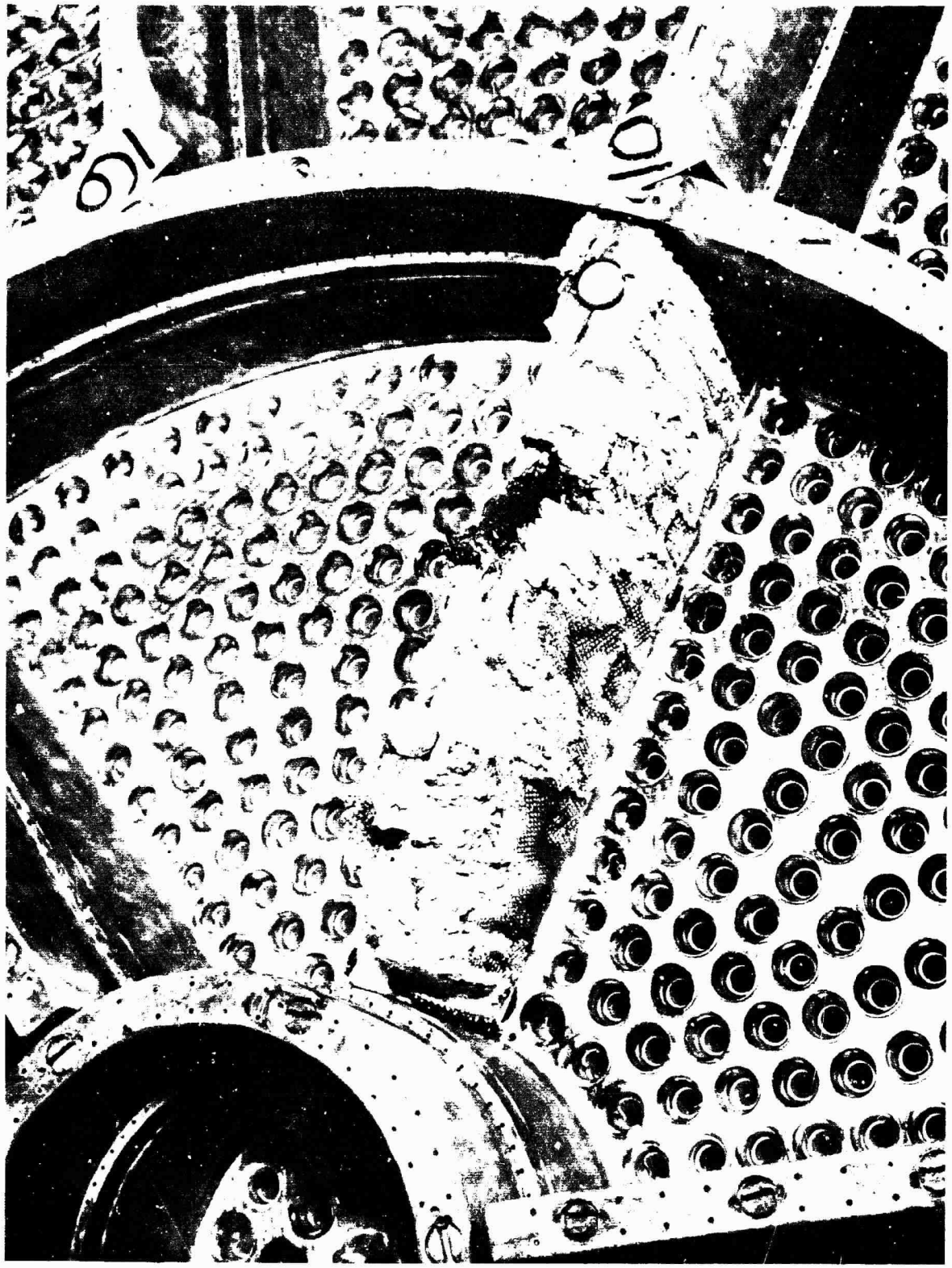

Figure 16. Inner Ablative Baffle Erosion After 132 sec of Steady-State Testing

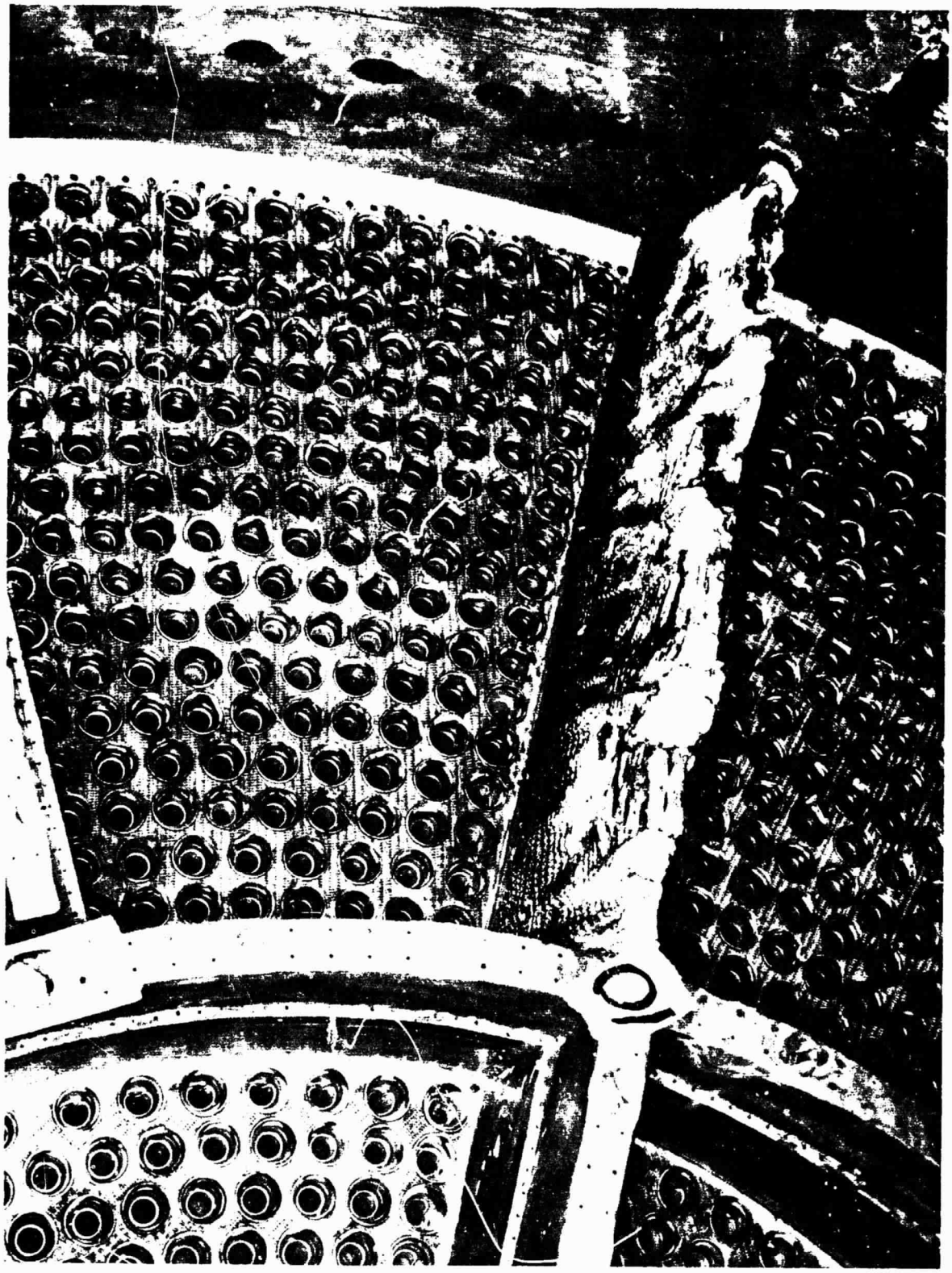

Figure 17. Outer Ablative Baffle Erosion After 120 sec of Steady-State Testing

3. Low-Cos Ablative Material Evaluation

Specimens from four general groups of ablative materials were tested by bolting them to the aft flange of the exit cone where they were subjected to exhaust gas flow at 570 psia chamber pressure. These materials were the silica-reinforced phenolics, asbestos-reinforced phenolics, cellulose-reinforced phenolics, and compounded materials. Figure No. 18 is a pre-test view of these attached specimens while Figure No. 19 is a post-test view.

The details of this evaluation are included as Appendix B of this report; however, the conclusions and recommendations are summarized below.

a. Conclusions

(1) The IBT-100 filled with silica had regression rates and char rates that were comparable with standard silica-reinforced phenolics.

(2) The performance of the vacuum bag grade silica-reinforced phenolics and epoxy novolacs was almost equivalent to the standard silica/phenolics; therefore, they should be considered as candidate exit cone liners for hand lay-up on a structural shell.

(3) Silica-reinforced phenolic is the lowest cost material based upon material degradation at the test conditions of a 2:1 area ratio ratio and a 570 psia chamber pressure.

(4) Asbestos-reinforced phenolic, cellulose-reinforced phenolics, and compounded materials would be lower in cost (based upon material degradation) at some higher area ratio and/or less severe use conditions.

b. Recommendations

(1) It is recommended that representative samples of the lower cost candidate materials be tested at high area ratios to determine their area of usefulness. Based upon the results and experience in other test programs, it appears that the asbestos-reinforced and cellulose-reinforced materials could be used at area ratios of 4:1 and higher. The compounded materials could have adequate performance at slightly higher area ratios and their cost of application makes their use desirable.

(2) It is recommended that an asbestos honeycombed core be used to retain the compounded materials in any further testing. Their tendency to spall and flake would be reduced by isolating and locking the indivi diaul cells of the compounded material.

D. THRUST CHAMBER PERFORMANCE

Thrust chamber performance was measured for each run to assure the maintenance of proper combustion conditions. No significant difference in vacuum specific impulse efficiency was noted when comparing performance at the

Figure 18. Pre-Test View of Attached Low-Cost Ablative Material Specimens

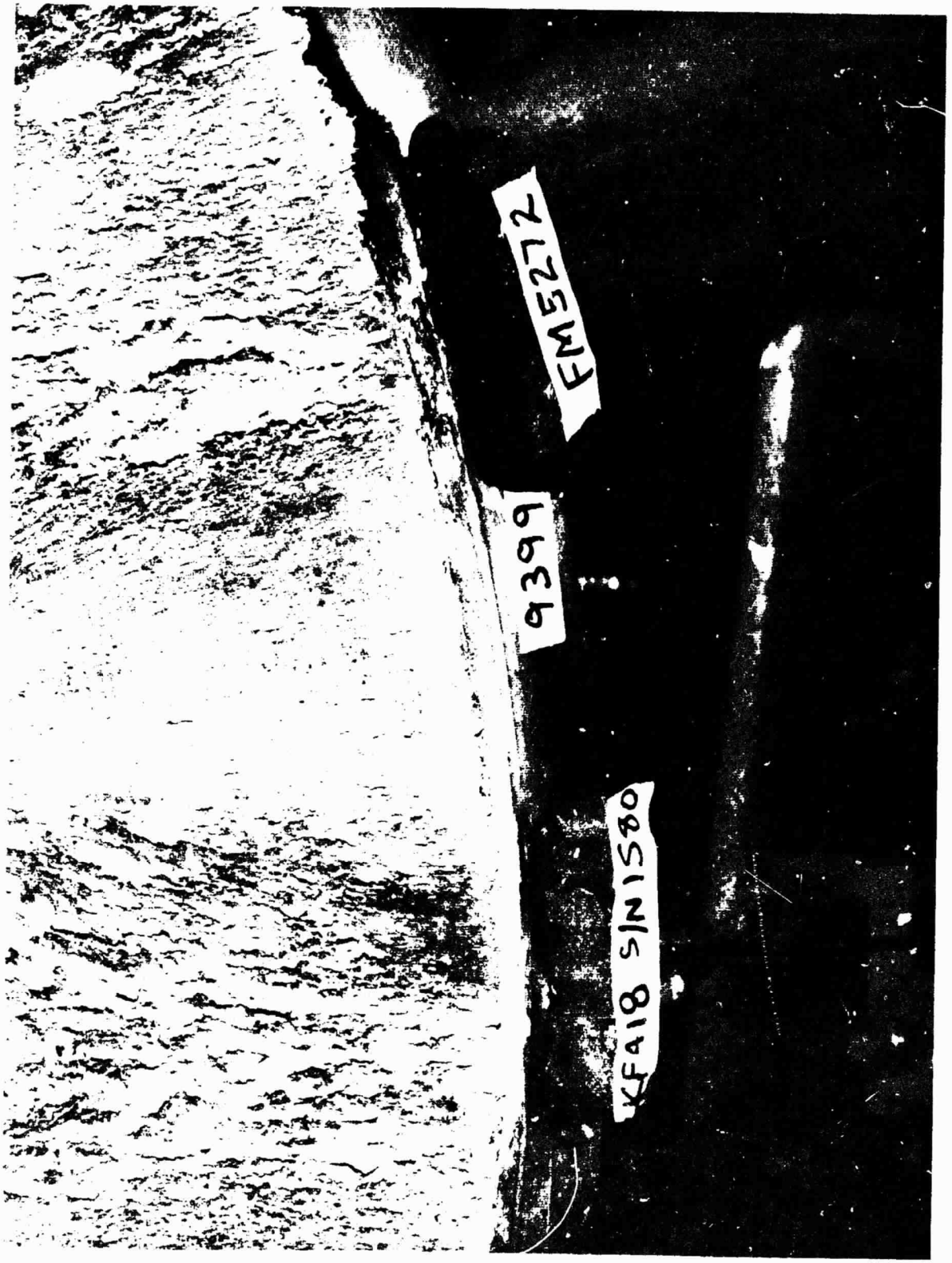

Figure 19. Post-Test View of Attached Low Cost Ablative Material Specimens

1040 psia chamber pressure and 570 psia chamber pressure levels. Vacuum specific impulse efficiency at a 2:1 expansion ratio, not including the nozzle geometry loss, at a nominal over-all mixture ratio of 5.5 was 96% to 96.5% at both chamber pressure levels. The M-1 combustion efficiency would result in only 94% specific impulse at an area ratio of 40:1.(7) The thrust chamber performance data are provided as Appendix F of this report.

E. COMBUSTION STABILITY

The thrust chamber exhibited very good stability under nominal operating conditions at both chamber pressure levels with respect to both low-frequency and high-frequency oscillations. Some low-frequency (1.5 cps) oscillations, which were caused by a "soft" fuel propellant system, occurred during two tests at 520 psia chamber pressure. (The chamber itself was not unstable, but it only followed the variations in fuel flow.) Increasing the chamber pressure to a minimum of 550 psia, along with position control of the fuel propellant system gaseous hydrogen supply valve, attenuated these oscillations. The fuel propellant system was "hardened" by increasing the system operating pressure and weight flow rate. Position control in place of pilot-feedback control of the mixer gas valve eliminated gaseous hydrogen flow oscillations.

1. Low-Frequency Stability

During the two chamber pressure steps of the staged-start transient, some low-frequency oscillations (chugging) existed, but they disappeared completely as chamber pressure and oxidizer flow rate increased. These occurred at a chamber pressure of 250 psia and a frequency of 220 cps with an amplitude of 40 psi to 50 psi peak-to-peak as well as at 450 psia and 250 cps with 20 psi to 25 psi peak-to-peak.

Low-frequency stability at both steady-state chamber pressure levels was excellent.

2. High-Frequency Stability

No indication of acoustic instability existed during any test under normal operating conditions at the two chamber pressure levels tested. Acoustic instability was induced by lowering the fuel temperature. The self-triggering temperature at an over-all mixture ratio of 4.9 was previously reported as 76°R to 81°R at 1000 psia chamber pressure.(8) In this program, the self-triggering temperature at an over-all mixture ratio of 4.9 was 74°R to 76°R at 570 psia chamber pressure. The instability disappeared as the temperature was raised to approximately 110°R.

Post-test hardware reviews following an instability usually showed minor increases in copper baffle erosion and an ultrasonic cleaning effect from the copper baffles.

---

(7) Barsotti, R. J., et al, op. cit.

(8) Contract NAS 3-2555

Review of motion pictures made during unstable operation clearly showed the disappearance of distinct hot gas streaks on the chamber wall which existed during steady-state operation. These streaks, which varied in intensity, resulted in differing regression rates circumferentially around the liner, downstream of the baffles as well as between the baffles. This is substantiated by studying Figure No. 20. The streaking during a test is caused by high local mixture ratios which possibly result from abnormal element or interelement mixing and/or local coolant flow variations. It appears as though better mixing along the wall, which results in lower local mixture ratios, occurs during unstable operation. Figure No. 21 shows the steady-state combustion and streaking characteristics as well as these same characteristics during unstable operation. Note the unstable combustion and the absence of wall streaking.

IV. CONCLUSIONS

The major conclusions resulting from the ablative thrust chamber testing accomplished in this program follow.

A. Silica-phenolic, tape-wrapped ablative chambers should be considered seriously for use in large, low-cost, long-duration oxygen/hydrogen engines with chamber pressures of up to 1040 psia.

B. The wall temperature at the throat must be lower than approximately 3600°R to obtain reasonable regression rates.

C. Materials other than tape-wrapped silica-phenolic show promise for use at area ratios of 2:1 or greater.

D. Existing analytical techniques provide sufficiently accurate predictions of ablative behavior for preliminary design purposes and must be used in connection with boundary layer mixture ratio prediction techniques.

E. Thrust chamber operation was stable within the 1040 psia to 550 psia chamber pressure range until hydrogen inlet temperature were reduced to below approximately 80°R.

F. Performance is approximately constant between chamber pressures of 1040 psia and 550 psia.

G. The thrust chamber is throttleable over the 1040 psia to 550 psia chamber pressure range.

H. The char material is structurally sound so long as hot gas does not leak behind the liner.

I. The ablative baffles performed satisfactorily during both steady-state and unstable conditions.

Figure 20. Post-Test View of Hot Gas Streaks on the Chamber Wall

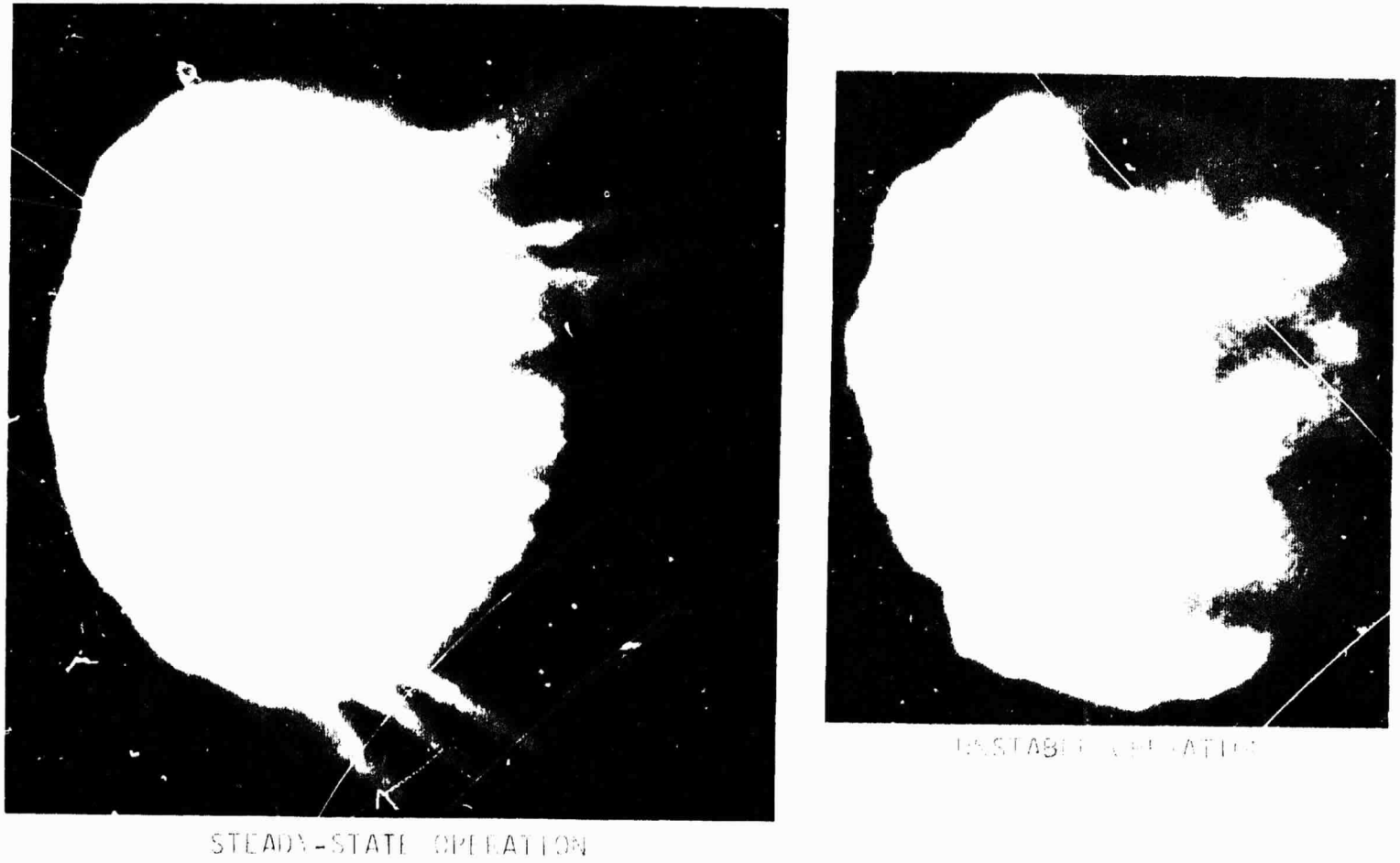

Figure 21. Combustion and Streaking Characteristics, Steady-State and Unstable Operation

APPENDIXES

APPENDIX A

REGRESSION AND CHAR DEPTH DATA AND ANALYSIS

I. INTRODUCTION

The basic objective of this contractual effort was to determine the duration capability of silica phenolic ablative thrust chamber liners for use in large oxygen/hydrogen liquid rocket engines. This appendix presents the regression and char depth data obtained with three ablative liners tested during this program as well as an analysis of these data.

II. SUMMARY

Three silica phenolic ablative liners were subjected to 18 tests. Five tests were conducted with liner S/N 001 at approximately 1040 psia thrust chamber pressure. Seven tests with liner S/N 002B and six tests with liner S/N 002C were conducted at 570 psia thrust chamber pressure. The liner from the throat to the exit was expelled during the last test with liner S/N 002C. Therefore, regression and char depth data at the throat is not valid and data downstream of the throat could not be obtained for this test.

The terms regression, degradation, and froth used in this report are defined as follows: regression is the erosion or loss of ablative material; degradation is the sum of the regression and ablative liner char depth; froth is a build-up of non-reinforced, reformed silica which is caused by the flow of molten silica that has lost the fabric reinforcement.

Sixty measurements were taken after each test for the regression evaluation. These measurements were taken as follows: The chamber and nozzle diameter was measured at 12 locations. Six measurements were taken in-line with the injector baffles and six measurements were taken equi-distant between baffles. These twelve peripheral measurements were taken at five axial locations varying from 14-in. from the injector face to 1/4-in from the nozzle exit.

Four char depth measurements also were taken, at each of the five axial locations, for a total of 20 char measurements after each test. Three char depth measurements, at each axial location, were taken between baffles and one measurement was taken in-line with a baffle.

The diametral measurements used for the regression evaluation and the char depth measurements are presented on Table III. Tests 001 through 005 were conducted at approximately 1040 psia thrust chamber pressure and tests 006 through 020 were conducted at approximately 570 psia thrust chamber pressure. Test durations above 90% of steady-state chamber pressure and the over-all thrust chamber mixture ratio for each test also are shown on the table. The diametral measurements in-line with baffles are designated by the whole numbers and those between baffles are designated as 1/2. Average diametral measurements, as well as averages in-line and between baffles also are shown on the table.

The total average regression at the throat obtained on liner S/N 001C was 0.25-in. for a total accumulated duration above 90% of steady-state chamber pressure of 144 sec. This total accumulated duration includes 54 sec of previous testing under Contract NAS 3-2555.

The total average regression at the throat obtained on liner SN 002B was 0.391-in. for a total accumulated duration of 265 sec.

The total average regression at the throat obtained on liner S/N 002C was 0.314-in. for an accumulated duration of 207 sec. The chamber liner actually experienced a total duration of 250 sec. However, as a result of the expulsion of the nozzle liner in the last test, the ablative was ripped away in throat region which invalidates this regression data.

Because the testing discussed above was conducted over a range of mixture ratios, the durations obtained on the liners do not represent the maximum capability for any one set of design conditions. Therefore, the data has been analyzed as a function of the over-all thrust chamber mixture ratio and boundary layer conditions for both 1040 psia and 570 psia pressure. Regression rates at the throat and both upstream and downstream of the throat can be estimated from these data for a particular set of design conditions. These data and analyses are presented in the sections which follow.

III. TECHNICAL DISCUSSION

A. TEST DATA ANALYSIS

This section presents the analysis of the regression and char depth test data shown on Table III.

1. Regression Analysis

The diametral measurements taken prior to the first test of each liner and after each test are shown on Table III. These data were used to determine the regression rates, for the specified test conditions, at the throat and in the convergent and divergent portions of the chamber and nozzle. The locations for these measurements are shown on the table.

The data shows that the regression in-line with baffles is less than that between baffles. This is expected because the additional baffle fuel film cooling reduces the boundary layer mixture ratio in-line with the baffles. Therefore, the data in-line and between baffles have been analyzed separately. Analysis of the data also shows that the average measurements both in-line and between baffles are severely affected by the material build-ups defined as froth. This frothing is obvious and can be identified on Table III by diameter decreases from one test to another. Because this froth would be washed away if the duration was extended, including these froth points in the analyses would not give a true indication of the regression and result in regression rates that are too low. Therefore, all the data points have

TABLE III

REGRESSION AND CHAR I

CHAMBER S/N	001 →			
TEST NO.	001*	002	003	004
TEST DURATION (FS_1 TO FS_2)-SEC	17.01	21.26	23.51	23.64
TEST DURATION (ABOVE 90% Pc)-SEC	13.81	17.36	19.61	19.64
ACCUM. TIME (ABOVE 90% Pc)-SEC	67.43**	84.79	104.40	124.14
OVER-ALL THRUST CHAMBER MR	5.35	5.37	5.11	5.45

	DISTANCE											
	14-IN.					25-IN.					THI	
DIAMETRAL MEASUREMENTS - IN.	PRE 001	POST 001	002	003	004	PRE 001	POST 001	002	003	004	PRE 001	POST 001
AFT OF BAFFLES 1 & 7	35.322	35.195	35.200	35.222	35.217	31.147	30.962	31.101	31.158	31.202	30.015	30.164
AFT OF BAFFLES 1½ & 7½	35.465	35.375	35.373	35.398	35.400	31.170	31.025	31.050	31.147	31.226	30.170	30.215
AFT OF BAFFLES 2 & 8	35.250	35.223	35.177	35.317	35.304	31.126	30.903	31.081	31.146	31.058	30.020	30.260
AFT OF BAFFLES 2½ & 8½	35.330	35.295	35.320	35.301	35.253	31.250	31.097	31.205	31.255	31.348	30.260	30.300
AFT OF BAFFLES 3 & 9	35.100	35.165	35.136	35.147	35.149	31.150	30.912	30.935	30.954	30.952	30.014	30.010
AFT OF BAFFLES 3½ & 9½	35.306	35.225	35.267	35.299	35.367	31.145	30.905	30.948	31.094	31.194	30.099	30.120
AFT OF BAFFLES 4 & 10	35.107	35.145	35.151	35.179	35.194	31.100	30.870	30.915	30.911	30.900	30.054	30.050
AFT OF BAFFLES 4½ & 10½	35.420	35.266	35.269	35.299	35.227	31.060	30.924	30.999	31.071	31.095	30.145	30.215
AFT OF BAFFLES 5 & 11	35.400	35.224	35.249	35.266	35.257	31.124	30.975	30.955	31.034	31.024	30.205	30.117
AFT OF BAFFLES 5½ & 11½	35.400	35.251	35.299	35.339	35.300	31.115	31.016	31.171	31.152	31.397	30.148	30.265
AFT OF BAFFLES 6 & 12	35.150	35.175	35.173	35.330	35.278	31.160	30.952	31.043	31.052	31.143	30.005	30.093
AFT OF BAFFLES 6½ & 12½	35.552	35.245	35.251	35.229	35.221	31.100	31.028	30.975	31.205	31.352	30.055	30.151
AVERAGE	35.342	35.252	35.239	35.277	35.264	31.137	30.965	31.052	31.098	31.158	30.099	30.165
AVE. INLINE WITH BAFFLES	35.272	35.188	35.181	35.244	35.233	31.135	30.926	31.005	31.043	31.047	30.052	30.116
AVE. BETWEEN BAFFLES	35.412	35.276	35.297	35.311	35.295	31.140	31.004	31.058	31.154	31.269	30.146	30.211
CHAP DEPTH - IN.												
AFT OF BAFFLE 1	.06	.09	.11	.13		.10	.14	.26	.26	.32***	.16	.13
BETWEEN BAFFLES 11 & 12	.08	.13	.22	.20	.27	.10	.13	.17	.19	.24	.18	.14
BETWEEN BAFFLES 12 & 1	.10	.08	.21	.16	.28	.11	.15	.23	.17	.26	.17	.11
BETWEEN BAFFLES 1 & 2	.07	.11	.21	.21	.26	.07	.16	.25	.19	.27	.16	.14

* COMPLETE RUN NO. 1198-D01-0C-001
** PREVIOUS ACCUMULATED DURATION >90% Pc ON LINER WAS 53.62 SEC
*** AREA BUILT UP BY MATERIAL FLOW
**** AREA OF EROSION STRE

TABLE III

SION AND CHAR DATA

DISTANCE FROM INJECTOR														
THROAT					THROAT + 8-IN.					EXIT - 1/4-IN.				
PRE 001	POST 001	002	003	004	PRE 001	POST 001	002	003	004	PRE 001	POST 001	002	003	004
30.015	30.164	30.241	30.287	30.283	36.995	37.385	37.421	37.361	37.364	42.526	42.952	42.972	42.937	42.908
30.170	30.215	30.324	30.363	30.408	36.802	37.492	37.417	37.473	37.395	42.512	43.006	43.012	43.003	42.964
30.020	30.260	30.331	30.383	30.430	36.765	37.468	37.344	37.265	37.261	42.560	43.009	42.990	42.960	42.954
30.260	30.300	30.409	30.445	30.492	36.587	37.460	37.387	37.458	37.205	42.525	42.962	42.966	42.984	43.010
30.014	30.010	30.012	30.103	30.090	36.830	37.435	37.385	37.507	37.411	42.565	42.940	42.909	42.955	42.933
30.099	30.120	30.203	30.256	30.450	36.645	37.385	37.408	37.438	37.357	42.568	42.963	42.911	42.920	42.993
30.051	30.050	30.154	30.146	30.212	36.865	37.435	37.388	37.436	37.385	42.580	42.975	42.885	42.910	42.940
30.145	30.215	30.231	30.257	30.261	36.690	37.512	37.412	37.480	37.387	42.600	42.978	42.913	42.937	42.945
30.205	30.117	30.155	30.186	30.056	36.960	37.453	37.414	37.493	37.361	42.620	42.924	42.904	42.905	42.920
30.148	30.265	30.431	30.422	30.653	36.722	37.440	37.333	37.489	37.512	42.635	43.006	42.966	43.016	43.064
30.005	30.095	30.216	30.225	30.322	36.840	37.491	37.392	37.470	37.444	42.600	43.016	42.976	42.979	42.940
30.05[illegible]	[illegible].151	30.186	30.357	30.583	36.732	37.491	37.444	37.447	37.118	42.630	42.986	43.045	43.019	42.822
30.099	30.163	30.239	30.286	30.353	36.786	37.454	37.395	37.443	37.350	42.577	42.976	42.954	42.960	42.948
30.052	30.116	30.182	30.222	30.232	36.876	37.445	37.391	37.422	37.371	42.575	42.969	42.941	42.941	42.929
30.146	30.211	30.297	30.350	30.475	36.696	37.463	37.400	37.464	37.329	42.578	42.985	42.969	42.980	42.966
.16	.13	.19	.20	.12****	.12	.13	.16	.18	.22	.15	.12	.18	.19	.24
.18	.14	.21	.19	.22	.15	.14	.21	.20	.25	.15	.16	.20	.17	.20
.17	.11	.19	.16	.20	.16	.14	.18	.18	.21	.16	.15	.20	.18	.23
.16	.11	.22	.23	.22	.17	.16	.21	.20	.24	.19	.19	.18	.1[illegible]	.21

TABLE III (cc

CHAMBER S/N	001	002B	002B
TEST NO.	005	006	007
TEST DURATION (FS_1 TO FS_2)-SEC	23.67	23.64	44.72
TEST DURATION (ABOVE 90% Pc)-SEC	19.77	20.64	41.90
ACCUM. TIME (ABOVE 90% Pc)-SEC	143.91	20.64	62.54
OVER-ALL THRUST CHAMBER MR	5.52	5.40*	5.50

	14-IN.				25-IN.				
DIAMETRAL MEASUREMENTS - IN.	POST 005	PRE 006	POST 006	POST 007	POST 005	PRE 006	POST 006	POST 007	POST 005
AFT OF BAFFLES 1 - 7	35.255	35.074	35.046	35.037	31.297	30.819	30.820	30.850	30.417
AFT OF BAFFLES 1½ - 7½	.391	.090	.042	.024	.328	.806	.775	.876	.552
AFT OF BAFFLES 2 -8	.301	.092	.067	.107	.031	.806	.822	.946	.491
AFT OF BAFFLES 2½ - 8½	.318	.094	.068	.006	.503	.805	.863	.964	.797
AFT OF BAFFLES 3 - 9	.153	.091	.052	.062	.004	.807	.823	.904	.143
AFT OF BAFFLES 3½ - 9½	.305	.094	.048	.053	.350	.812	.819	.973	.684
AFT OF BAFFLES 4 - 10	.151	.074	.050	.033	.500	.818	.800	.803	.311
AFT OF BAFFLES 4½ - 10½	.453	.070	.044	.023	.231	.819	.784	.847	.438
AFT OF BAFFLES 5 - 11	.254	.069	.045	.094	.010	.820	.822	.839	.214
AFT OF BAFFLES 5½ - 11½	.283	.070	.021	.012	.484	.823	.859	.932	.831
AFT OF BAFFLES 6 - 12	.325	.069	.033	.021	.180	.819	.824	.831	.240
AFT OF BAFFLES 6½ - 12½	.301	.071	.038	.028	.523	.821	.859	31.098	.841
AVERAGE	35.291	35.080	35.046	35.042	31.287	30.815	30.824	30.905	30.500
AVE. INLINE WITH BAFFLES	35.240	35.078	35.049	35.059	31.170	30.815	30.819	30.862	30.310
AVE. BETWEEN BAFFLES	35.342	35.082	35.044	35.024	31.403	30.814	30.827	30.948	30.690
CHAR DEPTH - IN.									
AFT OF BAFFLE NO. 1	.15	-	.12	.25	.28	-	.16	.29	.24
BETWEEN BAFFLES 11 & 12	.29	-	.21	.30	.25	-	.20	.30	.21
BETWEEN BAFFLES 12 & 1	.31**	-	.23	.30	.20	-	.20	.30	.20
BETWEEN BAFFLES 1 & 2	.21	-	.18	.29	.21	-	.15	.30	.19

* AVERAGE MIXTURE RATIO VALUE. OSCILLATING FLOW RATES WERE CAUSED BY TEST STAND-INDUCED LOW FR

** AREA HIGHLY FROTHED

II (cont.)

DISTANCE FROM INJECTOR											
THROAT				THROAT + 8-IN.				EXIT - 1/4-IN.			
POST 005	PRE 006	POST 006	POST 007	POST 005	PRE 006	POST 006	POST 007	POST 005	PRE 006	POST 006	POST 007
30.417	30.005	30.008	30.017	37.434	36.926	36.925	36.916	42.919	42.649	42.564	42.664
.552	.001	30.020	30.120	.210	.995	.931	.875	43.012	.690	.582	.685
.491	.000	29.970	30.106	.463	.989	.935	.940	42.934	.687	.559	.662
.797	.000	30.061	30.180	.497	.985	.932	.909	42.885	.689	.571	.682
.143	.001	29.999	30.067	.415	.975	.935	.942	42.933	.643	.560	.683
.684	.005	30.016	30.168	.533	.967	.925	.842	43.024	.630	.558	.633
.311	.010	29.968	29.968	.437	.975	.938	.935	42.914	.641	.562	.649
.438	.014	29.976	30.043	.460	.970	.942	.916	42.983	.645	.564	.627
.214	.017	29.991	30.040	.440	.968	.943	.926	42.934	.648	.587	.637
.831	.018	30.034	30.186	.354	.967	.933	.905	43.060	.675	.584	.649
.240	.016	30.000	30.019	.496	.944	.934	.919	42.999	.670	.613	.665
.841	.012	30.087	30.356	.283	.945	.936	.848	43.058	.646	.609	.602
30.500	30.008	30.011	30.106	37.419	36.967	36.934	36.906	42.971	42.659	42.576	42.653
30.310	30.008	29.989	30.036	37.448	36.963	36.935	36.930	42.939	42.656	42.574	42.660
30.690	30.008	30.032	30.176	37.390	36.972	36.935	36.883	43.004	42.663	42.578	42.646
.24	-	.17	.29	.25	-	.15	.26	.25	-	.15	.25
.21	-	.20	.27	.17	-	.19	.30	.20	-	.20	.31
.20	-	.19	.30	.22	-	.21	.30	.23	-	.23	.30
.19	-	.16	.30	.25	-	.23	.30	.25	-	.22	.29

OW FREQUENCY PERTURBATIONS.

FOLDOUT FRAME 2

TABLE III (cont.)

CHAMBER S/N	002B	002B	002B
TEST NO.	008	009	010
TEST DURATION (FS_1 TO FS_2)-SEC	30.06	44.82	47.34
TEST DURATION (ABOVE 90%Pc)-SEC	27.60	42.04	44.24
ACCUM. DURATION (ABOVE 90% Pc)-SEC	90.14	132.18	176.42
OVER-ALL THRUST CHAMBER MR	5.96*	5.70	4.20

	DISTANCE						
	14-IN.			25-IN.			
DIAMETRAL MEASUREMENTS - IN.	POST 008	POST 009	POST 010	POST 008	POST 009	POST 010	POST 008
AFT OF BAFFLES 1 - 7	35.047	35.045	35.068	30.983	30.950	31.135	30.210
AFT OF BAFFLES 1½ - 7½	.137	.144	.143	31.359	31.427	31.473	.612
AFT OF BAFFLES 2 - 8	.220	.324	.270	31.068	31.070	31.015	.196
AFT OF BAFFLES 2½ - 8½	.338	.344	.327	31.550	31.716	31.734	.804
AFT OF BAFFLES 3 - 9	.085	.033	.090	31.040	31.030	31.021	.164
AFT OF BAFFLES 3½ - 9½	.166	.192	.170	31.434	31.547	31.554	.723
AFT OF BAFFLES 4 - 10	.040	.052	.005	30.861	30.848	30.817	.088
AFT OF BAFFLES 4½ - 10½	.119	.143	.136	31.286	31.346	31.334	.552
AFT OF BAFFLES 5 - 11	.095	.099	.094	31.000	31.077	31.055	.226
AFT OF BAFFLES 5½ - 11½	.108	.092	.095	31.358	31.521	31.605	.702
AFT OF BAFFLES 6 - 12	.004	.022	.077	31.073	31.241	31.139	.190
AFT OF BAFFLES 6½ - 12½	.274	.366	.366	31.650	32.127	32.127	.944
AVERAGE	35.136	35.155	35.153	31.222	31.325	31.334	30.451
AVE. INLINE WITH BAFFLES	35.082	35.096	35.101	31.004	31.036	31.030	30.179
AVE. BETWEEN BAFFLES	35.190	35.214	35.206	31.440	31.614	31.638	30.723
CHAR DEPTH - IN.							
AFT OF BAFFLE NO. 1	.23	.28	.32	.28	.28	.33	.29
BETWEEN BAFFLES 11 & 12	.22	.33	.33	.12	.25	.32	.14
BETWEEN BAFFLES 12 & 1	.18	.29	.32	.11	.20	.26	.11
BETWEEN BAFFLES 1 & 2	.23	.30	.30	.15	.31	.31	.15

* AVERAGE MIXTURE RATIO VALUE. OSCILLATING FLOW RATES WERE CAUSED BY TEST STAND-INDUCE

(cont.)

DISTANCE FROM INJECTOR									
	THROAT			THROAT + 8-IN.			EXIT - 1/4-IN.		
POST 010	POST 008	POST 009	POST 010	POST 008	POST 009	POST 010	POST 008	POST 009	POST 010
.135	30.210	30.239	30.209	37.003	37.034	37.055	42.601	42.612	42.616
.473	.612	30.800	30.869	37.025	37.182	37.080	.621	.732	.706
.015	.196	30.267	30.261	36.899	36.897	37.058	.660	.671	.602
.734	.804	31.077	31.084	37.113	37.187	37.158	.636	.760	.830
.021	.164	30.243	30.277	36.865	36.924	36.938	.580	.648	.630
.554	.723	30.834	30.825	37.033	37.123	37.026	.573	.726	.711
.817	.088	30.073	30.079	37.009	37.043	37.001	.638	.623	.608
.334	.552	30.631	30.613	36.810	36.988	36.999	.605	.705	.705
.055	.226	30.258	30.302	36.792	37.002	36.925	.612	.652	.637
.605	.702	30.950	30.971	37.029	37.102	37.137	.637	.687	.757
.139	.190	30.460	30.447	37.009	37.030	37.000	.586	.662	.662
.127	.944	31.512	31.486	37.005	37.110	37.134	.561	.775	.733
.334	30.451	30.612	30.619	36.966	37.052	37.043	42.609	42.688	42.683
.030	30.179	30.257	30.263	36.930	36.988	36.996	42.613	42.645	42.626
.638	30.723	30.967	30.975	37.003	37.115	37.089	42.606	42.731	42.740
.33	.29	.33	.36	.28	.33	.33	.25	.31	.35
.32	.14	.21	.32	.27	.33	.33	.28	.35	.31
.26	.11	.21	.29	.30	.35	.32	.27	.31	.32
.31	.15	.33	.34	.30	.36	.34	.28	.35	.34

STAND-INDUCED LOW FREQUENCY PERTURBATIONS

FOLDOUT FRAME 2

TABLE III (cont.)

CHAMBER S/N	002B	002B
TEST NO.	011	012
TEST DURATION (FS_1 TO FS_2) - SEC	47.23	47.27
TEST DURATION (ABOVE 90% Pc) - SEC	44.08	44.12
ACCUM. DURATION (ABOVE 90% Pc) - SEC	220.50	264.62
OVER-ALL THRUST CHAMBER MR	5.07	5.00

	DISTANCE FROM INJECTOR									
	14-IN.		25-IN.		THROAT		THROAT + 8-IN.		EXIT - 1/4-IN.	
DIAMETRAL MEASUREMENTS - IN.	POST 011	POST 012	POST 011	POST 012	POST 011	POST 012	POST 011	POST 012	POST 011	POST 012
AFT OF BAFFLES 1 - 7	35.083	35.108	31.148	31.282	30.316	30.332	37.058	36.978	42.562	42.503
AFT OF BAFFLES 1½ - 7½	.125	.237	.720	.769	30.852	31.120	37.085	37.051	.725	.717
AFT OF BAFFLES 2 - 8	.284	.366	.129	.218	30.234	30.281	37.015	36.980	.632	.576
AFT OF BAFFLES 2½ - 8½	.400	.440	.981	.997	31.203	31.434	37.130	36.917	.692	.604
AFT OF BAFFLES 3 - 9	.068	.120	.073	.025	30.295	30.221	37.051	36.957	.626	.566
AFT OF BAFFLES 3½ - 9½	.207	.249	.625	.726	30.956	31.293	36.903	36.881	.678	.652
AFT OF BAFFLES 4 - 10	.080	.068	.000	.045	30.000	30.052	36.997	36.885	.624	.524
AFT OF BAFFLES 4½ - 10½	.123	.166	.381	.473	30.711	30.828	37.055	36.955	.632	.449
AFT OF BAFFLES 5 - 11	.221	.047	.090	.123	30.350	30.351	36.952	36.913	.625	.487
AFT OF BAFFLES 5½ - 11½	.161	.136	.581	.722	31.007	31.058	37.097	37.022	.689	.583
AFT OF BAFFLES 6 - 12	.023	.169	.288	.252	30.493	30.523	36.855	36.874	.502	.478
AFT OF BAFFLES 6½ - 12½	.386	.395	32.195	32.478	31.703	31.995	37.080	37.014	.691	.585
AVERAGE	35.180	35.208	31.434	31.509	30.677	30.791	37.023	36.952	42.640	42.560
AVE. INLINE WITH BAFFLES	35.127	35.146	31.121	31.158	30.281	30.293	36.988	36.931	42.595	42.522
AVE. BETWEEN BAFFLES	35.234	35.271	31.747	31.861	31.072	31.288	37.058	36.973	42.685	42.598
CHAR DEPTH - IN.										
AFT OF BAFFLE NO. 1	.32	.31	.34	.38	.33	.34	.34	.32	.33	.35
BETWEEN BAFFLES 11 & 12	.37	.40	.35	.37	.34	.33	.35	.34	.34	.34
BETWEEN BAFFLES 12 & 1	.31	.37	.32	.29	.33	.33	.33	.36	.35	.36
BETWEEN BAFFLES 1 & 2	.31	.35	.33	.35	.34	.37	.35	.38	.34	.38

TABLE III (cont.)

CHAMBER S/N	002C	002C
TEST NO.	014	016
TEST DURATION (FS_1 TO FS_2) - SEC	47.38	45.56
TEST DURATION (ABOVE 90% Pc) - SEC	44.20	42.15
ACCUM. DURATION (ABOVE 90% Pc) - SEC	44.20	86.35
OVER-ALL THRUST CHAMBER MR	5.75	5.51

	DISTANCE FROM INJECTOR														
	14-IN.			25-IN.			THROAT			THROAT + 8-IN.			EXIT - 1/4 IN.		
DIAMETRAL MEASUREMENTS - IN.	PRE 014	POST 014	POST 016	PRE 014	POST 014	POST 016	PRE 014	POST 014	POST 016	PRE 014	POST 014	POST 016	PRE 014	POST 014	POST 016
AFT OF BAFFLES 1 - 7	35.136	35.118	35.097	30.857	30.845	30.863	29.996	30.011	30.034	36.940	36.904	36.875	42.645	42.483	42.527
AFT OF BAFFLES 1½ - 7½	.139	.207	.198	.860	31.491	31.543	30.000	.629	30.754	.940	.936	.945	.646	.512	.624
AFT OF BAFFLES 2 - 8	.158	.317	.329	.871	.182	31.198	.006	.277	30.227	.945	.708	.829	.645	.384	.459
AFT OF BAFFLES 2½ - 8½	.164	.372	.476	.868	.355	31.783	.000	.475	30.909	.944	.935	.785	.645	.550	.461
AFT OF BAFFLES 3 - 9	.140	.119	.133	.860	30.834	30.899	29.998	29.923	29.999	.945	.823	.790	.645	.409	.458
AFT OF BAFFLES 3½ - 9½	.136	.099	.104	.850	31.398	31.501	.978	30.567	30.751	.945	.823	.825	.644	.457	.357
AFT OF BAFFLES 4 - 10	.120	.097	.094	.846	31.046	31.033	.975	.066	30.034	.944	.807	.827	.646	.412	.429
AFT OF BAFFLES 4½ - 10½	.122	.135	.107	.852	.329	31.502	.981	.515	30.752	.944	.850	.949	.646	.538	.430
AFT OF BAFFLES 5 - 11	.126	.103	.104	.860	.081	31.056	.989	.206	30.122	.943	.848	.858	.648	.460	.484
AFT OF BAFFLES 5½ - 11½	.135	.116	.159	.864	.183	31.321	.993	.363	30.503	.945	.909	.885	.647	.582	.537
AFT OF BAFFLES 5 - 12	.141	.145	.166	.859	.152	31.226	.995	.218	30.359	.943	.879	.859	.647	.481	.507
AFT OF BAFFLES 6½ - 12½	.136	.217	.201	.858	.421	31.602	.996	.597	30.875	.947	37.028	37.030	.645	.533	.496
AVERAGE	35.138	35.170	35.181	30.859	31.193	31.294	29.992	30.320	30.443	36.944	36.870	36.871	42.646	42.483	42.481
AVE. INLINE WITH BAFFLES	35.137	35.150	35.154	30.859	31.023	31.046	29.993	30.117	30.129	36.943	36.828	36.840	42.646	42.438	42.477
AVE. BETWEEN BAFFLES	35.139	35.191	35.208	30.859	31.363	31.542	29.991	30.524	30.757	36.944	36.912	36.903	42.646	42.529	42.484
CHAR DEPTH - IN.															
AFT OF BAFFLE NO. 1	-	.20	.25	-	.27	.30	-	.28	.33	-	.27	.35	-	.31	.32
BETWEEN BAFFLES 11 & 12	-	.34	.36	-	.25	.28	-	.23	.23	-	.34	.32	-	.33	.35
BETWEEN BAFFLES 12 & 1	-	.23	.33	-	.19	.29	-	.19	.26	-	.34	.35	-	.34	.36
BETWEEN BAFFLES 1 & 2	-	.33	.29	-	.27	.30	-	.33	.10	-	.38	.35	-	.33	.35

TABLE III (cont.)

CHAMBER S/N	002C	002C	002C	002C
TEST NO.	017	018*	019	020*
TEST DURATION (FS_1 TO FS_2) - SEC	46.89	38.45	44.89	46.51
TEST DURATION (ABOVE 90% Pc) - SEC	43.66	35.25	41.56	43.10
ACCUM. DURATION (ABOVE 90% Pc) - SEC	130.01	165.26	206.82	249.92
OVER-ALL THRUST CHAMBER MR	4.89	4.90	5.20	5.07**

	DISTANCE FRO									
	14-IN.				25-IN.				T	
DIAMETRAL MEASUREMENTS - IN.	POST 017	POST 018	POST 019	POST 020	POST 017	POST 018	POST 019	POST 020	POST 017	POST 018
AFT OF BAFFLES 1 - 7	35.089	35.106	35.096	35.170	30.851	30.876	30.877	31.562	29.989	30.034
AFT OF BAFFLES 1½ - 7½	.198	.185	.185	.222	31.538	31.503	31.652	.925	30.718	31.068
AFT OF BAFFLES 2 - 8	.328	.309	.314	.201	31.177	31.174	31.157	.448	30.201	30.372
AFT OF BAFFLES 2½ - 8½	.459	.434	.477	.120	31.846	31.914	32.086	32.375	30.975	31.070
AFT OF BAFFLES 3 - 9	.099	.319	.239	.074	30.890	30.919	30.919	31.480	29.994	30.011
AFT OF BAFFLES 3½ - 9½	.124	.127	.131	.203	31.536	31.527	31.637	.935	30.728	30.805
AFT OF BAFFLES 4 - 10	.106	.097	.096	.005	31.105	31.227	31.330	.452	.131	.235
AFT OF BAFFLES 4½ - 10½	.116	.098	.224	.199	31.601	31.605	31.719	.542	.880	.975
AFT OF BAFFLES 5 - 11	.103	.351	.184	.120	31.109	31.084	31.000	.497	.103	.173
AFT OF BAFFLES 5½ - 11½	.123	.129	.110	.083	31.336	31.376	31.454	.500	.552	.596
AFT OF BAFFLES 6 - 12	.159	.152	.146	.150	31.225	31.272	31.311	.592	.202	.372
AFT OF BAFFLES 6½ - 12½	.213	.137	.197	.137	31.654	31.748	31.838	.652	.963	31.046
AVERAGE	35.176	35.204	35.200	35.140	31.322	31.352	31.415	31.663	30.453	30.562
AVE. INLINE WITH BAFFLES	35.147	35.222	35.179	35.120	31.060	31.092	31.099	31.505	30.103	30.200
AVE. BETWEEN BAFFLES	35.206	35.185	35.221	35.160	31.585	31.612	31.731	31.822	30.803	30.927
CHAR DEPTH - IN.										
AFT OF BAFFLE NO. 1	.23	.29	.27	-	.28	.35	.37	-	.27	.33
BETWEEN BAFFLES 11 & 12	.33	.39	.44	-	.33	.36	.33	-	.25	.35
BETWEEN BAFFLES 12 & 1	.29	.35	.36	-	.24	.33	.35	-	.22	.34
BETWEEN BAFFLES 1 & 2	.29	.33	.32	-	.27	.35	.35	-	.27	.34

* STABILITY TEST

** AVERAGE VALUE. TEST CONDUCTED AT TWO STEADY-STATE MIXTURE RATIOS. MR = 4.88 FOR APPROXIMATELY 16 SECS PRIOR TO INDUCED INSTABILITY AND MR = 5.26 FOR ABOUT 16 SECS AFTER INSTABILITY.

*** NOZZLE LINER EXPELLED AT FS_1 + 24.9 SEC.

FOLDOUT FRAME

II (cont.)

	DISTANCE FROM INJECTOR											
	THROAT				THROAT + 8-IN.				EXIT - 1/4-IN.			
ST 0	POST 017	POST 018	POST 019	POST 020	POST 017	POST 018	POST 019	POST 020	POST 017	POST 018	POST 019	POST 020
562	29.989	30.034	30.142	30.900	36.890	36.854	36.916	***	42.514	42.598	42.523	***
925	30.718	31.068	31.103	31.296	.990	37.028	37.102		.573	.716	.626	
448	30.201	30.372	30.246	30.772	.855	36.972	36.828		.458	.593	.382	
375	30.975	31.070	31.313	30.775	.824	.803	36.934		.511	.611	.485	
480	29.994	30.011	30.037	30.648	.826	.828	.803		.405	.427	.383	
935	30.728	30.805	30.916	31.231	.903	.973	.830		.437	.558	.463	
452	.131	.235	30.242	30.577	.849	.855	.852		.407	.456	.451	
542	.880	.975	30.952	30.830	37.006	37.026	.475		.559	.635	.613	
497	.103	.173	30.238	30.655	36.851	36.898	.896		.484	.486	.463	
500	.552	.596	30.682	30.799	.948	.963	.927		.623	.608	.566	
592	.202	.372	30.328	30.866	.864	.875	.849		.492	.568	.577	
552	.963	31.046	31.194	31.034	.996	37.079	.990		.596	.720	.608	
563	30.453	30.562	30.620	30.865	36.900	36.930	36.869		42.505	42.581	42.512	
505	30.103	30.200	30.214	30.736	36.856	36.880	36.857		42.460	42.521	42.463	
922	30.803	30.927	31.027	30.994	36.944	36.979	36.881		42.550	42.641	42.560	
	.27	.33	.36	-	.32	.38	.35		.30	.34	.36	
	.25	.35	.31	-	.31	.41	.38		.31	.40	.39	
	.22	.34	.35	-	.35	.40	.40		.30	.37	.40	
	.27	.34	.35	-	.29	.36	.37		.31	.34	.37	

S

been analyzed and those which show a decrease in diameter have been eliminated. Tables IV through VIII show the average pre-test and post-test diameters in-line and between baffles for the five axial locations with the froth points eliminated. To obtain the average regression, the companion pre-test dimension also is eliminated for each froth point. The average regression rates shown on these tables are defined as the difference in the average radius divided by the duration above 90% of steady-state thrust chamber pressure. Also noted on these tables are data points which do not correlate with the others or which are based upon 50% or less of the six measurements taken in-line or between baffles for a particular axial location. For the cases in which 50% or less of the six measurements taken in-line or between baffles for a particular axial location. For the cases in which 50% or less of the data is used, frothing is the cause for data elimination and the remaining points showing regression could be either too low, if the area had been protected by froth, or too high if the local mixture ratio was significantly different than the average over-all thrust chamber mixture ratio. In either case, plots of the regression data identify the data which is inconsistent with the rest and the notes on the table, in most instances, present the factors contributing to this inconsistency.

Figures No. 22 and No. 23 show the average regression rate at the throat as a function of the over-all thrust chamber mixture ratio for 1040 psia and 570 psia thrust chamber pressures, respectively. These figures illustrate that the regression rate is higher between baffles for a given over-all thrust chamber mixture ratio and the regression rates at 1040 psia thrust chamber pressure are greater than those at 570 psia, as a result of the higher shear forces and heat transfer coefficient. The data from test 001 appears to be erroneous. This is particularly apparent from the data point in-line with baffles plotted at an over-all mixture ratio of 5.35 on Figure No. 22 and from the regression rates shown on Tables V and VI for the nozzle. No reason for the error in this data could be established although it appears that the pre-test measurements could be bad. It should be noted that liner S/N 001 used in test 001 had previously accumulated 54 sec test duration at 1040 psia thrust chamber pressure under Contract NAS3-2555.

The test data called out by the notes on Table IV is identified by the test number next to the symbol on Figure No. 23. It should be noted that the data for test 018, a stability test, appears to be high, as expected, because of pressure spikes. The liner was charred through in the throat region between baffles; therefore, the data point for test 012 also is high. The data for test 006 appears to be low and this probably results from the large amount of frothing that occurred, with the froth protecting the liner in this region for part of the test duration. Tests 006 and 008 also were affected by test stand-induced, low-frequency perturbations causing a mixture ratio variation and hence, the over-all mixture ratio for these tests only is an estimate of the average. Only one data point was obtained in-line with baffles for test 017. This data point was in-line with baffles 4 and 10. For this test, ablative baffles were placed in these locations and hence regressions similar to those between baffles could be expected. This is substantiated by the test data as noted by the data point between baffles shown on the figure. Although only 50% of the data was valid for test 010, the regression rates obtained appear to be reasonable.

TABLE IV

REGRESSION EVALUATION AT THE THROAT

LINER NO.	TEST NO.	THRUST CHAMBER PRESSURE PSIA	OVER-ALL THRUST CHAMBER MIXTURE RATIO	TEST DURATION ABOVE 90% Pc, SEC	AVERAGE PRE-TEST DIAMETER INLINE WITH BAFFLES, IN.	AVERAGE PRE-TEST DIAMETER BETWEEN BAFFLES, IN.	AVERAGE POST-TEST DIAMETER INLINE WITH BAFFLES, IN.	AVERAGE POST-TEST DIAMETER BETWEEN BAFFLES, IN.	AVERAGE REGRESSION RATE INLINE WITH BAFFLES, IN/SEC	AVERAGE REGRESSION RATE BETWEEN BAFFLES, IN/SEC	BOUNDARY LAYER MIXTURE RATIO INLINE WITH BAFFLES	BOUNDARY LAYER MIXTURE RATIO BETWEEN BAFFLES	WALL TEMP. INLINE WITH BAFFLES °R	WALL TEMP. BETWEEN BAFFLES °R
001	001(1)	1040	5.35	13.81	30.013	30.146	30.172	30.211	.00576	.00235	2.04	2.42	3310	3760
	002		5.37	17.36	30.116	30.211	30.182	30.297	.00190	.00248	2.05	2.43	3320	3770
	003		5.11	19.61	30.182	30.271	30.222	30.336	.00102	.00166	1.94	2.33	3190	3650
	004		5.45	19.74	30.251	30.350	30.321	30.475	.00177	.00317	2.07	2.46	3350	3800
	005		5.52	19.77	30.214	30.475	30.315	30.690	.00285	.00544	2.10	2.50	3380	3840
002B	006(2)	570	5.40(3)	20.64	30.005	30.007	30.008	30.044	.000073	.00090	2.06	2.44	3330	3775
	007		5.50	41.90	29.989	30.032	30.036	30.176	.00056	.00172	2.09	2.49	3370	3830
	008		5.96(3)	27.60	30.036	30.176	30.179	30.723	.00259	.00991	2.30	2.73	3620	4100
	009		5.70	42.04	30.197	30.723	30.293	30.967	.00114	.00523	2.18	2.58	3480	3940
	010(4)		4.20	44.24	30.191	30.942	30.219	30.975	.00032	.00037	1.60	2.07	2760	3350
	011		5.07	44.08	30.309	30.996	30.364	31.110	.00062	.00136	1.93	2.31	3170	3630
	012(5)		5.00	44.12	30.279	31.072	30.308	31.288	.00033	.00245	1.90	2.30	3140	3620
002C	014		5.75	44.20	29.992	29.991	30.156	30.524	.00186	.00603	2.20	2.61	3500	3960
	016		5.51	42.15	30.050	30.524	30.131	30.757	.00096	.00276	2.10	2.49	3380	3830
	017(6)		4.89	43.66	30.034	30.760	30.131	30.843	.00111	.00095	2.26	2.26	3570	3570
	018(7)		4.90	35.25	30.103	30.803	30.200	30.927	.00138	.00176	1.86	2.26	3090	3570
	019		5.20	41.56	30.165	30.917	30.207	31.042	.00051	.00150	1.98	2.37	3240	3700

(1) REGRESSION DATA APPEARS TO BE ERRONEOUS; PARTICULARLY INLINE WITH BAFFLES FOR THIS CASE.
(2) ONLY ONE REGRESSION READING INLINE WITH BAFFLES 1-7 AND FIVE READINGS BETWEEN BAFFLES.
(3) AVERAGE MIXTURE RATIO VALUE. OSCILLATING FLOW RATES WERE CAUSED BY TEST STAND-INDUCED LOW FREQUENCY PERTURBATIONS.
(4) ONLY THREE REGRESSION READINGS BOTH INLINE AND BETWEEN BAFFLES.
(5) LAST TEST ON THIS LINER AND THE LINER WAS COMPLETELY CHARRED THROUGH AT THE THROAT BETWEEN BAFFLES WHICH ACCOUNTS FOR THE HIGH REGRESSION.
(6) ONLY ONE REGRESSION POINT INLINE WITH BAFFLES 4-10. ABLATIVE BAFFLES WERE LOCATED IN THESE POSITIONS FOR THIS TEST AND THEREFORE THE BOUNDARY LAYER CONDITIONS ARE CLOSER TO THOSE BETWEEN BAFFLES.
(7) STABILITY TEST. HIGHER THAN NORMAL REGRESSIONS.

TABLE V

REGRESSION EVALUATION 8-IN. DOWNSTREAM OF THE THROAT (ϵ =1.5)

LINER NO.	TEST NO.	THRUST CHAMBER PRESSURE, PSIA	AVERAGE PRE-TEST DIAMETER INLINE WITH BAFFLES IN.	AVERAGE PRE-TEST DIAMETER BETWEEN BAFFLES IN.	AVERAGE POST-TEST DIAMETER INLINE WITH BAFFLES IN.	AVERAGE POST-TEST DIAMETER BETWEEN BAFFLES IN.	AVERAGE REGRESSION RATE INLINE WITH BAFFLES IN/SEC	AVERAGE REGRESSION RATE BETWEEN BAFFLES IN/SEC	BOUNDARY LAYER MIXTURE RATIO INLINE WITH BAFFLES	BOUNDARY LAYER MIXTURE RATIO BETWEEN BAFFLES	WALL TEMP. INLINE WITH BAFFLES °R	WALL TEMP. BETWEEN BAFFLES °R
001	001 (1)	1040	36.876	36.696	37.445	37.463	.0206	.0278	2.37	2.81	3550	4040
	002 (2)		37.385	37.385	37.421	37.408	.00104	.00066	2.38	2.82	3570	4050
	003		37.395	37.400	37.477	37.464	.00209	.00163	2.26	2.72	3430	3940
	004 (3)		37.361	37.489	37.364	37.512	.000076	.00058	2.42	2.86	3610	4100
	005		37.371	37.292	37.448	37.397	.00195	.00266	2.46	2.89	3660	4130
002B	006	570	NO VALID DATA. FROTHING OCCURRED AT ALL LOCATIONS									
	007 (4)		36.935	-	36.941	-	.00015	-	2.45	2.88	3650	4120
	008		36.923	36.876	37.007	37.041	.00100	.00197	2.70	3.15	3920	4400
	009		36.936	37.003	37.007	37.115	.00129	.00203	2.56	2.98	3770	4220
	010 (5)		36.952	37.067	37.017	37.090	.00077	.00027	1.98	2.46	3100	3660
	011 (6)		36.973	37.040	37.020	37.070	.00053	.00034	2.24	2.70	3410	3920
	012 (7)		36.855	-	36.874	-	.00022	-	2.21	2.68	3370	3900
002C	014 (8)		-	36.947	-	37.028	-	.00092	2.58	3.01	3790	4260
	016 (9)		36.788	36.870	36.838	36.906	.00059	.00043	2.46	2.88	3660	4120
	017		36.841	36.878	36.857	36.934	.00018	.00064	2.16	2.64	3310	3860
	018 (10)		36.849	36.969	36.886	37.014	.00053	.00064	2.17	2.65	3330	3870
	019 (11)		36.854	36.916	36.916	37.018	.00197	.00123	2.30	2.75	3470	3980

NOTES

(1) REGRESSION DATA APPEARS TO BE ERRONEOUS.
(2) ONLY ONE REGRESSION READING BOTH INLINE (1-7) AND BETWEEN BAFFLES (3½ - 7½).
(3) ONLY ONE REGRESSION READING BOTH INLINE (1-7) AND BETWEEN BAFFLES (5½ - 11½).
(4) FROTHING OCCURRED AT ALL LOCATIONS BETWEEN BAFFLES. TWO REGRESSION READINGS INLINE WITH BAFFLES (2-8 AND 3-9).
(5) THREE REGRESSION READINGS BOTH INLINE AND BETWEEN BAFFLES.
(6) THREE REGRESSION READINGS INLINE WITH BAFFLES AND TWO BETWEEN.
(7) FROTHING OCCURRED AT ALL LOCATIONS BETWEEN BAFFLES. ONE REGRESSION READING INLINE (6-12).
(8) FROTHING OCCURRED AT ALL LOCATIONS INLINE WITH BAFFLES. ONE REGRESSION READING BETWEEN (6' - 12½).
(9) THREE REGRESSION READINGS BOTH INLINE AND BETWEEN BAFFLES.
(10) STABILITY TEST.
(11) ONLY ONE REGRESSION READING INLINE WITH BAFFLES (1-7) AND TWO BETWEEN (1½ - 7½ AND 2½ - 8½).

TABLE VI

REGRESSION EVALUATION 1/4-IN. FROM THE EXIT (ϵ = 2.0)

LINER NO.	TEST NO.	THRUST CHAMBER PRESSURE, PSIA	AVERAGE PRE-TEST DIAMETER INLINE WITH BAFFLES IN.	AVERAGE PRE-TEST DIAMETER BETWEEN BAFFLES IN.	AVERAGE POST-TEST DIAMETER INLINE WITH BAFFLES IN.	AVERAGE POST-TEST DIAMETER BETWEEN BAFFLES IN.	AVERAGE REGRESSION RATE INLINE WITH BAFFLES IN/SEC	AVERAGE REGRESSION RATE BETWEEN BAFFLES IN/SEC	BOUNDARY LAYER MIXTURE RATIO INLINE WITH BAFFLES	BOUNDARY LAYER MIXTURE RATIO BETWEEN BAFFLES	*ALL TEMP. INLINE WITH BAFFLES °R	*ALL TEMP. BETWEEN BAFFLES °R
001	001 (1)	1040	42.575	42.578	42.969	42.983	.0143	.0147	2.57	3.05	3710	4240
	002 (2)		42.952	42.985	42.972	43.008	.00058	.00066	2.58	3.06	3730	4250
	003		42.923	42.939	42.948	42.964	.00064	.00064	2.45	2.95	3570	4130
	004 (3)		42.906	42.964	42.930	43.003	.00061	.00099	2.62	3.10	3770	4280
	005		42.923	42.931	42.944	43.019	.00053	.00223	2.56	3.14	3820	4320
002B	006	570	NO VALID DATA. FROTHING OCCURRED AT ALL LOCATIONS.									
	007		42.574	42.572	42.660	42.655	.00103	.00099	2.65	3.13	3810	4310
	008		NO VALID DATA. FROTHING OCCURRED AT ALL LOCATIONS.									
	009		42.608	42.606	42.649	42.731	.00049	.00149	2.77	3.24	3940	4420
	010 (4)		42.637	42.717	42.639	42.764	.000023	.00053	2.03	2.70	3070	3860
	011 (5)		42.605	42.706	42.628	42.725	.00026	.00022	2.42	2.94	3540	4120
	012		NO VALID DATA. FROTHING OCCURRED AT ALL LOCATIONS.									
002C	014		NO VALID DATA. FROTHING OCCURRED AT ALL LOCATIONS.									
	016 (6)		42.438	42.512	42.477	42.624	.00046	.00133	2.66	3.13	3820	4310
	017 (7)		42.471	42.456	42.471	42.545	0	.00108	2.34	2.88	3440	4060
	018 (8)		42.460	42.535	42.521	42.648	.00087	.0016	2.35	2.89	3460	4070
	019 (9)		42.566	-	42.577	-	.000011	-	2.49	2.99	3620	4170

NOTES

(1) REGRESSION DATA APPEARS TO BE ERRONEOUS.
(2) ONLY ONE REGRESSION READING INLINE (1-7) WITH BAFFLES AND THREE BETWEEN.
(3) TWO REGRESSION READINGS INLINE (4-10 AND 5-11) WITH BAFFLES AND FOUR BETWEEN.
(4) TWO REGRESSION READINGS INLINE (1-7 AND 6-12) WITH BAFFLES AND THREE BETWEEN.
(5) TWO REGRESSION READINGS INLINE (2-8 AND 4-10) WITH BAFFLES AND ONE BETWEEN (1½ - 7½).
(6) ONLY ONE REGRESSION READING BETWEEN BAFFLES (1½ - 7½). EVIDENCE OF REGRESSION AT ALL LOCATIONS INLINE.
(7) FROTHING AT FOUR OR SIX LOCATIONS INLINE WITH BAFFLES WITH NO REGRESSION EVIDENT AT THE OTHER TWO LOCATIONS. REGRESSION EVIDENT AT FIVE OR SIX LOCATIONS BETWEEN.
(8) STABILITY TEST.
(9) FROTHING OCCURRED AT ALL LOCATIONS BETWEEN BAFFLES. ONLY ONE REGRESSION POINT INLINE WITH BAFFLES (6-12).

TABLE VII

REGRESSION EVALUATION 14-IN. FROM THE INJECTOR FACE

LINER NO.	TEST NO.	THRUST CHAMBER PRESSURE PSIA	AVERAGE PRE-TEST DIAMETER INLINE WITH BAFFLES IN.	AVERAGE PRE-TEST DIAMETER BETWEEN BAFFLES IN.	AVERAGE POST-TEST DIAMETER INLINE WITH BAFFLES IN.	AVERAGE POST-TEST DIAMETER BETWEEN BAFFLES IN.	AVERAGE REGRESSION RATE INLINE WITH BAFFLES IN/SEC	AVERAGE REGRESSION RATE BETWEEN BAFFLES IN/SEC	BOUNDARY LAYER MIXTURE RATIO INLINE WITH BAFFLES	BOUNDARY LAYER MIXTURE RATIO BETWEEN BAFFLES	WALL TEMP. INLINE WITH BAFFLES	WALL TEMP. BETWEEN BAFFLES °R
001	001[1]	1040	35.104	-	35.155	-	.00185	-	0.98	1.42	1820	2510
	002		35.188	35.256	35.200	35.281	.00035	.00072	0.99	1.43	1830	2520
	003		35.181	35.302	35.244	35.334	.00161	.00082	0.92	1.35	1700	2400
	004[2]		35.163	35.349	35.172	35.384	.00023	.00089	1.01	1.45	1860	2570
	005[3]		35.215	35.234	35.244	35.357	.00073	.00311	1.03	1.48	1890	2600
002B	006	570	NO VALID DATA. FROTHING OCCURRED AT ALL LOCATIONS.									
	007[4]		35.055	35.048	35.088	35.053	.00039	.00006	1.02	1.47	1870	2590
	008		35.067	35.024	35.097	35.190	.00034	.00301	1.15	1.65	2080	2840
	009		35.090	35.207	35.124	35.238	.00040	.00037	1.08	1.54	1970	2700
	010[5]		35.033	35.229	35.079	35.231	.00051	.00002	0.67	1.07	1220	1960
	011		35.105	35.239	35.167	35.284	.00066	.00031	0.90	1.33	1640	2370
	012		35.115	35.248	35.191	35.297	.00086	.00056	0.89	1.31	1660	2340
002C	014[6]		35.150	35.140	35.231	35.233	.00092	.00105	1.10	1.56	2010	2720
	016		35.171	35.196	35.183	35.246	.00014	.00059	1.02	1.48	1870	2610
	017[7]		35.094	35.153	35.106	35.163	.00014	.00012	0.85	1.27	1600	2280
	018[8]		35.097	35.124	35.259	35.128	.00230	.00006	0.86	1.28	1600	2300
	019		35.309	35.190	35.314	35.243	.00006	.00057	0.94	1.37	1750	2430
	020[9]		35.121	35.150	35.160	35.213	.00045	.00064	0.90	1.33	1680	2370

NOTES

(1) TWO REGRESSION READINGS INLINE WITH BAFFLES (3-9 AND 4-10). FROTHING OCCURRED AT ALL LOCATIONS BETWEEN BAFFLES.
(2) TWO REGRESSION READINGS INLINE WITH BAFFLES (3-9 AND 4-10) AND TWO REGRESSION READINGS BETWEEN BAFFLES (1½ - 7½ AND 3½ - 9½).
(3) THREE REGRESSION READINGS BOTH INLINE AND BETWEEN BAFFLES.
(4) THREE REGRESSION READINGS INLINE WITH BAFFLES BUT ONLY ONE BETWEEN BAFFLES (3½ - 9½).
(5) THREE REGRESSION READINGS INLINE WITH BAFFLES. FROTHING VERY EVIDENT BETWEEN BAFFLES WITH A TWO MINOR REGRESSION READINGS AT 5½ - 11½ AND 6½ - 12½.
(6) TWO REGRESSION READINGS INLINE WITH BAFFLES (2-8 AND 4-12) AND FOUR BETWEEN.
(7) ONE REGRESSION READING INLINE WITH BAFFLES (4-10) AND FOUR BETWEEN.
(8) STABILITY TEST HENCE REGRESSION IS EXPECTED TO BE HIGHER THAN NORMAL. THREE REGRESSION READINGS INLINE WITH BAFFLES ARE HIGH; HOWEVER, FROTHING OCCURS BETWEEN BAFFLES AND ONLY TWO MINOR REGRESSION READINGS AT 3½ - 9½ AND 5½ - 11½ ARE NOTED.
(9) TWO REGRESSION READINGS INLINE WITH BAFFLES (1-7 AND 6-12) AND TWO BETWEEN (1½ - 7½ AND 3½ - 9½). THIS WAS ALSO A STABILITY TEST.

TABLE VIII

REGRESSION EVALUATION 25-IN. FROM THE INJECTOR FACE

LINER NO.	TEST NO.	THRUST CHAMBER PRESSURE PSIA	AVERAGE PRE-TEST DIAMETER INLINE WITH BAFFLES IN.	AVERAGE PRE-TEST DIAMETER BETWEEN BAFFLES IN.	AVERAGE POST-TEST DIAMETER INLINE WITH BAFFLES IN.	AVERAGE POST-TEST DIAMETER BETWEEN BAFFLES IN.	AVERAGE REGRESSION RATE INLINE WITH BAFFLES IN/SEC	AVERAGE REGRESSION RATE BETWEEN BAFFLES IN/SEC	BOUNDARY LAYER MIXTURE RATIO INLINE WITH BAFFLES	BOUNDARY LAYER MIXTURE RATIO BETWEEN BAFFLES	WALL TEMP. INLINE WITH BAFFLES	WALL TEMP. BETWEEN BAFFLES °R
001	001	1040	NO VALID DATA. FROTHING OCCURRED AT ALL LOCATIONS.									
	002		30.916	30.999	31.015	31.075	.00256	.00219	1.81	2.18	3050	3520
	003		31.023	31.035	31.069	31.154	.00117	.00303	1.71	2.09	2920	3400
	004(1)		31.105	31.154	31.173	31.269	.00172	.00291	1.84	2.21	3090	3550
	005		31.049	31.269	31.245	31.403	.00496	.00339	1.86	2.25	3110	3600
002B	006	570	31.813	31.815	31.823	31.850	.00024	.00085	1.82	2.20	3060	3540
	007		30.819	30.827	30.862	30.948	.00051	.00144	1.85	2.24	3100	3590
	008		30.862	30.948	31.004	31.440	.00257	.00891	2.04	2.46	3340	3840
	009		31.047	31.440	31.129	31.614	.00098	.00207	1.93	2.33	3200	3690
	010(2)		30.950	31.668	31.135	31.699	.00209	.00035	1.38	1.81	2460	3050
	011		31.030	31.644	31.121	31.780	.00103	.00154	1.70	2.07	2900	3380
	012		31.092	31.747	31.167	31.861	.00085	.00129	1.67	2.05	2870	3350
002C	014		30.859	30.859	31.115	31.363	.00290	.00570	1.95	2.35	3230	3720
	016		31.003	31.363	31.047	31.542	.00051	.00212	1.85	2.24	3100	3590
	017		31.045	31.542	31.107	31.595	.00071	.00061	1.62	2.01	2800	3300
	018(3)		31.018	31.609	31.074	31.661	.00081	.00074	1.63	2.02	2810	3320
	019		31.074	31.612	31.109	31.731	.00042	.00143	1.75	2.12	2970	3440
	020(3)		31.099	31.707	31.505	31.934	.00471	.00263	1.70	2.07	2900	3380

NOTES

(1) TWO REGRESSION READINGS INLINE WITH BAFFLES (1-7 AND 6-12). REGRESSION EVIDENT AT ALL LOCATIONS BETWEEN.
(2) ONE REGRESSION READING INLINE WITH BAFFLES (1-7). REGRESSION EVIDENT AT FIVE OF SIX LOCATIONS BETWEEN BAFFLES.
(3) STABILITY TEST. HIGHER THAN NORMAL REGRESSIONS EXPECTED.

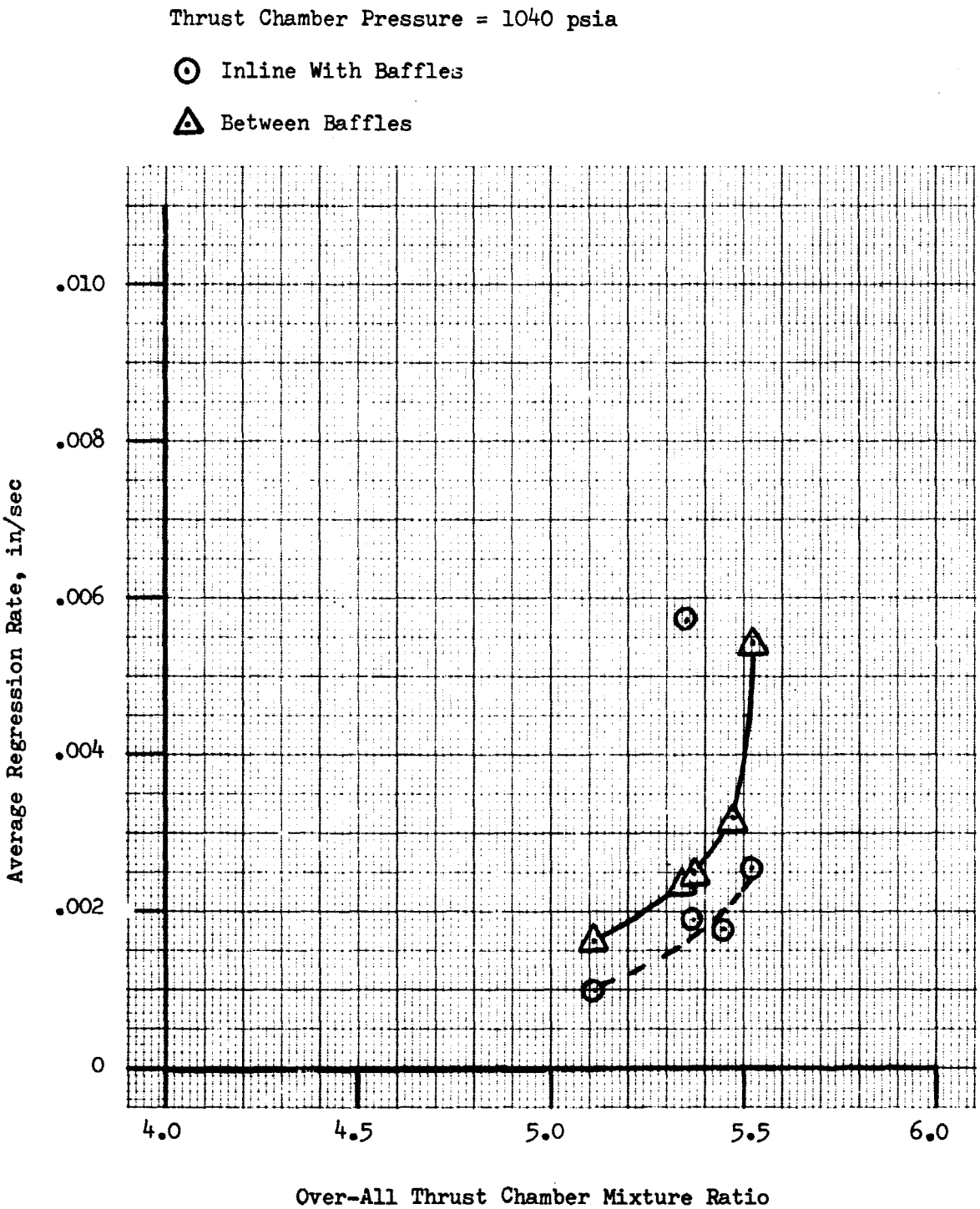

Figure 22. Average Regression Rate at the Throat vs Over-all Thrust Chamber Mixture Ratio (Thrust Chamber Pressure = 1040 psia

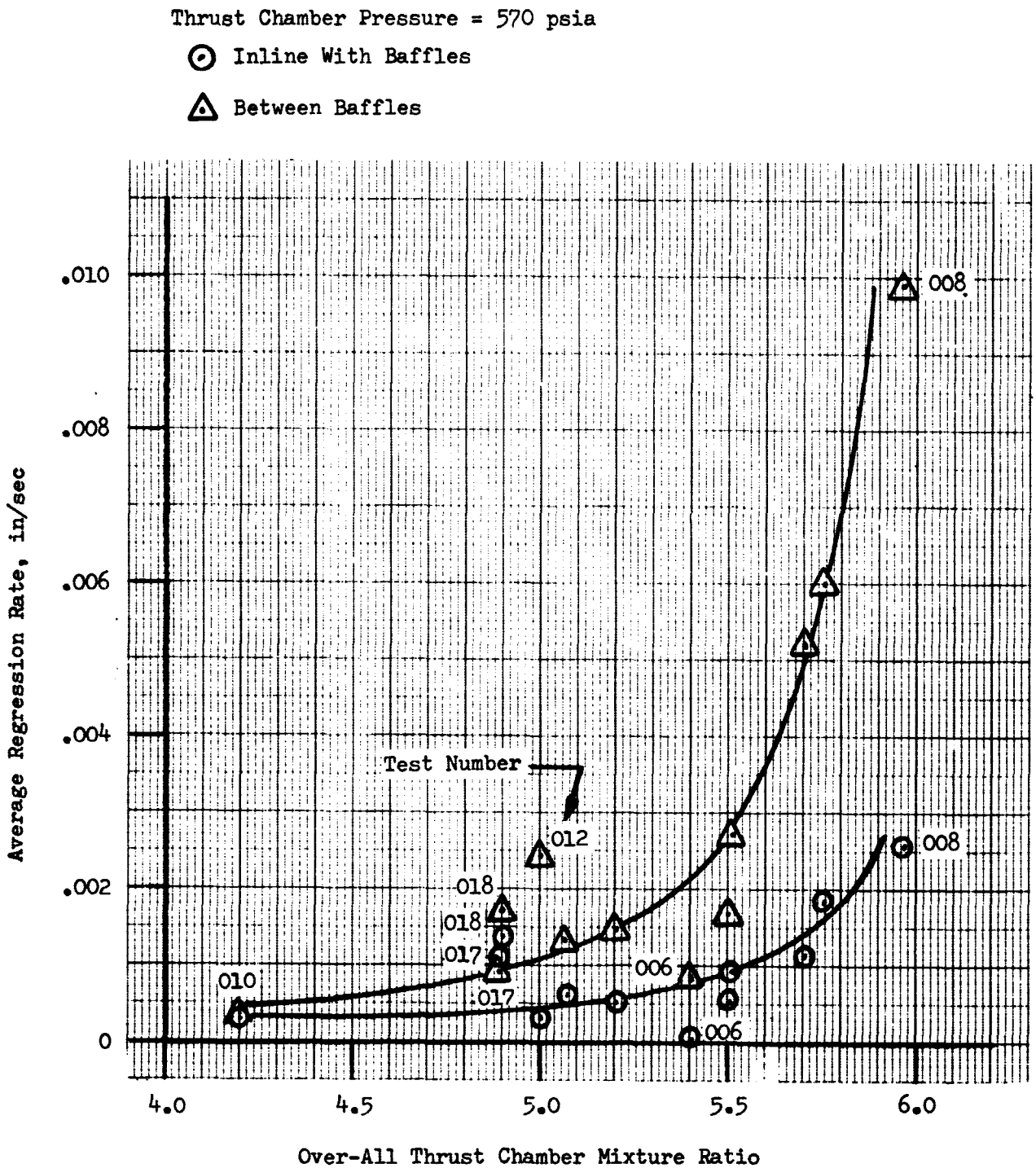

Figure 23. Average Regression Rate at the Throat vs Over-all Thrust Chamber Mixture Ratio (Thrust Chamber Pressure = 570 psia)

Because it is apparent from Figures No. 22 and No. 23 that the regression rates are a function of the boundary layer conditions, the data were correlated as a function of the wall temperature (boundary layer recovery temperature). No temperature measurements or fluid samples of the boundary layer were taken during the test program. Therefore, it was necessary to use analytical techniques to predict the boundary layer mixture ratio and the wall temperature as a function of the axial distance from the injector face. The methods used and the boundary layer analysis is presented in Appendix E, "Theoretical Analysis of Ablative Chamber Thermal Behavior." The predicted boundary layer conditions are shown on Figures No. 24 through No. 26. Any future programs of this nature should include an experimental determination of the boundary layer conditions to reliably correlate the regression data and provide back-up for the analytical models. Figure No. 24 and No. 25 show the estimated boundary layer mixture ratio as a function of the over-all thrust chamber mixture ratio for the five axial locations of interest. Because of the additional fuel film cooling, the boundary layer mixture ratio in-line with baffles shown on Figure No. 24 is significantly lower than that between baffles shown on Figure No. 25. The wall temperature is shown as a function of the boundary layer mixture ratio on Figure No. 26 for the chamber and nozzle. Using Figures No. 24 and No. 25, the boundary layer mixture ratios were determined in-line and between baffles at each axial location for each test over-all thrust chamber mixture ratio. The wall temperature then was determined for these boundary layer mixture ratios as a function of axial location from Figure No. 26. The boundary layer mixture ratios and wall temperatures predicted for the test conditions are shown on Tables IV through VIII.

Figures No. 27 through No. 36 show the regression rate as a function of wall temperature for the five axial locations of interest at thrust chamber pressures of 1040 psia and 570 psia. Data from tests 001, 018, and 020 have not been included on these plots. The test 001 data was eliminated because it is obviously erroneous. The data from tests 018 and 020 have not been plotted because these were stability tests and the regression data is inconsistent as a result of pressure surges causing higher than normal regressions in most cases. Test 012 was the last test with liner 002B and the liner was completely charred through at the throat between baffles. This resulted in higher than normal regressions and therefore, this data point has not been plotted on Figure No. 28. All the remaining data were plotted and those affected by frothing are identified. The data for the shaded points on the plots also is identified and explained by the notes on Tables IV and VIII.

Figures No. 27 and No. 28 present the regression rate data at the throat for thrust chamber pressures of 1040 psia and 570 psia, respectively. It can be noted from these figures that the regression data for both in-line and between baffles reasonably fit one curve at both thrust chamber pressures. Therefore, the wall temperature is a practical correlating parameter. At 3600°R, approximately the melting point of the silica, the regression rate at 1040 psia thrust chamber pressure is 0.002-in./sec compared to 0.0013-in./sec at 570 psia chamber pressure. This difference of 0.7 mils/sec

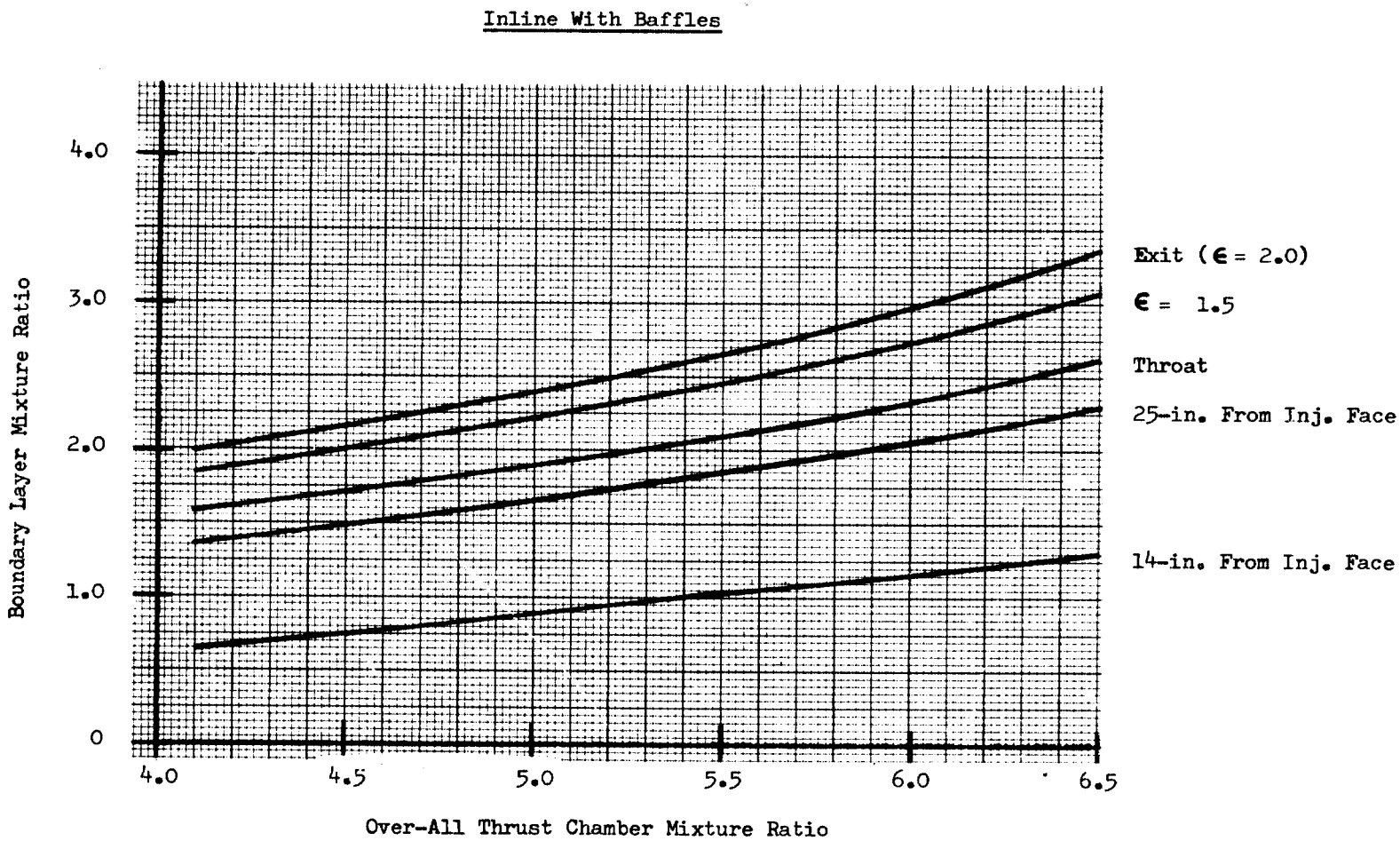

Figure 24. Boundary Layer Mixture Ratio vs Over-all Thrust Chamber Mixture Ratio (In-Line with Baffles)

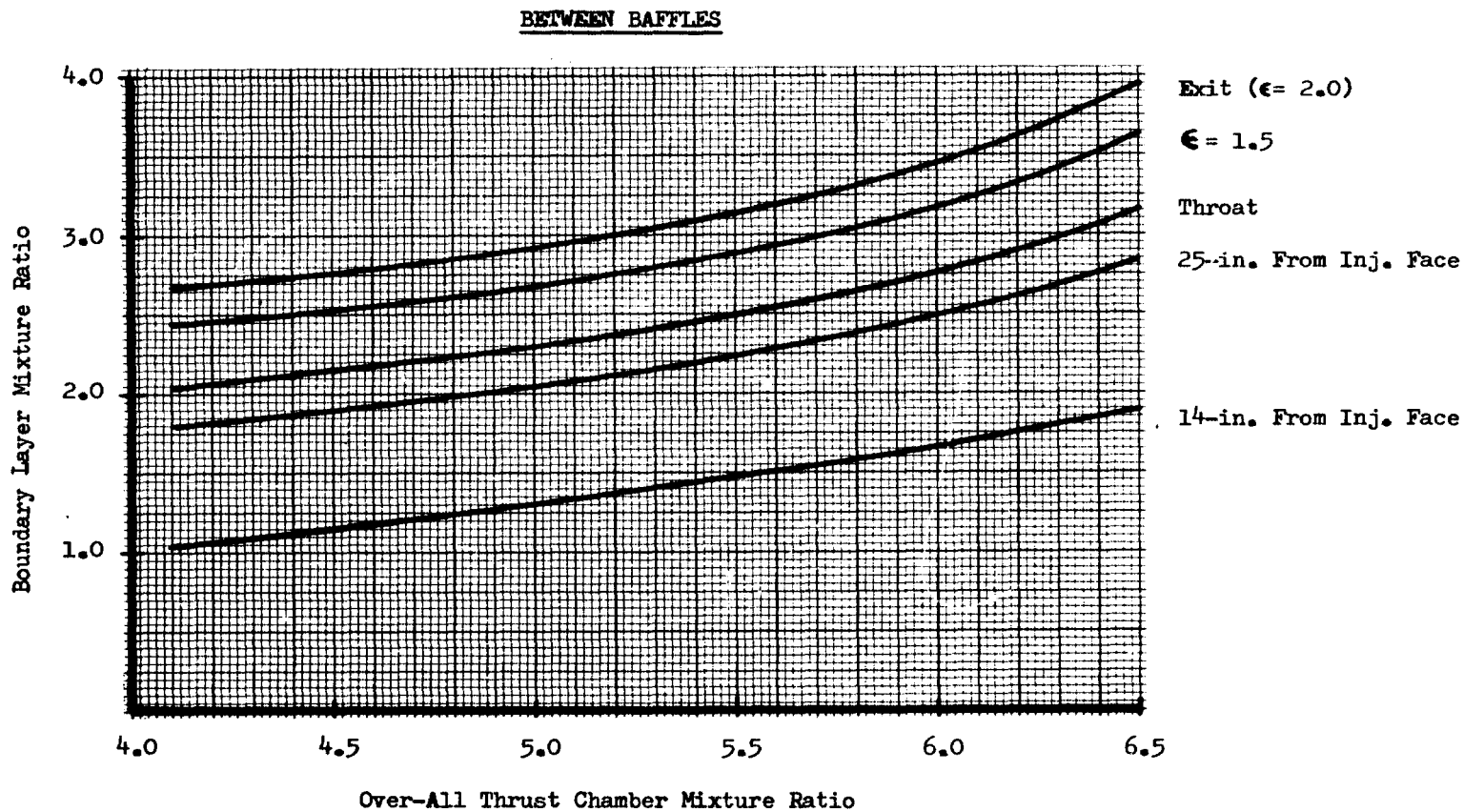

Figure 25. Boundary Layer Mixture Ratio vs Over-all Thrust Chamber Mixture Ratio (Between Baffles)

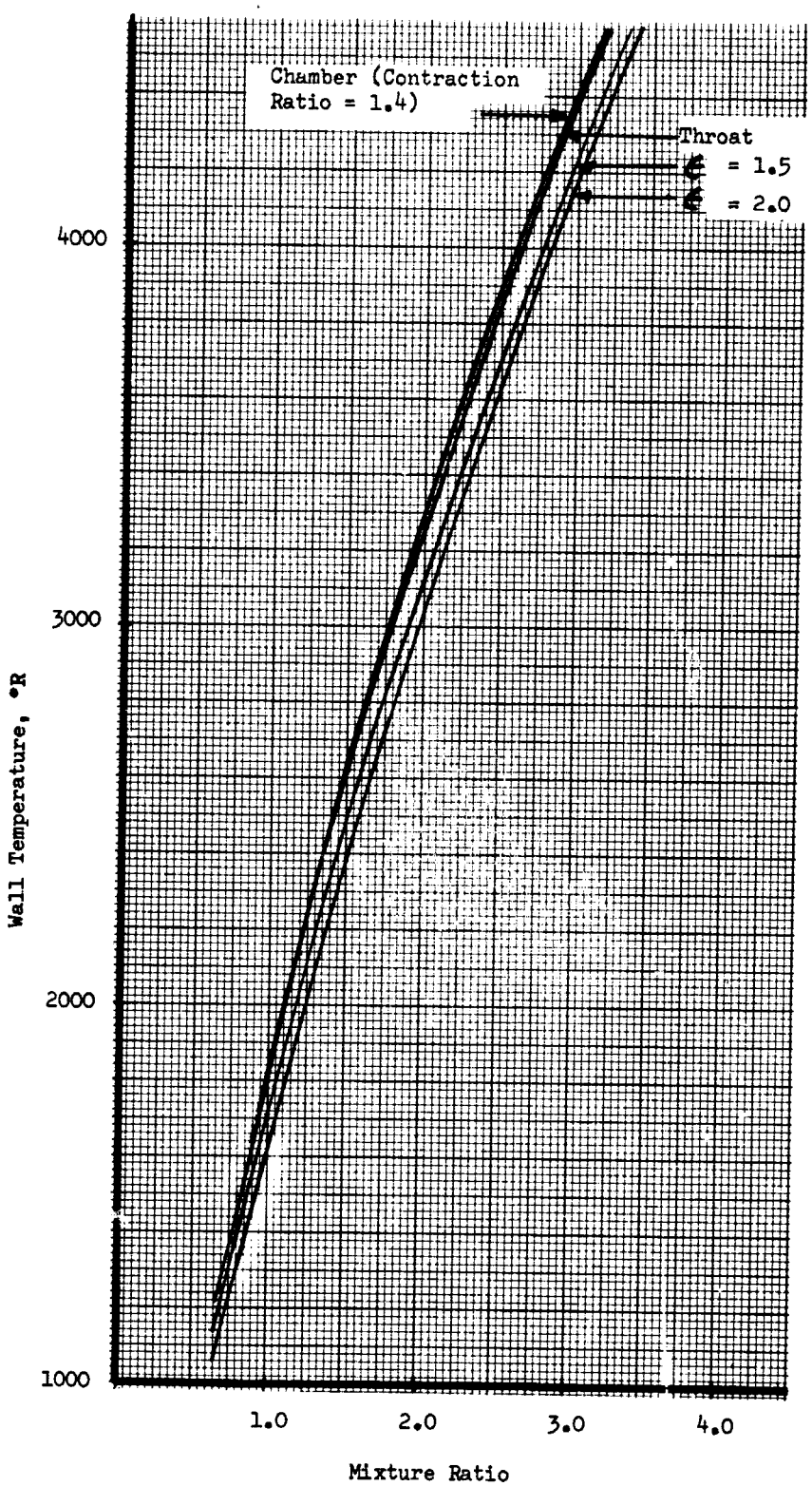

Figure 26. Wall Temperatures vs Mixture Ratio

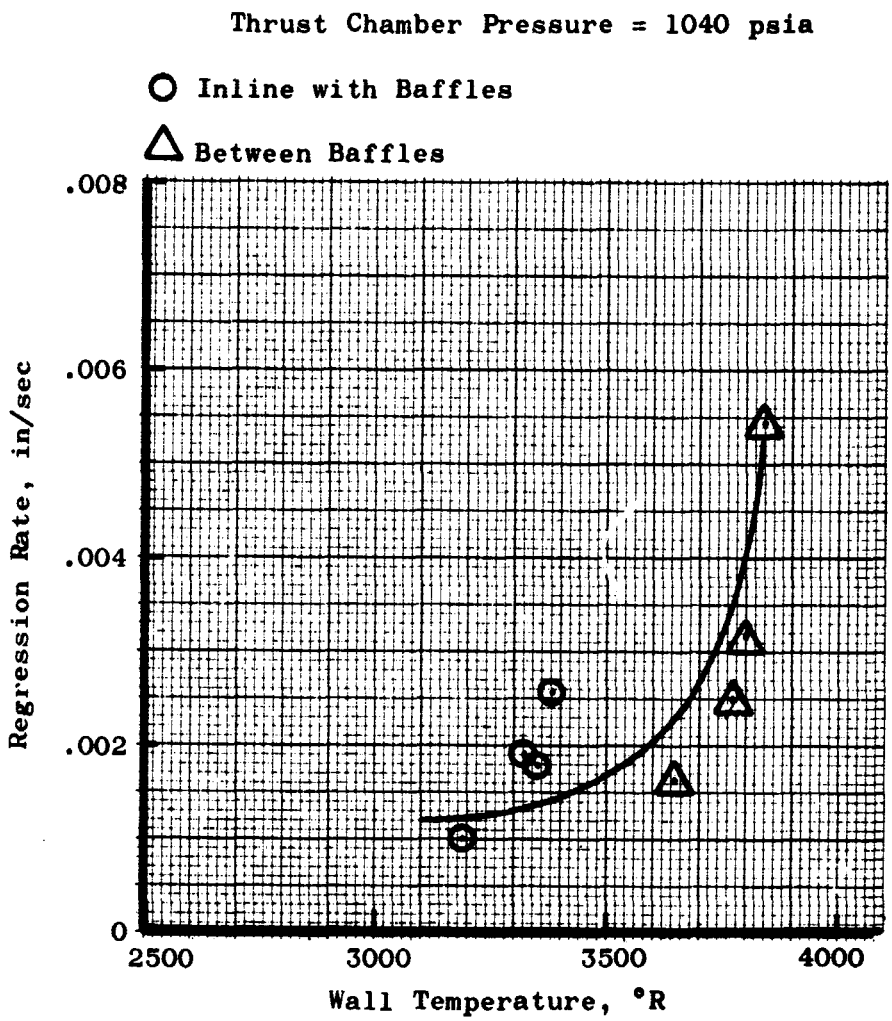

Figure 27. Regression Rate at the Throat vs Wall Temperature (Thrust Chamber Pressure = 1040 psia)

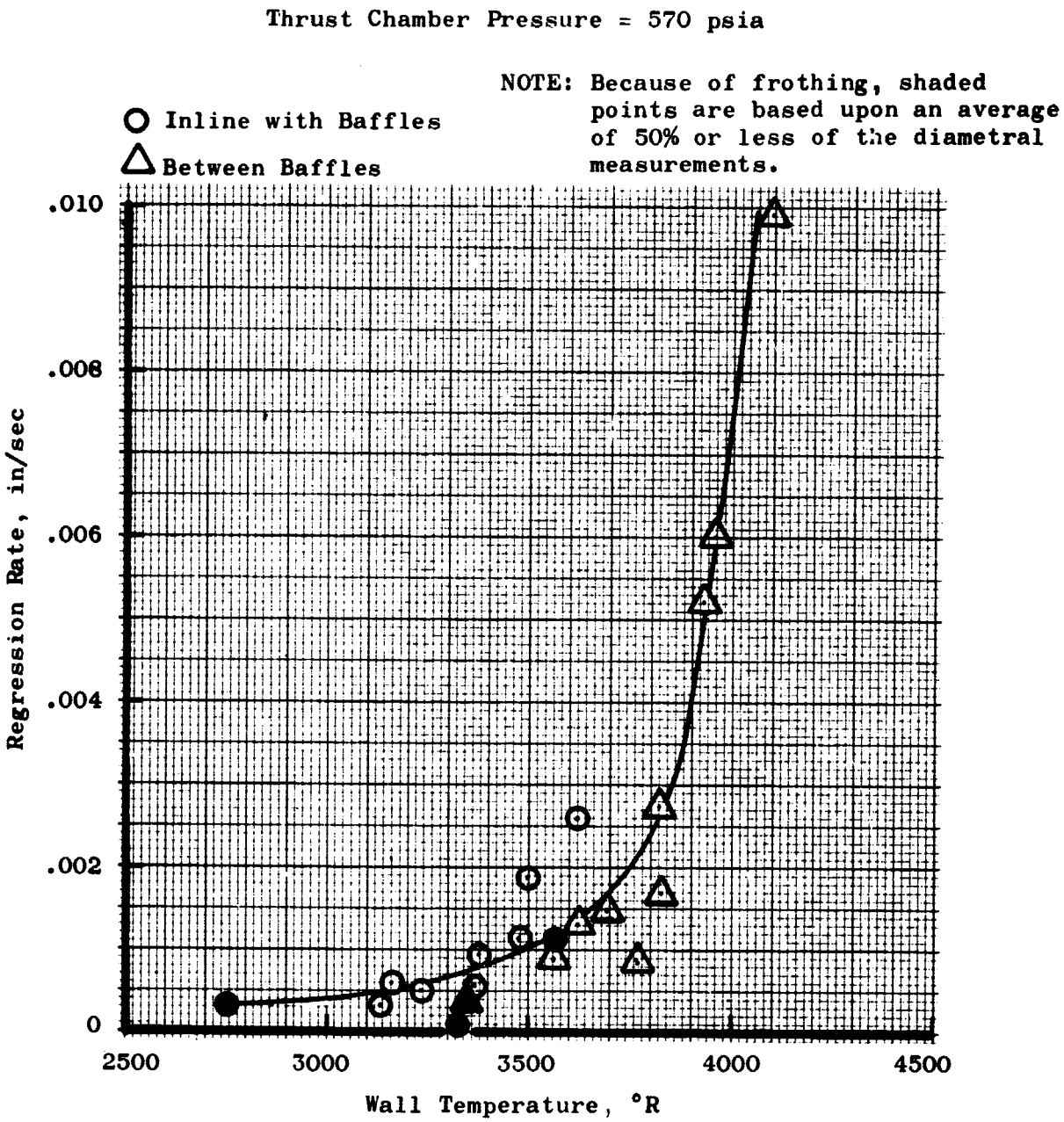

Figure 28. Regression Rate at the Throat vs Wall Temperature (Thrust Chamber Pressure = 570 psia)

in the regression rate remains essentially constant below 3600°R. Above a temperature of 3600°R, the regression rate increases exponentially. This exponential increase would cease after the temperature corresponding to the stoichiometric mixture ratio was reached. The high regression at higher pressure is probably attributable to the increased shear forces and the higher heat flux caused by the increased heat transfer coefficient. This suggests that the heat transfer coefficient or heat flux also could be a reasonable correlating parameter.

Based upon Figures No. 27 and No. 28, the throat regression rates can be limited to approximately 1.2 mils/sec and 0.5 mils/sec at thrust chamber pressures of 1040 psia and 570 psia, respectively, if the wall temperature does not exceed a value of approximately 3200°R.

Figures No. 29 and No. 30 present the regression data 8-in. downstream of the throat; nozzle area ratio is approximately equal to 1.5 at this point. As a result of the limited number of data points and data scatter at 1040 psia thrust chamber pressure, the curve shown on Figure No. 29 is based upon the trend shown at the throat. It can be noted from these figures that the regression rates for a given wall temperature are less than at the throat. This can be attributed to the fact that the heat flux at an area ratio of 1.5 is substantially reduced as a result of the reduced heat transfer coefficient. It also should be noted that a large amount of frothing occurred downstream of the throat and the curves shown are a best estimate of the trends.

Based upon these figures, the regression rates at an area ratio of 1.5 can be limited to approximately 1.2 mils/sec at 1040 psia chamber pressure and 0.5 mils/sec at 570 psia chamber pressure by maintaining the wall temperature at 3700°R or less.

Figures No. 31 and No. 32 present the regression data at the exit for 1040 psia and 570 psia thrust chamber pressures, respectively. The nozzle area ratio at the exit is approximately equal to 2.0. Frothing again significantly affected the majority of the data points and hence, the curves only serve to illustrate trends. Regression rates are substantially less than those experienced at the throat because of the reduced heat flux. Within the accuracy limits of the data, the regression rates at an area ratio of 2.0 are approximately the same as those at an area ratio of 1.5 for a wall temperature below 3900°R. Above a 3900°R temperature, the regression rates at the exit are less than those at an area ratio of 1.5. These figures indicate that the regression rates at the exit for both chamber pressures can be limited to 0.5 mils/sec if the wall temperature does not exceed 3900°R.

The regression data upstream of the throat is presented on Figures No. 33 through No. 36. Figures No. 33 and No. 34 show the regression rates 14-in. from the injector face. Because a substantial amount of the fuel film coolant is still not mixed with the main stream at this location, the boundary layer mixture ratios and hence, wall temperatures, are low. Therefore, the regression rates also are much lower than those experienced at the throat.

Note: Because of frothing, shaded points are based upon an average of 50% or less of the diametral measurements.

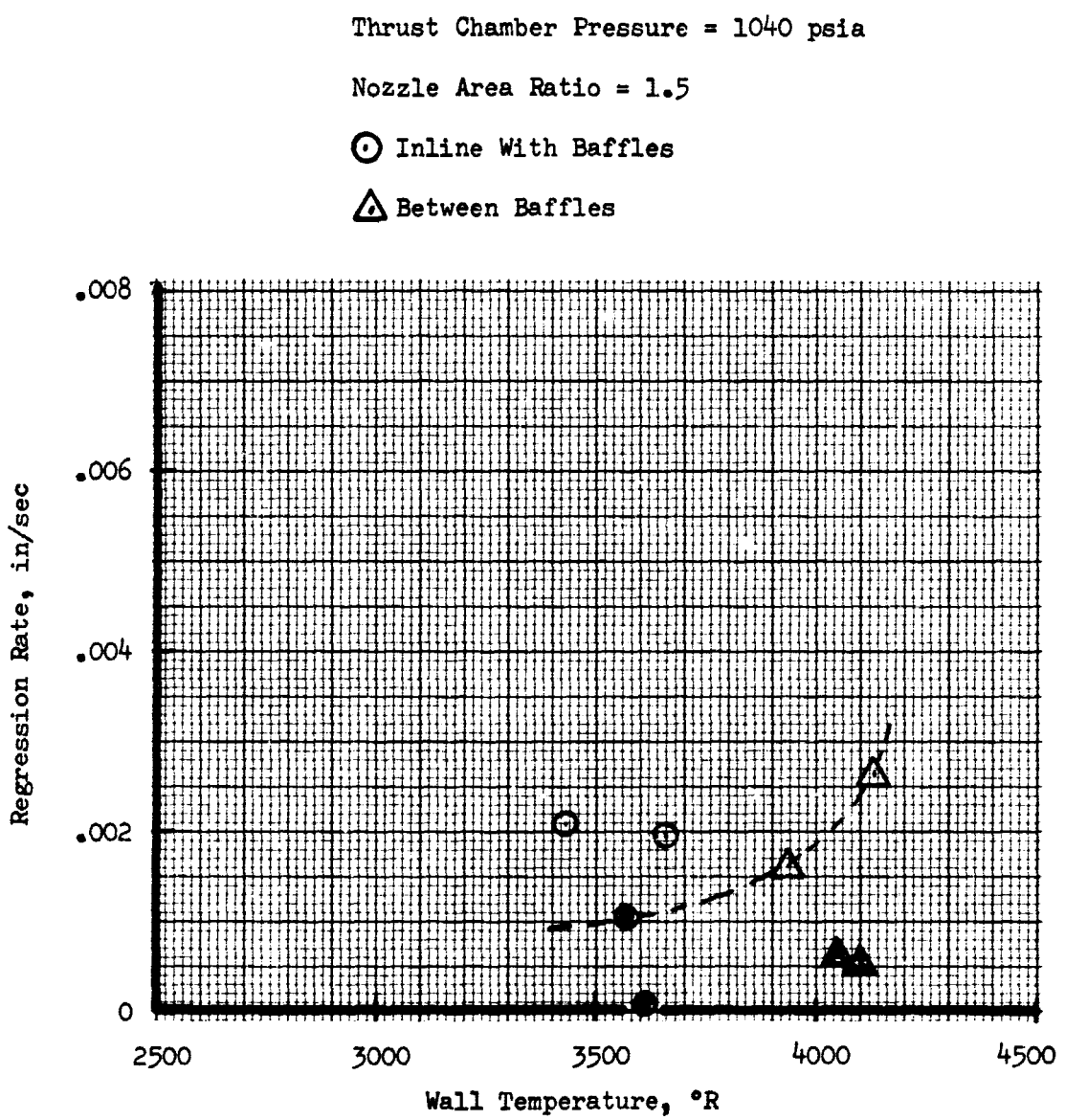

Figure 29. Regression Rate 8-in. Downstream of the Throat vs Wall Temperature (Thrust Chamber Pressure = 1040 psia)

Note: Because of frothing, shaded points are based upon an average of 50% or less of the diametral measurements.

Thrust Chamber Pressure = 570 psia

Nozzle Area Ratio = 1.5

⊙ Inline With Baffles

△ Between Baffles

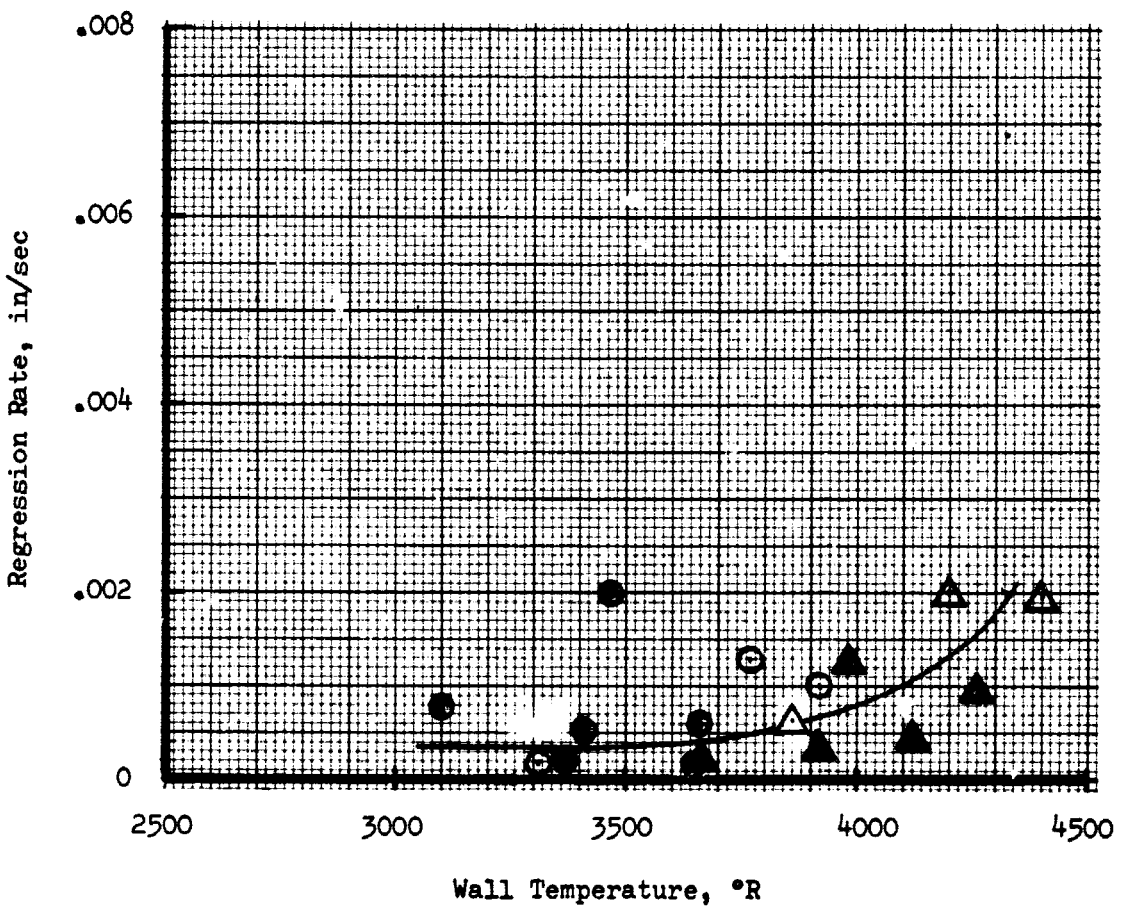

Figure 30. Regression Rate 8-in. Downstream of the Throat vs Wall Temperature (Thrust Chamber Pressure = 570 psia)

Note: Because of frothing, shaded points are based upon an average of 50% or less of the diametral measurements.

Thrust Chamber Pressure = 1040 psia

Nozzle Area Ratio = 2.0

⊙ Inline With Baffles

△ Between Baffles

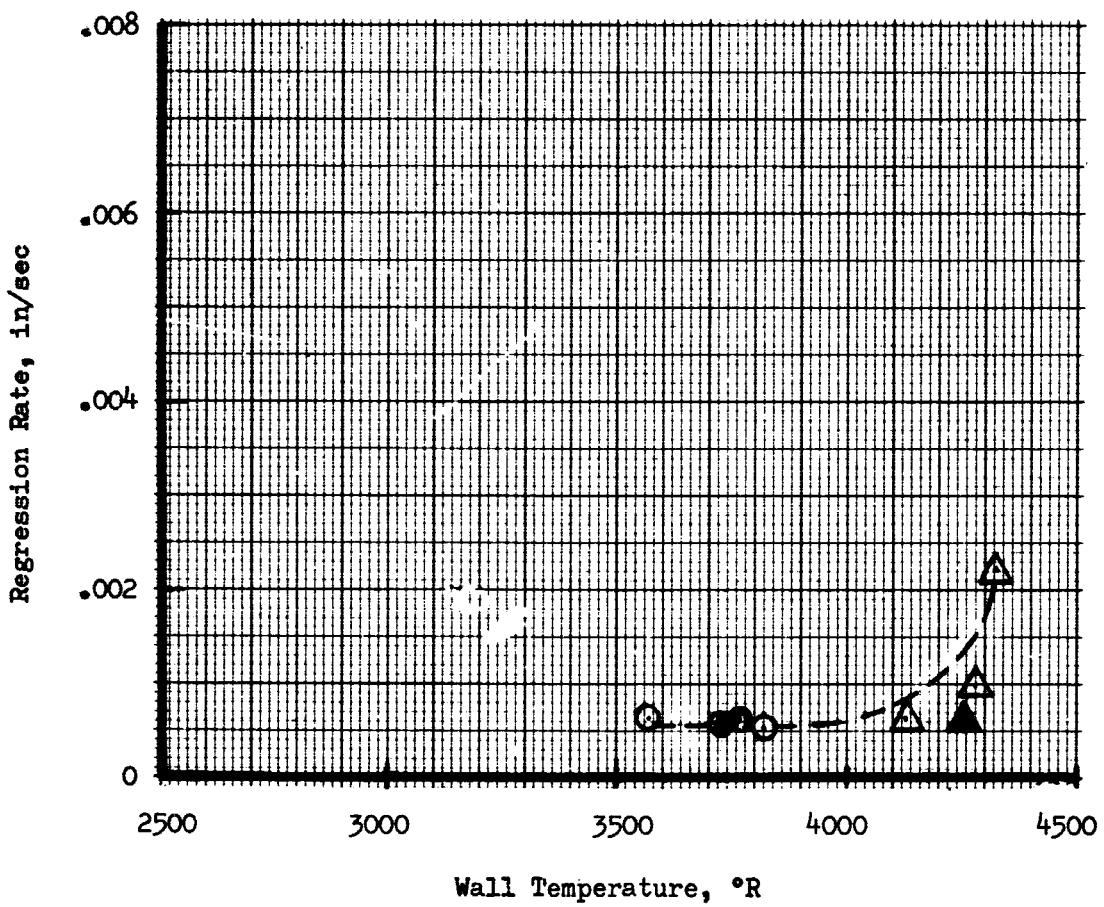

Figure 31. Regression Rate 1/4-in. from the Exit vs Wall Temperature (Thrust Chamber Pressure = 1040 psia)

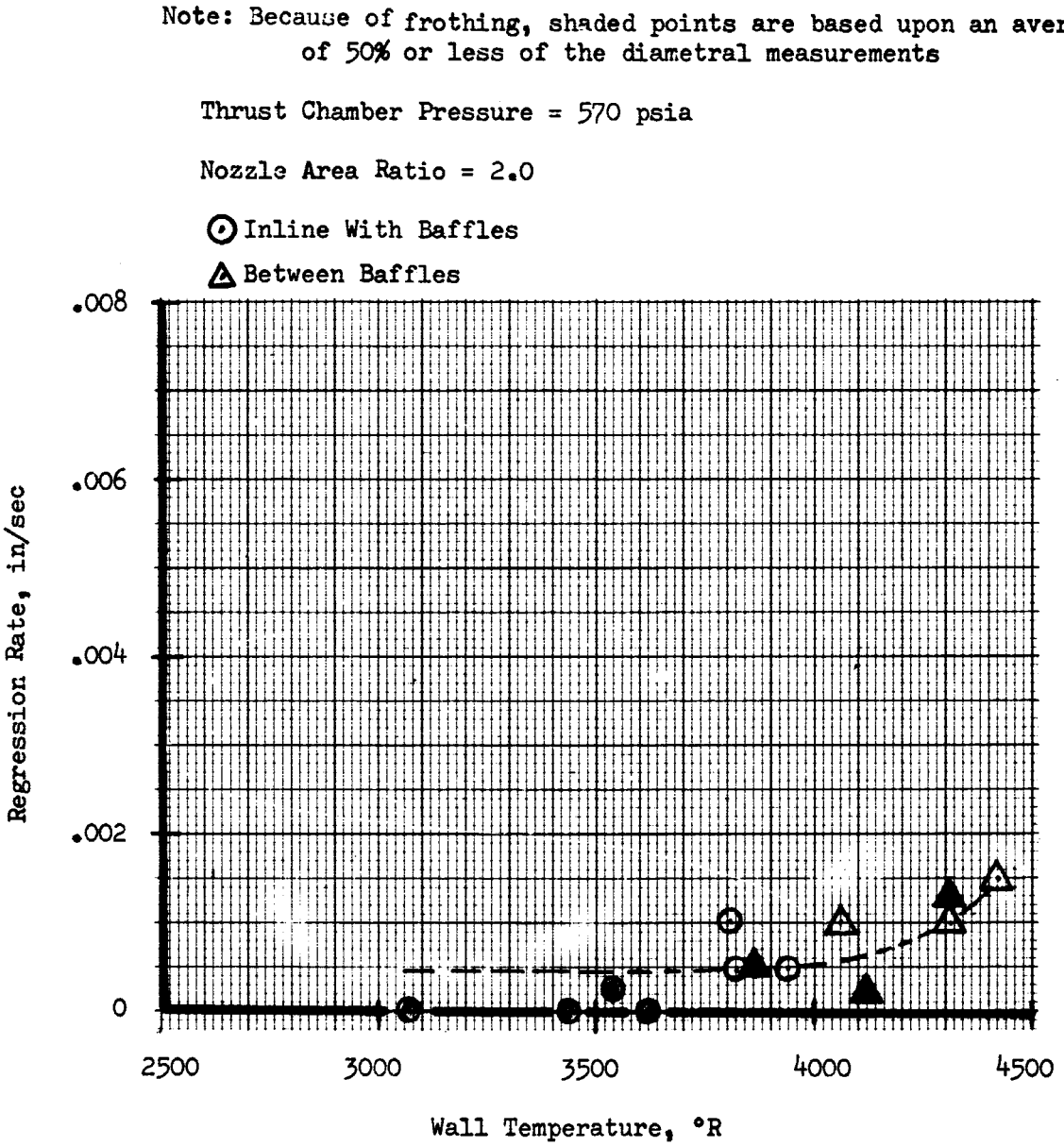

Figure 32. Regression Rate 1/4-in. from the Exit vs Wall Temperature (Thrust Chamber Pressure = 570 psia)

Note: Because of frothing, shaded points are based upon an average of 50% or less of the diametral measurements.

Thrust Chamber Pressure = 1040 psia

⊙ Inline With Baffles

△ Between Baffles

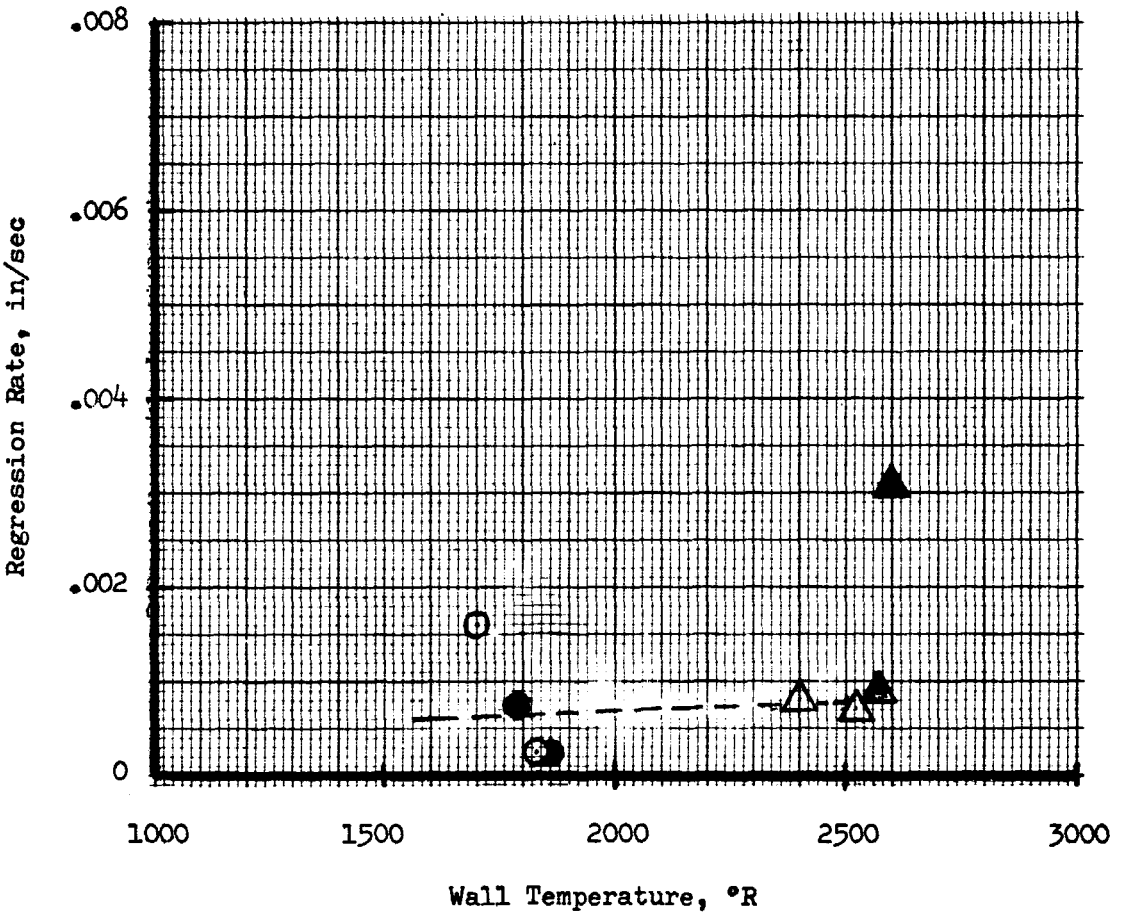

Figure 33. Regression Rate 14-in. from the Injector Face vs Wall Temperature (Thrust Chamber Pressure = 1040 psia)

Note: Because of frothing, shaded points are based upon an average of 50% or less of the diametral measurements.

Thrust Chamber Pressure = 570 psia

⊙ Inline With Baffles

△ Between Baffles

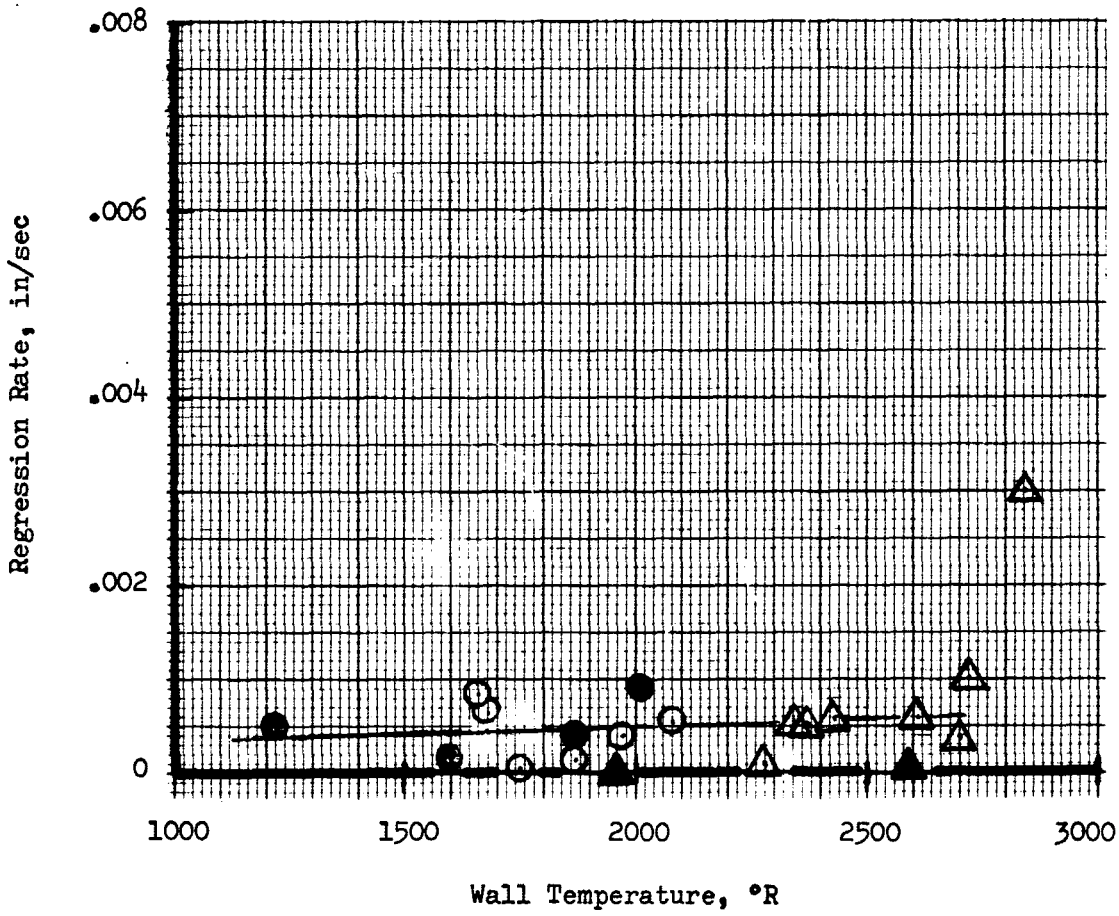

Figure 34. Regression Rate 14-in. from the Injector Face vs Wall Temperature (Thrust Chamber Pressure = 570 psia)

Note: Because of frothing, shaded points are based upon an average of 50% or less of the diametral measurements.

Thrust Chamber Pressure = 1040 psia

⊙ Inline With Baffles

△ Between Baffles

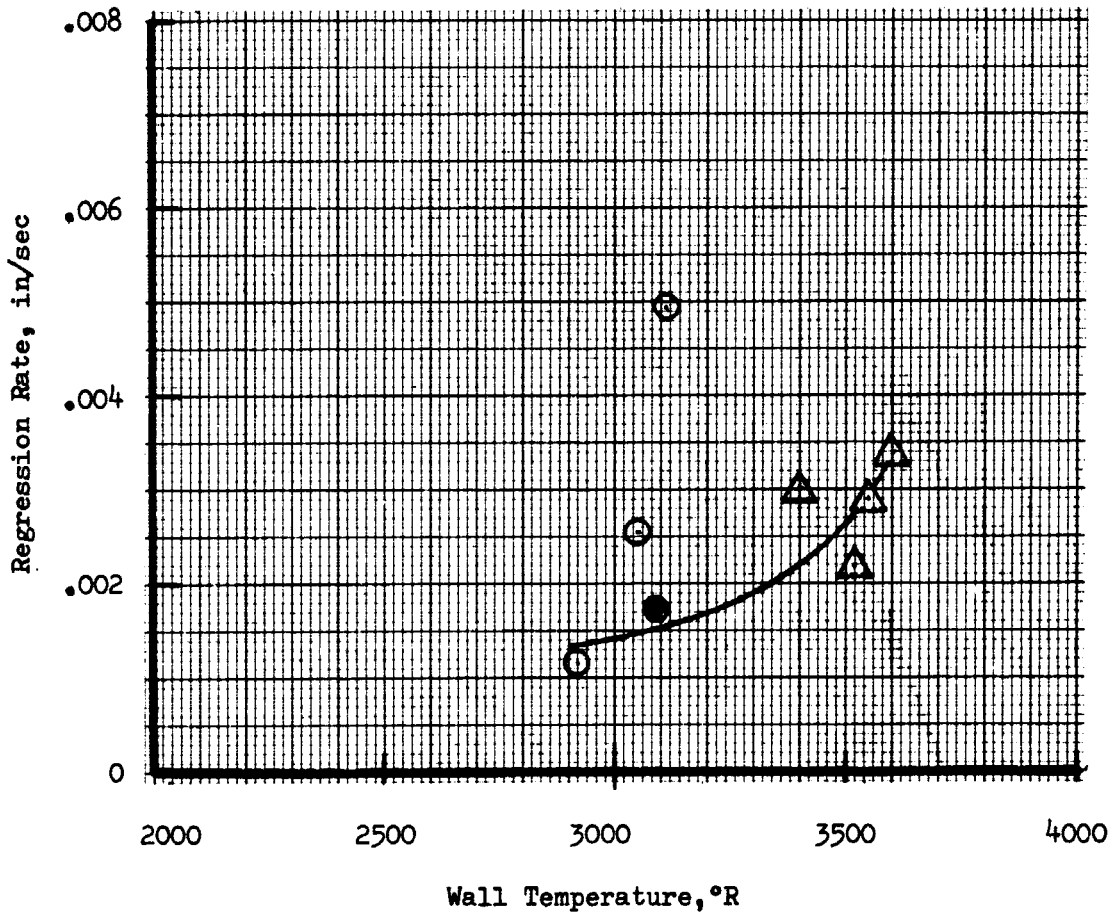

Figure 35. Regression Rate 25-in. from the Injector Face vs Wall Temperature (Thrust Chamber Pressure= 1040 psia)

NOTE: Because of frothing, shaded points are based upon an average of 50% or less of the diametral measurements.

Thrust Chamber Pressure = 570 psia

○ Inline with Baffles

△ Between Baffles

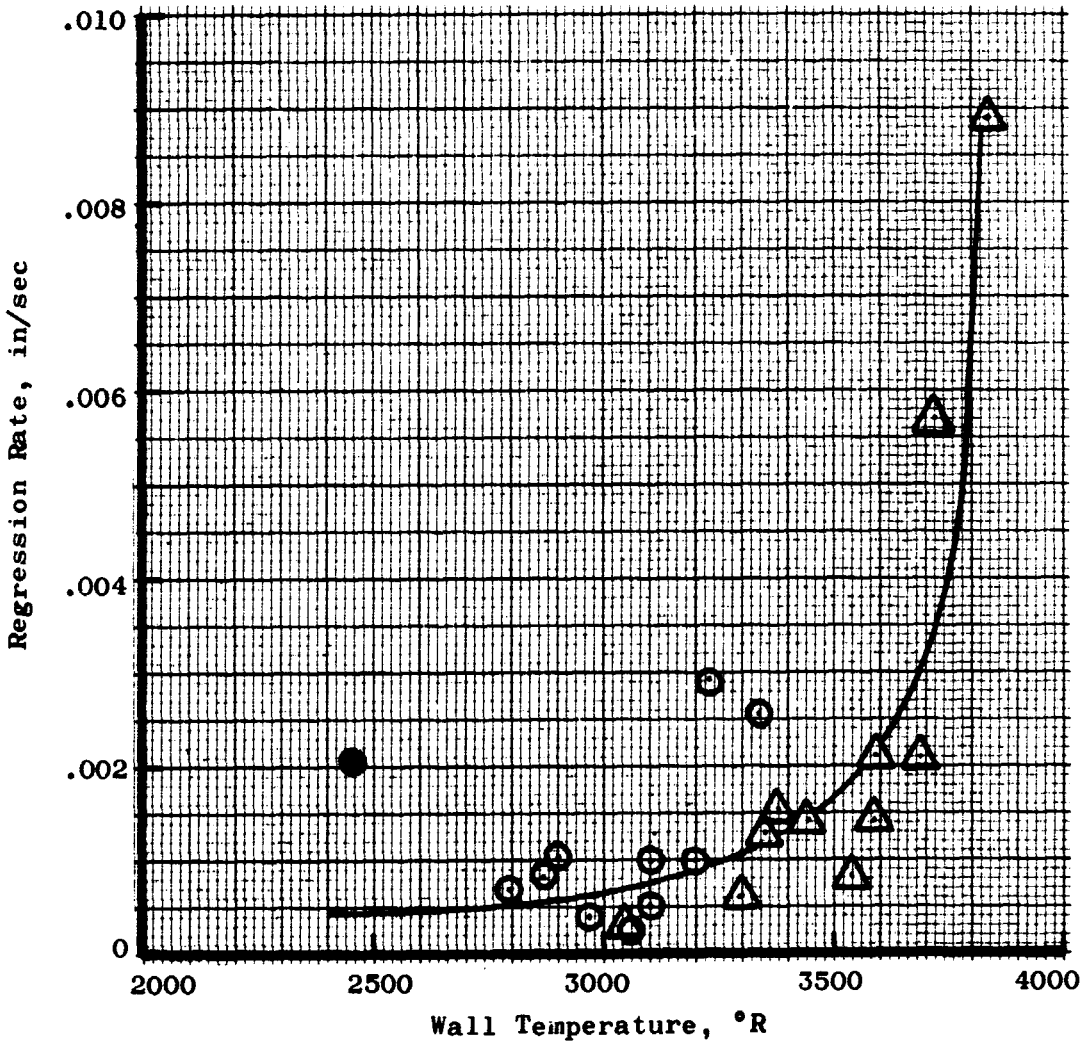

Figure 36. Regression Rate 25-in. from the Injector Face vs Wall Temperature (Thrust Chamber Pressure = 570 psia)

Valid data at 1040 psia thrust chamber pressure is very limited and hence the line shown on Figure No. 33 is a best estimate based upon a comparison with the 570 psia thrust chamber data. Frothing also significantly affects the data at this location. The one data point at a regression rate of 3 mil/sec on Figure No. 34 which appears to be inconsistent with the rest was obtained during test 008 which was conducted at a high mixture ratio (5.96). Regression occurred at all locations between baffles for this test and the data is apparently valid. However, because data at higher mixture ratios and hence, wall temperatures, was not obtained, the trend shown by this one data point cannot be justified.

Figures No. 35 and No. 36 present the regression data 25-in. from the injector face. The regression rates at this location are similar to those at the throat which is located 30-in. from the injector face. However, the regression rates for any particular wall temperature appear to be slightly higher at this location than at the throat.

2. Char Depth Analysis

The char depth measurements taken after each test and the locations of these measurements are shown on Table III. Three of the measurements were taken between baffles and one measurement was taken in-line with a baffle. Examination of the data shows that at all locations and for almost all tests, there is either very little difference between the char depth in-line and between baffles or the char depth is slightly higher in-line with baffles than between. Larger in-line char depths are expected because the regressions are less. The effect of the baffle location, as well as the over-all thrust chamber mixture ratio upon the char depth has been analyzed in greater detail at the throat.

Table IX summarizes the test parameters and the char depth data at the throat. The char depths between baffles shown on this table are an average of the three measurements taken. The char data points are plotted as a function of the accumulated test duration on Figures No. 37 and No. 38 for 1040 psia and 570 psia thrust chamber pressures, respectively. These figures show the tendency toward slightly higher char depths in-line than between the baffles. Because of an erosion streak, one point on Figure No. 37 in-line with the baffles shows a low char depth. The figures also show that the char depth reaches an essentially constant value and increases in the accumulated duration do not affect the char depth. This equilibrium char depth is approximately 0.2-in. and 0.35-in. for 1040 psia and 570 psia thrust chamber pressures, respectively. Char depth decreases with increasing thrust chamber pressure because the regression increases. Figure No. 38 also seems to indicate that the over-all thrust chamber mixture ratio has very little or no effect upon the char depth after reaching an equilibrium value, although greater char depths are expected at low mixture ratio because the regression is less. Therefore, the char depth data at the throat has been plotted as a function of over-all thrust chamber mixture ratio on Figures No. 39 and No. 40.

TABLE IX

CHAR EVALUATION AT THE THROAT

LINER NO.	TEST NO.	THRUST CHAMBER PRESSURE, PSIA	OVER-ALL THRUST CHAMBER MIXTURE RATIO	TEST DURATION ABOVE 90% Pc, SEC	CHAR DEPTH INLINE WITH BAFFLES,	AVERAGE CHAR DEPTH BETWEEN BAFFLES, IN.	ACCUM. TIME ABOVE 90% Pc, SEC.
001	001	1040	5.35	13.81	.13	.14	67.43(1)
	002		5.37	17.36	.19	.207	84.79
	003		5.11	19.61	.20	.193	104.40
	004		5.45	19.74	.12(2)	.213	124.14
	005		5.52	19.77	.24	.20	143.91
002B	006	570	5.40	20.64	.17	.183	20.64
	007		5.50	41.90	.29	.290	62.54
	008		5.96	27.60	.29	.133	90.14
	009		5.70	42.04	.33	.25	132.18
	010		4.20	44.24	.36	.317	176.42
	011		5.07	44.08	.33	.337	220.50
	012		5.00	44.12	.34	.343	264.62
002C	014		5.75	44.20	.28	.25	44.20
	016		5.51	42.15	.33	.197	86.35
	017		4.89	43.66	.27	.247	130.01
	018		4.90	35.25	.33	.343	165.26
	019		5.20	41.56	.36	.337	206.82

(1) 53.62 SECS ACCUMULATED UNDER PREVIOUS CONTRACT NAS 3-2555.
(2) AREA OF EROSION STREAK

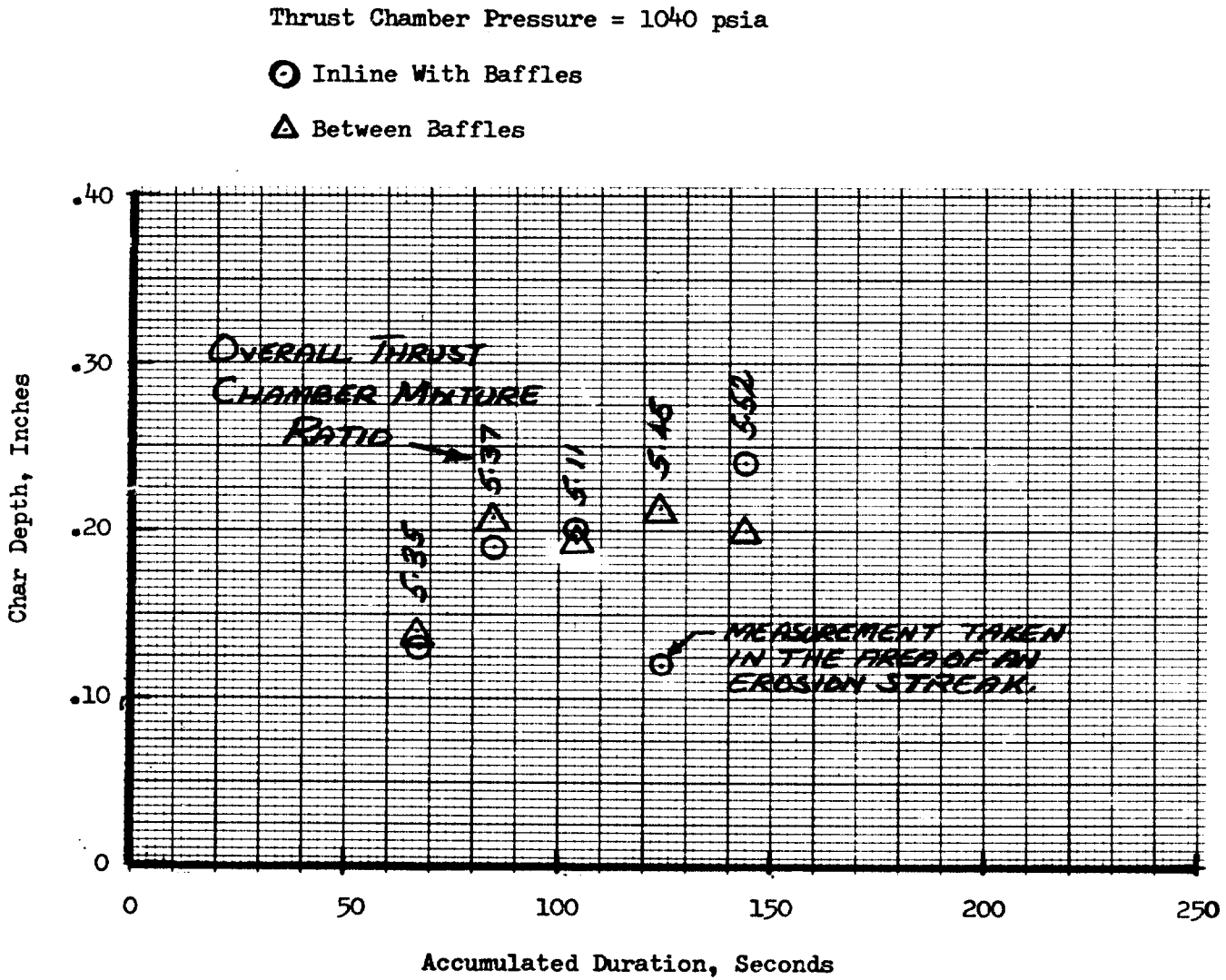

Figure 37. Char Depth at the Throat vs Accumulated Duration (Thrust Chamber Pressure = 1040 psia)

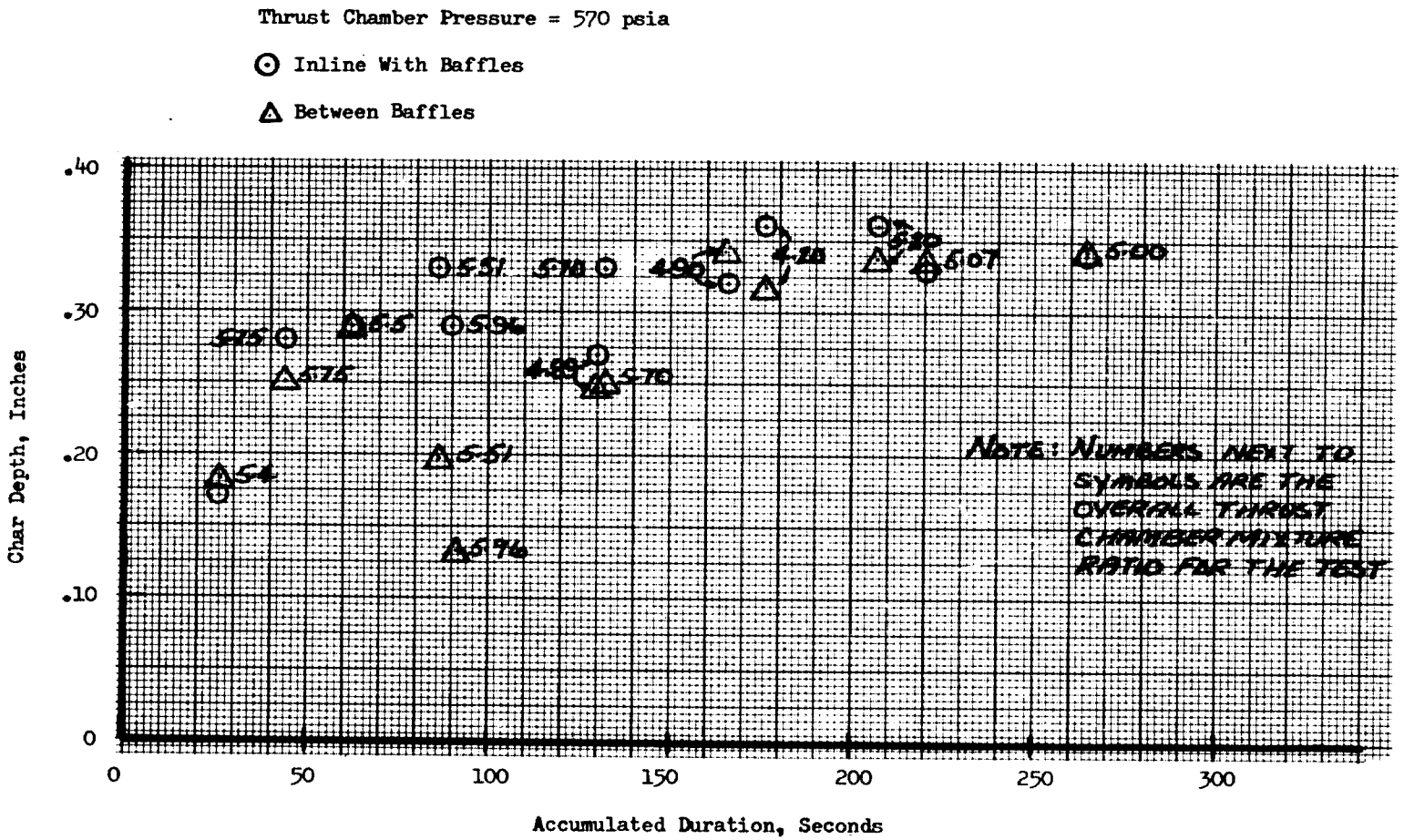

Figure 38. Char Depth at the Throat vs Accumulated Duration (Thrust Chamber Pressure = 570 psia)

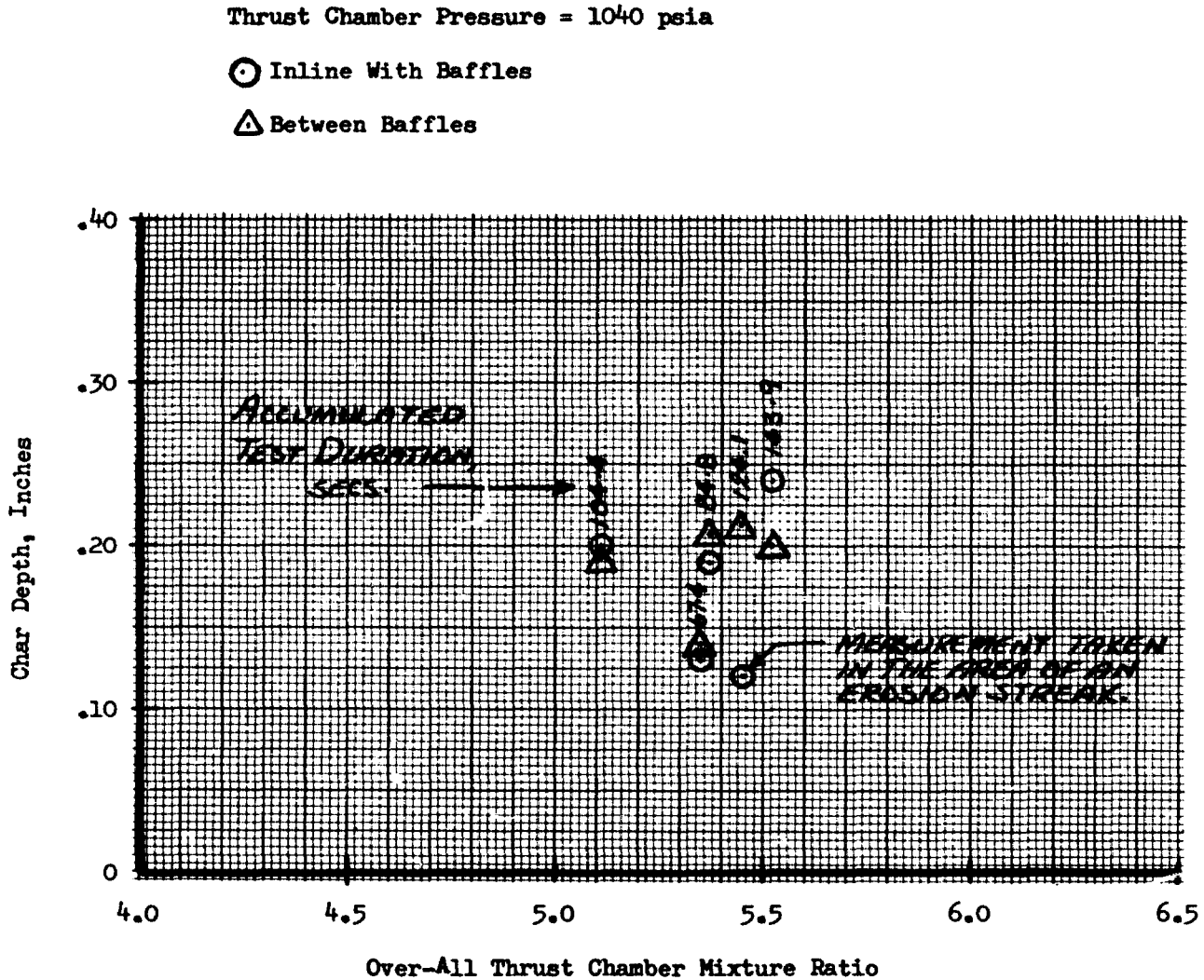

Figure 39. Char Depth at the Throat vs Over-all Thrust Chamber Mixture Ratio (Thrust Chamber Pressure = 1040 psia)

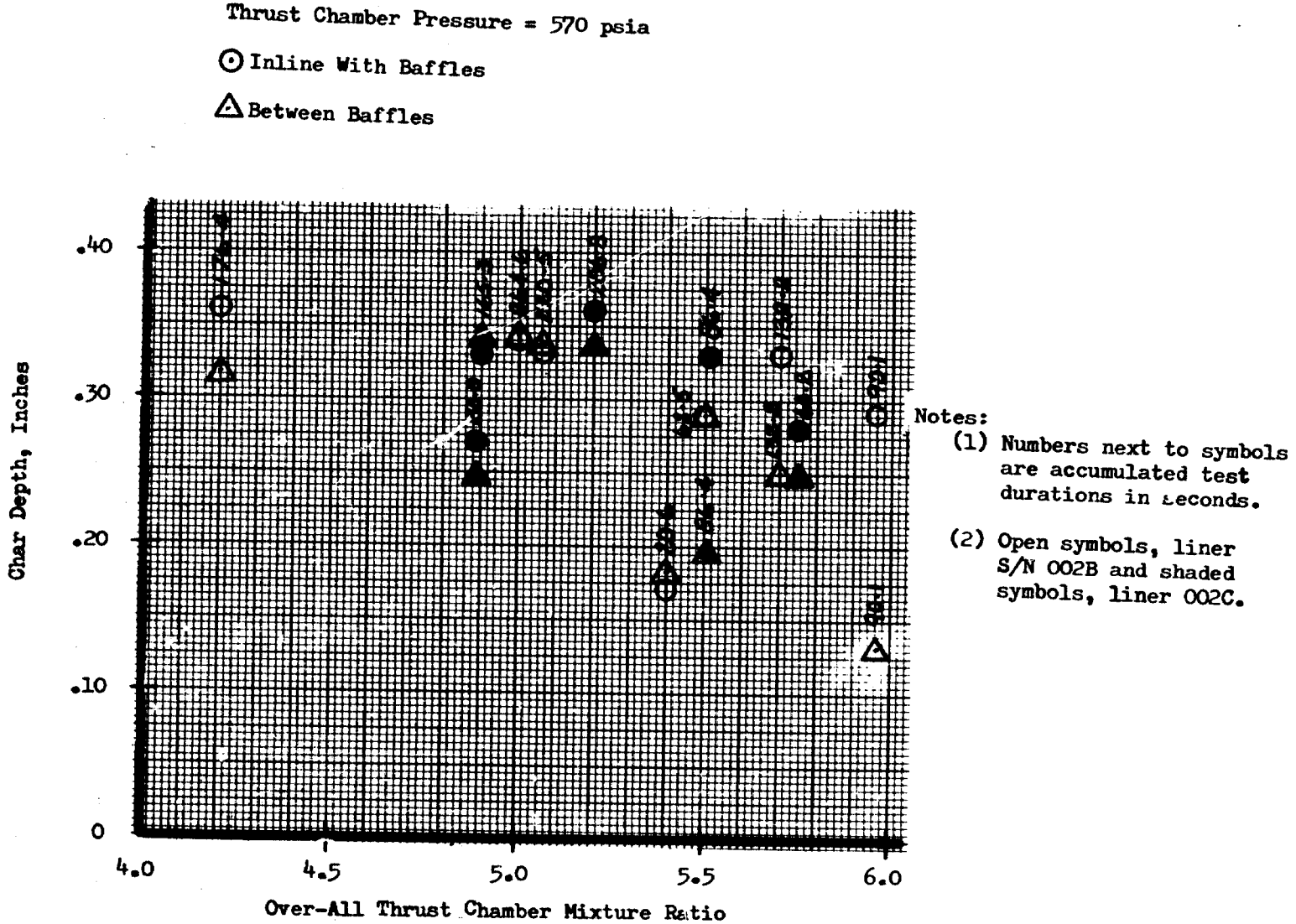

Figure 40. Char Depth at the Throat vs Over-all Thrust Chamber Mixture Ratio (Thrust Chamber Pressure = 570 psia)

Because of the small number of data points over a narrow mixture ratio range at 1040 psia thrust chamber pressure, the char depth appears to remain essentially constant after accumulating over 80 sec test duration as shown on Figure No. 39.

Figure No. 40 for 570 psia thrust chamber pressure shows that there is an increase in char depth with decreasing mixture ratio after the liner has accumulated 80 sec to 90 sec of test duration. This increase in char depth in-line with baffles was approximately 0.05-in. and 0.18-in. between baffles for liner S/N 002B over a mixture ratio range of 4.2 to 5.96. For liner S/N 002C, the char depth increases were approximately 0.02-in. in-line with baffles and 0.14-in. between baffles over a mixture ratio range of 4.89 to 5.51.

Because of the large amount of data scatter, the data at all locations are summarized on Figure No. 41 without distinction in respect to the location of the baffles or the over-all mixture ratios. The bands shown on the figure represent the maximum and minimum values experienced for the two thrust chamber pressures as a function of the distance from the injector face. For high mixture ratios and thrust chamber pressures, low char depths and high regressions can be expected.

B. APPLICATIONS OF THE DATA

Based upon the figures presented in the previous section of this appendix, ablative liner thickness requirements for oxygen/hydrogen engines in a 400K to 1 million lb thrust class can be determined. Because regression in the throat region is the most critical, it is desirable to design the engine for a minimal throat regression rate. This means that the film cooling requirements and hence, the boundary layer conditions in the rest of the chamber and nozzle are dictated by the throat requirements. For example, if a throat regression rate of 0.5 mils/sec at a thrust chamber pressure of 570 psia is not to be exceeded, Figure No. 28 shows that the wall temperature of 3200°R or less must be maintained. Therefore, the injector must be designed to supply sufficient fuel film cooling to achieve this wall temperature value. Figure No. 26 shows that this wall temperature of 3200°R corresponds to a boundary layer mixture ratio at the throat of 1.96. To determine the film coolant requirements, plots of boundary layer mixture ratio as a function of the over-all thrust chamber mixture ratio with variations in the fuel film coolant percentage are required. This can be accomplished through the use of analytical techniques similar to those described in Appendix E. With the film cooling requirement at the throat established, the boundary layer mixture ratios and hence, wall temperatures then must be determined for the chamber and nozzle. Chamber and nozzle regression rates can be determined for the resulting wall temperatures from Figures No. 29 through No. 36.

Assuming a 0.5 mil/sec throat regression rate, 570 psia thrust chamber pressure and a 200 sec engine duration as design criteria, the ablative liner will regress 0.1-in. From Figure No. 41, a char depth of 0.25-in. to

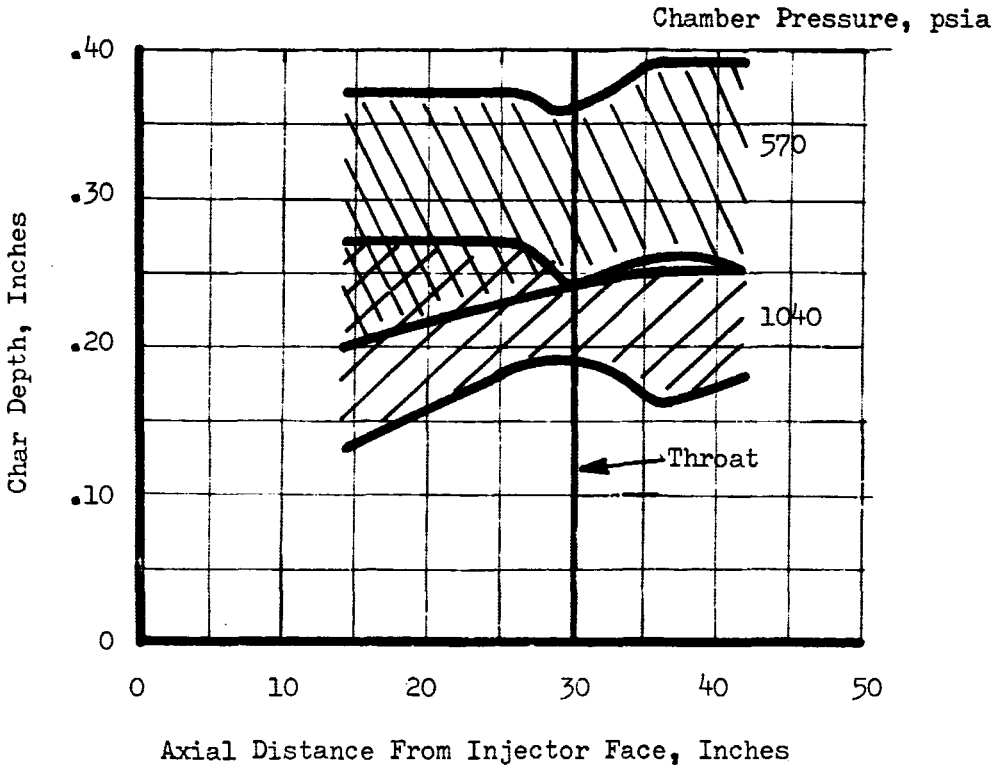

Figure 41. Char Depth vs Axial Distance for the Injector Face

0.36-in. can be expected at the throat. Using the more conservative char depth value, a total degradation of 0.46-in. can, therefore, be expected for this particular set of design conditions. Some margin of safety, approximately 0.25-in., should be allowed. Therefore, the total required ablative liner thickness at the throat is approximately 0.75-in.

For engine designs at other thrust chamber pressures and thrust levels with different throat sizes than the hardware tested under this program, the allowable wall temperature must be estimated by considering the total heat transfer problem. Because the heat flux is a product of the heat transfer coefficient and temperature difference across the wall, the contribution of the heat transfer coefficient as a driving force in addition to the wall temperature must be considered. The heat transfer coefficient is directly proportional to the eight-tenths power of the static density and hence, thrust chamber pressure and inversely proportional to the two-tenths power of the diameter. Therefore, it is obvious that for engines at higher thrust chamber pressures and/or smaller throat sizes, the heat transfer coefficient increases and the allowable wall temperature would be reduced.

Figure No. 42 shows that the data at the throat for the two thrust chamber pressures correlates very well using the eight-tenths power of density parameter. A single curve reasonably fits all the data points at the two pressures and a comparison of this figure with Figures No. 27 and No. 28 show that this curve goes through the same data points. Therefore, the correlating parameter would appear to be practical. The diameter factor also has been included to assist in scaling; however, because all of the hardware used in this program had the same throat size, data for other throat sizes is required to verify the use of this parameter. The heat transfer coefficient also is proportional to velocity to the eight-tenths power. Therefore, including this term in the correlating parameters can be a way of scaling the data obtained in this program to other area ratios.

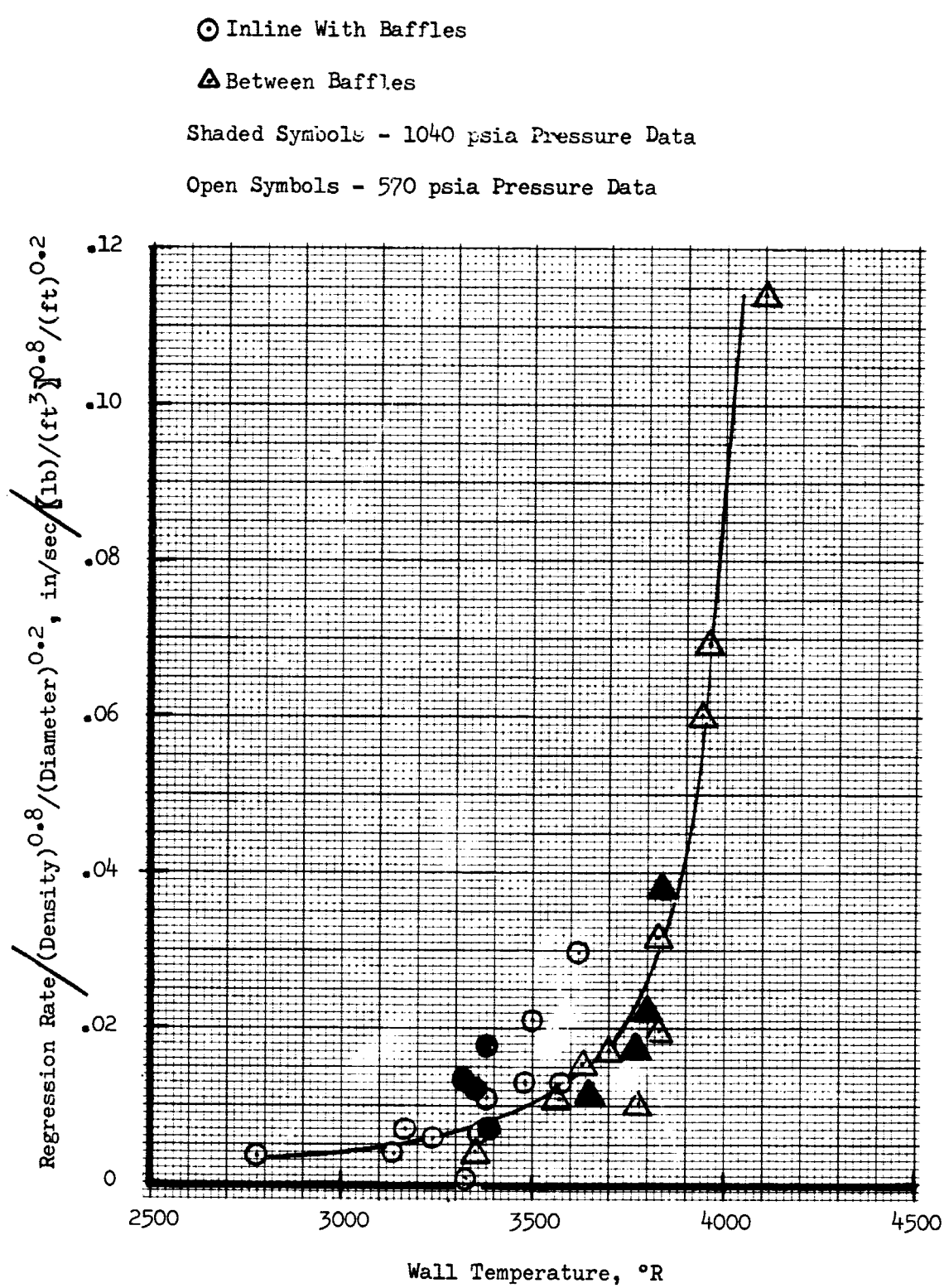

Figure 42. Ratio of Regression Rate at the Throat to Heat Flux Correlating Parameter vs Wall Temperature

APPENDIX B

LOW-COST ABLATIVE MATERIAL DATA

Appendix B

I. INTRODUCTION

The following four general groups of low-cost ablative materials were evaluated.

- Silica-Reinforced Phenolics
- Asbestos-Reinforced Phenolics
- Cellulose-Reinforced Phenolics
- Compounded Materials

Test specimens were bolted to the aft flange of the exit cone and subjected to exhaust gas flow at 570 psia chamber pressure. These specimens were exposed to the conditions and firing durations listed on Table X.

TABLE X

TEST FIRING PARAMETERS

Test Specimen No.	Test Run No.	Firing Duration (sec)	Chamber Pressure (psia)	Mixture Ratio
1 through 7	008(*)	30.052	430 to 530	4.5 to 7.5
1 through 7	009	44.814	553	5.8 to 5.4
8 through 14	011	47.227	550	5.07
13 and 14	012	47.226	550	5.00
15** through 23	014	47.4	544	5.75
24 through 27	016	45.6	567	5.51
24 through 27	017	46.9	566	4.89

NOTES: * Run No. 008 experienced test stand-induced flow oscillations

** Specimen No. 15 (40SA40 with asbestos honeycomb) was lost during Test Run No. 14.

The char depth and regression of each specimen was measured and recorded after each test firing. Average char and regression rates were calculated and are shown on Table XI. The conclusions and recommdnations resulting from this evaluation were presented in the main text.

TABLE XI

REGRESSION AND CHARRING RATES OF LOW-COST ABLATIVE MATERIALS

Spec. No.	Material Designation	Type Material	Material Supplier	Firing Duration sec	Regression Rate mils/sec	Rate of Charring mils/sec
1	4S5107	SiO_2/Phenolic(Thick C-100-96-SiO_2)	Coast	74.866	2.54	6.41
2	1BT 100	PBAN Epoxy Asbestos	AGC	74.866	5.27	7.62
3	4A6605	24 RPD (Cork Filled/Phenolic)	Coast	74.866	10.15	12.4
4	WB 2230	SiO_2/Phenolic	Western Backing	74.866	1.47	6.53
5	V61	Epoxy-Polysulfite Asbestos	General Tire	74.866	8.68	9.88
6	4A6305	20 RPD (SiO_2 Microballoons) /Phenolic	Coast	74.866	8.01	8.14
7	4A6005	Chrysotile Asbestos/ Phenolic	Coast	74.866	7.34	9.21
8	MXS 213	Silica/Phenolic	Fiberite	47.227	2.12	7.83
9	FM 5525	Crocidolite Asbestos/ Phenolic	U.S.P.	47.227	11.00	13.1
10	FM 5272	Kraft Paper/Phenolic	U.S.P.	47.227	10.8	11.6
11	MXA 6012	Crocidolite Asbestos/ Phenolic	Fiberite	47.227	11.6	12.7
12	KF 418	Canvas Duck/Phenolic	Fiberite	47.227	13.5	14.4
13	SP 8030-96	Thick C-100-96 SiO_2/ Phenolic	Armour	94.453	1.06	5.51
14	WB 2230	SiO_2/Phenolic	Western Backing	94.453	0.21	6.35

TABLE XI (cont.)

Spec. No.	Material Designation	Type Material	Material Supplier	Firing Duration sec	Regression Rate mils/sec	Rate of Charring mils/sec
15(*)	40SA40 Asbestos H.C.	Polyurethane/Asbestos Honeycomb	American Polytherm			
16	40SA40 Asbestos H.D.	Polyurethane/Asbestos Honeycomb	American Polytherm	47.4	6.76	8.44
17	IBT-100/SiO_2 Asbestos H.C.	Polybutadiene-Acrylonitrile with SiO_2 & Asbestos Honeycomb	AGC	47.4	0.00	4.64
18	Epotuf 2909	Epoxy Novolac/Silica (Vacuum Bag Grade)	AGC	47.4	1.26	4.85
19	C-100-48, F502	Silica/Phenolic (Vaccum Bag Grade)	USP	47.4	0.00	6.33
20	DEN 431-2910	Epoxy Novolac/Silica (Vacuum Bag Grade)	AGC	47.4	2.53	7.59
21	56,614-01	Trowelable Phenolic Reinforced with Asbestos Fibers	Haveg	47.4	5.90	6.32
22	56,614-01	Trowelable Phenolic Reinforced with Asbestos Fibers	Haveg	47.4	6.53	8.44
23	WB 2230	Silica Phenolic	Western Backing	47.4	0.00	4.22
24	C-100-48	Epoxy Novolac	Western Backing	92.5	-0.76	3.59
25	C-100-96	Silica Phenolic (Heavy Weight Silica Fabric)	Western Backing	92.5	0.00	2.81
26	UC-100-48	Silica Phenolic (Unstabilized Silica Fabric)	Western Backing	92.5	1.30	3.78
27	C-100-48 (WB 2230)	Silica/Phenolic (WB 2230)	Western Backing	92.5	0.00	4.22

(*) Specimen No. 15 was lost during Test Run No. 014

II. SILICA-REINFORCED PHENOLICS

The calculated regression rates of the silica-reinforced materials ranged from 0.21 mils/sec to 2.54 mils/sec. Differences in firing parameters, including location in relationship to the baffles, contributed to the seemingly large variation. The control material, WB 2230, exhibited a lower regression rate during both firing durations; however, the regression rate variance was very large (0.21 to 1.47). Identical conditions, including relative positions to the baffle locations, would have to be maintained to establish reliable data.

The MXS 213 demonstrated the feasibility of using lower density silica-reinforced phenolics and fiber tapes in place of fabric tapes. However, the regression rate and char rate were higher for the MXS 213 than for the fabric-reinforced phenolics. The char integrity was questionable because some of the char layer cracked off during firing. The MXS 213 might be unsuitable for multiple firing cycles because of the poor integrity of the char.

The specific gravity of the MXS 213 was 1.0 as compared to 1.70 for the standard silica-reinforced phenolic materials. Based upon the char depth measurements, the weight advantage gained would be approximately 50%. Calculations based upon one square inch of exposed surface coupled with the char results show that 0.044 lb would be required for the MXS 213 to provide the same protection as 0.061 lb of silica-reinforced phenolic. The cost per lb of the MXS 213 is higher than for the standard silica phenolic; however, the over-all cost would be lower because a lesser amount (lb) is required.

The 4S5107 exhibited the highest regression rate of the four silica-reinforced phenolics; however, the char rate was one of the lowest of the materials tested. Both of the double-thickness silica fabric materials had low char rates indicating lower conductivities could be obtained as well as lower fabrication cost for the SP 8030-96 and 4S5107.

The material cost of WB 2230 is $0.599 per cubic inch and it costs $1.44 per cubic inch to fabricate using parallel-to-centerline tape-wrap techniques. The SP 8030-96 cost $0.491 per cubic inch and $1.107 per cubic inch to fabricate. Assuming equivalent performance, the SP 8030-96 would be approximately 25% lower in cost.

III. ASBESTOS-REINFORCED PHENOLICS

The asbestos-reinforced phenolics did not perform as well as expected. Temperature and shear conditions at the 2:1 area ratio exceeded the capabilities of asbestos reinforcement. The fusion point of the asbestos (ranging from 2180°F to 2770°F) was exceeded so that melting and shearing of the melt occurred very readily. Asbestos could be expected to perform quite well at some higher ratio because silica performs well at this area ratio and its fusion temperature is 3100°F.

The area ratio at which asbestos performance would make it competitive with silica-phenolic in price would have to be established by higher nozzle area ratio testing. Standard chrysotile asbestos-reinforced phenolic cost $1.473 per cubic inch as fabricated compared to $1.743 for silica-reinforced phenolic. Therefore, asbestos char rates that exceed silica char rates by at least 20% are not competitive because of the lower regression rates of the silica-phenolic. This factor will change for very large components where the material cost is a higher percentage of the total cost.

IV. CELLULOSE-REINFORCED PHENOLICS

Two general types of cellulose-reinforced phenolics were evaluated. The KR 418 is a "canvas duck" reinforced system and the FM 5272 is a "Kraft paper" reinforced phenolic. Previous test results indicated that at area ratios higher than 4:1, the cellulose materials were equivalent to asbestos in regression rates and char depths.

Test results (see Table XI) show the regression to be higher than the silica-phenolics by an order of magnitude. Char rates were twice as high as the silica-phenolic materials. However, at higher area ratios, KF 418 and FM 5272 materials would be cost competitive with asbestos and/or silica because of their low char rate.

Both materials have very poor char integrity and tend to flake or spall very easily. This characteristic is not acceptable in a chamber which has a multiple stop-start duty cycle. However, the char thickness is less than 0.100-in.; therefore, loss of the char layer in an exit cone would not be detrimental to performance.

V. COMPOUNDED MATERIALS

Two compounded materials were tested. The IBT 100 is a PBAN epoxy system filled with asbestos. The V-61 is an asbestos filled epoxy-polysulfide NBR.

These materials were tested during runs -008 and -009. The majority of the material loss occurred in Test No. -008. Although the materials were present during Test No. -009, they were somewhat protected by the exit cone. Therefore, the regression and char rates shown on Table XI are not comparable with the control WB 2230.

The char contained cracks and appeared to have flaked-off in some areas. Regression was non-uniform. However, the potential of these materials to perform as ablatives without catastrophic failures was demonstrated. In less severe environmental conditions, materials of this type will be cost competitive.

This general class of materials also would be useful for refurbishing and/or short duration firings. The raw material can be applied to the existing hardware and cured in-place. Higher reinforcement contents and higher char

yielding resin could be expected to improve the resistance of the compounded materials to regression.

"Standard" silica-reinforced resins also were tested. These resins could be made from cut patterns or by hand lay-up, cured at low pressures (vacuum bag), and materials that can be troweled or cast.

Two other materials selected for evaluation were a heavy weight (thick) silica fabric, C-100-96, and an unstabilized silica fabric in a phenolic matrix, UC-100-48. The heavy weight silica reduces tape wrapping time by approximately one-half and the unstabilized silica is lower in price by approximately $1.00/lb. Two of the compounded materials, 40SA40 and IBT-100, were cast in asbestos honeycomb (cell size 1/2-in.) to reduce the cracking and flaking of the char. The 40SA40 is filled with silica, and the IBT-100 contains chopped silica-fiber-reinforcement. Another material that can be troweled is an asbestos-filled phenolic, designated 56, 614-01, which is supplied by Haveg. The compounded materials 40SA40 and 56,614-01 had high regression and low char depths. Regression rates of these materials exceeded the silica-reinforced resins by 3 mils/sec to 6 mils/sec. One compounded material, which contained a silica-reinforcement, had a regression rate of zero and a char depth resembling the "standard" silica phenolics. The silica reinforcement provided a dramatic improvement in performance over the asbestos-reinforced IBT-100. The char, which is usually swept away, was held intact by the asbestos honeycomb and the silica reinforcement did not melt sufficiently to be swept away.

The IBT-100 sample was covered with the fused silica from the exit liner material. The effect of the silica covering upon the ultimate performance of the material is not known; however, it is apparent that silica-filled IBT-100, a trowelable material, is a good candidate exit cone liner material.

All of the silica fabric-reinforced materials performed well. Two of the control samples, Specimen No. 23 and No. 27, had zero regression.

The unstabilized silica, DEN 431 and Epotuf 2909, had regression rates greater than 1 mil/sec. All but one of the silica fabric materials had regression rates less than 1 mil/sec. The silica fabric-reinforced epoxy novolac supplied by Western Backing Coproration had a negative regression rate. This is attributed to delaminations and to the characteristic high thermal expansion of the epoxy novolac resins.

All of the silica-reinforced systems are potential candidate materials for a low-cost exit cone with the exception of the UC-100-48/phenolic, which delaminated, and the DEN 431-2910, which had a regression rate of 2.53. However, the DEN 431 epoxy novolac resin has a low viscosity at room temperature and could be considered as a candidate for a resin injection fabrication process.

Both the F502/C-100-48 vacuum grade silica phenolic and the vacuum grade epoxy novolac are candidates for liner materials laid-up on a structural shell. They can be cured in a forced air oven or on-site using a heating

blanket or heat lamps. The silica-filled IBT-100 can be troweled or cast into a structural shell liner with asbestos honeycomb to the thickness required and cured in place.

The data is questionable for those materials with comparatively high regression rates because after the initial regression, the specimens were somewhat protected by the silica phenolic exit cone liner. Also, many specimens were coated with a layer of SiO_2 melt from the exit cone, which provided additional protection from the exhaust gases. Therefore, reported values should be considered minimum for both the char and regression of the materials tested.

One of the 40SA40/asbestos honeycomb specimens was lost during Test No. -014 and no data are reported for this specimen.

APPENDIX C

CORE SAMPLE COMPOSITION DATA

Appendix C

Table XII is a listing of the results from post-test char sample analyses for elemental and metallic content.

The char samples were taken from four locations; at the 25-in. axial station, in-line with Baffle No. 1, and from between Baffles No. 11 and No. 12, No. 12 and No. 1, and No. 1 and No. 2.

Analysis by means of x-ray diffraction revealed the presence of an amorphous substance indicating virgin material. A few of the samples showed traces of silicon carbide, apparently a composite of reinforcement and char.

The samples were analyzed for C, H, N, and O content utilizing Coleman Carbon-Hydrogen, Nitrogen, and Oxygen Analyzers. Measurement accuracy was within $\pm$ 0.3%. The resulting data show an increase in carbon content as mixture ratio increased. A higher carbon content also was evident in locations between the baffles as compared to those in-line with the baffles.

Emission spectrographic analysis showed the major metallic constituents to be SiO_2, Al_2O_3, and TiO_2 with traces of Zr, Ca, B, Mg, Cr, and Cu also being present. The measurement accuracy of this analysis method was $\pm$ 10%.

TABLE XII

SAMPLE ELEMENT AND METALLIC CONTENT DATA

			ELEMENTAL ANALYSIS				SPECTRAL EMISSION ANALYSIS		
Sample Location	Test No.	Liner S/N	%C	%H	%N	%O	SiO_2*	TiO_2*	Al_2O_3*
In-Line Baffle No. 1	002	001	6.60	0.54	0.18	0.77	95.0	-	0.4
	003		7.48	0.31	0	nil	90.0	0.2	0.6
	004		4.96	0.38	nil	0.29	95.0	0.3	0.3
	005		4.67	0.15	nil	0.31	95.0	0.8	0.3
	006	002B	9.12	0.37	0	0.45	85.0	0.7	0.4
	007		8.04	0.35	nil	0.48	90.0	0.6	0.5
	008		13.20	0.24	nil	0.44	84.0	1.5	0.4
	009		10.20	0.15	0.15	1.28	83.0	1.3	0.3
	010		6.54	0.50	nil	nil	88.0	1.0	0.8
	011		7.09	0.33	nil	nil	85.0	0.5	0.4
	012		10.00	0.22	nil	nil	85.0	0.5	0.4
	014	002C	8.75	0.35	nil	nil	85.0	0.5	0.7
Between Baffles No. 11 & 12	002	001	11.20	0.44	nil	nil	90.0	-	0.5
	003		6.72	nil	0	0	95.0	0.1	0.2
	004		11.50	nil	nil	0	80.0	0.1	0.2
	005		10.80	0.16	nil	0.25	93.0	0.9	0.5
	006	002B	13.90	0.12	0.31	0.21	80.0	0.4	0.6
	007		11.50	0.12	nil	0.30	85.0	0.5	0.4
	008		16.10	0.23	nil	0.60	84.0	1.8	0.4
	009		14.80	0.16	nil	0.31	83.0	1.5	0.3
	010		13.80	0.28	nil	nil	82.0	0.8	0.8
	011		14.80	0.11	0.12	0.14	82.0	0.5	0.4
	012		12.80	nil	0.12	0.30	80.0	0.4	0.3
	014	002C	16.50	0.16	nil	nil	80.0	0.6	0.6
Between Baffles No. 12 and 1	002	001	5.98	0.27	nil	nil	95.0	-	0.4
	003		10.80	nil	0	nil	90.0	0.2	0.2
	004		12.40	0.24	0	nil	85.0	0.2	0.2
	005		12.20	0.16	nil	0.37	90.0	0.6	0.3
	006	002B	17.20	0.25	0.14	0.70	75.0	0.4	0.4
	007		11.30	0.41	0	0.56	85.0	0.4	0.3
	008		14.50	0.27	0	0.35	85.0	1.8	0.4
	009		15.30	0.15	0.08	0.51	80.0	0.9	0.2
	010		14.00	0.14	nil	0.26	85.0	0.9	0.7
	011		13.40	0.26	nil	0.37	83.0	0.5	0.4
	012		11.50	0.23	0.15	0.66	85.0	0.5	0.5
	014	002C	16.30	0.27	nil	nil	78.0	0.3	0.5
Between Baffles No. 1 and 2	002	001	4.87	0.28	0.12	0.37	95.0	-	0.5
	003		8.98	0.27	0	nil	90.0	0.2	0.5
	004		7.56	0.22	nil	0	85.0	0.1	0.2
	005		12.80	0.18	nil	0.48	90.0	0.4	0.1
	006	002B	15.80	0.21	0.32	0.78	75.0	0.4	0.3
	007		11.90	0.21	0.20	0.42	85.0	0.5	0.4
	008		15.00	0.27	nil	0.47	85.0	1.7	0.4
	009		14.60	0.10	0.13	nil	80.0	1.2	0.4
	010		7.31	0.17	nil	0.30	87.0	1.6	1.0
	011		14.00	0.21	nil	nil	83.0	0.4	0.3
	012		13.20	nil	0.16	nil	85.0	0.4	0.4
	014	002C	10.70	0.50	0.27	0.70	83.0	0.6	0.9

*Quantitative percentages of the three major constituents only; SiO_2, TiO_2, and Al_2O_3

APPENDIX D

SECTIONED LINER DATA

Appendix D

The ablative liners were sectioned for appraisal of their condition. These sections were visually inspected and measured for degradation profile characteristics.

I. LINER S/N 001

The total duration accumulated with liner S/N 001 at the 1040 psia chamber pressure level was 144 sec. The chamber portion of the liner was longitudinally sectioned at the thickest and thinnest places for visual observation of the char profile (see Figure No. 43 for a comparison of the two sections).

II. LINER S/N 002B

The total duration experienced by S/N 002B liner was 265 sec.

Char-through of the liner occurred between baffles 8 and 9 at the throat chamber-liner to nozzle-liner joint.

Char depth measurements were taken at 2-in. intervals along the liner contour from 10-in. aft of the injector face to 13-in. aft of the throat on the three longitudinal sections shown on Figure No. 44. These sections were located aft of baffle No. 1 and between baffles 8 and 9 and baffles 12 and 1. The data for each section are listed on Table XIII.

The liners were also sectioned circumferentially at five axial stations; 14-in. and 25-in. aft of the injector face, throat, and 8-in. and 13-in. aft of the throat. See Figures No. 45 through No. 49, respectively, for comparative degradation profiles.

III. LINER S/N 002C

The total duration for liner S/N 002C was 250 sec. The nozzle liner was expelled at approximately 25 sec into the last test firing. Liner S/N 002C had charred completely through between baffles No. 8 and No. 9 extending longitudinally from 26-in. aft of the injector face to the throat. Char-through also occurred in the throat between baffles No. 3 and No. 4, baffles 12 and 1 and baffles No. 7 and No. 8. A circumferential crack 1 to 2-in. forward of the throat and running between baffles No. 5 and 8 and a similar crack between baffles No. 8 and No. 9 extending into the char-through area were noted.

Char depth measurements were taken on three circumferential sections; 14-in. aft of the injector flange (Figure No. 50), 25-in. aft of the injector flange (Figure No. 51), and at the chamber throat (Figure No. 52). The char penetration was measured at 5-degree intervals, clockwise, looking forward with 0-degrees at the No. 1 baffle. Data for the three sections are recorded on Table XIV, XV, and XVI.

TABLE XIII

CHAR DEPTHS MEASURED ON LONGITUDINAL SECTIONS OF ACT LINER S/N 002B

Distance Aft of Injector Face in.	Char Depth - inches		
	At Baffle No. 1	Between Baffles No. 8 and No. 9	Between Baffles No. 12 and No.1
10	.21	.27	.22
12	.21	.28	.25
14	.24	.35	.34
16	.23	.32	.34
18	.23	.31	.35
20	.27	.34	.32
22	.27	.33	.31
24	.29	.27	.29
26	.32	.28	.30
28	.30	.32	.27
30	.31	.29	.27
31	.32	.30	.26
Throat	.25	.35	.25
Distance Aft of Throat in.			
2	.33	.33	.26
4	.38	.34	.35
6	.33	.36	.32
8	.33	.37	.36
10	.29	.35	.37
12	.34	.41	.35
13	.31	.40	.46

TABLE XIV

LINER CHAR PROFILE OF S/N 002C CHAMBER CIRCUMFERENTIAL SECTION AT 14-IN. AFT OF INJECTOR

Baffle No.	Radial Location[1] Degrees	Total Thickness in.	Remainder Uncharred in.	Baffle No.	Radial Location Degrees	Total Thickness in.	Remainder Uncharred in.
1[2]	0	1.25	0.98	7	180	1.12	0.80
	5	1.25	0.98		185	1.20	1.01
	10	1.13	0.94		190	1.23	0.92
	15	1.25	0.94		195	1.07	0.68
	20	1.24	0.98		200	1.10	0.77
	25	1.24	0.99		205	1.20	0.88
2	30	1.24	0.98	8	210	1.15	0.70
	35	1.05	0.78		215	1.00	0.80
	40	1.24	0.92		220	1.20	0.90
	45	0.97	0.74		225[2]	1.15	0.85
	50	1.08	0.87		230	0.90	0.63
	55	1.20	0.87		235	1.12	0.87
3	60	1.24	0.91	9	240	1.25	0.97
	65	1.20	1.06		245	1.07	0.89
	70	1.12	0.91		250	1.26	0.98
	75	1.06	0.77		255	1.20	0.91
	80	1.17	0.88		260	1.28	0.96
	85	1.13	0.83		265	1.23	0.94
4	90	1.08	0.83	10	270	1.27	1.00
	95	1.09	0.90		275	1.27	1.00
	100	1.25	0.97		280	1.25	1.03
	105	1.00	0.85		285	1.23	0.87
	110	0.97	0.78		290	1.23	0.86
	115	1.07	0.85		295	1.23	0.87
5	120	1.26	1.03	11	300	1.24	0.90
	125	1.04	0.80		305	1.24	0.95
	130	0.94	0.75		307.5[2]	1.00	0.82
	135	1.17	0.87		310	1.06	0.83
	140	1.26	0.97		315	1.26	0.88
	145	1.26	0.95		320	1.25	0.88
6	150	1.27	0.93	12	330	0.96	0.72
	155	1.25	0.97		335	1.25	0.98
	160	1.27	1.00		390	1.03	0.83
	165	1.18	0.86		345[2]	1.24	0.89
	170	1.23	0.86		350	1.15	0.86
	175	1.20	0.90		355	1.05	0.75

(1) Measured clockwise looking forward
(2) Location of longitudinal section

TABLE XV

LINER CHAR PROFILE OF S/N 002C CHAMBER CIRCUMFERENTIAL SECTION AT 25-IN. AFT OF INJECTOR

Baffle No.	Radial Location[1] Degrees	Total Thickness in.	Remainder Uncharred in.	Baffle No.	Radial Location Degrees	Total Thickness in.	Remainder Uncharred in.
1[2]	0	1.43	1.12	7	180	0.91	0.63
	5	1.46	1.15		185	1.45	1.12
	10	1.34	1.07		190	1.17	0.88
	15	1.42	1.11		195	0.36	0.12
	20	1.20	0.95		200	0.92	0.48
	25	1.37	1.05		205	1.07	0.6[illegible]
2	30	1.44	1.08	8	210	1.15	0.79
	35	1.09	0.80		215	1.43	1.17
	40	1.12	0.85		220	1.12	0.81
	45	1.25	0.92		225[2]	1.27	0.91
	50	1.42	1.12		230	0.17	0.03
	55	1.10	0.76		235	0.92	0.51
3	60	1.30	0.91	9	240	1.25	0.88
	65	1.52	1.18		245	1.40	1.14
	70	1.40	1.12		250	1.35	1.07
	75	0.93	0.62		255	1.06	0.73
	80	1.00	0.67		260	1.20	0.91
	85	0.85	0.57		265	1.18	0.92
4	90	1.40	1.09	10	270	1.27	0.96
	95	1.35	1.11		275	1.32	0.94
	100	1.37	1.09		280	1.48	1.12
	105	1.18	0.87		285	1.13	0.77
	110	1.07	0.73		290	1.03	0.67
	115	1.37	1.00		295	0.97	0.61
5	120	1.48	1.17	11	300	0.95	0.56
	125	1.46	1.15		305	1.28	0.97
	130	1.25	0.92		307.5[2]	1.32	1.05
	135	1.17	0.85		310	1.27	0.93
	140	1.31	1.04		315	1.16	0.82
	145	1.22	0.85		320	1.08	0.71
6	150	1.23	0.87	12	330	1.00	0.71
	155	1.30	0.94		335	1.34	1.00
	160	1.43	1.07		340	1.06	0.82
	165	0.92	0.57		345[2]	1.34	1.00
	170	0.90	0.52		350	0.94	0.59
	175	1.09	0.73		355	0.76	0.51

(1) Measured clockwise looking forward
(2) Location of longitudinal section

TABLE XVI

LINER CHAR PROFILE OF S/N 002C CHAMBER CIRCUMFERENTIAL SECTION AT THROAT

Baffle No.	Radial Location[1] Degrees	Total Thickness in.	Remainder Uncharred in.	Baffle No.	Radial Location Degrees	Total Thickness in.	Remainder Uncharred in.
1[2]	0	1.46	1.09	7	180	1.00	0.72
	5	1.60	1.27		185	1.55	1.26
	10	1.54	1.25		190	1.23	0.89
	15	1.53	1.23		195	0.45	0.00
	20	1.38	1.07		200	0.72	0.00
	25	1.43	1.08		205	0.85	0.34
2	30	1.50	1.17	8	210	1.20	0.69
	35	1.37	1.08		215	1.67	1.29
	40	1.50	1.16		220	1.32	0.99
	45	1.34	1.01		225	1.13	0.82
	50	1.57	1.27		230[2]	0.28	0.00
	55	1.29	0.97		235	1.13	0.57
3	60	1.45	1.10	9	240	1.41	1.07
	65	1.75	1.44		245	1.59	1.28
	70	1.50	1.19		250	1.58	1.27
	75	1.02	0.00		255	1.20	0.87
	80	1.07	0.00		260	1.30	0.87
	85	0.94	0.00		265	1.29	0.99
4	90	1.28	0.00	10	270	1.37	1.02
	95	1.59	1.32		275	1.46	1.13
	100	1.59	1.30		280	1.63	1.30
	105	1.34	0.95		285	1.32	1.00
	110	1.08	0.78		290	1.24	0.84
	115	1.43	1.08		295	1.06	0.68
5	120	1.62	1.37	11	300	1.00	0.69
	125	1.62	1.35		305	1.47	1.18
	130	1.35	1.04		307.5[2]	1.51	1.23
	135	1.27	0.93		310	1.44	1.15
	140	1.50	1.18		315	1.32	0.95
	145	1.33	1.04		320	1.11	0.74
6	150	1.37	1.04	12	330	1.20	0.93
	155	1.46	1.16		335	1.43	1.14
	160	1.42	1.06		340	1.06	0.85
	165	0.92	0.37		345[2]	1.46	1.12
	170	1.04	0.58		350	1.05	0.00
	175	1.04	0.68		355	0.95	0.00

(1) Measured clockwise looking forward
(2) Location of longitudinal section

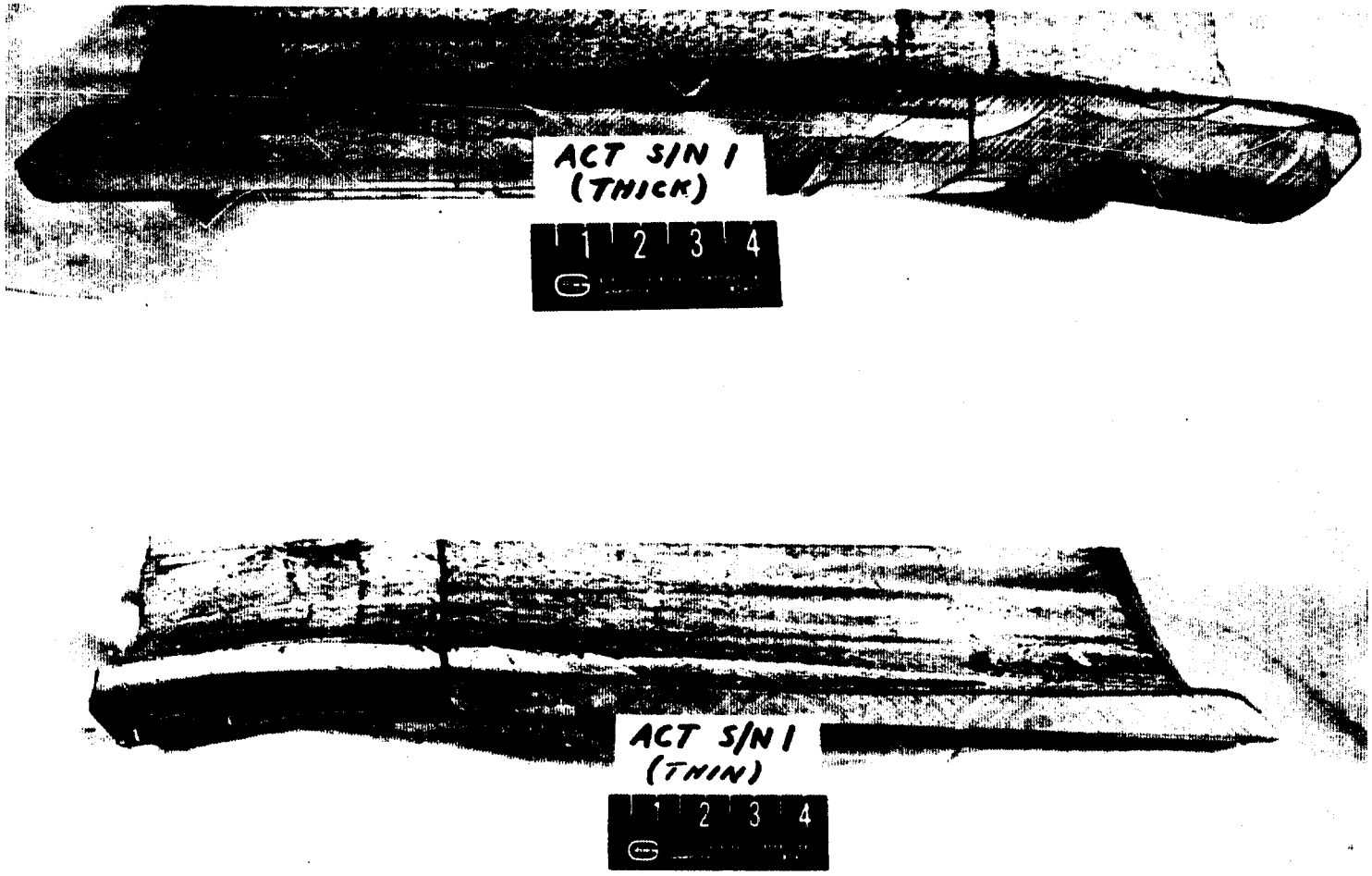

Figure 43. Longitudinal Sections (Thick and Thin) of S/N 001 Liner

Figure 44. Three Longitudinal Sections of S/N 002B Liner

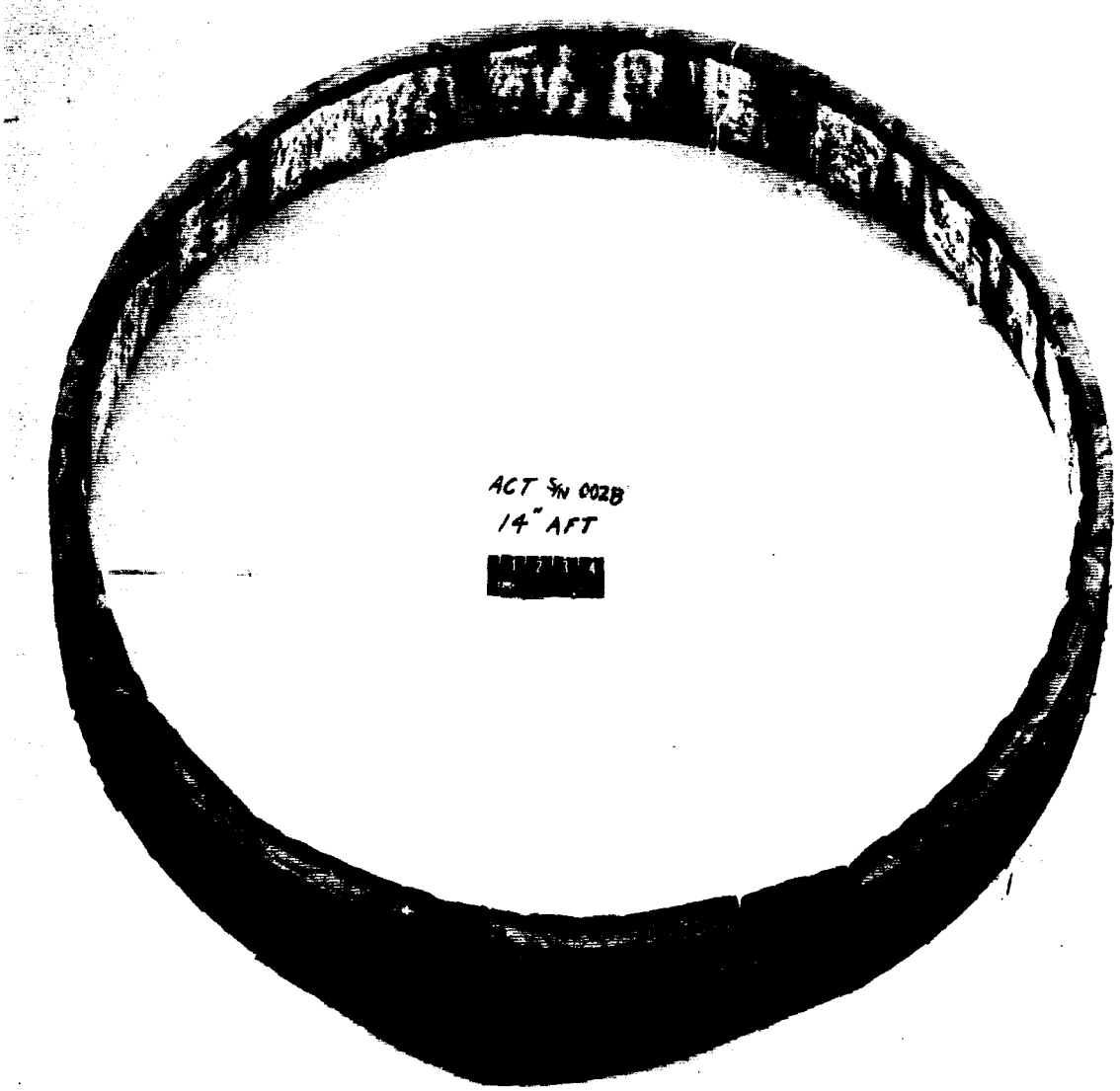

Figure 45. Circumferential Section of Liner S/N 002B, 14-in. Aft of Injector

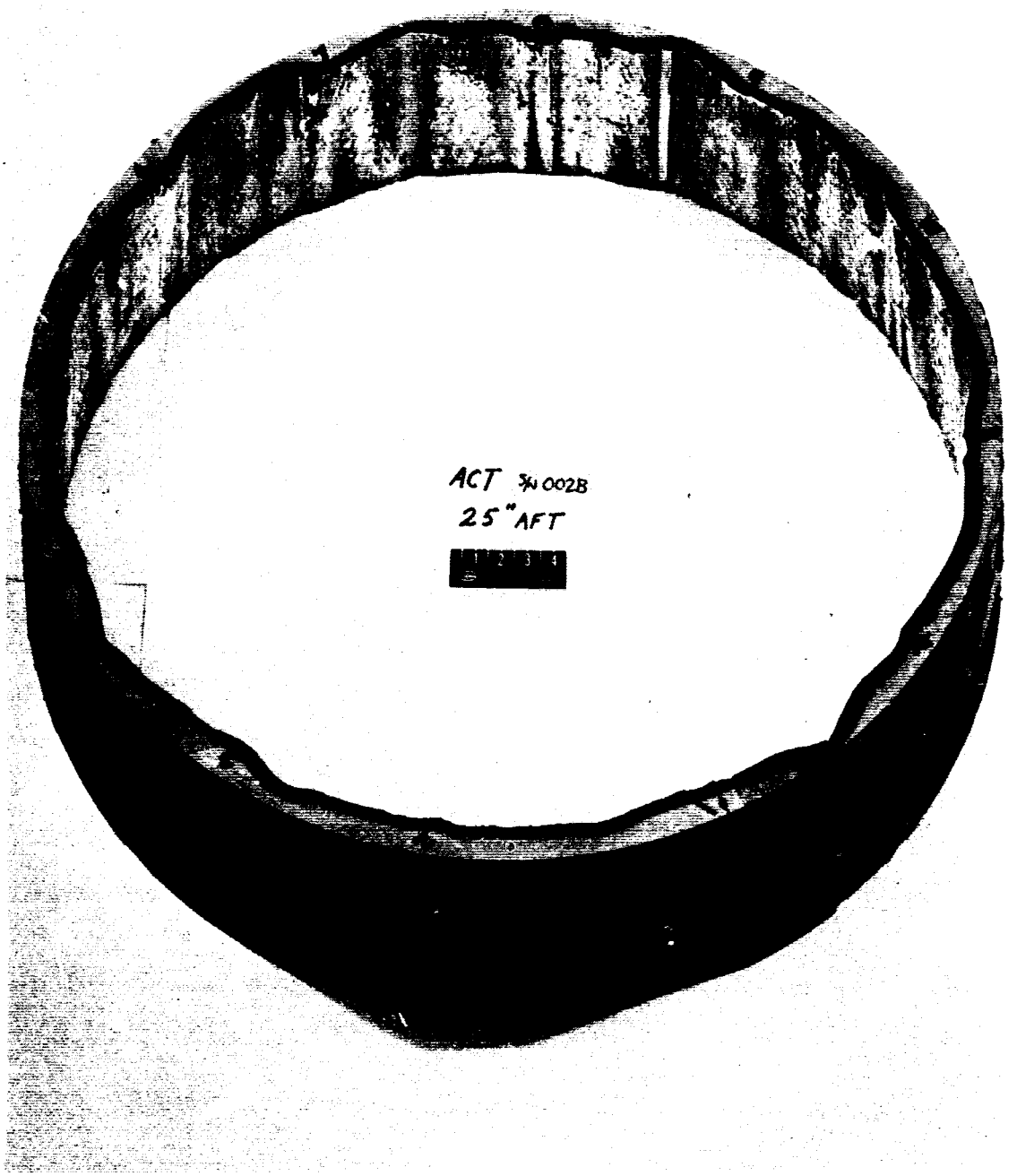

Figure 46. Circumferential Section of Liner S/N 002B, 25-in. Aft of Injector

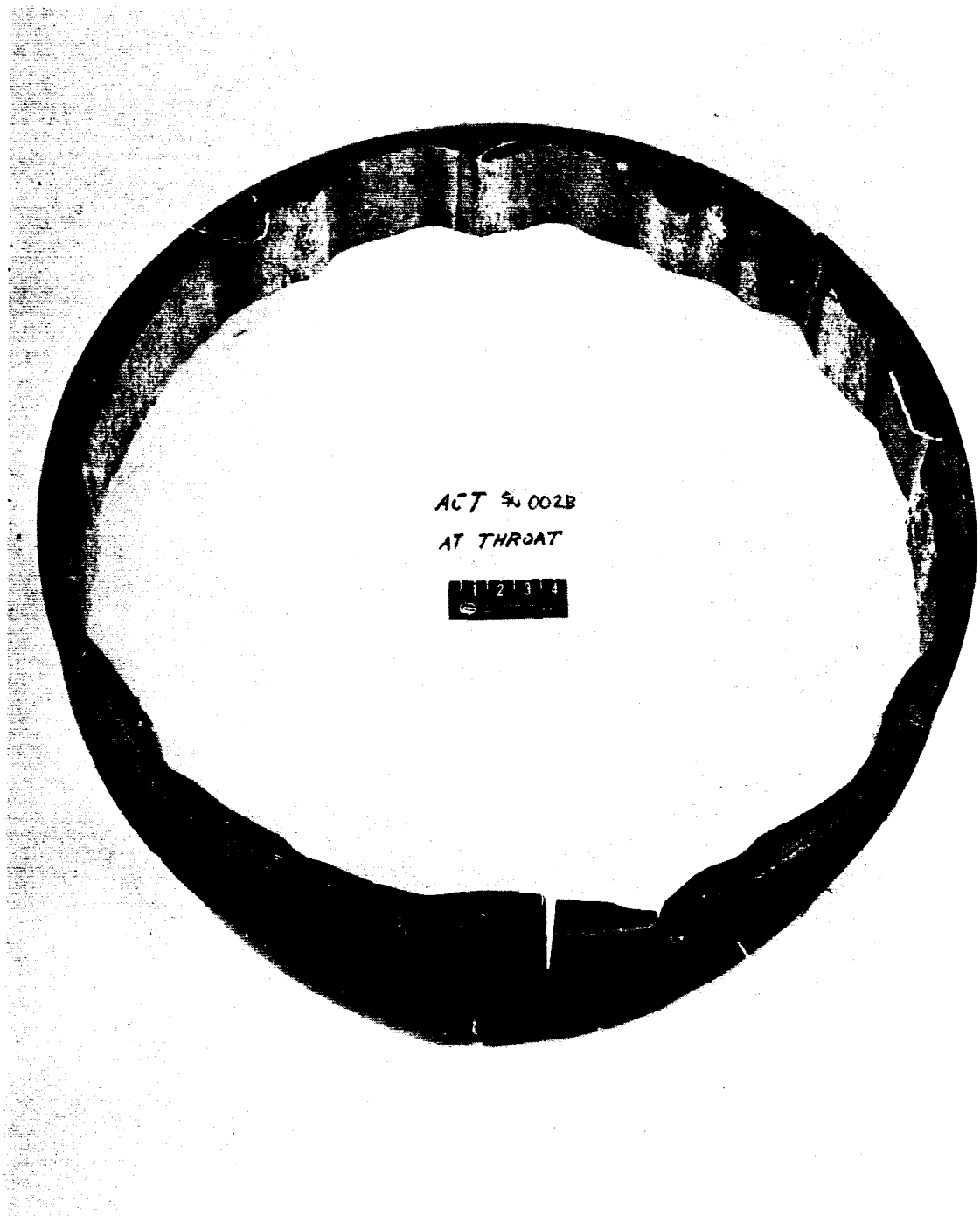

Figure 47. Circumferential Section of Liner S/N 002B, at the Throat

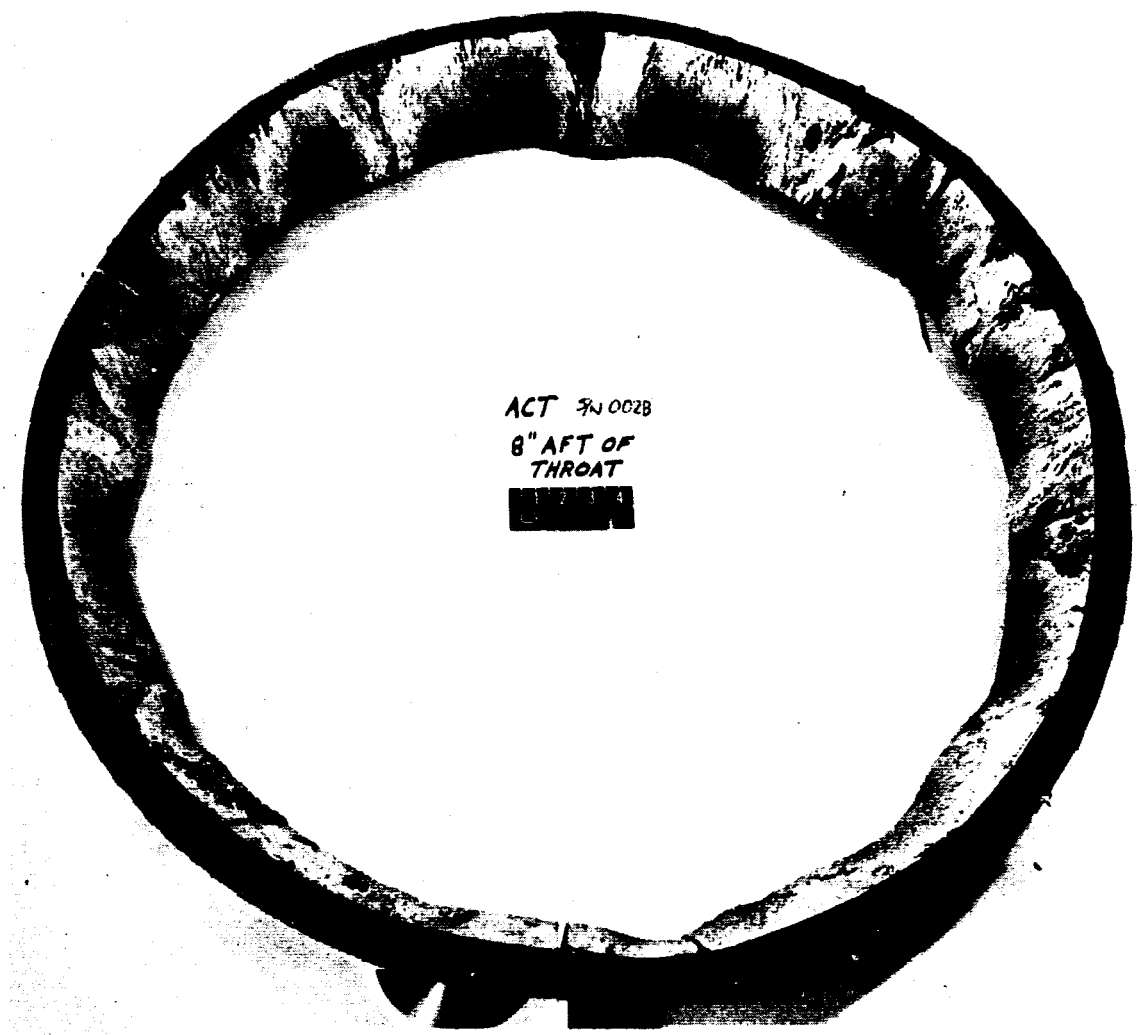

Figure 43. Circumferential Section of Liner S/N 002B, 8-in. Aft of Throat

Figure 49. Circumferential Section of Liner S/N 002B, 13-in. Aft of Throat

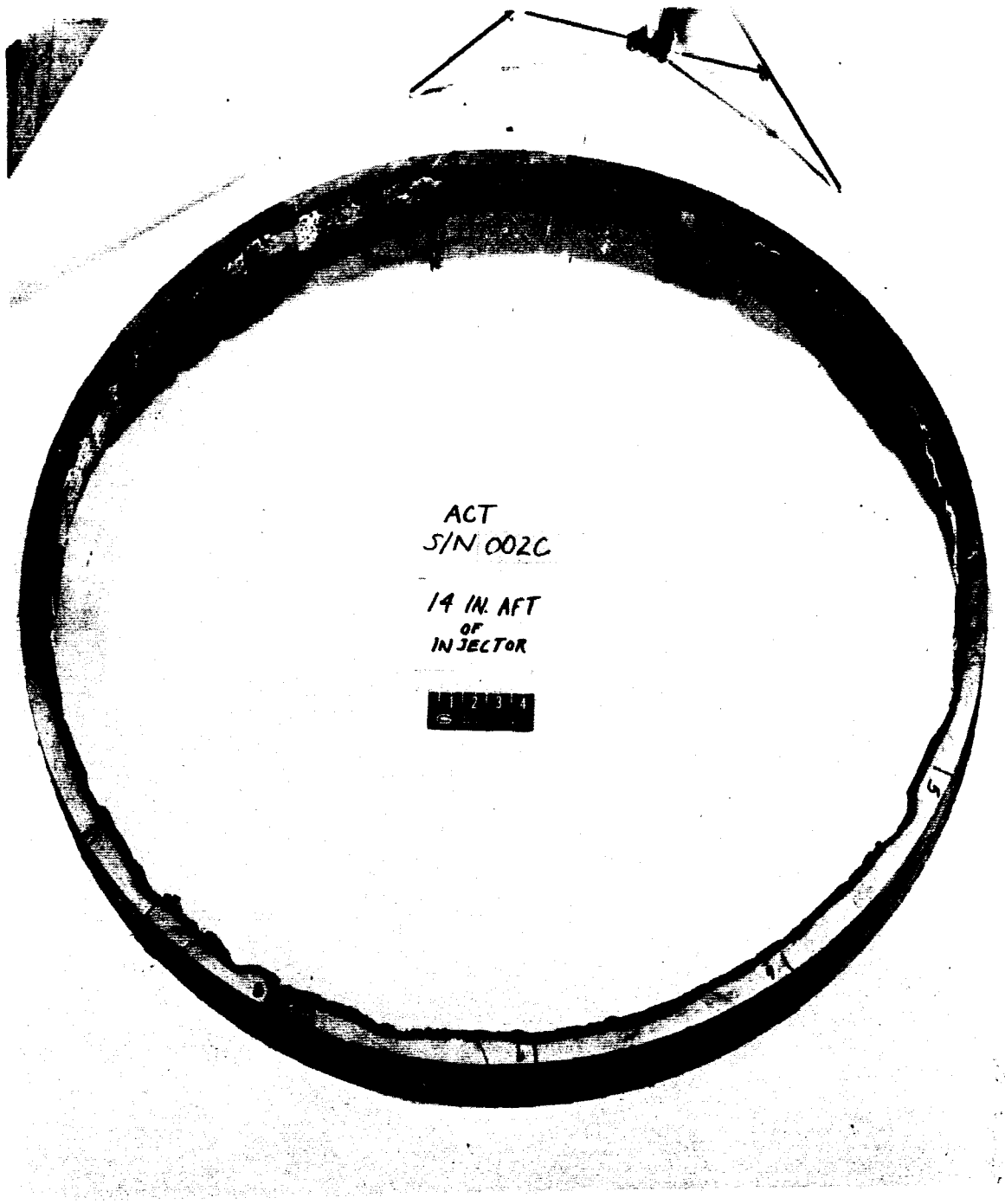

Figure 50. Circumferential Section of Liner S/N 002C, 14-in. Aft of Injector

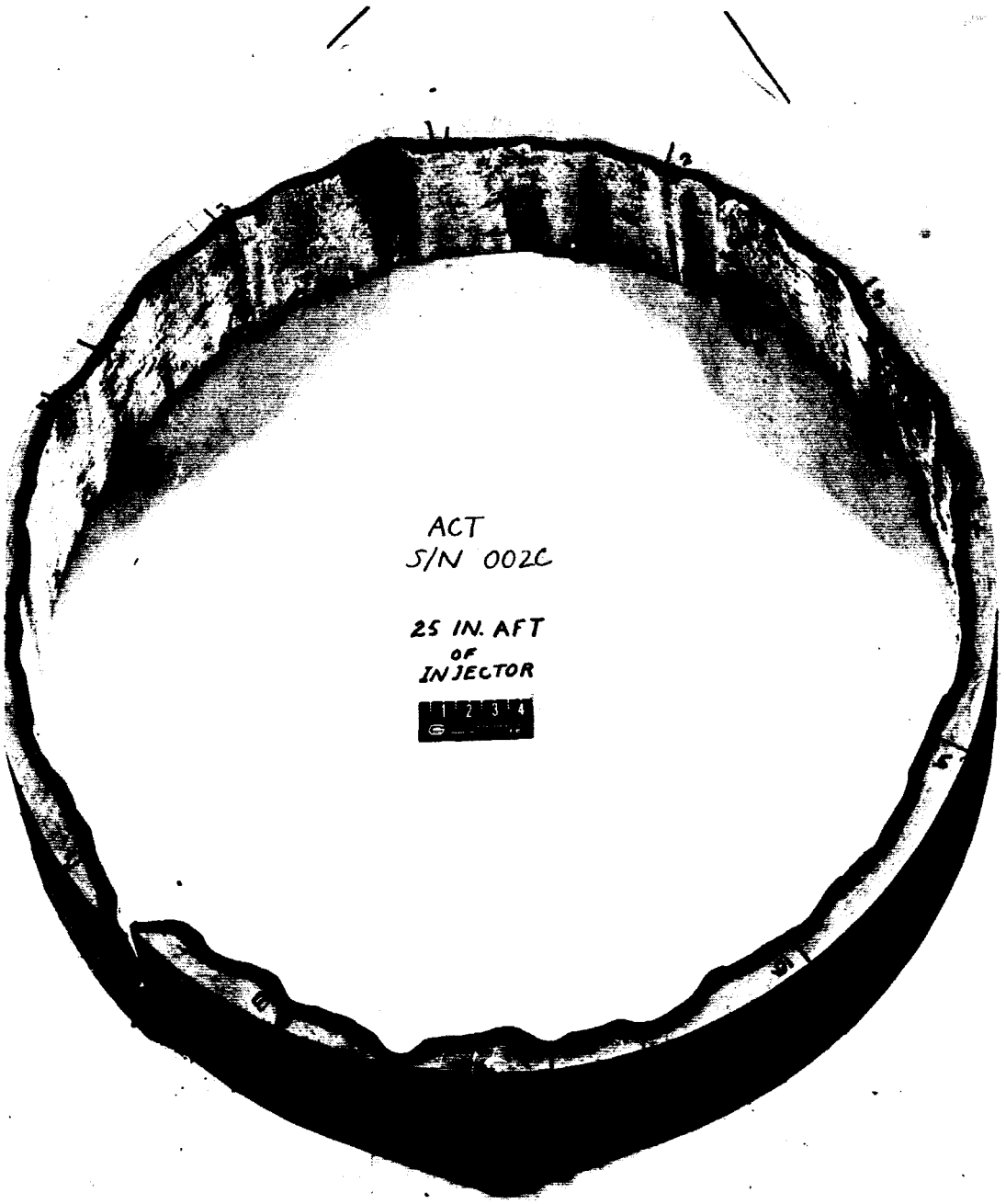

Figure 51. Circumferential Section of Liner S/N 002C, 25-in. Aft of Injector

Figure 52. Circumferential Section of Liner S/N 002C, at the Throat

Appendix D

Char depth also was measured on the four longitudinal sections shown on Figure No. 53. These sections were located as follows:

At baffle No. 1	- 0-degrees
Between baffles No. 8 and 9	- 230-degrees
Between baffles No. 11 and 12	- 307.5-degrees
Between baffles No. 12 and 1	- 345-degrees

The radial locations (0-degrees, 230-degrees, 307.5-degrees, and 345-degrees) were measured clockwise, looking forward, from 0-degrees at the No. 1 baffle. The char depth was measured at 2-in. intervals along the liner contour from the throat to 10 in. aft of the injector face. The data for each section are listed on Table XVII. A 100% char depth was observed on the 230-degree section at 26-in. and 28-in. aft of the injector face and at the throat.

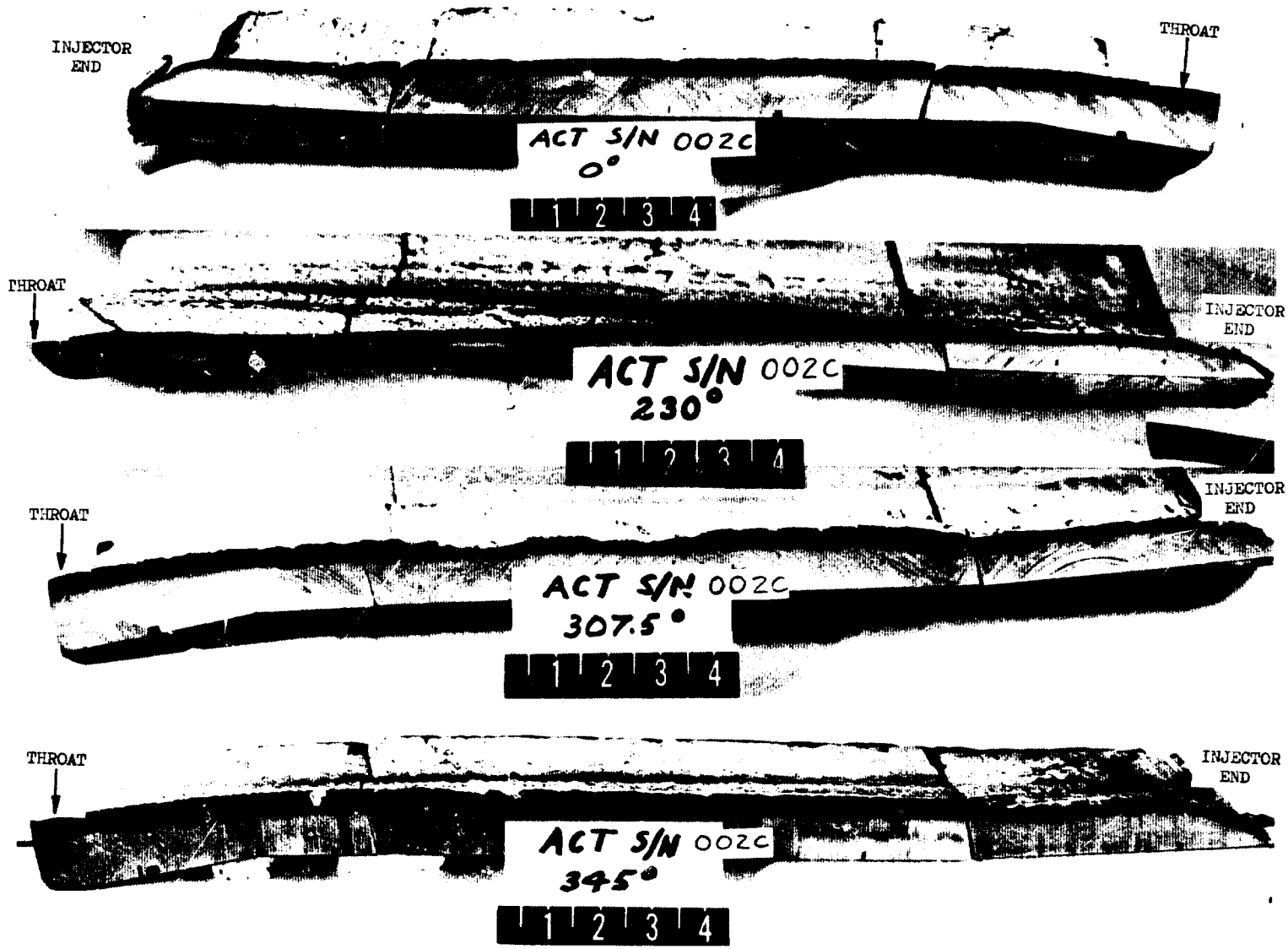

Figure 53. Four Longitudinal Sections of Liner S/N 002C

TABLE XVII

LINER CHAR PROFILE OF S/N 002C CHAMBER LONGITUDINAL SECTIONS AT 0-DEGREES, 230-DEGREES, 307.5-DEGREES, and 345-DEGREES

Baffle Location / Radial Location[2]	1		8 - 9		11 - 12		12 - 1	
	0-Degrees		230-Degrees		307.5-Degrees		345-Degrees	
Distance Aft of Injector in.	Total Thk. in.	Remain. Unchar in.	Total Thk. in.	Remain. Unchar in.	Total Thk. in.	Remain. Unchar in.	Total Thk. in.	Remain. Unchar in.
10	1.00	0.86	0.77	0.59	0.92	0.76	1.04	0.88
12	1.08	0.86	0.79	0.64	0.98	0.80	1.00	0.82
14[1]	1.25	0.98	0.90	0.63	1.00	0.82	1.24	0.89
16	1.25	0.97	0.94	0.61	1.24	0.92	1.27	0.97
18	1.34	1.02	0.78	0.47	1.26	0.97	1.31	1.00
20	1.32	1.00	0.57	0.40	1.32	0.90	1.33	0.99
22	1.37	1.07	0.42	0.25	1.28	1.00	1.34	1.00
24	1.37	1.05	0.27	0.13	1.15	0.97	1.31	1.00
25[1]	1.43	1.12	0.17	0.03	1.32	1.05	1.34	1.00
26	1.42	1.04	0.14	0.00	1.35	1.04	1.34	0.99
28	1.35	0.96	0.03	0.00	1.33	1.00	1.36	0.97
30	1.47	1.14	0.35	0.20	1.50	1.22	1.47	1.11
Throat[1]	1.46	1.09	0.28	0.00	1.51	1.23	1.46	1.12

(1) Circumferential sections at these points
(2) Measured clockwise looking forward with 0-degrees at baffle No.1

APPENDIX E

THEORET CAL ANALYSIS OF ABLATIVE CHAMBER THERMAL BEHAVIOR

Appendix E

I. INTRODUCTION

The primary objective of this analysis is to theoretically predict thermal behavior-temperature responses as well as erosion and char rates of the ablative liner at various axial and circumferential locations. To accomplish this, a number of subsidiary analyses are required. These include: analysis of the injector hydraulic system to determine propellant flow distribution; analysis of the boundary layer in the chamber to determine how the mixture ratio varies locally with injector flow distribution and gas core mixture ratio; and analysis of the ablative liner to determine how erosion varies locally with boundary layer mixture ratio.

II. INJECTOR HYDAULIC ANALYSIS - OXIDIZER CIRCUIT

The hydraulic analysis of the oxidizer circuit was undertaken to find the flow rate from each orifice and to determine any azimuthal variations that may exist because of inlet effects, etc. The study was made with a specially written computer program for the IBM 1130 machine. It is concluded that the oxidizer flow pattern is very uniform and that circumferential variations are of the order of a few percent.

The method of analysis involves dividing the injector assembly into discrete channels for which flow resistance values could be calculated. Figure No. 54 shows this breakdown. Resistance R is used to calculate pressure drop from the equation

$$\Delta P = R \dot{W}^2 \qquad \text{Eq. (E1)}$$

where ΔP is in terms of psia and $\dot{W}$ is in lb-in./sec

Resistance is defined by

$$R = \frac{3.62 f \frac{l}{d}}{\rho d^4} \qquad \text{Eq. (E2)}$$

where l is the passage length in inches, d the passage diameter in inches, ρ the fluid density in lbm/ft^3, and f is the Crane friction factor. The injector assembly is represented by the series/parallel resistance network shown on Figure No. 55. Each of the 12 segments of the injector is subdivided into element groups with the outermost row of elements (Row 33) represented by the 15 individual elements, as shown on Figure No. 56. The flow distribution is solved by simplifying the resistance network into a single equivalent resistance to find the over-all pressure drop, given the total flow rate, and then determining the flow rate to the separate segments and individual orifices in each segment.

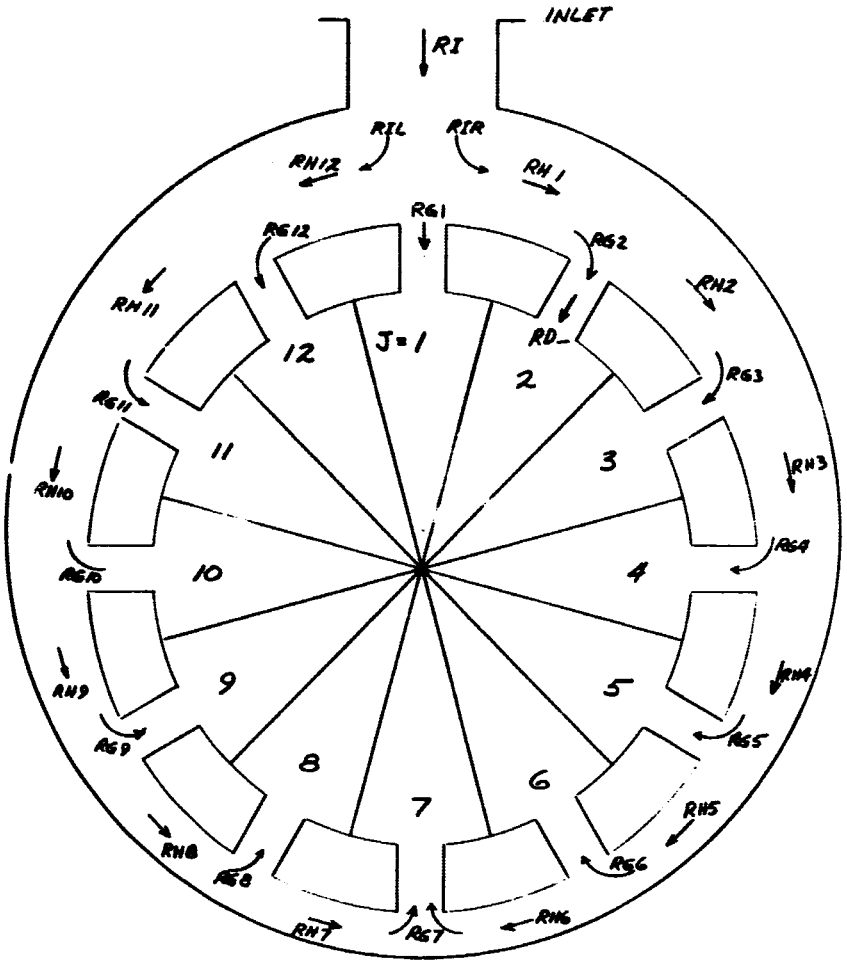

* RC = resistance of channel between elements

RT = resistance of turn into each element

R = resistance of element

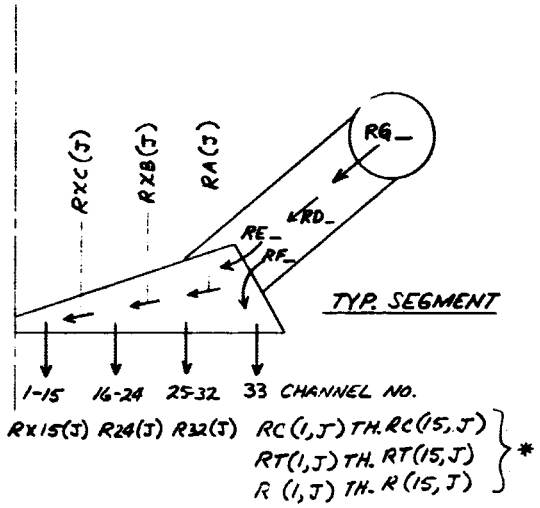

Figure 54. M-1 Injector Oxidizer Circuit, Resistance Nomenclature

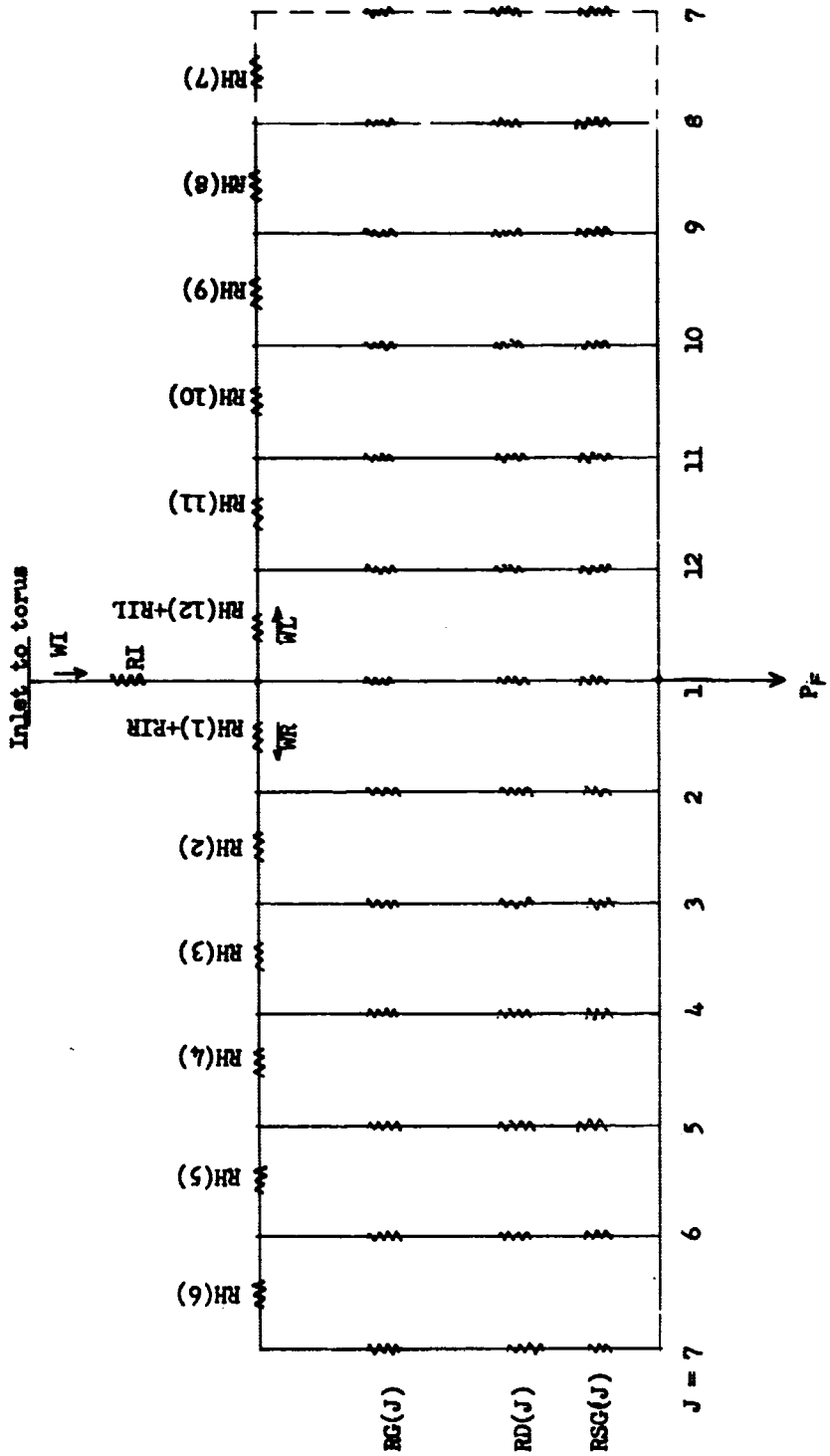

Figure 55. Injector Series/Parallel Resistance Network

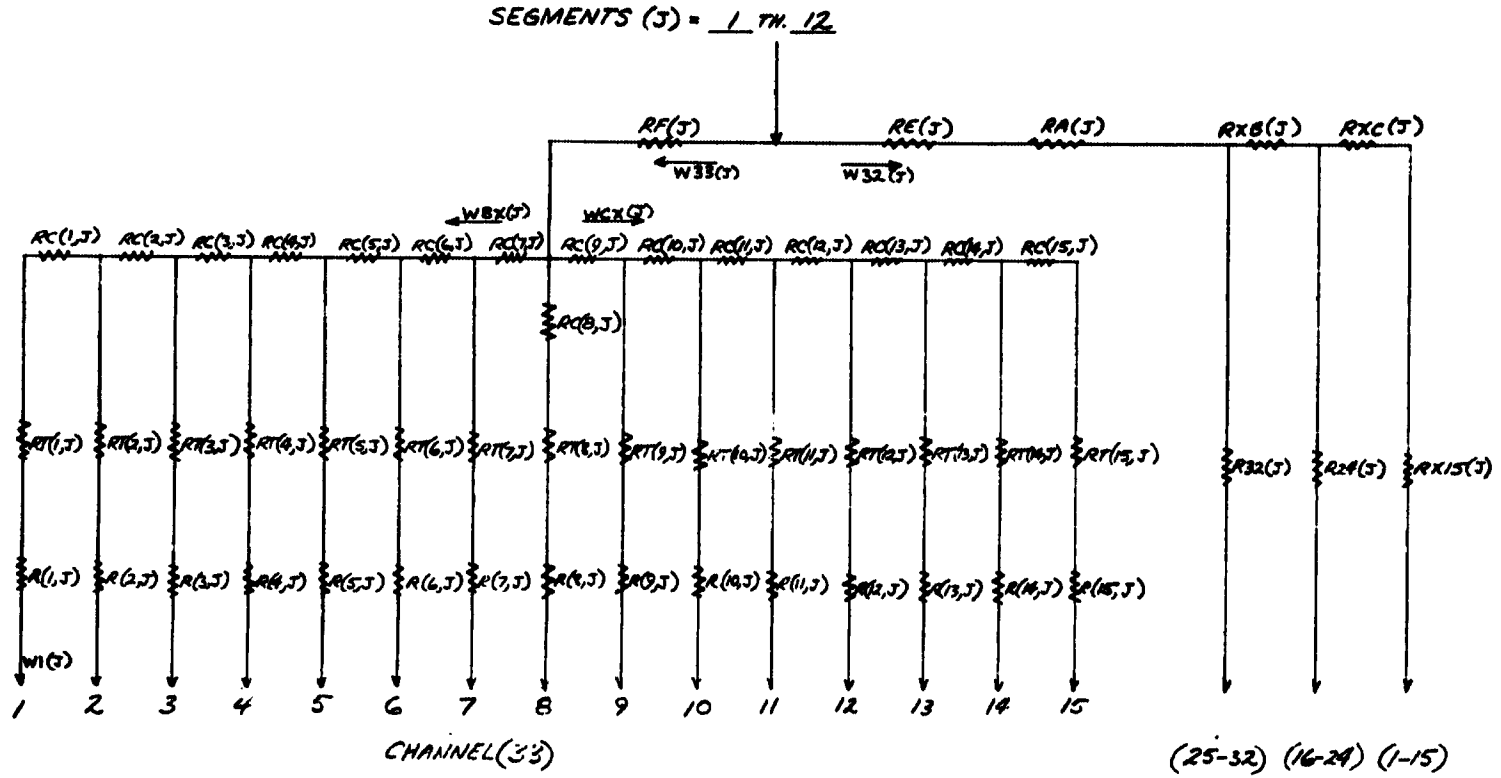

NOTE: SUBSCRIPT (J) DENOTES SEGMENT

Figure 56. Segmented Injector

Table XVIII presents the analytical results for the full thrust and half-thrust cases. The striking conclusion is that the circumferential variation in flow rate is very small. The injector segment nearest the oxidizer header receives about 2.2% more flow than the average value, and the diametrically opposite segment receives about 0.6% less than the average; these two locations representing extremes. The greatest total variation in circumferential flow rate from the outermost row (33) of orifices is 1.5% in any particular segment.

III. INJECTOR HYDRAULIC ANALYSIS - FUEL CIRCUIT

The injector fuel circuit hydraulic analysis was done using a computer program developed to perform Titan Injector hydraulics analyses. The program uses an electric analog to calculate the flow distribution and pressure drop throughout the circuit. The program, which was written for the IBM 1130 computer, was converted to the GE 235 Mark II system for this analysis because of storage limitations in the former machine.

The analysis involved dividing the flow circuit into a series/parallel network of flow resistances, as was done for the oxidizer circuit analysis. These resistances comprise the fuel element, rigimesh wall, and baffle resistance as well as the manifold resistance. The latter is based upon Jakob's formula for flow through a staggered tube bank. Figure No. 57 shows the flow network. Azimuthal variations are ignored because of the complexities that would arise if such variations were considered. Large azimuthal flow variations are not expected to occur in this fuel circuit.

The results are summarized on Table XIX for a chamber pressure of 1000 psia and Table XX for 500 psia pressure. These results are compared to experimental pressure drop data at 1000 psia chamber pressure obtained with injectors S/N 012 and S/N 020 (see Figure No. 58). The predicted fuel pressure drop is in reasonably good agreement with the fuel pressure drops obtained experimentally, and it is concluded that the predicted fuel flow distribution must be a good representation of the actual flow distribution, although there are no flow distribution data available to check this.

IV. BOUNDARY LAYER MIXTURE RATIO

To accurately predict and/or correlate ablative erosion rates as a function of engine operating conditions, it is necessary that wall gas-side boundary conditions are known. The following paragraphs describe an analysis by which the boundary layer mixture ratio was determined for the subject ablative thrust chamber.

In summary, the boundary O/F is a function of the following parameters:

TABLE XVIII

SUMMARY OF RESULTS FROM OXIDIZER FLOW ANALYSIS

Pc 100C

Ox flowrate to injector torus = 2872.0 lbm/sec Pressure differential (torus inlet to PF) = 452.12 psia

Segment flowrates (1 through 12, lbm/sec)	244.58	237.86	238.64	238.72	238.76	239.75	239.90	239.75	238.76	238.72	238.64	237.86
Segment pressures (1 through 12, psia)	399.69	378.02	380.50	380.76	380.91	384.07	384.56	384.07	380.91	380.76	380.50	378.02

Segment No.	Channel 33 Flowrate 1	2	3	4	5	6	7	8	9	10	11	12	13	14	15	Channel 25-32	Channel 16-24	Channel 1-15
1	.913	.913	.914	.922	.925	.926	.924	.906	.926	.926	.925	.923	.915	.914	.914	104.392	74.239	52.140
2	.888	.888	.889	.897	.899	.900	.898	.901	.901	.900	.900	.897	.890	.889	.888	101.522	72.198	50.706
3	.891	.891	.892	.900	.902	.903	.901	.904	.904	.903	.903	.900	.893	.892	.891	101.854	72.435	50.872
4	.891	.891	.893	.900	.902	.903	.902	.904	.904	.903	.903	.900	.893	.892	.892	101.890	72.460	50.890
5	.892	.892	.893	.900	.903	.904	.902	.904	.904	.904	.903	.901	.893	.892	.892	101.909	72.474	50.900
6	.895	.895	.896	.904	.906	.907	.906	.908	.908	.907	.907	.904	.897	.896	.896	102.332	72.774	51.111
7	.896	.896	.897	.904	.907	.908	.906	.909	.908	.908	.907	.905	.897	.896	.896	102.336	72.820	51.143
8	.895	.895	.896	.904	.906	.907	.906	.908	.908	.907	.907	.904	.897	.896	.896	102.332	72.774	51.111
9	.892	.892	.893	.900	.903	.904	.902	.904	.904	.904	.903	.901	.893	.892	.892	101.909	72.474	50.900
10	.891	.891	.893	.900	.902	.903	.903	.902	.904	.903	.903	.900	.893	.892	.892	101.890	72.460	50.890
11	.891	.891	.892	.900	.902	.903	.901	.904	.904	.903	.903	.900	.893	.892	.891	101.854	72.435	50.872
12	.888	.888	.889	.897	.899	.900	.898	.901	.901	.900	.900	.897	.890	.889	.888	101.522	72.198	50.706

Pc 50C

Ox flowrate to injector torus = 1436 lbm/sec Pressure differential (torus inlet to PF) = 108.03 psia

Segment flowrates (1 through 12, lbm/sec)	122.29	118.93	119.32	119.36	119.38	119.87	119.95	119.87	119.38	119.36	119.32	119.93
Segment pressures (1 through 12, psia)	99.92	94.50	95.12	95.19	95.22	96.03	96.14	96.01	95.22	95.19	95.12	94.50

Segment No.	1	2	3	4	5	6	7	8	9	10	11	12	13	14	15	Channel 25-32	Channel 16-24	Channel 1-15
1	.456	.456	.457	.461	.462	.463	.462	.463	.463	.463	.462	.461	.457	.457	.457	52.196	37.119	26.070
2	.444	.444	.444	.448	.449	.450	.449	.450	.450	.450	.450	.448	.445	.444	.444	50.761	36.099	25.353
3	.445	.445	.446	.450	.451	.451	.450	.452	.452	.451	.451	.450	.446	.446	.445	50.927	36.217	25.436
4	.445	.445	.446	.450	.451	.451	.451	.452	.452	.451	.451	.450	.446	.446	.446	50.945	36.230	25.445
5	.446	.446	.446	.450	.451	.452	.451	.452	.452	.452	.451	.450	.446	.446	.446	50.954	36.237	25.450
6	.447	.447	.448	.452	.453	.453	.453	.454	.454	.453	.453	.452	.448	.448	.448	51.166	36.387	25.555
7	.448	.448	.452	.453	.454	.453	.454	.454	.454	.454	.453	.452	.448	.448	.448	51.198	36.410	25.571
8	.447	.447	.448	.452	.453	.453	.453	.454	.454	.453	.453	.452	.448	.448	.448	51.166	36.387	25.555
9	.446	.446	.446	.450	.451	.452	.451	.452	.452	.452	.451	.450	.446	.446	.446	50.954	36.237	25.450
10	.445	.445	.446	.450	.451	.451	.451	.452	.452	.451	.451	.450	.446	.446	.446	50.945	36.230	25.445
11	.445	.445	.446	.450	.451	.451	.450	.452	.452	.451	.451	.450	.446	.446	.445	50.927	36.217	25.436
12	.444	.444	.444	.448	.449	.450	.449	.450	.450	.450	.450	.448	.445	.444	.444	50.761	36.099	25.353

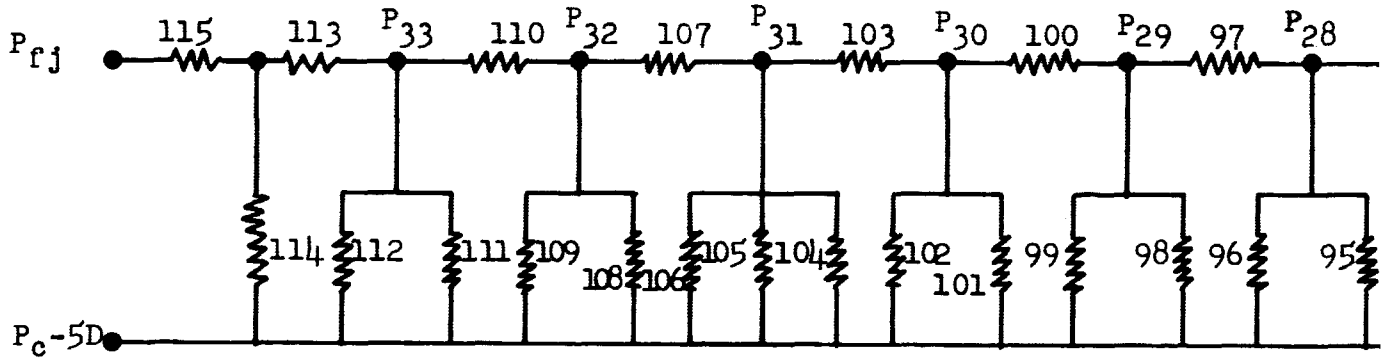
P_{fj}
115
113
P_{33}
110
P_{32}
107
P_{31}
103
P_{30}
100
P_{29}
97
P_{28}
114
112
111
109
108
106
105
104
102
101
99
98
96
95
P_c-5D

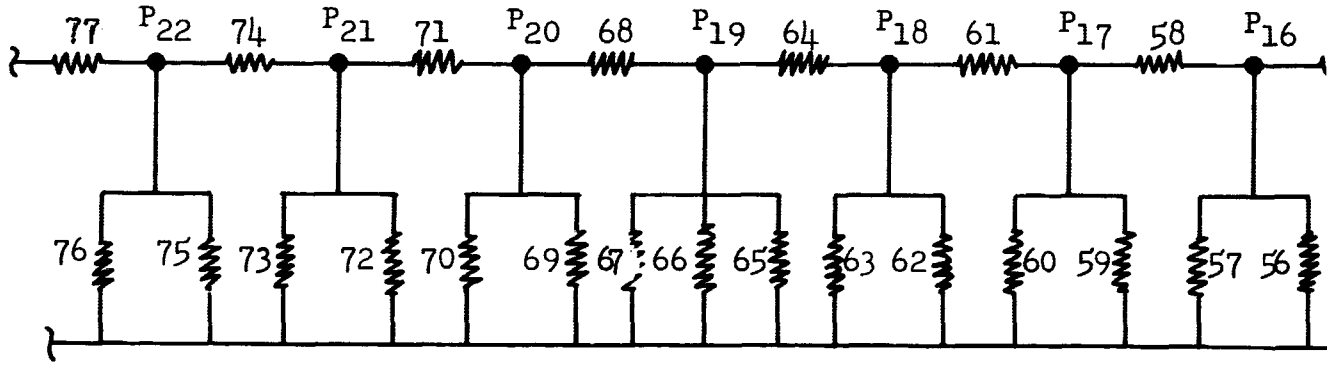
77
P_{22}
74
P_{21}
71
P_{20}
68
P_{19}
64
P_{18}
61
P_{17}
58
P_{16}
76
75
73
72
70
69
67
66
65
63
62
60
59
57
56

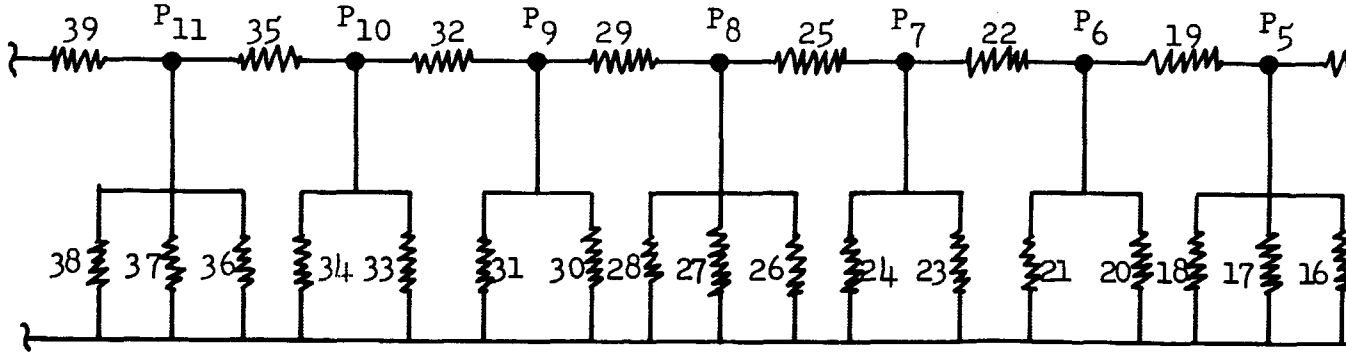
39
P_{11}
35
P_{10}
32
P_9
29
P_8
25
P_7
22
P_6
19
P_5
38
37
36
34
33
31
30
28
27
26
24
23
21
20
18
17
16

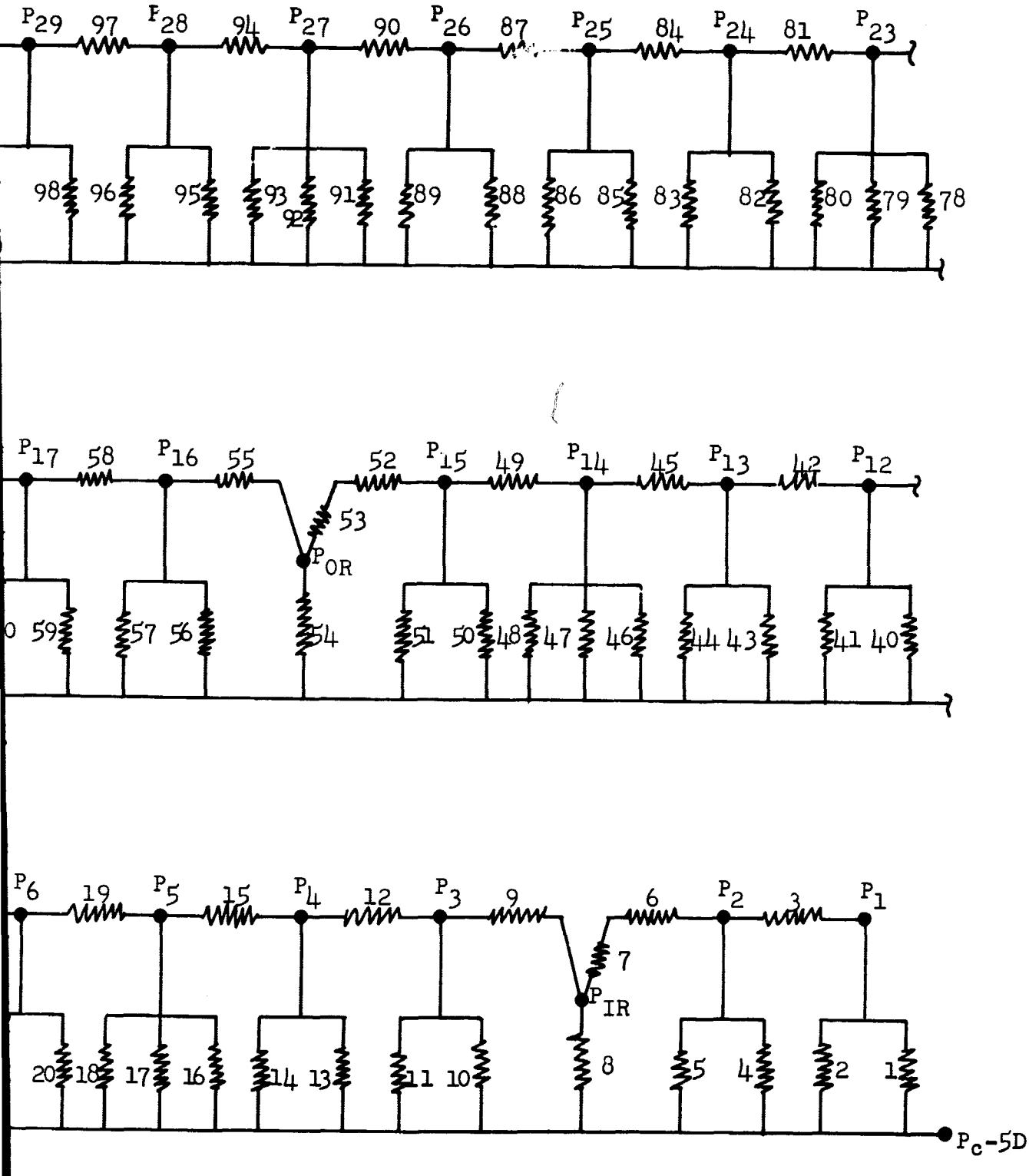

Figure 57. M-1 Injector Fuel Side Hydraulic Circuit

FOLDOUT FRAME 2

TABLE XIX

PREDICTED FUEL FLOW DISTRIBUTION FOR P_c = 1000 PSIA

Row No.	Element	Rigimesh	Baffle	Total
1	.785	.08034	---	.8657
2	1.2564	.03742	---	1.2938
Inner Ring	1.1454	---	---	1.1454
3	2.0008	.04976	---	2.0506
4	2.3910	.2476	---	2.6386
5	3.2592	.0721	.5605	3.8917
6	3.8532	.08172	---	3.9349
7	4.4514	.09108	---	4.5425
8	4.4958	.09012	.5799	5.1658
9	4.5210	.1274	---	4.6484
10	6.2400	.22698	---	6.4670
11	6.8640	.13146	.59052	7.5860
12	7.5060	.1420	---	7.6480
13	8.1600	.1530	---	8.3130
14	8.232	.1531	.6066	8.9917
15	8.322	.1536	---	8.4756
Outer Ring	4.0872	---	---	4.0872
16	13.0080	.7776	---	13.7856
17	14.9040	1.230	---	16.1340
18	14.9700	.2760	---	15.246
19	16.9020	3.804	2.9808	23.6868
20	16.9860	.3108	---	17.2968
21	18.954	.4153	---	19.3693
22	19.0560	3.4608	---	22.5168
23	21.0540	.4236	3.0384	24.5161
24	21.1860	.3805	---	21.5665
25	23.2260	.5196	---	23.7456
26	23.3700	.4208	---	23.7908
27	25.4580	.5278	3.1080	29.0938
28	25.6260	.4597	---	26.0857
29	27.7620	.5680	---	28.3300
30	27.9480	.4994	---	28.4474
31	30.1320	.6090	3.1884	33.9294
32	30.3660	.5412	---	30.9072
33	30.5820	.6096	---	31.1916

TABLE XX

PREDICTED FUEL FLOW DISTRIBUTION FOR P_c = 500 PSIA

Row No.	Element	Rigimesh	Baffle	Total
1	.39306	.04021	---	.43327
2	.62880	.01873	---	.64753
Inner Ring	.57312	---	---	.57312
3	1.0050	.2490	---	1.2540
4	1.1964	.1239	---	1.3203
5	1.6308	.03607	.28044	1.94731
6	1.9278	.04089	---	1.9687
7	2.2278	.04557	---	2.27338
8	2.2500	.045108	.29016	2.58527
9	2.2626	.06378	---	2.32638
10	3.1224	.11358	---	3.2360
11	3.4362	.06576	.29550	3.7974
12	3.7566	.07104	---	3.8276
13	4.0818	.07656	---	4.15836
14	4.1196	.07662	.3036	4.4998
15	4.1628	.07686	---	4.23966
Outer Ring	2.0454	---	---	2.0454
16	6.5100	.3891	---	6.8991
17	7.4580	.6156	---	8.07360
18	7.4880	.1381	---	7.6261
19	8.4600	.1904	1.4916	10.1420
20	8.49600	.15552	---	8.6515
21	9.486	.20784	---	9.6938
22	9.53400	.17316	---	9.7072
23	10.5360	.21198	1.5204	12.2684
24	10.6020	.19038	---	10.7924
25	11.6220	.2600	---	11.88204
26	11.6940	.2106	---	11.9046
27	12.7380	.2641	1.5552	14.5573
28	12.8220	.2300	---	13.0520
29	13.8900	.2842	---	14.1742
30	13.9860	.2499	---	14.23[illegible]
31	15.0780	.3047	1.5954	16.9[illegible]1
32	15.1920	.2708	---	15.4628
33	15.3060	.3051	---	15.6112

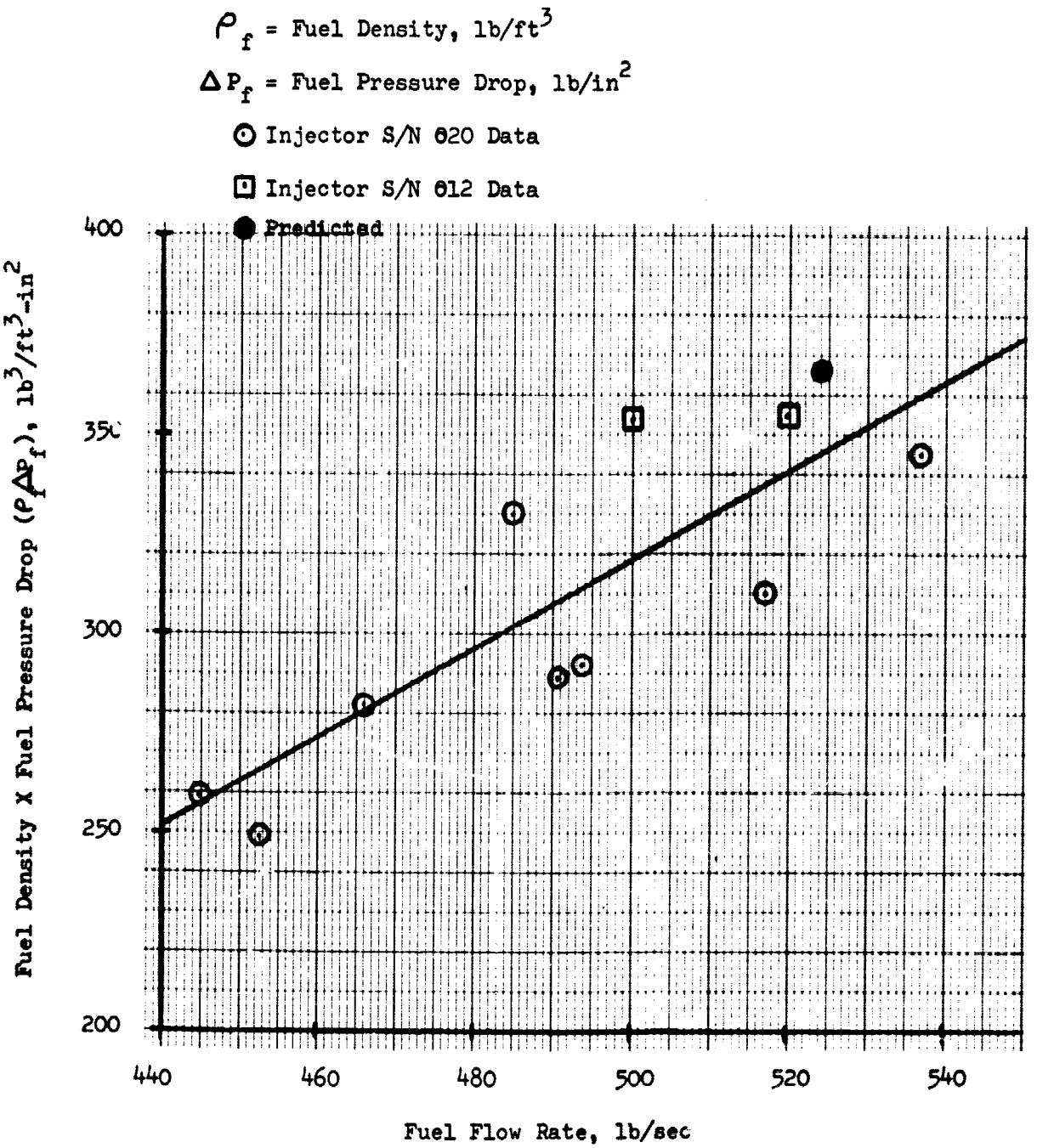

Figure 58. Coaxial Element Injector Fuel Density x Fuel Pressure Drop vs Fuel Flow Rate

- The mass flow in the boundary layer.

- The circumferential and axial distribution of fuel film coolant.

- The circumferential and axial distribution of free stream mixture ratio.

If the total mass flow in the boundary layer can be computed as a function of length and the amount of fuel film coolant is known, the amount of entrained free stream gases can be computed by difference. That is, the film coolant mass flow subtracted from the boundary layer mass flow yields the amount of entrained free stream gases at their local O/F. With the local O/F computed as a function of length and circumferential location, the boundary layer mixture as a function of the same parameters is the quotient, of the amount of oxidizer contributed by the entrained free stream gases and the sum of the boundary layer fuel contributed by the film coolant and entrained gases.

As can be seen from the brief overview above, the boundary O/F can be specified completely by knowledge of the amount of mass flow in the boundary, the fuel film coolant flow rate, and the local free stream O/F. The boundary layer total flow rate can be found by many computational techniques found in the literature. The film coolant flow rate as a function of circumferential location can be found by a hydraulic analysis of the injector. The local free stream O/F is a function of the propellant vaporization and the net movement of resultant chamber gases "chamber cross winds." The analytical models describing these latter two processes are termed the vaporization and gas dynamic models. The following paragraphs describe the analytical techniques used to determine each of the necessary physical components of this boundary layer analysis.

A. TOTAL BOUNDARY LAYER FLOW RATE

There are a number of analytical techniques which may be used to find the boundary layer flow rate. The development of the equation used in this analysis follows: the growth of a boundary layer m_{BL} is given by the equation:

$$\dot{M}_{bL} = \int_{o}^{\delta} \rho U_{(y)} d_y \qquad \text{Eq. (E3)}$$

where ρ is the fluid density and is considered constant in the boundary layer (i.e., $\rho = \rho_\infty$), $U_{(y)}$ is the local velocity and δ is the boundary layer thickness.

If it is assumed that similar velocity profiles exist in the boundary layer as it develops from the point of injection and that this profile is only a function of the freestream conditions, then

$$U_{(y)} = U_\infty \left(\frac{y}{\delta}\right)^{\frac{1}{n}} \qquad \text{Eq. (E4)}$$

where U_∞ is the freestream velocity and n is a function of the freestream Reynolds number. Combining Equations (E3) and (E4) gives

$$\dot{M}_{BL} = \int_0^\infty \rho_\infty \; U_\infty \left(\frac{y}{\delta}\right)^{\frac{1}{n}} dy = \frac{n}{n+1} \; \rho_\infty \; U_\infty \; \delta \qquad \text{Eq (E5)}$$

It can be show that for a developing boundary layer the thickness can be expressed as:

$$\delta = x^{\frac{n+1}{n+3}} \left[\left(\frac{n \; C_n}{(n+2)(n+3)} \right)^{\frac{2n}{n+1}} \left(\frac{\rho_\infty \; U_\infty}{\mu_\infty} \right)^{\frac{2}{n+1}} \right]^{\frac{-(n+1)}{(n+3)}} \qquad \text{Eq. (E6)}$$

In this case X is the distance in which the boundary layer has been developing, C_n is a function of n (9) and μ_∞ is the freestream velocity.

Combining and rearranging gives the form:

$$\dot{M}_{BL} = 0.82 \left[\left(\frac{n}{n+1} \right) \left(\frac{nC_n^{\frac{-2n}{n+1}}}{(n+2)(n+3)} \right)^{\frac{-(n+1)}{n+3}} \mu_\infty^{\frac{2}{n+3}} \left(\rho_\infty \; U_\infty\right)^{\frac{n+1}{n+3}} \right] X^{\frac{n+1}{n+3}} \qquad \text{Eq. (E7)}$$

The constant 0.82 is an empirical value derived from the work of J. L. Stollery and A. A. M. El-Ehwany.(10)

The above equation is a solution of the flat-plate boundary problem and inherent in this solution is the assumption of a constant $\rho(U)_\infty$ product over the length of developing boundary layer. However, this is not the case in this rocket thrust chamber, with two factors affecting this assumption. The first being that there is not a constant combustion gas flow rate throughout the length of the chamber. This is caused by incomplete propellant vaporization which effectively adds vaporizing oxidizer to the combustion gases as they traverse the length of the chamber, thus increasing the $\rho(U)_\infty$ product as function of axial length. The magnitude of this increase was computed using the vaporization model described in the following section. The second factor affecting the boundary layer solution is the area change of thrust chamber. This also drives the $\rho(U)_\infty$ product higher as a function of combustor length. To account for these varying freestream conditions, the $\rho(U)_\infty$ product, as a function of length, was computed at three engine over-all mixture ratios (4.5, 5.5, and 6.5). The flow rate in the boundary layer then was computed using

(9) Schlichting, Dr. H., Boundary Layer Theory, McGraw-Hill, 4th Edition, 1960, page 503

(10) Stollery, J. L. and El-Ehwany, A.A.M., "A Note on the Use of Boundary Layer Model for Correlating Film Cooling Data," Heat Mass Transfer, Vol. 8, pp 55-65, Pergamon Press, 1965

Equation (E7) for $\rho(U)_\infty$ products corresponding to axial lengths of 0.5, 1.0, 1.5, 2.0 and 2.5 feet. From these solutions, the derivative $d\dot{m}_{BL}/dL$ was approximated graphically at each of the points above. The flow in the boundary layer then was found by summing the individual contribution of each delta $\dot{m}_{BL}$ at its particular length and $\rho(U)_\infty$ product, with the assumption that the slope $\Delta\dot{m}_{BL}/\Delta$length was constant for 0.5 feet. The resulting boundary layer flow rate gradient is shown on Figure No. 59 for the 5.5 over-all engine mixture ratio case.

A more sophisticated solution could be found using methods such as those of Elliott, Bartz and Silver.(11) However, the close correlation of the resulting data (see Appendix A) indicate the basic validity of this approach.

B. FUEL FILM COOLANT FLOW RATE

The fuel film coolant flow rate was found analytically from a hydraulic analysis of the subject injector. The injector assembly was divided into discrete channels for which resistance values could be calculated. The injector assembly then was represented by a series and parallel resistance network. A combustor solution of this network first reduces the network into a single equivalent resistance to permit determination of the over-all pressure differential. Then, the flow for each element or groups of element was determined.

C. THE VAPORIZATION MODEL

As mentioned previously, the local O/F freestream is a necessary prerequisite to the solution of the boundary O/F. Upon injection, the fuel is in the gaseous state and the oxidizer in a liquid state. It can be reasoned qualitatively, therefore, that near the injector face, the combustion products are very fuel rich and tend towards the operating O/F as they proceed down the chamber. This characteristic is depicted on Figure No. 60 for an over-all engine O/F of 5.5. Similar curves were generated for engine operating mixture ratios of 4.5 and 6.5.

At the outset, the term vaporization model, when applied to supercritical propellants, is a misnomer. A better name would be propellant preparation model because the model here computes that amount of propellant entering into the combustion process. The model used here is functionally similar to vaporization models existent in the literature with the difference that it has been biased using the results of hot firing data. The model described below has been used for other supercritical propellants and has generated good results, thus indicating the basic validity of this approach.

(11) Elliot, Bartz, and Silver, Calculation of Turbulent Boundary-Layer Growth and Heat Transfer in Axi-Symmetric Nozzles, JPL TR No. 32-387, 15 February 1963

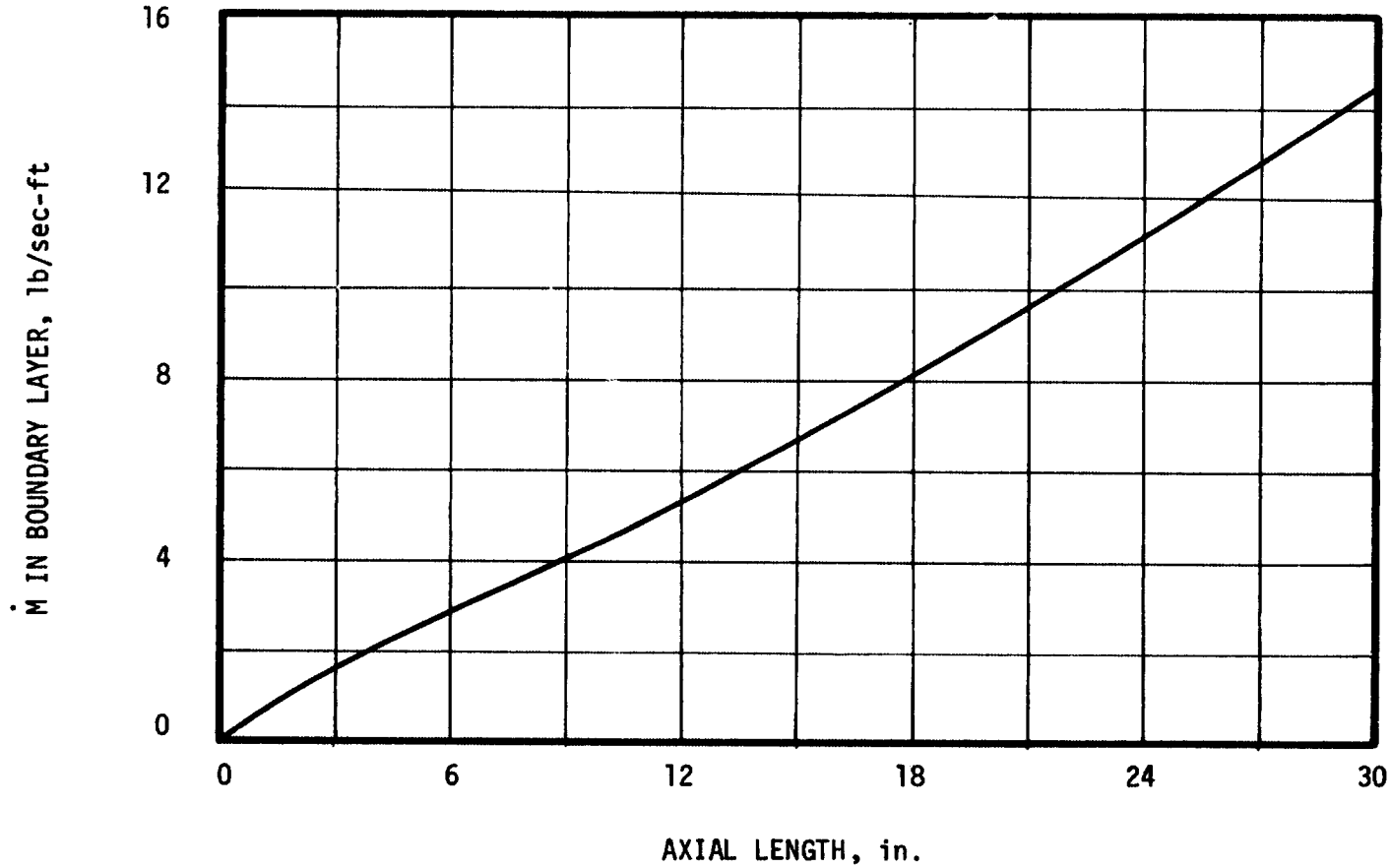

Figure 59. Boundary Layer Flow Rate as a Function of Axial Length

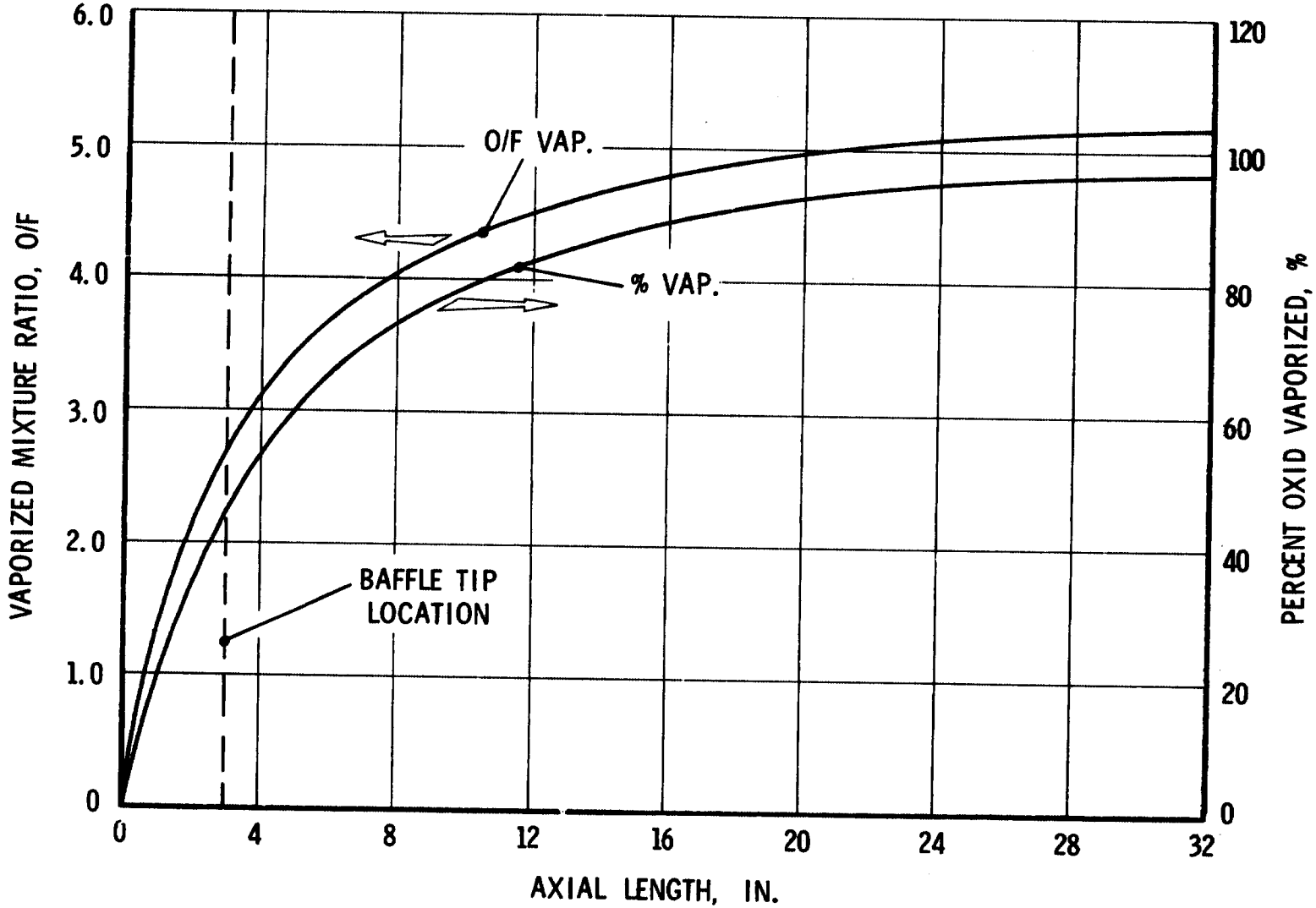

Figure 60. Mixture Ratio and Percent Oxid Vaporized vs Axial Length

Appendix E

The basic vaporization model used for this analysis was developed by Priems and Heidman(12) and later modified by Beltran(13) and Aerojet-General. The Beltran modification accounts for the decomposition reaction of Hydrazine base fuels. The Aerojet-General contribution adds the impingement angle, momentum, and elements type effects to the basic model.

The model as developed by Priem solves the combined energy, momentum, and mass transfer processes acting upon a statistically defined droplet distribution. Functional relationships between the combustion related variables and vaporized propellants were generated using an iterative computer solution of the various transfer processes. These solutions resulted in simplified equations relating chamber pressure, injection velocity, chamber geometry, orifice diameter, propellant, and injection temperature to injector-chamber performance.

The basic computer model simultaneously solves the heat transfer, mass transfer, and aerodynamic momentum transfer (drag) between the combustion gas and the liquid droplet. Heat input to the droplet raises the liquid droplet temperature and superheats the vapor drop mantle. The heat flux is influenced by drop differential velocity between the drop and the surrounding gas, chamber pressure, thermal transport properties of the propellants, and vapor mantle thickness surrounding the droplet. With hydrazine base fuels, in the region where drop relative velocities are low, the two flame decomposition reaction is the heat source of the vaporization process. Residence time of the drops is determined by simultaneously solving with the mass and heat transfer equations and the ballistic equations using empirical drag coefficients. Those drops that survive the vaporization process contain energy, unavailable to the combustion process, which is a direct measure of combustion performance.

To date, inadequate treatment of drop size distributions in a hot firing environment had compromised the utility of any vaporization model. Work is progressing in this area, but solutions which supply accurate analytical predictions are not yet available. This problem has been circumvented by empirically determining effective drop sizes. Using the functional relationships developed by Priem, effective drop sizes and distributions have been extrapolated from experimental engine data covering a wide variety of operating constraint. Drop sizes of this sort do not represent actual drop sizes or distributions and contain whatever deficiencies are implicit in the original model. However, experience indicates that the model has remained valid over a wide range of designs and operating points. Extrapolation to design ranges outside those of empirical data constraints must be suspect. In the particular case of this engine, drop sizes relationships were developed based upon the

(12) Priem, R. J. and Heidman, M. F., Propellant Vaporization as a Design Criterion for Rocket Engine Combustion Chambers, TR-R-67, NASA Technical Report, 1960

(13) Beltran, M. R., et. al., Liquid Rocket Engine Combustion Instability Studies, Final Report, AFRPL-TR-66-125, 1 July 1966

steady-state performance of the thrust chamber assembly. These basically empirical correlations allowed the accurate computation of the vaporization rate as a function of length, culminating in the work presented on Figure No. 60.

D. THE DYNAMIC FORCE MODEL

Gas dynamic forces on the wall of a combustion chamber result from nonaxial flow of gases in the chamber which, in turn, result from nonuniform mass and mixture ratio distribution across the injector face, or unevenly distributed combustion in the chamber. The compatibility model allows evaluation of the magnitude and direction of this nonaxial flow, so that critical zones along the combustion chamber wall can be identified and design changes specified to minimize the gas dynamic forces in these zones. In this particular case, the combustion chamber wall between the baffles and under the baffles were identified as the critical zones. The resulting analysis was directed at determining the net movement of combustion gases from the injector matrix to the areas under the baffles.

The input information required to apply the gas dynamic force model is as follows: mass and mixture ratio distribution across the injector face; resultant momentum and direction of effluent from each element; and energy release profile as a function of axial distance. This information can be readily determined for a given injector-chamber design. The gas dynamic force model then is applied by assuming that each element forms a stream tube of combustion gases, which is represented by a geometric shape characteristic of the element design. The cross-sectional area of each stream tube is a function of the mass flow rate within the stream tube and the relative degree of vaporization achieved by the propellants. The stream tube initiates at the physical location of each element in the injector face and then moves to a new position determined by the energy release pressure profile. This movement is represented by a vector from the center of the original location to the center of its relaxed location. The magnitude and direction of this vector represents the gas dynamic force effect. This effect is shown on Figure No. 61. For this particular case observation, Figure No. 61 reveals that in effect, two stream tubes move from the injector matrix to the area under the baffles. The oxidizer and fuel swept into this zone from the matrix in addition to the baffle coolant, when summed, produce the freestream mixture ratio under the baffles. From inspection of Figure No. 61, note that relatively little gas movement occurs between the baffles. Thus, the local O/F is identical to the vaporized matrix mixture ratio.

E. RESULTS

From Figure No. 59, 14.5 lb/sec-ft mass flow is in the boundary layer at the throat. Between the baffles for an over-all engine mixture ratio of 5.5, this total flow is comprised of 2.2 lb/sec-ft film coolant and 12.30 lb/sec-ft entrained freestream gases. Inspection of Figure 60 reveals that these gases have local freestream O/F at the throat of 5.2. The quotient of

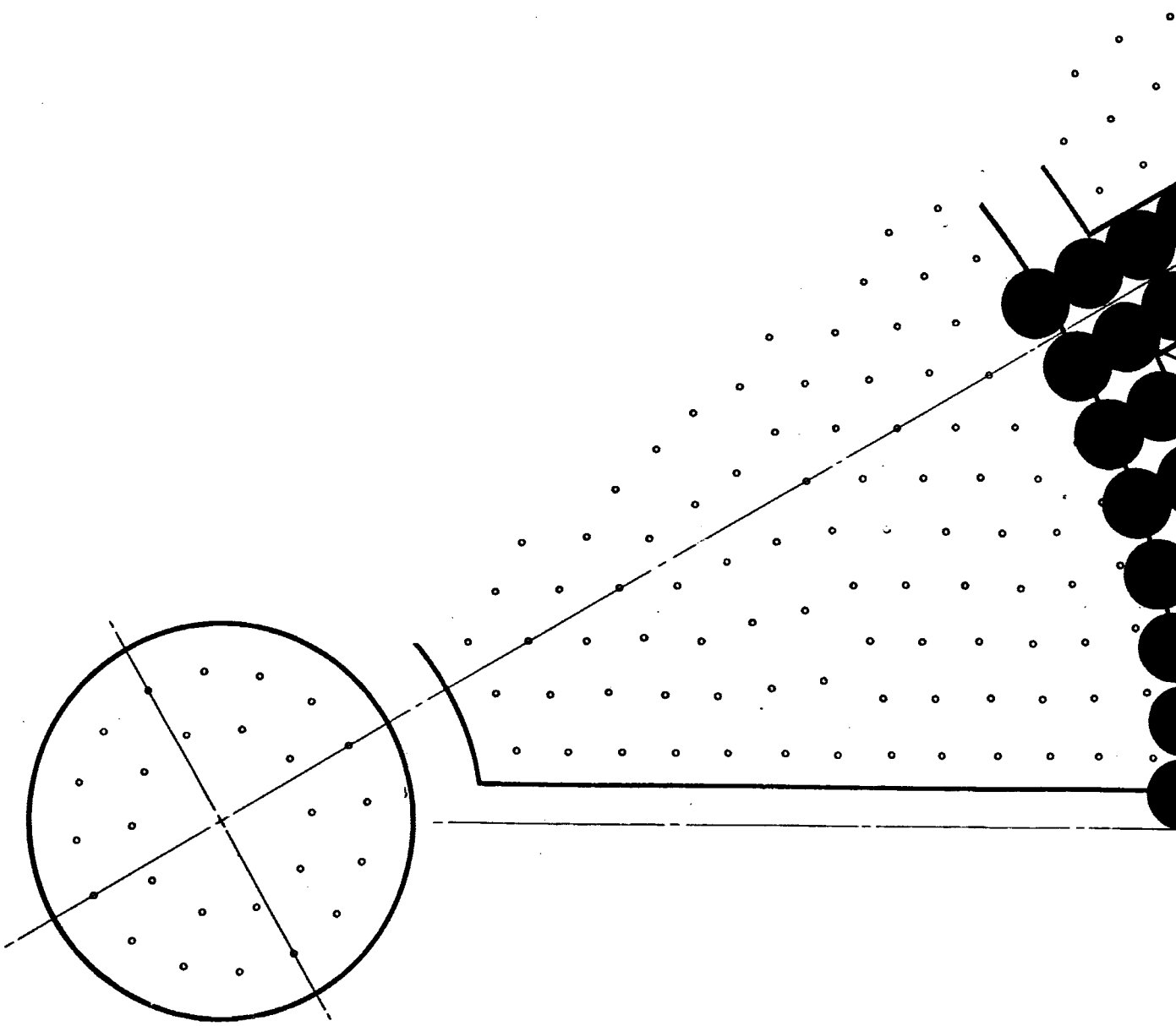

FOLDOUT FRAME 1

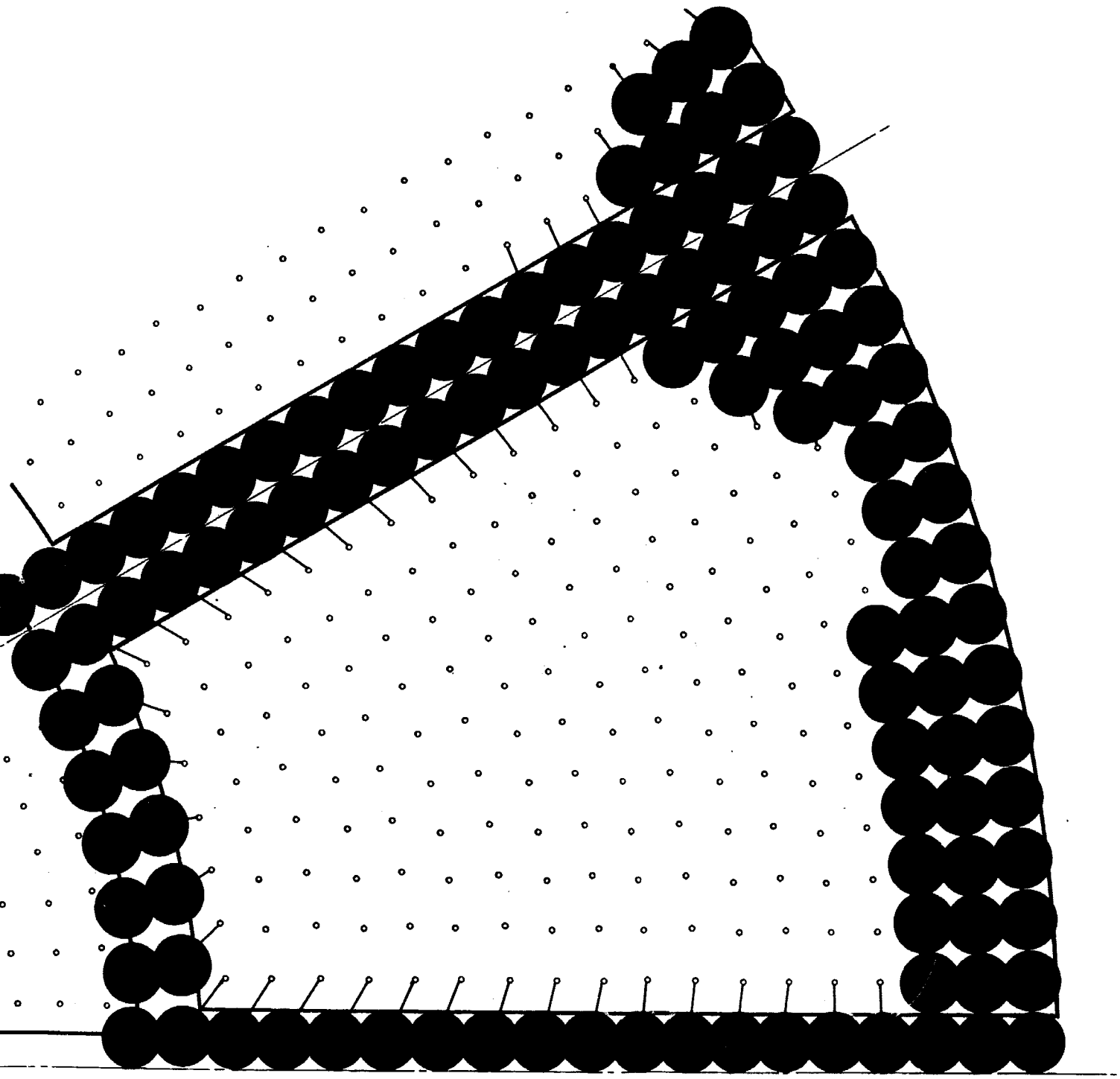

Figure 61. Injector Configuration

the oxidizer to fuel in the boundary layer yields an O/F of 2.5 at the throat. The axial change of mixture ratio for between baffle locations is depicted on Figure No. 62 for over-all engine mixture ratios of 4.5, 5.5 and 6.5.

Under the baffles, the local mixture ratio is 4.4 at throat and the amount of film coolant is 2.3 lb/sec-ft. The entrained 12.20 lb/sec-ft combustion gases when combined with the fuel film coolant yield a local mixture ratio under the baffles lower than that between the baffles. This is depicted on Figure No. 63 at over-all engine mixture ratios of 4.5, 5.5 and 6.5. When the results of this analysis are used to plot the erosion rate data, good correlations were obtained. This data is presented in Appendix A.

V. ABLATIVE CHAMBER ANALYSIS

The analysis of the ablative chamber to determine the temperature response, char, and erosion rates at different axial locations for various boundary layer mixture ratios, was accomplished by the Aerotherm Corp. of Mountain View, California. Aerotherm has developed highly sophisticated computer programs for ablation analysis, and these are not yet available for general use throughout the industry.

The complete Aerotherm Final Report (No. 68-43), entitled "Theoretical Predictions of the Variation of Silica Phenolic Ablation with Liquid Propellant Mixture Ratio," by M. R. Wool and C. B. Moyer is included as Attachment 1 to this appendix.

VI. AVERAGE EROSION RATE IN TERMS OF BOUNDARY LAYER MIXTURE RATIO OR RECOVERY TEMPERATURE

The Aerotherm report (Appendix B to Attachment 1) also presents the predicted erosion rate in terms of the non-dimensional parameter.

$$B'_{ave} = \frac{\rho_{char}\ \dot{S}_{ave}}{\rho_e\ V_\infty\ C_h}$$

and the mass fraction of oxygen in the boundary layer. While the non-dimensional form is meaningful to the analyst, a dimensional form also is of general interest. Thus, the Aerotherm results have been replotted in terms of the actual erosion rate and the boundary layer mixture ratio and recovery temperature. Figures No. 64 through No. 66 show the average erosion rate at the throat, exit, and chamber respectively versus mixture ratio. Figures No. 67 through No. 69 show the same data in relationship to recovery temperature. Recovery temperature here is evaluated at the given mixture ratio.

The pattern of the predictions is as much the same as in the non-dimensional plots. However, there is, a greater separation between indicated values for the two chamber pressure; less severe erosion accompanies lower pressure at a given mixture ratio, as would be expected. In the non-dimensional

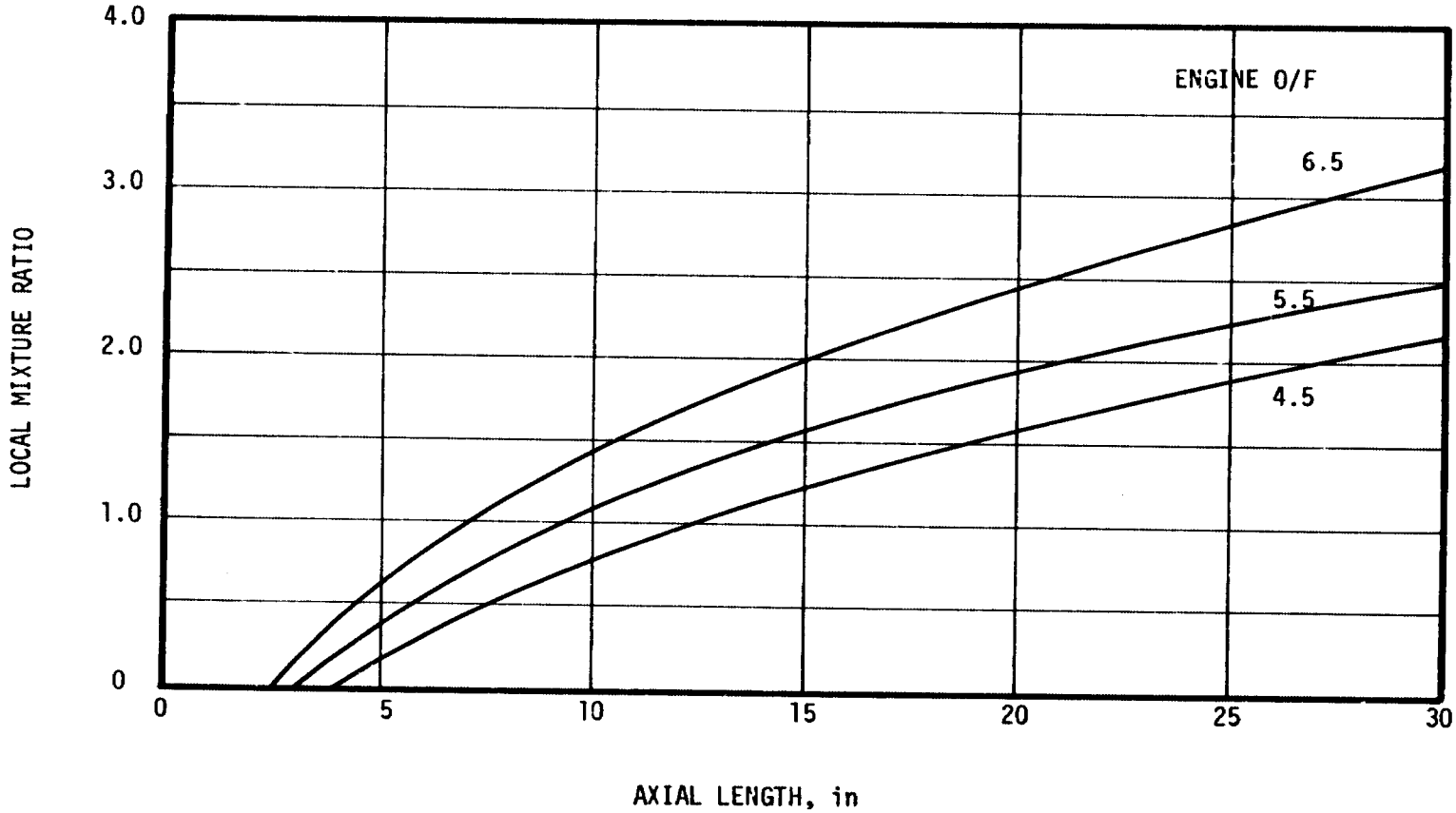

Figure 62. Between Baffles Local Mixture Ratio Profile

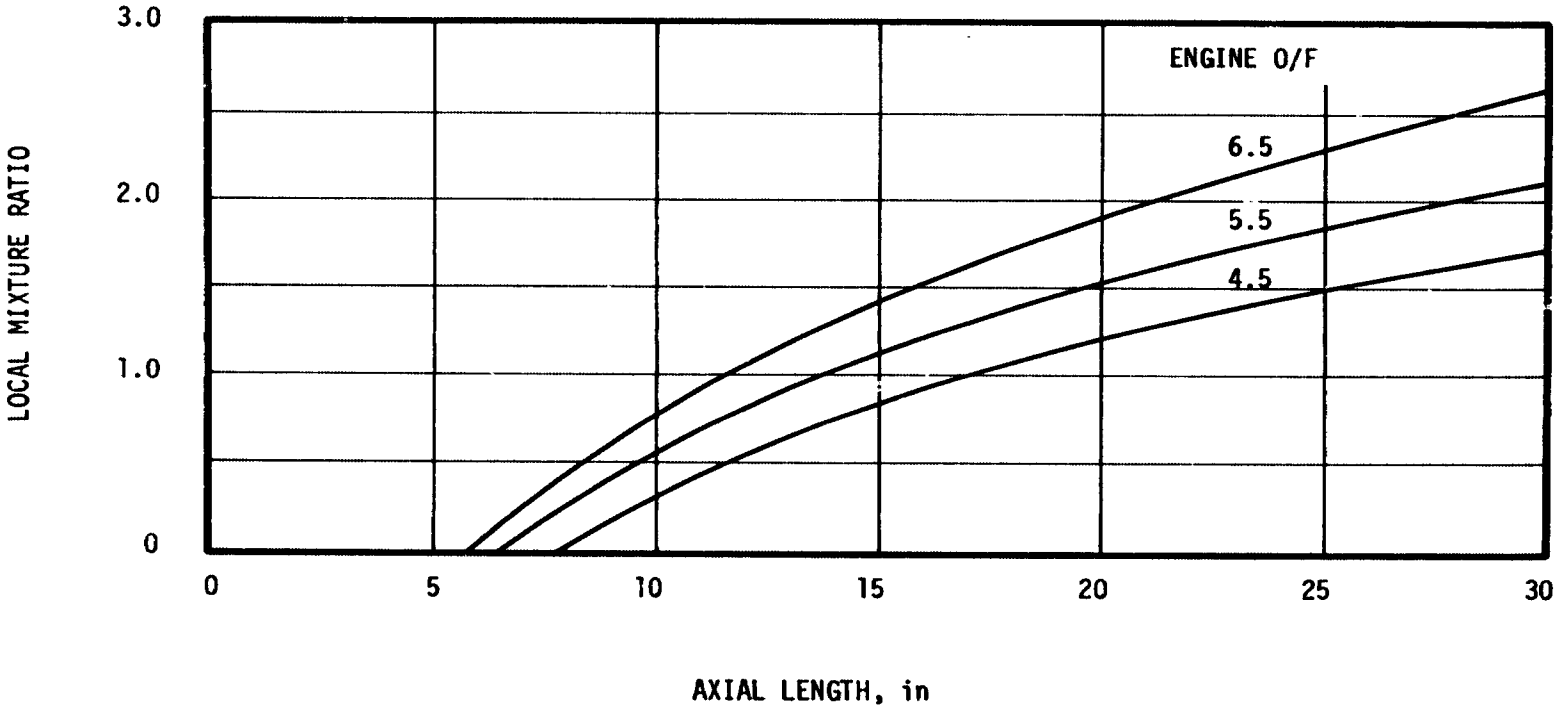

Figure 63. Under Baffles Local Mixture Ratio Gradient

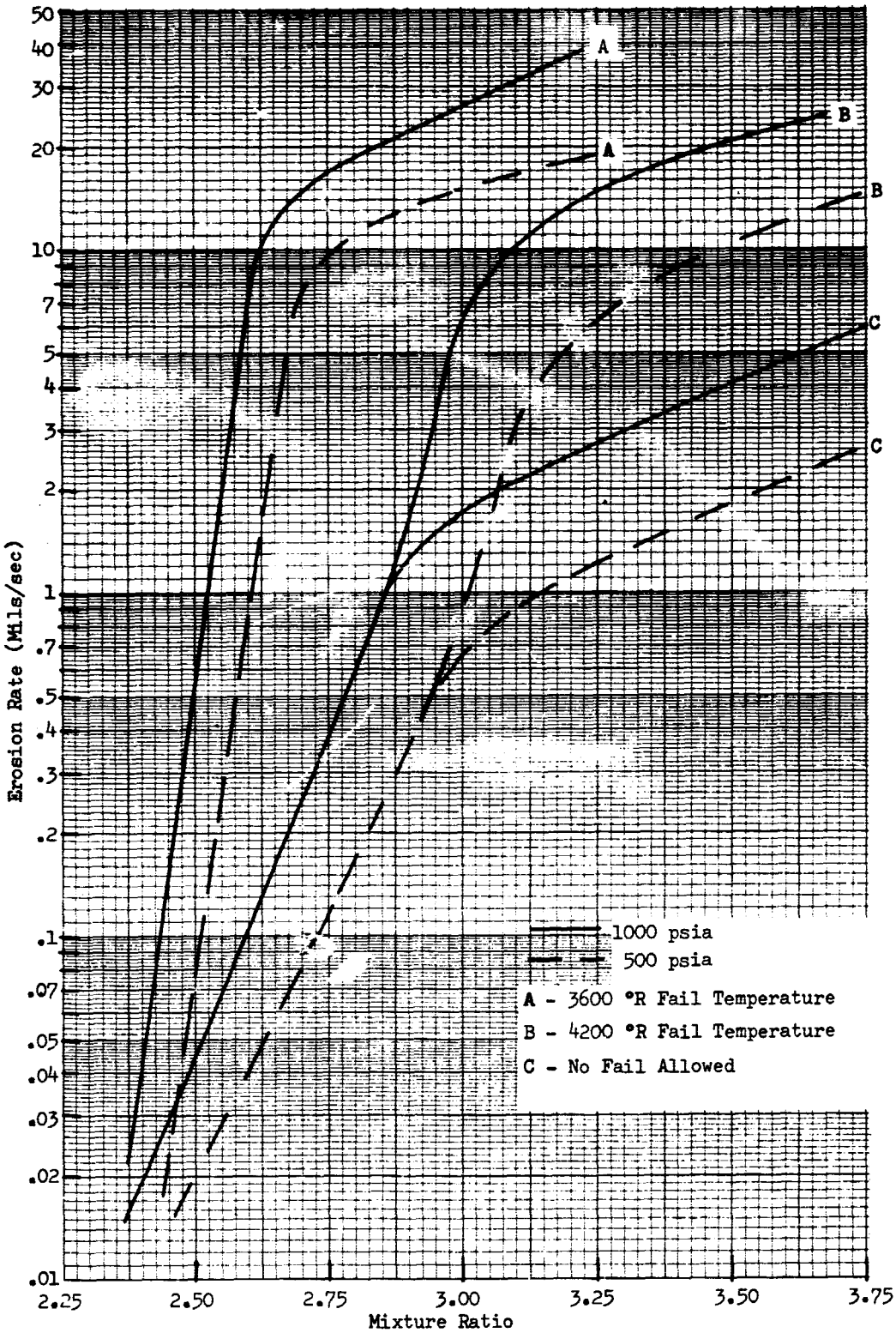

Figure 64. Average Erosion Rates vs Mixture Ratio of Boundary Layer (Throat)

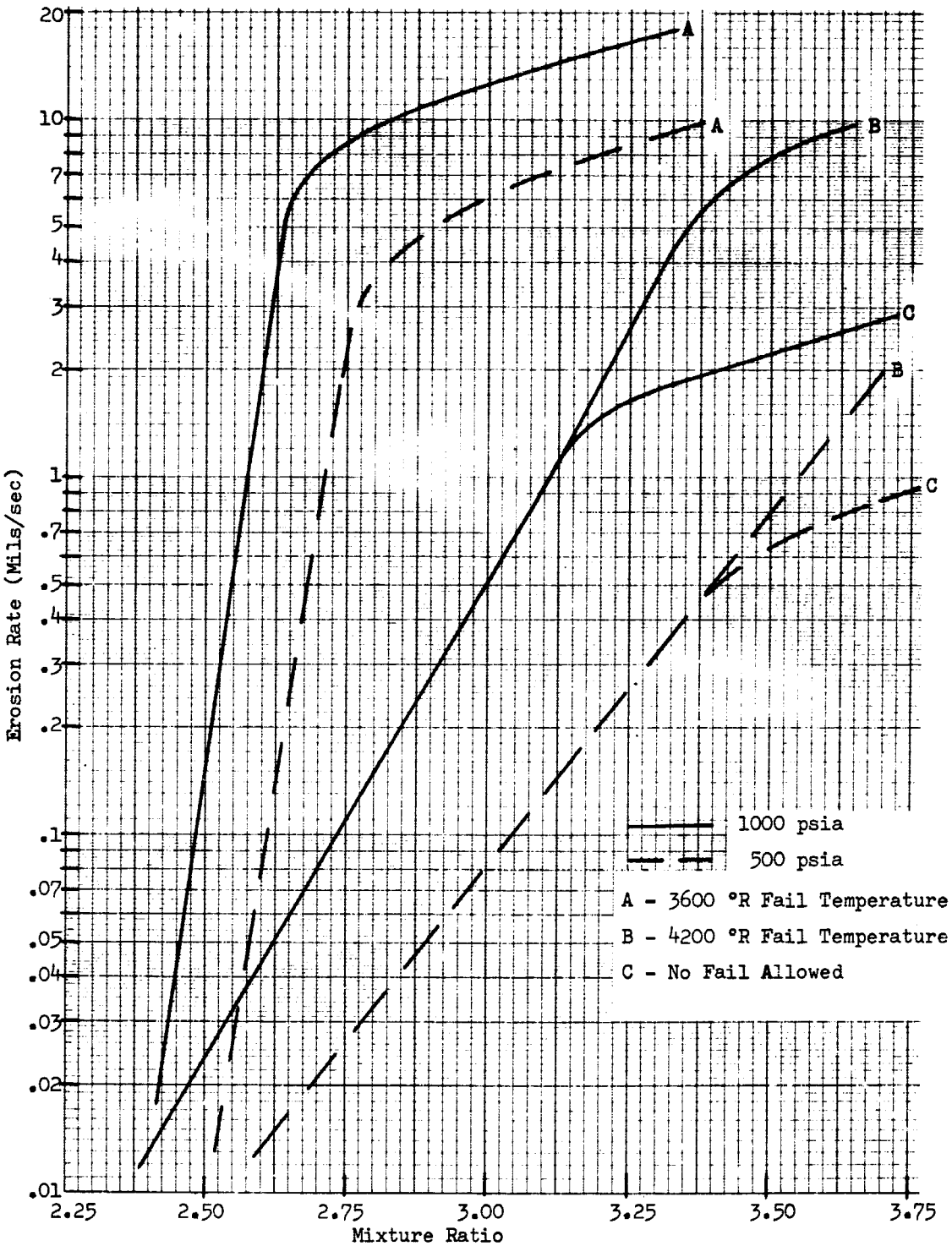

Figure 65. Average Erosion Rates vs Mixture Ratio of Boundary Layer (Chamber)

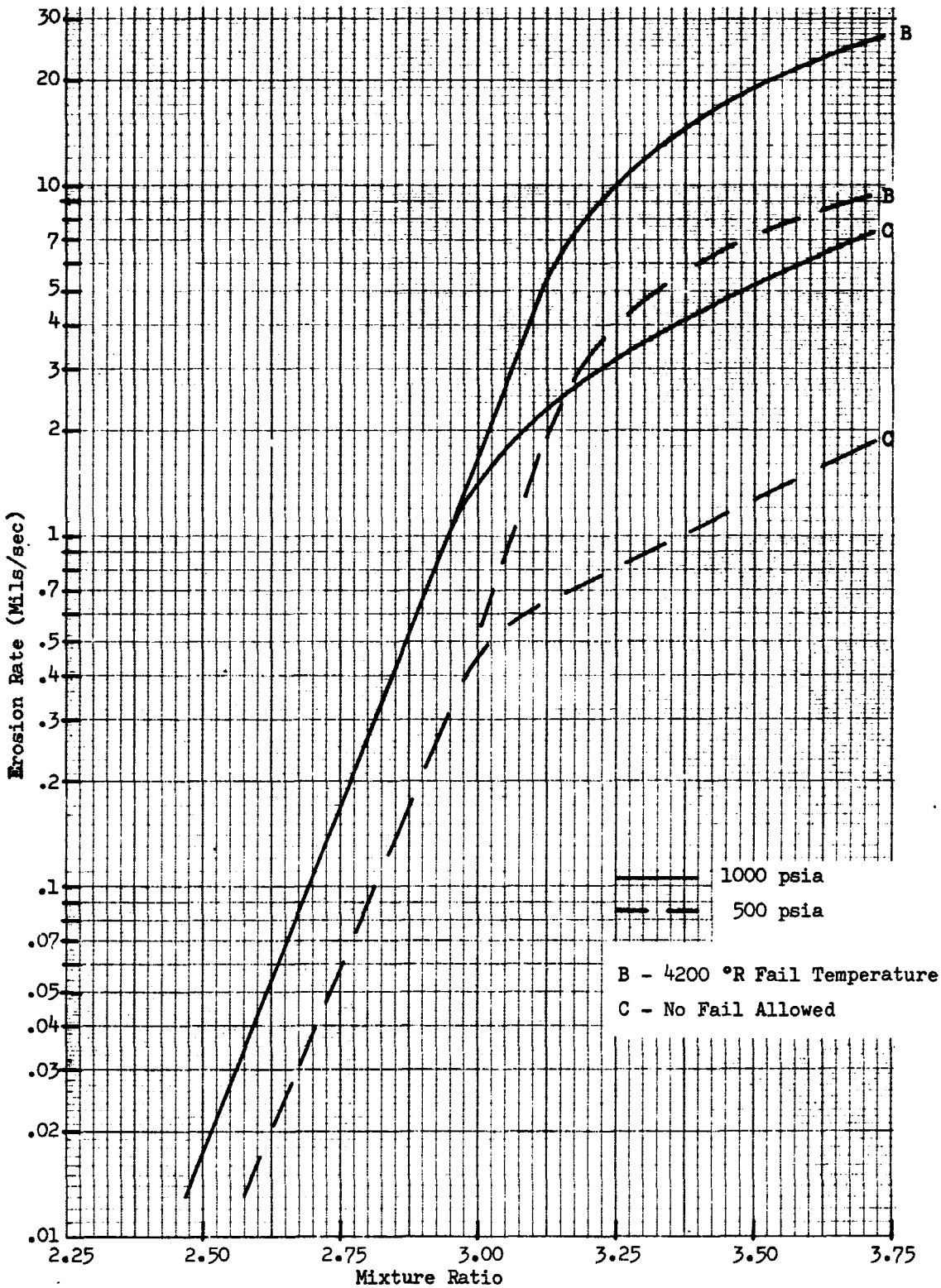

Figure 66. Average Erosion Rates vs Mixture Ratio of Boundary Layer (Chamber)

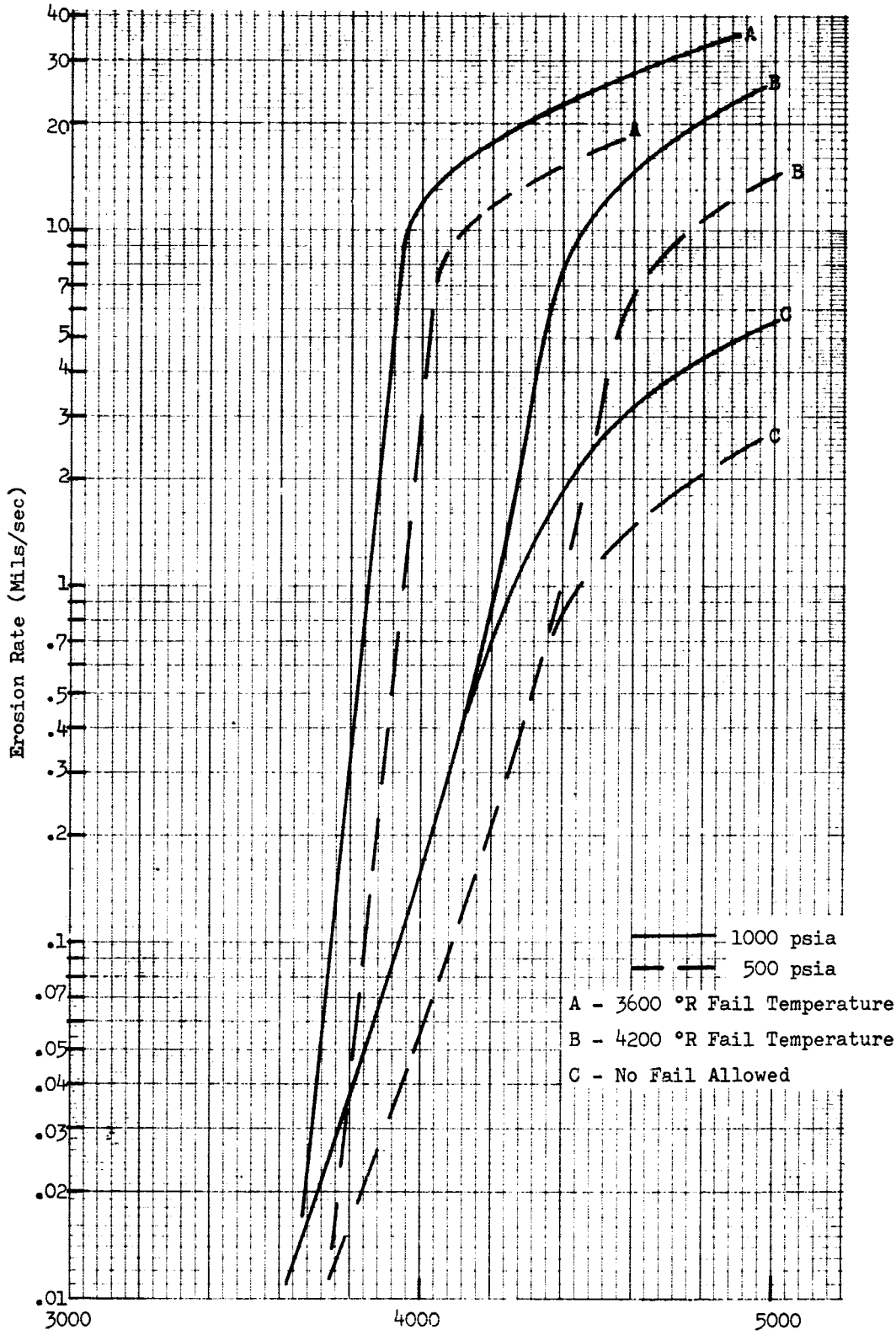

Figure 67. Average Erosion Rates vs Boundary Layer Temperature (Throat)

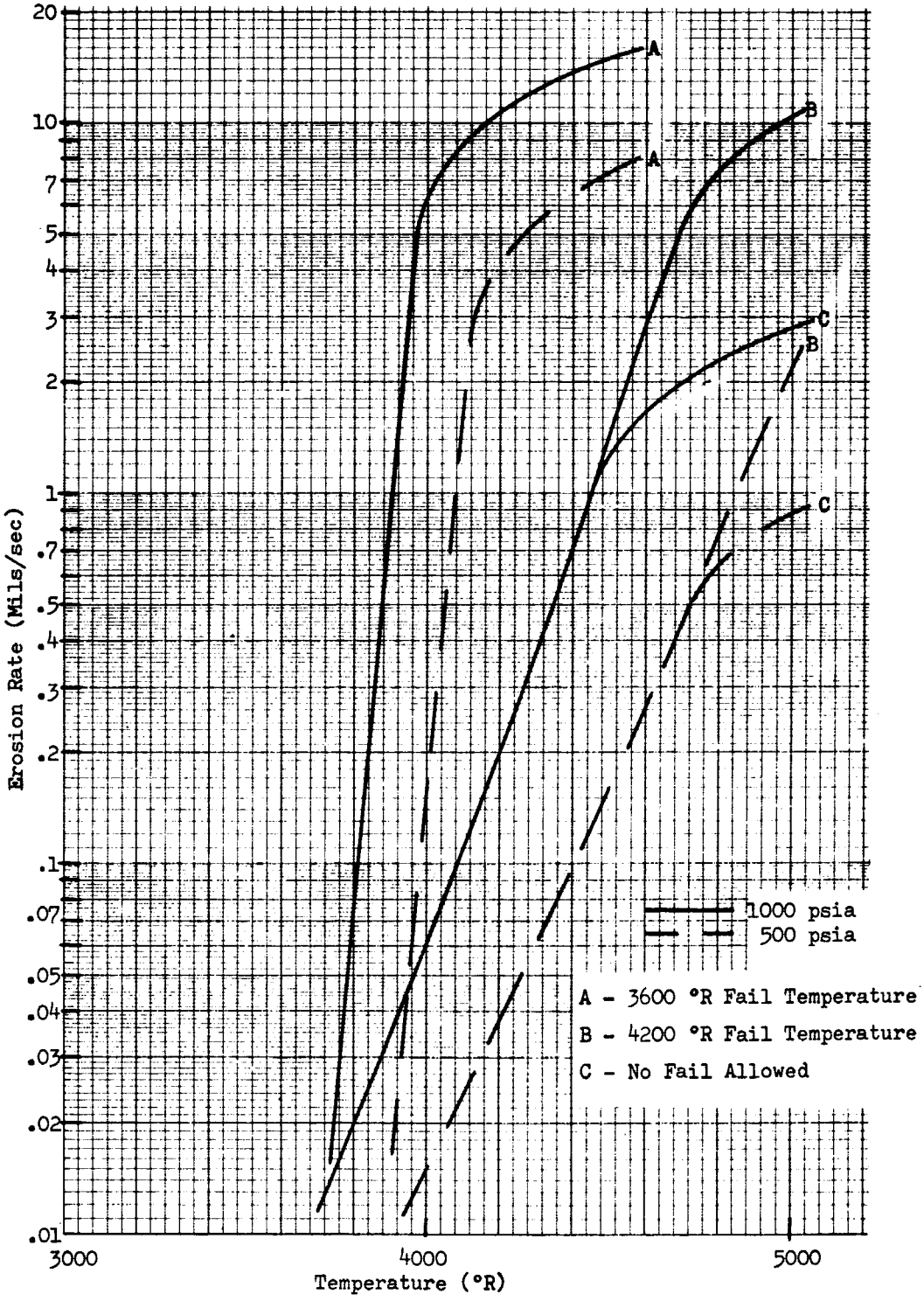

Figure 68. Average Erosion Rates vs Boundary Layer Temperature (Exit)

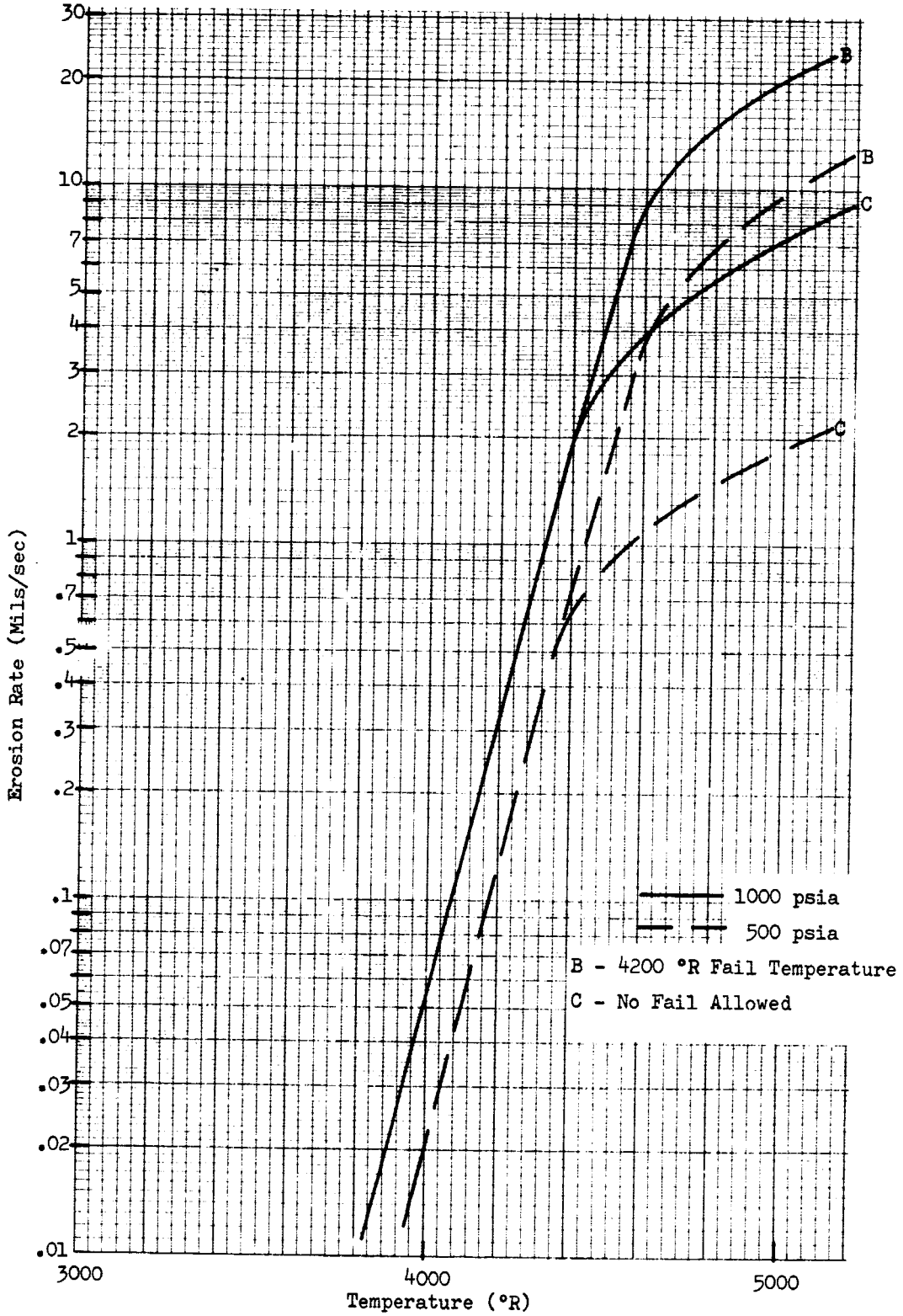

Figure 69. Average Erosion Rates vs Boundary Layer Temperature (Chamber)

plots, the smaller heat transfer coefficient, C_h, at the lower pressure compensates for the lower erosion rate, and yields comparable non-dimensional rates for both pressures in several cases.

The figures again illustrate the sensitivity of erosion rate to the boundary layer composition, regardless of the assumed material fail temperature. Also, they highlight the difficulty of matching measured erosion rates with predicted values.

Aerotherm

Final Report No. 68-43

THEORETICAL PREDICTIONS OF THE VARIATION OF SILICA PHENOLIC ABLATION WITH LIQUID-PROPELLANT MIXTURE RATIO

by

Mitchell R. Wool
Carl B. Moyer

Prepared for

Aerojet-General Corporation
Sacramento, California

Purchase Order No. 104487 Aerotherm Project No. 6085

Appendix E, Attachment 1

TABLE OF CONTENTS

List of Tables

List of Figures

List of Symbols

A	nozzle flow area
B_i	pre-exponent for the ith component in the decomposition equation
B'	nondimensional ablation rate ($= \dot{m}/\rho_e U_e C_M$), various subscripts
β	one of three specific heat curve fit constants
C_h	Stanton number heat transfer coefficient
C_M	mass transfer coefficient
∂	partial derivative
E_{a_i}	activation energy of the ith component in the decomposition equation
ϵ_w	surface emissivity
F	radiation view factor, various subscripts
Γ	resin volume fraction
h	enthalpy, various subscripts
K	mass fraction
$\dot{m}$	mass flux, various subscripts
P	pressure
Pr	Prandtl number
Ψ_i	density exponent for the ith component in the decomposition reaction
q	energy flux, various subscripts
Qr	net radiant efflux from a given nozzle location
R	gas constant
ρ	density, various subscripts
$\dot{s}$	surface recession rate
σ	time
U,v	velocity

Subscripts

A,B,C	components of decomposition reaction
c	char
e	edge gas
g	pyrolysis gas
i	symbolic component of decomposition reaction
o	total or nonablating or original or oxygen
r	recovery or radiant or residual
s	static or surface
ss	steady state
v	virgin material
w	surface
x	moles of O_2Si per mole of C_6H_6O in virgin material
y	constant depth below ablating surface

Superscripts

*	throat location or condensed phase
~	elemental

THEORETICAL PREDICTIONS OF THE VARIATION OF SILICA PHENOLIC ABLATION WITH LIQUID PROPELLANT MIXTURE RATIO

1. Introduction

Aerotherm Corporation has performed computer solutions for the transient thermal ablative response of WBC 2230, silica phenolic nozzle insulation material for five O_2/H_2 liquid rocket propellant mixture ratios ranging from 2.50 to 3.75. Three nozzle locations ($A/A^* = -1.4$, 1.0 and 2.0) for each of two chamber pressures (500 psia and 1000 psia) were predicted. The matrix of cases is defined more completely in Section 3. The primary purpose of the study was to explore the effect of boundary layer mixture ratio on the predicted total recession allowing both thermochemical and mechanical (melting) ablation. The computer codes utilized in the analysis are described in Section 2. Input quantities to the surface thermochemistry code are presented in Section 3, and results of the calculations are described in Section 4. Additional input quantities required to perform the transient heating calculations are given in Section 5. These results are then presented and summarized in Section 6.

2. Computer Codes Employed

The basic thermal response was calculated utilizing the Aerotherm Charring Material Ablation (CMA) computer program. This code performs the transient in-depth heat conduction plus pyrolysis generation computation and couples it to a surface energy balance boundary condition. The solution procedure is briefly described in Appendix A and more completely in References 1-4.

The surface thermochemical input required by CMA to calculate the surface energy balance boundary condition is prepared utilizing the Aerotherm Chemical Equilibrium (ACE) computer program. In the surface equilibrium mode, this code computes the thermochemically controlling surface species and accounts for heated surface mass balances for each chemical element in the system allowing for all possible surface equilibrium reactions. In the case where the gas phase

equilibrium temperature computed for non-failing ablation is higher than the specified melt temperature of the candidate surface species, that species will be "mechanically" removed from the surface until either the computed surface temperature equals the fail temperature or the species no longer controls the surface equilibrium. Additional discussion of the ACE program are included in Appendix A and References 5 and 6.

3. Surface Thermochemical Calculation Input

The equilibrium surface thermochemical response of the WBC 2230 silica phenolic to a variation of the O_2/H_2 liquid propellant mixture ratio was evaluated utilizing the ACE computer program. At the outset, it was assumed that equal diffusion coefficients could be employed to accurately characterize the diffusion of species to the surface. This simplification reduces both the required input to the ACE computation and the number of cases needed to evaluate the material response with only a slight reduction of accuracy (see Sections 4 and 6). Considering only equal diffusion coefficients, the input required to obtain the necessary surface thermochemical data is described and presented below.

The quantities which must be supplied to the ACE program are as follows:

System pressure

Relative masses of components in a particular solution (per unit of edge gas diffused)

Fail temperatures for all candidate surface species

Elemental composition of boundary layer edge gas, pyrolysis gas, and charred material

Thermodynamic data for all species considered

To sufficiently define the response of the WBC 2230 silica phenolic to the varying environments considered in the analysis, an extensive matrix of surface calculations was performed. The ranges of input quantities are summarized below:

Mixture ratios of 3.75, 3.25, 3.00, 2.75, 2.50

O_2Si fail temperatures of 3600 ^{o}R, 4200 ^{o}R and ∞

Pressures of 4, 16 and 60 atmospheres for each mixture ratio and fail temperature

Ablation rates (Both B'_{char} and B'_{gas}) from 0.0 to 3.0 for each pressure.

The range of O_2Si * fail temperatures employed provides a means of evaluating the importance of this effect. The values of pressure were chosen to enable accurate interpolation to the pressures at the various nozzle locations. Similarly, sufficient B' values were computed to ensure accurate interpolations in each surface thermochemistry table. The complete matrix of cases is summarized in Table 1.

The elemental compositions of the boundary layer edge gases were defined for each mixture ratio and are presented in Table 2. To define the compositions of the pyrolysis gas and char constituents, data from References 7 and 8 were obtained and compared. A consistent set of data for the WBC 2230 silica phenolic was not attained. However, the compositions of char and pyrolysis gas were computed by making several reasonable and experimentally substantiated assumptions. These are:

Reinforcement molecular composition	O_2Si
Resin molecular composition *	C_6H_8O
Resin residual molecular composition	C
Fraction of resin remaining as residual (by mass)	0.40
Fraction of virgin material which is resin (by mass)	0.31

The calculated relative elemental composition for the pyrolysis gas and char are presented in Table 3. It should be noted that these compositions are within the apparent experimental error of the available data.

The thermodynamic data required as input to the ACE computer program is as follows:

Heat of formation at 298 ^{o}K

Sensible enthalpy rise from 298 ^{o}K to 3000 ^{o}K

Curve fit constants (β_o, β_1, β_2) to evaluate specific heat (Cp) from $Cp = \beta_o + \beta_1 T + \beta_2 T^{-2}$ where T is temperature in deg.K.

Entropy at 3000 ^{o}K and 1 atmosphere

Species phase designation

* See Reference 9

4. Equilibrium Surface Thermochemistry Results

In this section, a few of the more interesting ACE results are discussed. First, in the range of ablation where the solutions were found, the surface species was always silica, O_2Si^*, and in most cases it was being failed mechanically. The selection of the fail temperature for O_2Si^* of 3600 ^oR and 4200 ^oR caused silica to fail from the surface for values of B'_{char} above 0.01 for all mixture ratios considered.

By inspection and comparison of several ACE results, the primary mechanisms of surface removal were qualitatively defined for both non-failing and fail allowed cases. When the silica species is allowed to fail, the carbon in the char is consumed through the attack by the H_2O diffusing from the boundary layer edge, in an amount necessary to achieve the specified B'_{char}. To obtain the same B'_{char} without allowing failing, the silicon species are removed either by vaporization (O_2Si vapor) or by reduction of the O_2Si^* to OSi (vapor), most notably by the following reaction:

$$O_2Si^* + C^* \rightarrow OSi + CO$$

For either of these reactions to occur, however, the surface temperature and enthalpy must be increased above the fail allowed value, and the relative amount of energy required to obtain a given B'_{char} solution is increased. Hence, as expected, a given energy input results in a higher recession with fail allowed than with no fail allowed.

A second point of interest concerns the effects of assuming equal diffusion on the ACE results. From the above discussion, for a failing silica surface, H_2O diffusion would be expected to affect the surface recession. However, since there is an excess of H_2O available at the surface for all mixture ratios, a small change of H_2O diffusion rate would not be expected to alter the resulting ablation rates. In addition, because O_2Si^* remains as the controlling surface species for the fail temperatures specified in these systems, carbon consumption does not affect the recession except as it alters the energy events at the surface.

5. Input to the Transient Material Ablation Prediction

The transient in-depth heat conduction plus pyrolysis generation performed by the CMA computer program requires as input the following property data:

- Thermal conductivity of virgin and charred materials
- Specific heats of virgin and charred materials
- Heats of formation at 298 ^{o}K for virgin material, char and pyrolysis gas.
- Sensible enthalpy of pyrolysis gas above 298 ^{o}K
- Virgin and residual densities of three decomposition components
- Resin volume or mass fraction
- Kinetic constants in the three decomposition reactions
- Layout of nodal network
- Surface boundary condition specification

The values of these variables utilized in this analysis are presented and discussed in Section 5.1.

For this study the surface boundary condition was defined by coupling the in-depth response to a surface energy balance calculation. The input required for this option is as follows:

- Surface thermochemical energy terms as a function of pressure, B'_{gas} and B'_{char} (computed by the ACE program)
- Heat transfer coefficient
- Ratio of heat to mass transfer coefficients
- Surface emissivity and view factor
- Incident radiation heat flux
- Boundary layer edge gas recovery enthalpy

These input quantities are described in Section 5.2.

5.1 In-depth Response Computation Input

The property data required to solve the in-depth conduction and decomposition problem were supplied by Reference 7. Thermal conductivity and specific heat values for both virgin and fully charred materials are presented in Figures 1 and 2. Heats of formation of virgin material, char and pyrolysis gas are summarized below:

Material	Heat of Formation at 298 ^{o}K (Btu/lb)
Plastic	-4875.0
Char	-5670.0
Pyrolysis Gas	-2000.0

The resin mass fraction was 0.31

Pyrolysis gas sensible enthalpies and decomposition kinetic constants were also provided by Reference 7 but slight adjustments were required to obtain a consistent problem formulation. As noted in Section 3, the composition of the pyrolysis gas was recalculated. The equilibrium variation of enthalpy with temperature for the revised composition was utilized in the material response predictions. A linear variation of the sensible enthalpy increase above 298 ^{o}K was assumed. At 5500 ^{o}R, the enthalpy increase was 6800 Btu/lb. The heat of formation value given above was not altered.

In a few initial CMA calculations where kinetic constants from Reference 7 were utilized, a substantial portion of the resin was not pyrolyzed at temperatures where complete charring should have occurred. When the nondecomposed resin enters the surface node, computational as well as physically unrealistic problems are encountered. Since only char material with a density of 59.2 lb/ft^3 can leave the surface (computational constraint) and since the incompletely charred material is substantially more dense than the char, a net build up of material on the surface occurs until the computation becomes unstable. In order to insure that complete pyrolysis would occur, kinetic decomposition data reported in Reference 10 was utilized with density values specified by Reference 7. The two sets of data are compared in Table 4. Also, typical density versus temperature curves generated using the two sets of kinetic data are compared in Figure 3. It is apparent that the kinetics of Reference 10 produce faster decomposition above 2000 ^{o}R.

The nodal network utilized in the CMA predictions was selected so that stable solutions were ensured. A stability criterion utilized to determine node sizes is discussed in Reference 1. A typical nodal network used in this study is shown schematically in Figure 4.

5.2 Surface Energy Balance Input

The equilibrium surface thermochemistry tables were generated utilizing the ACE computer program as described in Sections 2 and 3.

The net radiant energy efflux from a given nozzle location to cold surfaces was defined by Reference 7 as,

$$Q_r = F\epsilon_w \sigma T_w^4$$

where F = the view factor from the nozzle location to all cold surfaces (fuel injector and exit plane)

ϵ_w = surface emissivity = 0.95 (Reference 7)

σ = Stefan-Boltzmann's constant

T_w = surface temperature

The radiant energy interchange between two hot nozzle locations is assumed to be zero. The table below summarizes the radiation view factors defined by Reference 7.

Location	Area Ratio	$F_{injector}$	F_{exit}	F_{total}
Chamber	-1.4	0.279	0.084	0.363
Throat	1.0	0.082	0.272	0.354
Exit	2.0	0.0	0.738	0.738

The heat transfer coefficient values defined by Reference 7 are presented in Figure 5 as a function of normalized axial pressure drop for both 1000 psia and 500 psia chamber pressures. These transfer coefficient values from Reference 7 were evaluated utilizing the simplified Bartz equation (Reference 11). For this analysis, it was assumed that heat and mass transfer coefficients were equal, thus substantially reducing the computational requirements for the program. Note that errors introduced by this assumption are within the uncertanties introduced by the Bartz approximation.

The boundary layer edge recovery enthalpy was defined by adding the static enthalpy at the sonic location to a recovery factor corrected kinetic energy term for the entire range of mixture ratios, according to the following formula:

$$h_r = h_s + (Pr)^{1/3} Cp(T_o - T_s)$$

where h_r is recovery enthalpy

h_s is static enthalpy at sonic location
T_o is total temperature
T_s is static temperature at sonic location

For each mixture ratio computed, total temperature was defined as the adiabatic flame temperature of that mixture. The recovery enthalpy is presented in Figure 6 as a function of mixture ratio. The recovery enthalpy was assumed independent of nozzle location.

6. Presentation and Discussion of Transient Ablation Predictions

Table 5 presents a summary of the results of all transient CMA predictions. For all predictions, the surface temperature, recession rate, and B'_{char} rise within a few seconds to a value which remains fairly steady for the problem duration. The surface temperature values given in Table 5 are at a duration of 25 seconds. The recession rate ($\dot{s}_{ave}$) was defined as the total recession divided by the duration, and the average B'_{char} (B'_{ave}) was defined by:

$$B'_{ave} = \frac{\rho_{char}\dot{s}_{ave}}{\rho_e U_e C_{h_o}}$$

A better overview of the surface recession variation with mixture ratio is given in Figures 7a, b and c (throat, exit and chamber locations, respectively). The graphs show the very strong dependence of B'_{ave} on the mass fraction of oxygen in the boundary layer edge gas ($\tilde{K}_{o_e}$). Figures 8a, b and c, again for throat, exit and chamber locations, show the surface temperatures (at 25 seconds) for the same cases and reveal, again, a strong dependence on $\tilde{K}_{o_e}$. Figure 8, also demonstrates where the specification of O_2Si^* fail temperature effects ablation prediction. When surface temperature is below the specified fail temperature, only thermochemical ablation occurs. For solutions at the specified fail temperature, melt removal occurs.

Both the strong B'_{char} and surface temperature trends with $\tilde{K}_{o_e}$ are primarily due to the same effect: the model utilized to define the edge gas recovery enthalpy caused the recovery temperature to rise drastically with $\tilde{K}_{o_e}$ (probably at a linear rate suggested by the

slope of the lines in Figure 8). The energy input to the surface is, of course, strongly dependent on the edge recovery temperature. Moreover, this effect is substantiated by a brief inspection of the ACE output at a typical surface solution point. Even at a mixture ratio of 2.50 ($\tilde{K}_{o_e}$ = 0.714), ample oxygen in the form H_2O is available at the surface for oxidation of all carbon in the char and pyrolysis gases. In a given problem, the recession rate is therefore dependent on the energy available to melt and remove the O_2Si^* surface, because the carbon in the char is screened and protected by the silica on the surface. In the problems that are strongly transient, pyrolysis gases also tend to inhibit char carbon oxidation.

In this respect it may be noted that detailed study of the CMA output indicates that the results for cases where recession rates are low ($B'_{char} < 0.02$) represent highly transient situations (even though the wall temperature is fairly steady), whereas for $B'_{char} > 0.05$ the prediction approaches a quasi-steady state solution.

An interesting and important steady state reference ablation rate ($B'_{c_{ss}}$) is derived in Appendix B. The analysis is based on the assumption that carbon (C*) and not silica (O_2Si^*) is the controlling surface species, and that the carbon is only allowed to ablate by combination with oxygen at the surface to form carbon monoxide gas (CO). This would occur if all O_2Si^* at the surface were required to be mechanically removed. The analysis requires that all elemental oxygen diffusing to the surface must consume free (non oxidized) carbon. Thus ablation is limited by the rate of oxygen diffusion. The result is as follows:

$$B'_{c_{ss}} = 2.62\, \tilde{K}_{o_e}$$

Figures 7 and 8 reveal another important conclusion: predicted recession rates in the range of mixture ratios studied is a strong function of the assumed fail temperature. As explained earlier, the assumed fail temperature strongly effects the surface energy terms. In the analysis of materials whose melt temperatures are accurately known, this situation can be accepted with equanimity. With silica, however, there is no single temperature where a total phase change occurs. Rather, the material becomes gradually less viscous over a range of temperatures between 3400 ^{o}R and 4400 ^{o}R. Without a fixed

melt temperature, the actual surface melt phenomena are determined by complex liquid-layer physics and probably cannot be very well simulated by the fail temperature approach. Thus the selection of the fail temperature for silica almost requires that the surface temperature "answer" be known in advance.

Fortunately, for silica phenolic the "answer" is known. Firstly, observations of the temperature of silica phenolic surfaces during ablation in oxidation environments tend to cluster at around 4000 ^{o}R to 4200 ^{o}R. Secondly, there is abundant evidence that the silica and carbon in the char begin to react rapidly at around 4000 ^{o}R (References 12 and 13). This destroys the carbon matrix in the neighborhood of the surface and allows the silica to flow away. Thus a reasonably accurate estimate for a silica fail temperature is 4200 ^{o}R. To define the effective recession extremes, several calculations were also done for 3600 ^{o}R fail temperature and for no failing (infinite fail temperature). The expected ablation answers, however, are in the neighborhood of the 4200 ^{o}R results.

References

1. Moyer, C.B., and Rindal, R.A.: Finite Difference Solution for the In-Depth Response of Charring Materials Considering Surface Chemical and Energy Balances. Aerotherm Corporation, Palo Alto, California, Final Report 66-7, Part II, March 14, 1967 (also NASA CR-1061, June, 1968).

2. Aerotherm Corporation, Palo Alto, California: Users Manual, Aerotherm Charring Material Ablation Program, Version 2, January, 1966.

3. Aerotherm Corporation, Palo Alto, California: Fortran Variable Names, Aerotherm Charring Material Ablation Program, Version 2, February, 1966.

4. Aerotherm Corporation, Palo Alto, California: Flow Charts, Aerotherm Charring Material Ablation Program, Version 2, April 1966.

5. Aerotherm Corporation, Mountain View, California: Users Manual, Aerotherm Chemical Equilibrium Program (ACE), in preparation.

6. Kendall, R.M.: A General Approach to the Thermochemical Solution of Mixed Equilibrium - Nonequilibrium, Homogeneous Systems. Aero-Therm Report No. 66-7, Part V. March 14, 1967 (also NASA CR-1064, June, 1968).

7. Private Communication with Aerojet Personnel, Roy Michel and Frank Miller. November 6, 1968.

8. Ladacki, M., Hamilton, J.V., and Cohz, S.N.: Heat of Pyrolysis of Resin in Silica-Phenolic Ablator. AIAA Journal, Vol. 4, No. 10, October, 1966, pp. 1798-1802.

9. Sykes, G.F.Jr.: Decomposition Characteristics of Char-Forming Phenolic Polymer Used for Ablative Composites. NASA TN D-3810, February, 1967.

10. Schaefer, J.W. and Dahm, T.J.: Studies of Nozzle Ablative Material Performance for Large Solid Boosters. NASA CR-72080, Aerotherm Report No. 66-2, December 15, 1966.

11. Bartz, D.R.: A Simple Equation for Rapid Estimation of Rocket Nozzle Convective Heat-Transfer Coeffecients. Jet Propulsion January, 1957, p. 49.

12. Rindal, R.A., Clark, K.J., Moyer, C.B.,and Flood, D.T.: Experimental and Theoretical Analysis of Ablative Material Response in a Liquid-Propellant Rocket Engine. Aerotherm Corporation, Palo Alto, California, NASA CR-72301, September 1, 1967.

References Concluded

13. Seader, J.D., Larsen, J.V., Thompson, R.W., and Chidley, J.D., Catalysis of Internal Endothermic Ablative Reactions between Char and Reinforcement. AIAA Paper No. 68-505, June, 1968

14. Schaefer, J.W., Dahm, T.J., Rodriguez, D.A., Reese, J.J.Jr., and Wool, M.R.: Studies of Ablative Material Performance for Solid Rocket Nozzle Applications. NASA CR-72429, Contract NAS 7-534, Aerotherm Report No. 68-30, March 1, 1968.

Table 1

Matrix of ACE Tables Generated*

Fail Temperature (^{O}R)	Mixture Ratio	Pressure (atm)
∞	3.75	4.0 16.0 60.0
4200.	3.75	4.0 16.0 60.0
	3.25	4.0 16.0 60.0
	3.00	4.0 16.0 60.0
	2.75	4.0 16.0 60.0
	2.50	4.0 16.0 60.0
3600.	3.75	4.0 16.0 60.0
	3.25	4.0 16.0 60.0
	2.75	4.0 16.0 60.0

* Each ACE Table Includes an 8 x 11 B'_g, B'_c matrix

Table 2

Elemental Mass Fractions of Edge Gas Systems

Element	Mixture Ratio				
	3.75	3.25	3.00	2.75	2.50
Hydrogen, H	0.211	0.236	0.250	0.266	0.286
Oxygen, O	0.789	0.761	0.750	0.734	0.714

Table 3

Elemental Compositions of Char, and Pyrolysis Gas*

Element	Elemental Mass Fractions	
	Char	Pyrolysis Gas
Hydrogen, H	-	0.107
Carbon, C	0.151	0.611
Oxygen, O	0.452	0.282
Silicon, Si	0.397	-

* WBC 2230, Silica Phenolic:
31 % resin fraction, 40% residual mass, C_6H_6O resin formula

Table 4

Comparison of Internal Decomposition Kinetic Data

Component	Densities		Pre Exponential Factor	Density Exponent	Activation Energy Factor	Reaction Zone Temperature
	Initial	Residual				
i	ρ_{o_i}, lb/ft^3	ρ_{r_i}, lb/ft^3	B_i, (sec)$^{-1}$	ψ_i	E_{a_i}/R, ^oR	T_{min}, ^oR
Reference 7						
A	19.35	0.00	9.13×10^{-2}	1.43	4.32×10^3	560.
B	37.10	0.00	3.52×10^{14}	4.07	4.89×10^4	1200.
C	112.00	112.00	0.0	0.0	0.0	9000.
Reference 10						
A	19.35	0.00	1.40×10^4	3.00	1.54×10^4	1000.
B	37.10	0.00	4.48×10^9	3.00	3.68×10^4	600.
C	112.00	112.00	0.0	0.0	0.0	90000.

Table 5

Summary of Ablation Prediction Results
a) Silica Fail Temperature of 4200 ^{o}R

Mixture Ratio	$\tilde{K}_{o_e}$	Location	$\dot{s}_{ave}$ (mils/sec)	B'_{ave}	T_{wall} @ 25 sec. (^{o}R)	Local Pressure (atm)	Local $\rho_e U_e C_h$ (lb/ft^2 sec)
High Pressure							
3.75	0.789	Throat	26.95	0.1425	4200.	38.4	0.933
3.25	0.765	"	15.32	0.0811	4200.	"	"
3.00	0.750	"	6.25	0.0330	4200.	"	"
2.75	0.734	"	0.390	0.0021	4037.	"	"
2.50	0.714	"	0.045	0.00024	3783.	"	"
3.75	0.789	Exit	10.90	0.1228	4200.	8.06	0.438
3.25	0.765	"	2.98	0.0336	4199.	"	"
3.00	0.750	"	0.532	0.0060	4078.	"	"
2.75	0.734	"	0.120	0.0014	3874.	"	"
2.50	0.714	"	0.025	0.00028	3650.	"	"
3.25	0.765	Chamber	10.49	0.0804	4200.	58.8	0.644
2.75	0.734	"	0.161	0.00123	4008.	"	"
2.50	0.714	"	0.013	0.0001	3757.	"	"
Low Pressure							
3.75	0.789	Throat	14.97	0.1605	4200.	19.2	0.459
3.25	0.765	"	6.63	0.0714	4200.	"	"
3.00	0.750	"	0.678	0.00727	4174.	"	"
2.75	0.734	"	0.115	0.00125	3950.	"	"
2.50	0.714	"	0.019	0.00020	3710.	"	"
3.75	0.789	Exit	2.500	0.0571	4200.	4.03	0.216
3.25	0.765	"	0.250	0.0057	4025.	"	"
3.00	0.750	"	0.0894	0.00204	3867.	"	"
2.75	0.734	"	0.026	0.00059	3690.	"	"
2.50	0.714	"	0.0006	0.00001	3494.	"	"
3.75	0.789	Chamber	10.16	0.1430	4200.	29.4	0.351
3.25	0.765	"	4.26	0.0600	4200.	"	"
2.75	0.734	"	0.050	0.00071	3912.	"	"

Table 5 - concluded

b) No Fail Allowed

Mixture Ratio	$\tilde{K}_{o_e}$	Location	$\dot{s}_{ave}$ $\left(\frac{mils}{sec}\right)$	B'_{ave}	T_{wall} @ 25 sec. (^{o}R)	Local Pressure (atm)	Local $\rho_e U_e C_{h_o}$ (lb/ft^2 sec)
High Pressure							
3.75	0.789	Throat	5.85	0.0310	4759.	38.40	0.933
|	|	Exit	2.91	0.0328	4473.	8.06	0.438
|	|	Chamber	7.76	0.0594	4988.	58.80	0.644
Low Pressure							
3.75	0.789	Throat	2.89	0.0310	4625.	19.20	0.459
|	|	Exit	0.918	0.0210	4274.	4.03	0.216
|	|	Chamber	1.959	0.0276	4680.	29.40	0.351

c) Silica Fail Temperature of 3600 ^{o}R

Mixture Ratio	$\tilde{K}_{o_e}$	Location	$\dot{s}_{ave}$ $\left(\frac{mils}{sec}\right)$	B'_{ave}	T_{wall} @ 25 sec. (^{o}R)	Local Pressure (atm)	Local $\rho_e U_e C_{h_o}$ (lb/ft^2 se
High Pressure							
3.75	0.765	Throat	39.92	0.2070	3600.	38.40	0.933
2.75	0.734	|	16.19	0.0855	|	|	|
3.25	0.765	Exit	16.38	0.1840	3600.	8.06	0.435
2.75	0.734	|	9.98	0.1120	|	|	|
Low Pressure							
3.25	0.765	Throat	18.78	0.2020	3600.	19.20	0.459
2.75	0.734	|	10.62	0.1142	|	|	|
3.25	0.765	Exit	8.29	0.1895	3600.	4.03	0.216
2.75	0.734	|	2.68	0.0612	|	|	|

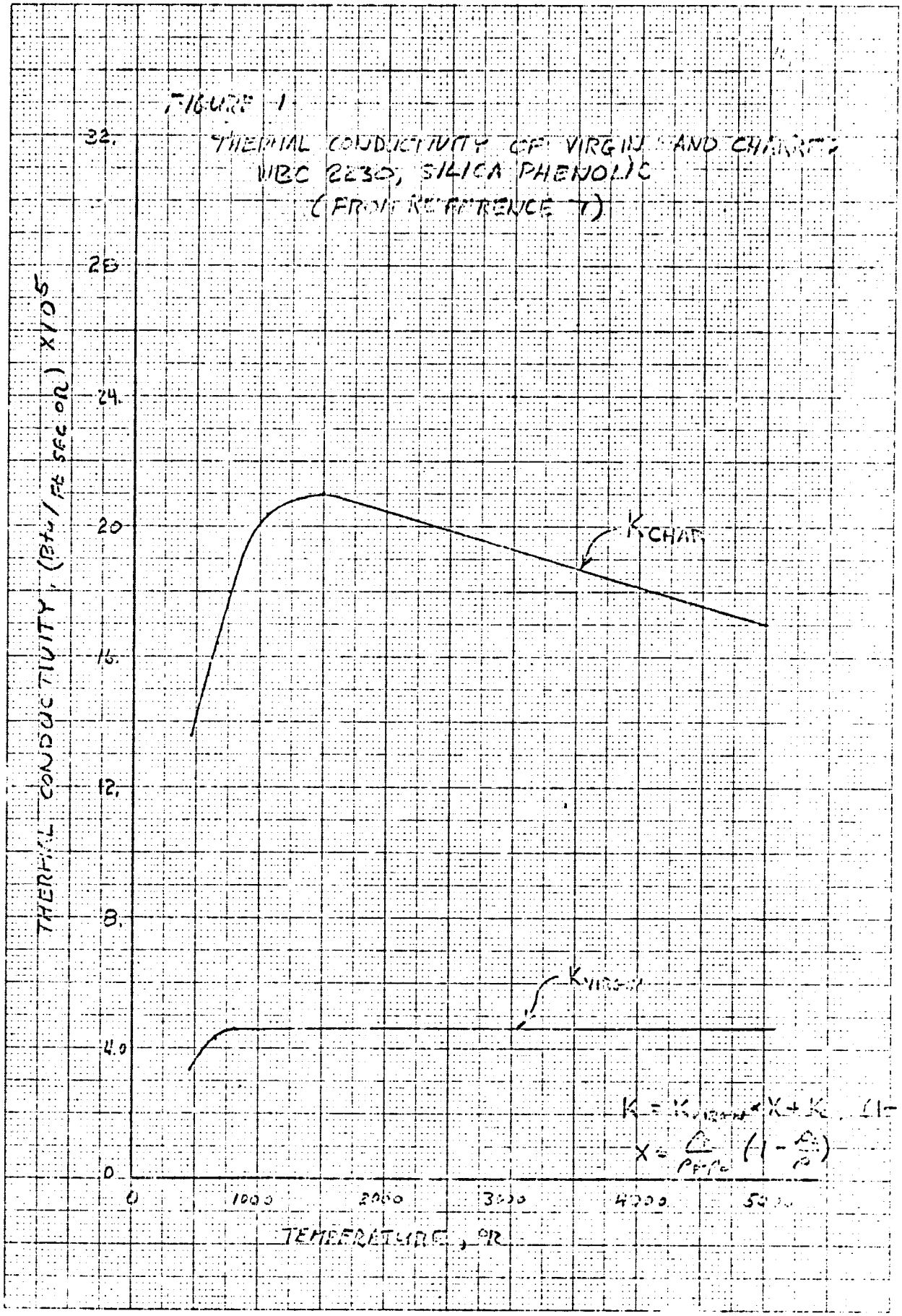

FIGURE 2 SPECIFIC HEAT OF VIRGIN AND CHARRED WBC 2030, SILICA PHENOLIC (FROM REFERENCE 7)

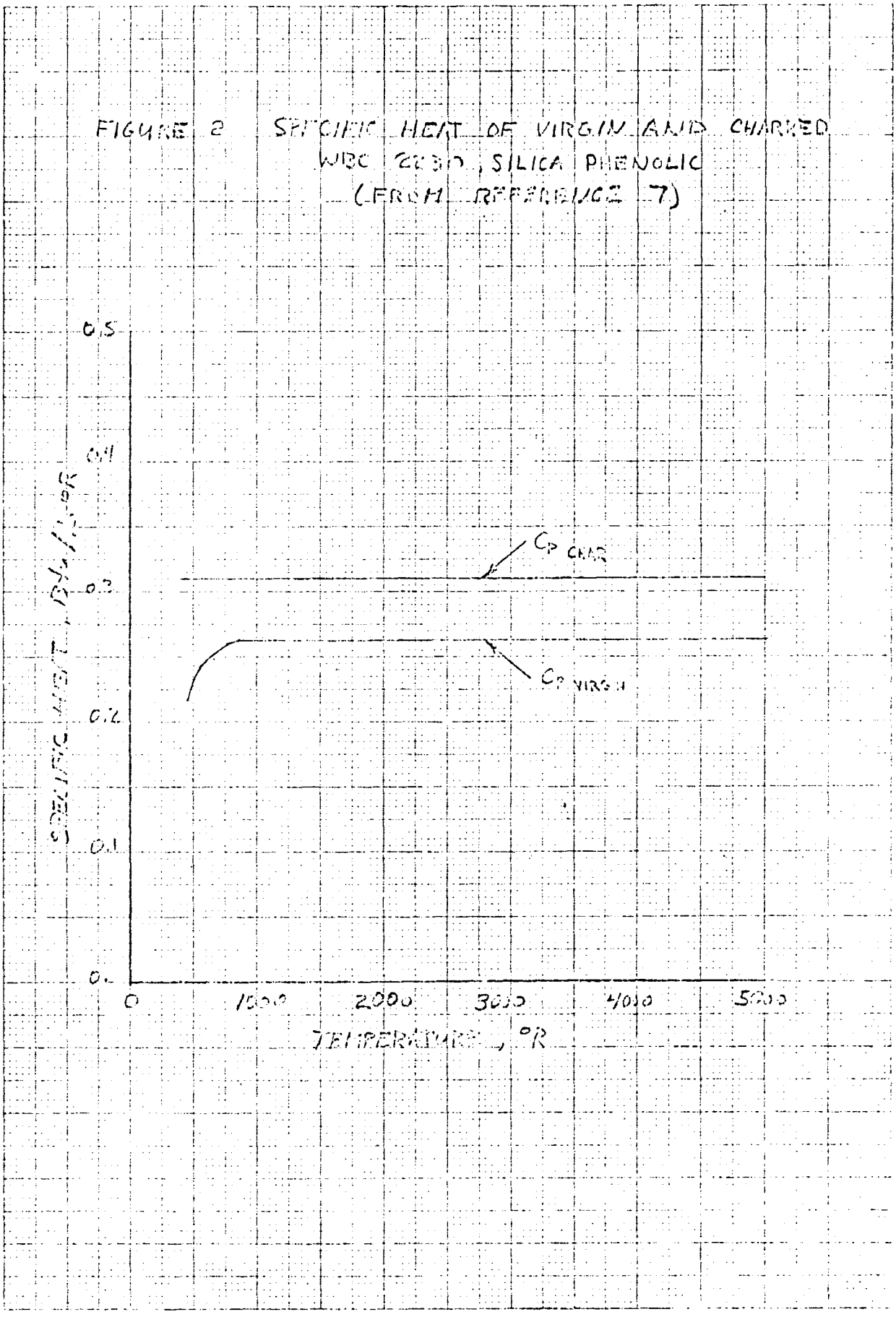

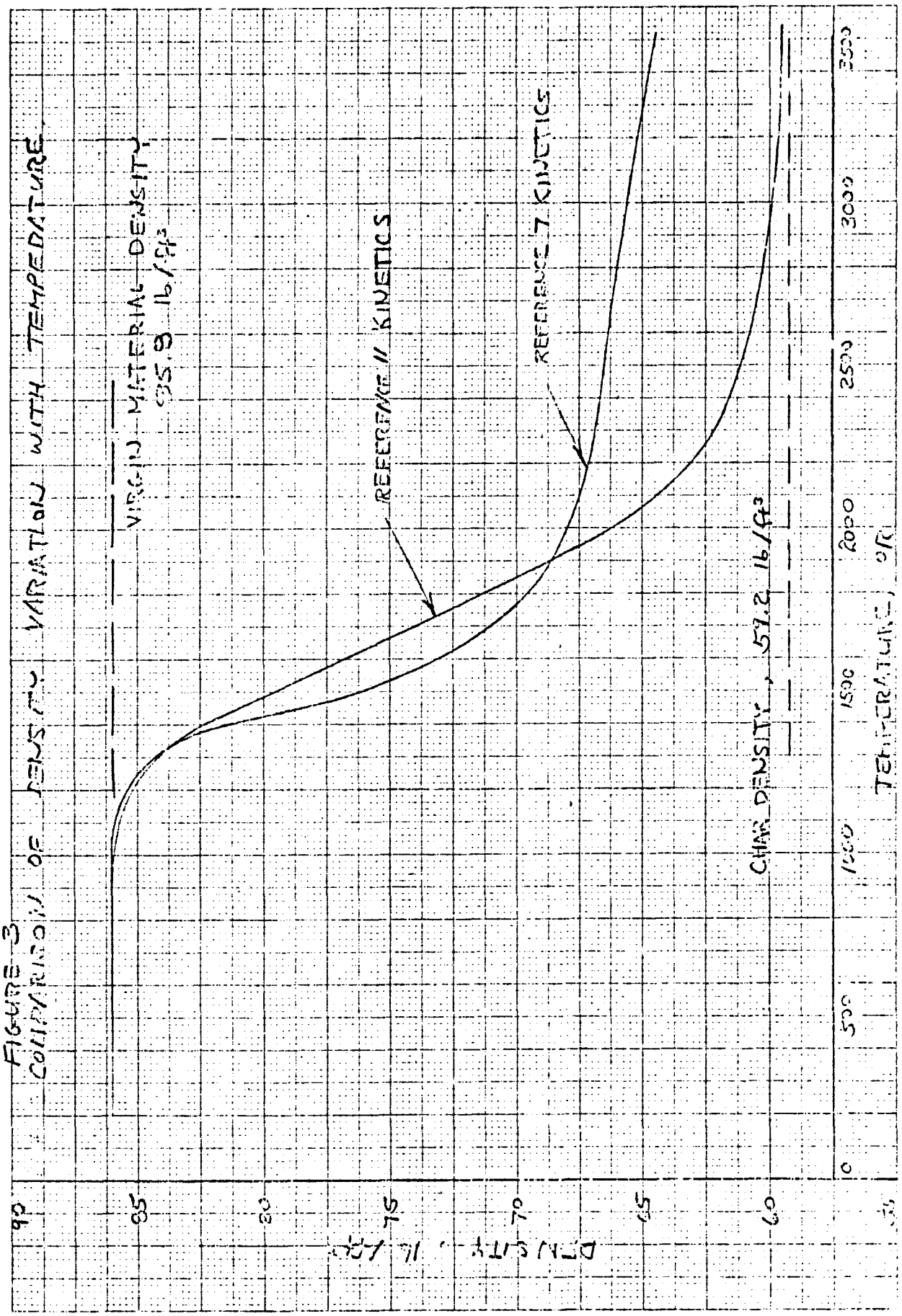
FIGURE 3
COMPARISON OF DENSITY VARIATION WITH TEMPERATURE
VIRGIN MATERIAL DENSITY
CSS 16/ft³
REFERENCE 11 KINETICS
REFERENCE 7 KINETICS
CHAR DENSITY, 57.2 16/ft³
DENSITY, lb/ft³
TEMPERATURE, °R
90
85
80
75
70
65
60
0
500
1000
1500
2000
2500
3000
3500

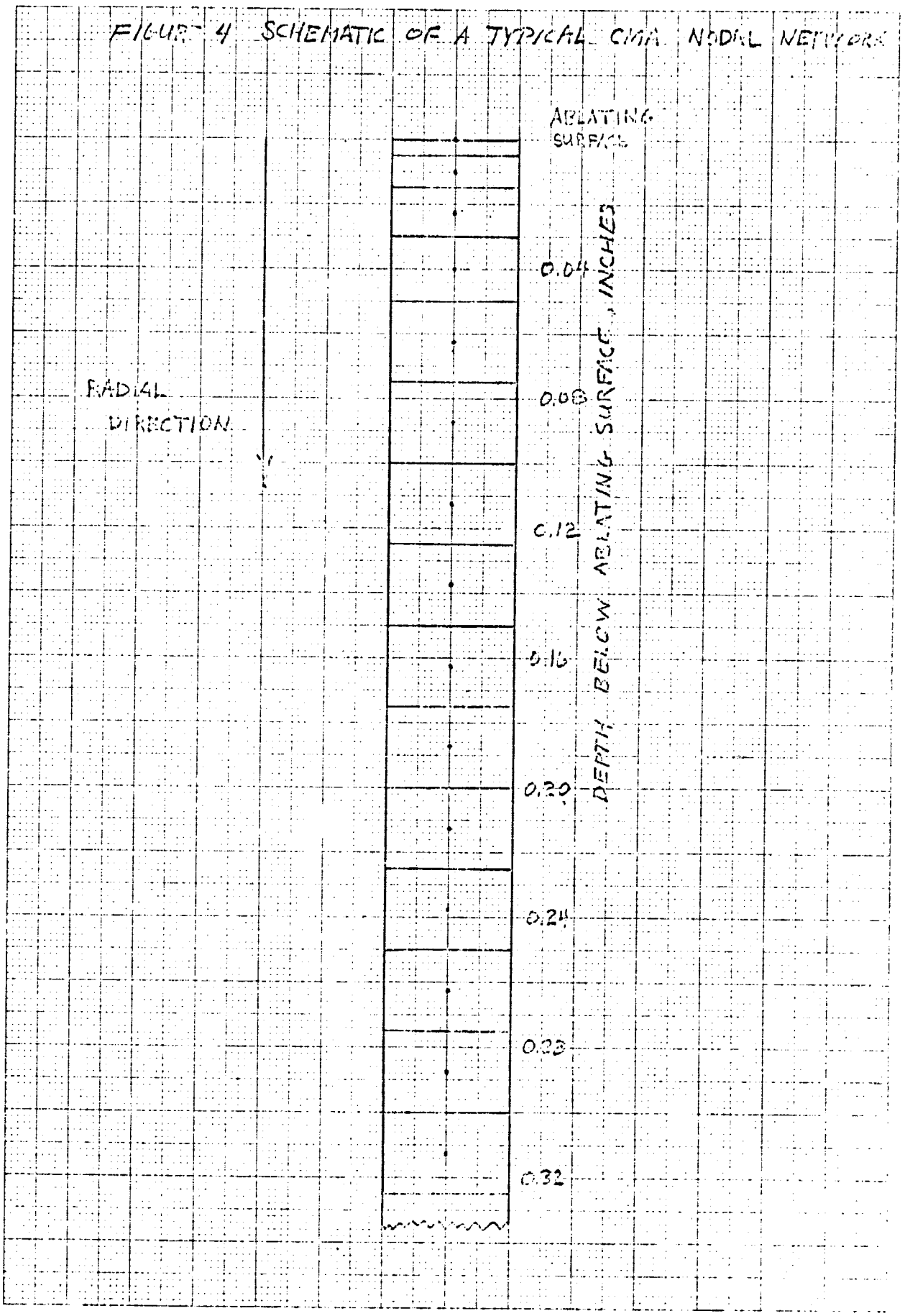

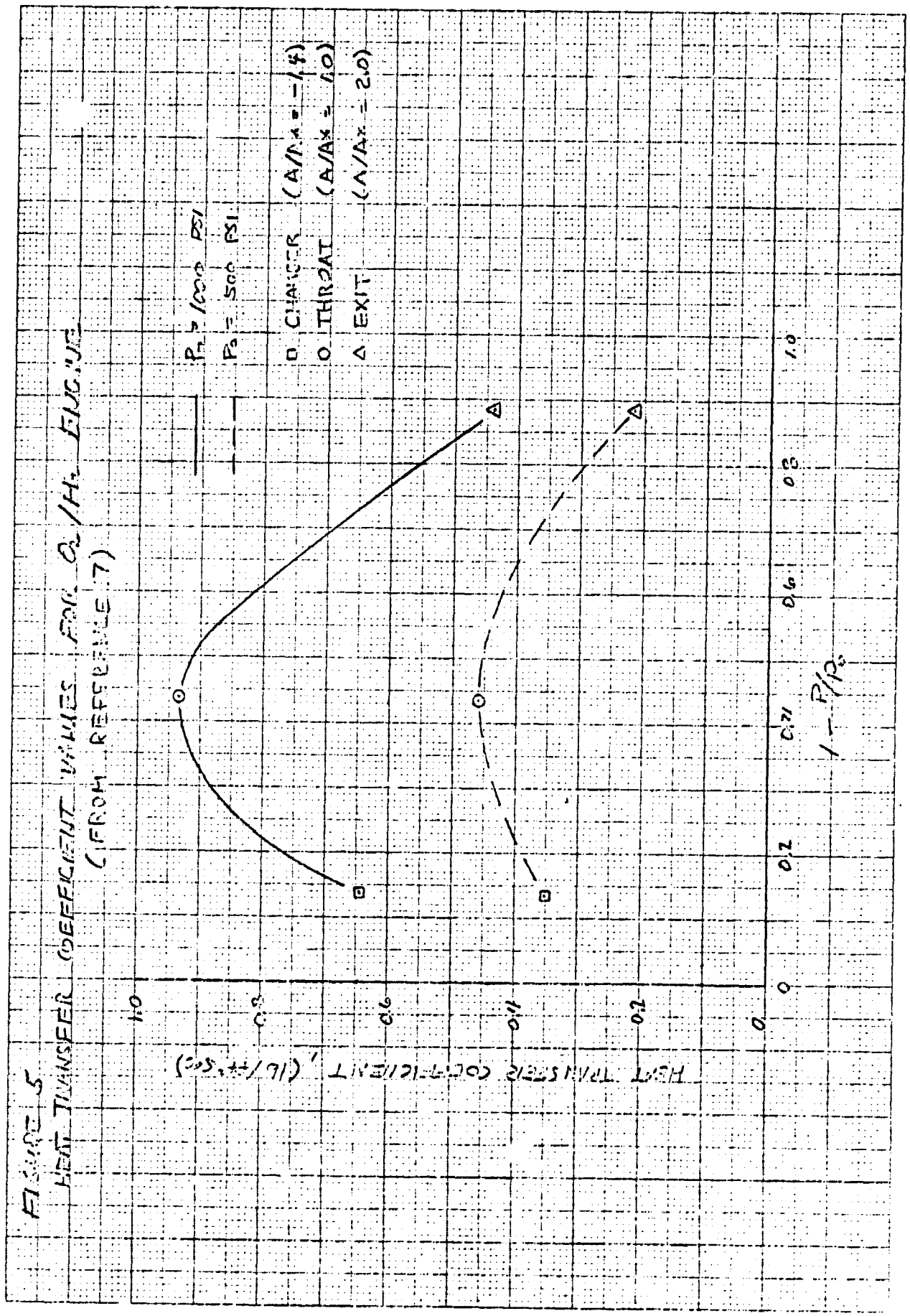
FIGURE 5
HEAT TRANSFER COEFFICIENT VALUES FOR O2/H2 ENGINE
(FROM REFERENCE 7)
Pc = 1000 PSI
Pc = 500 PSI
□ CHAMBER (A/At = 1.4)
○ THROAT (A/At = 1.0)
△ EXIT (A/At = 2.0)
HEAT TRANSFER COEFFICIENT, (BTU/ft²-sec)
1 - P/Pc
0
0.2
0.4
0.6
0.8
1.0

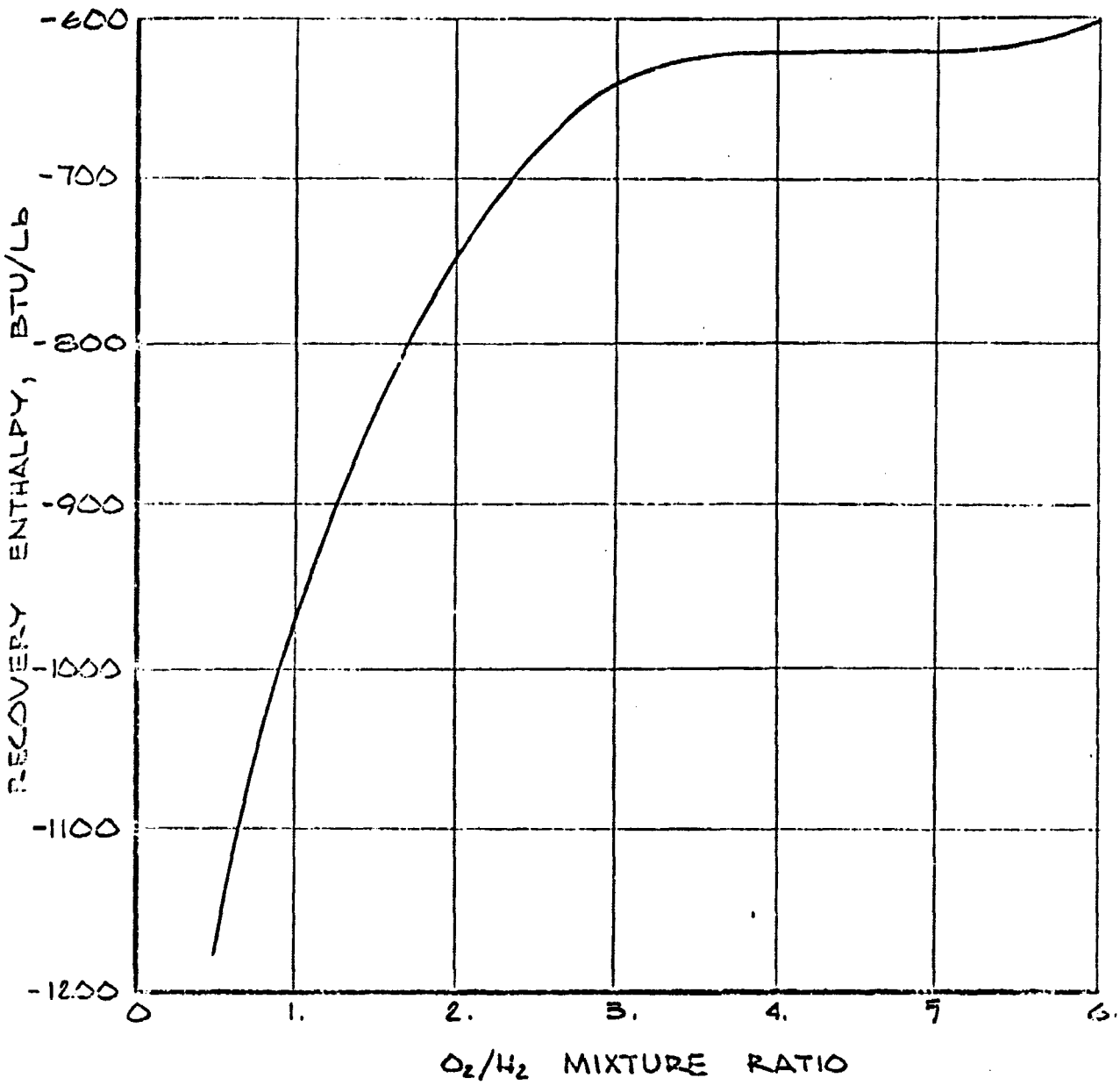

FIGURE 6 RECOVERY ENTHALPY AS A FUNCTION OF O_2/H_2 MIXTURE RATIO

Figure 7 VARIATION OF SURFACE RESPONSE WITH EDGE GAS OXYGEN MASS FRACTION

a) THROAT LOCATION

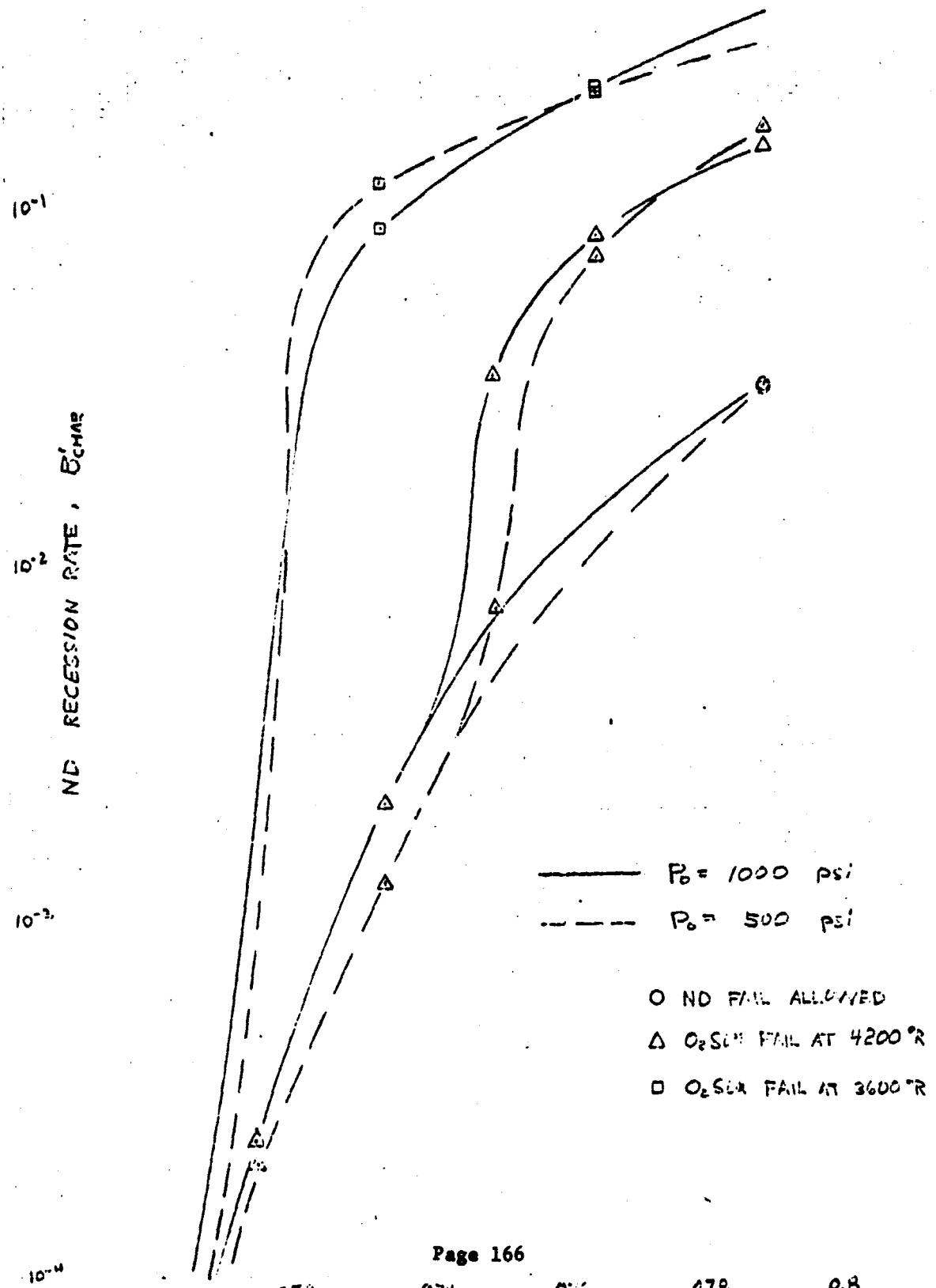

FIGURE 7 , CONTINUED

b) EXIT LOCATION

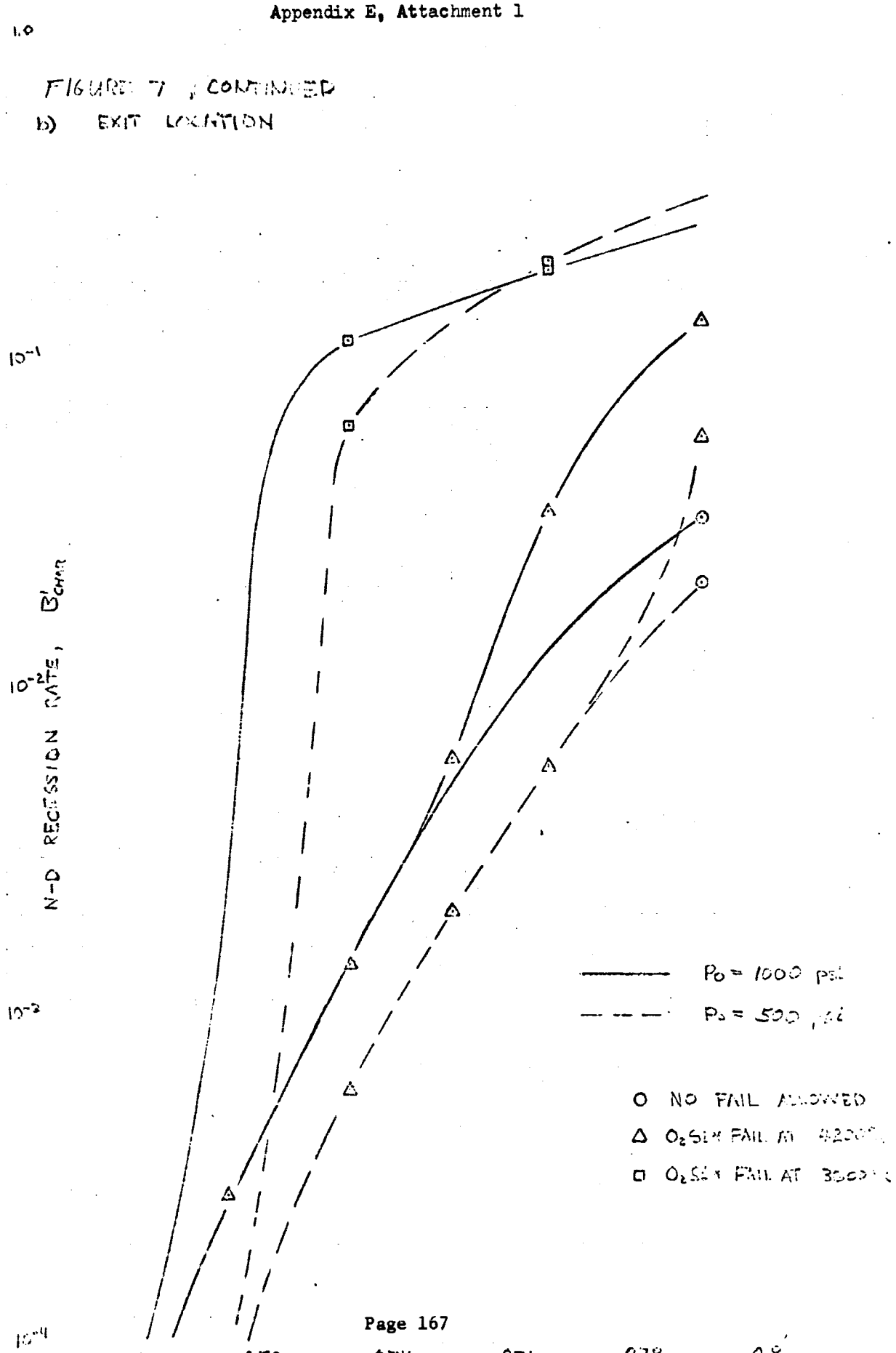

FIGURE 7, CONTINUED

c) CHAMBER LOCATION

——— P_o = 1000 psi

– – – P_o = 500 psi

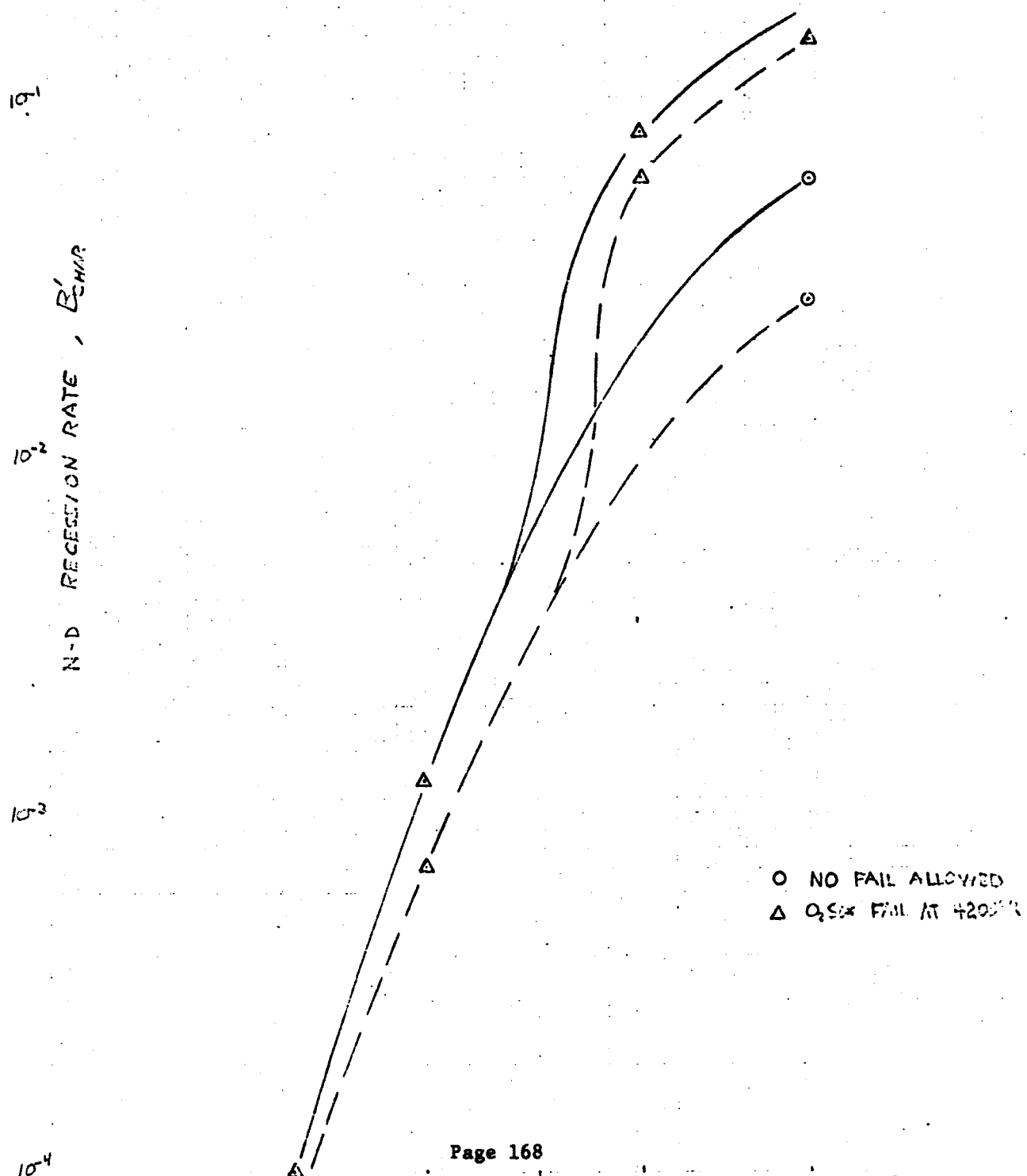

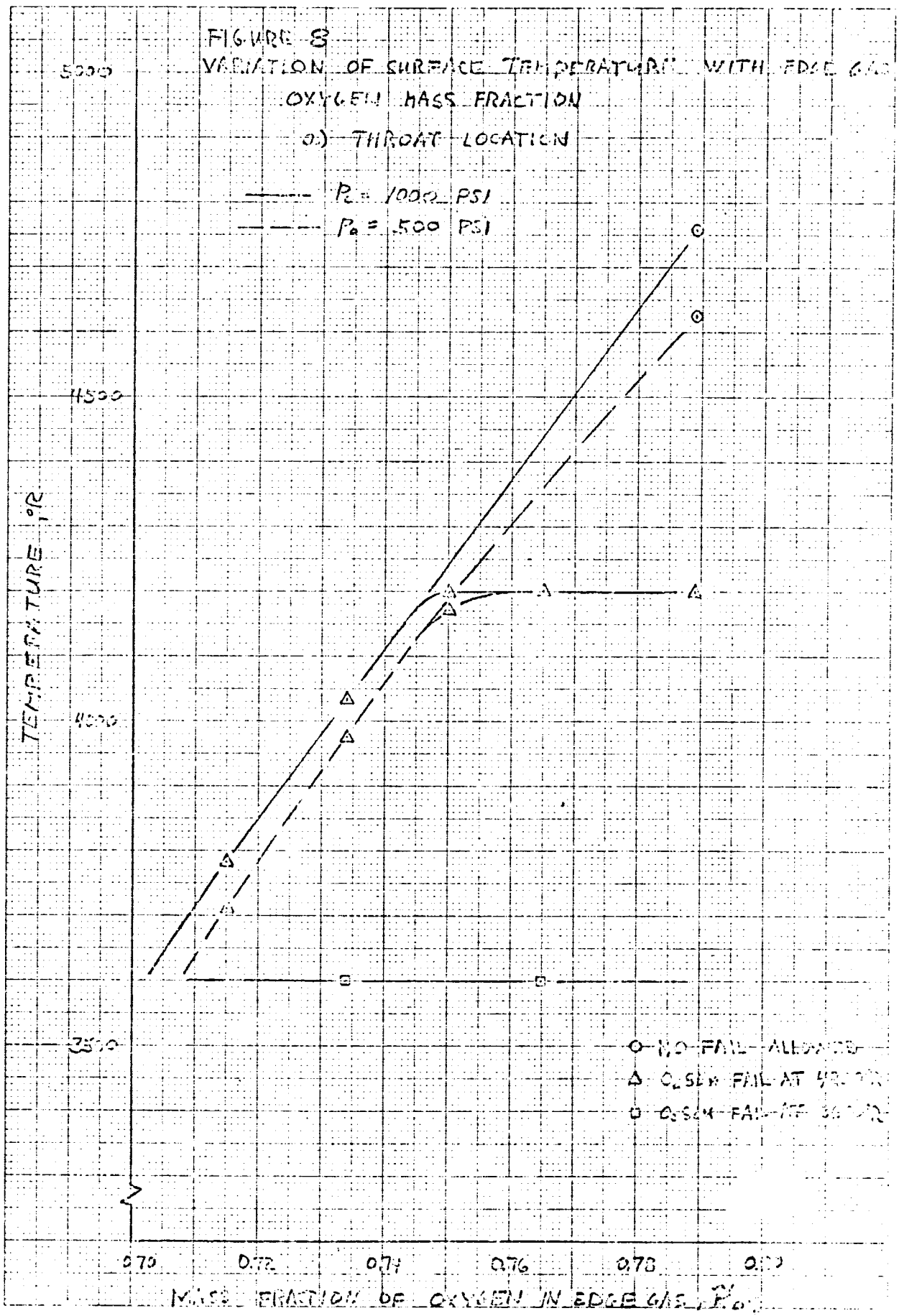
FIGURE 8
VARIATION OF SURFACE TEMPERATURE WITH EDGE GAS
OXYGEN MASS FRACTION
a) THROAT LOCATION
P_c = 1000 PSI
P_c = 500 PSI
5000
4500
4000
3500
TEMPERATURE °R
0.70
0.72
0.74
0.76
0.78
0.80
MASS FRACTION OF OXYGEN IN EDGE GAS, F_o
NO FAIL ALLOWED
O2 SEM FAIL AT
O2 SEM FAIL AT

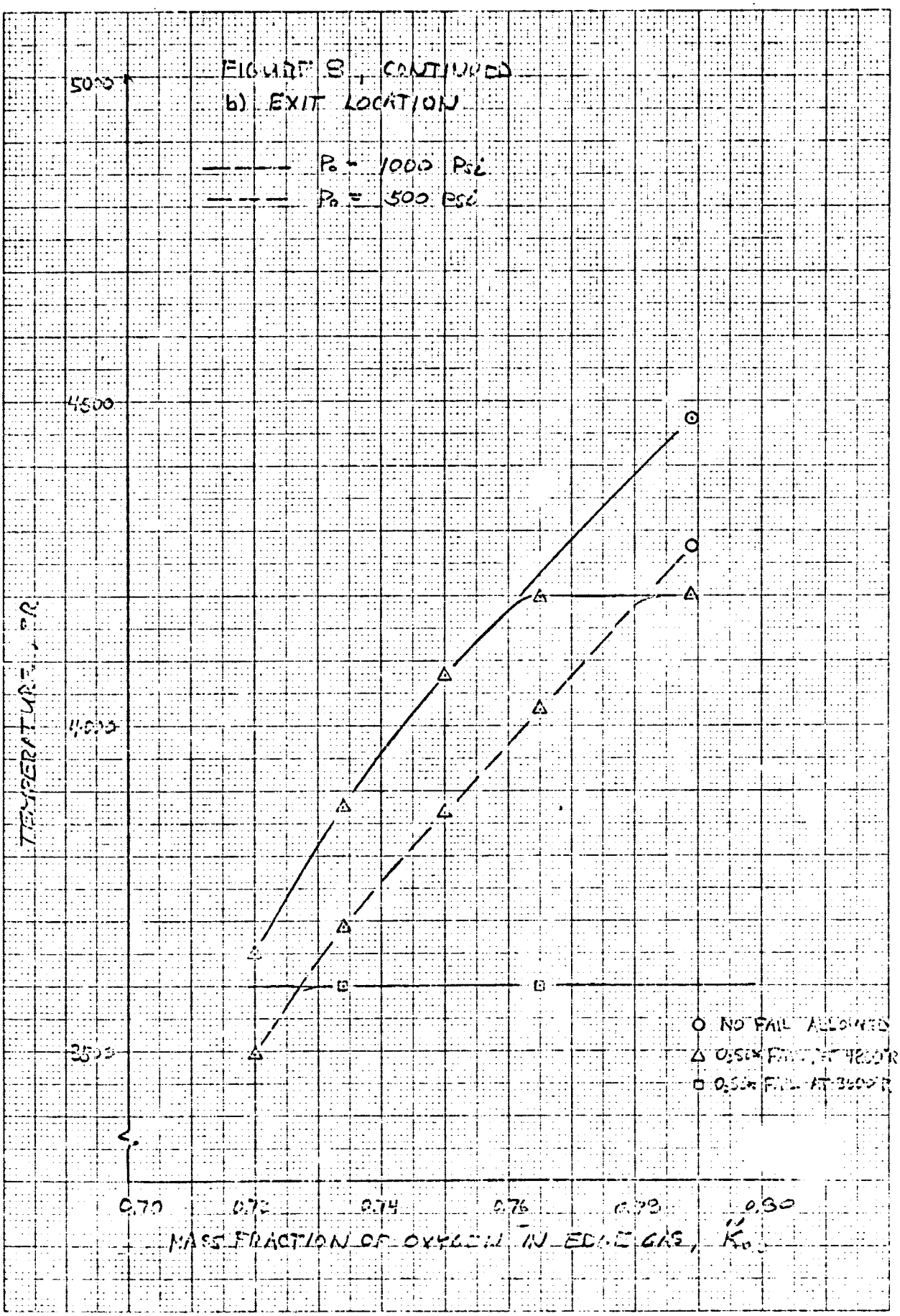

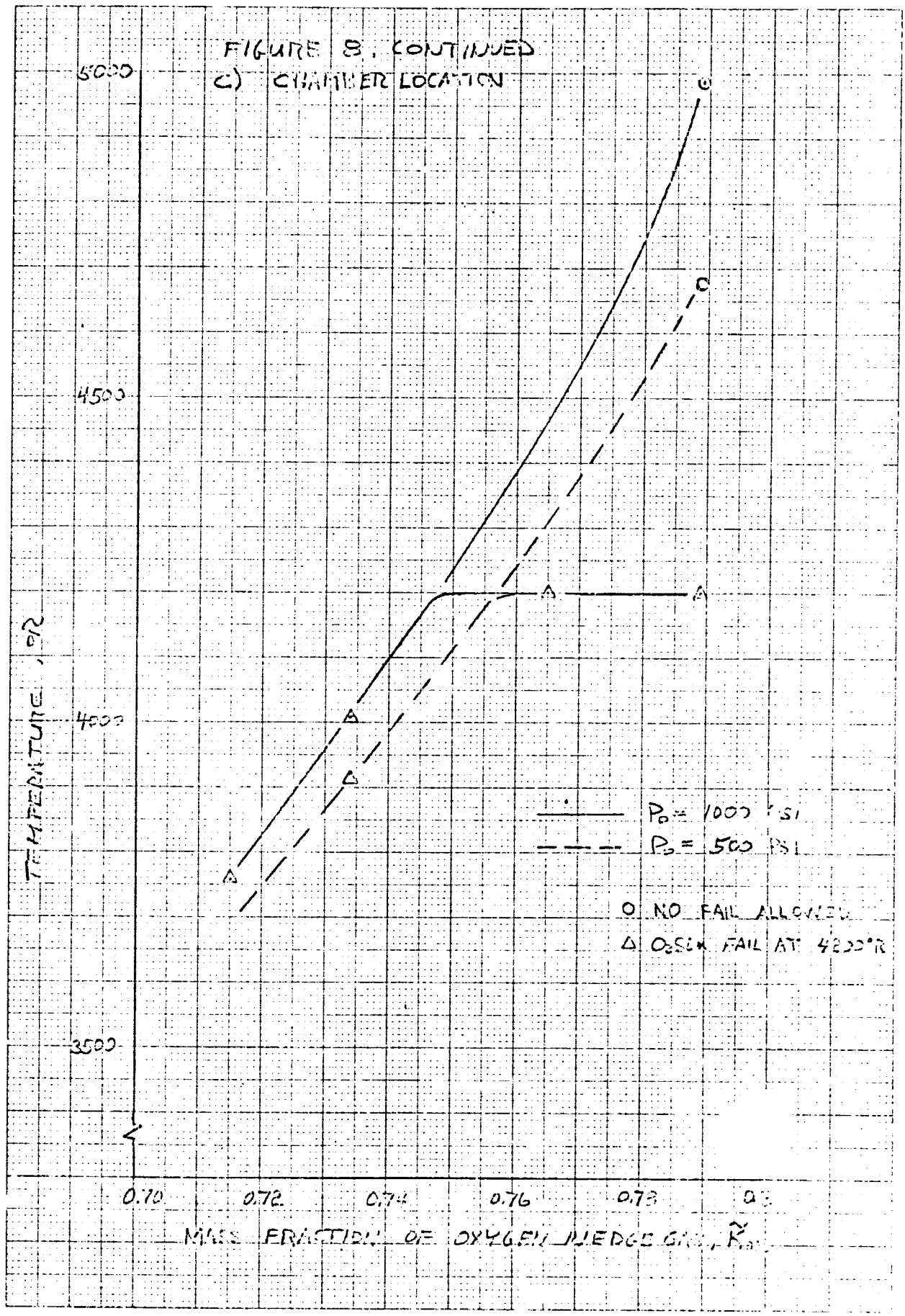

APPENDIX A

THE DESCRIPTION OF RELEVANT COMPUTER CODES

1. The Aerotherm Charring Material Ablation Program (CMA)

1.1 General Description

The CMA program is a coded procedure for calculating the in-depth thermal response of a charring, ablating material. The basic physics included correspond to simple charring of the form

$$\text{plastic} \rightarrow \text{char} + \text{gas}$$

according to a three component Arrhenius rate law where

$$\rho = \Gamma(\rho_A + \rho_B) + (1-\Gamma)\,\rho_C \qquad (1)$$

and

$$\left(\frac{\partial \rho}{\partial \theta}\right)_y = B_i \rho_{o_i} \left(\frac{\rho_i - \rho_{r_i}}{\rho_{o_i}}\right)^{\Psi_i} \exp(-E_{a_i}/RT) \qquad (2)$$

Usually components A and B represent constituents of the resin or plastic binder and Γ is the volume fraction of resin in the composite material, while component C represents a more refractory reinforcement. Initial versions of the program were described in Reference 1, and subsequently a more complete description of the physics and mathematical treatment was given in Reference 2.

The program is an implicit, finite-difference computational proc edure for computing the one-dimensional transient transport of thermal energy in a three-dimensional isotropic material which can ablate from a front surface and which can decompose in depth. Decomposition (pyrolysis) reactions are based on a three-component model. The program permits up to eight different backup materials of arbitrary thickness. The back wall of the composite material may transfer energy by convection and radiation.

The ablating surface boundary condition may take one of three forms:

OPTION 1 - Film coefficient model convection-radiation heating with coupled mass transfer, including the effects of unequal heat and mass transfer coefficients (non-unity Lewis number) and unequal mass diffusion coefficients. Surface thermochemistry computations need not presume chemical equilibrium at the surface.

OPTION 2 - Specified surface temperature and surface recession rate.

OPTION 3 - Specified radiation view factor and incident radiation flux, as functions of time, for a stationary surface.

Any combination of the first three options may be used for a single computation. Option 3 is appropriate to cooldown after termination of convective heat input and is often useful in conjunction with Options 1 and 2.

The program permits the specification of a number of geometries, including plane, cylindrical or annular, and spherical. In the most general case, area may vary arbitrarily with depth.

The rear surface of the last node may be specified as insulated, or may experience convective and radiative heat transfer to a "reservoir" at a specified reservoir temperature if a rear surface convection coefficient and an emissivity are input.

Material properties such as thermal conductivity, specific heat, and emissivity are input as functions of temperature for virgin plastic and char. For partially decomposed material, the program performs an appropriate averaging on density to determine effective material properties.

The basic solution procedure is by a finite difference approach. For each time step, the decomposition relations are solved and then the in-depth energy fluxes constructed in general terms. These are then harmonized with a surface energy balance (if a surface energy balance option is being used) and the in-depth temperatures determined. New material property values are set up and the solution is ready for the next time increment.

The CMA program outputs instantaneous mass ablation rates and blowing parameters for char and pyrolysis gas, total integrated mass ablation of char and pyrolysis gas, total recession and recession rates of surface, of the char line, and of the pyrolysis line. It also outputs the surface energy flux terms, namely, the energy convected in, energy radiated in, energy reradiated out, chemical generation, and conduction away (q_{cond}). Further, it describes how the input energy of q_{cond} is "accommodated" or "partitioned" in the solid material. Part of the energy is consumed in decomposing the plastic, part is consumed in sensible enthalpy changes of the solid, and part is "picked up" by the pyrolysis gases as they pass through the char. Thermocouple and isotherm output can also be called for.

1.2 Some Surface Energy Balance Details

In calculations under Option 1, the in-depth solution is coupled to a general film-coefficient boundary condition. The following sketch

shows the various energy fluxes of interest:

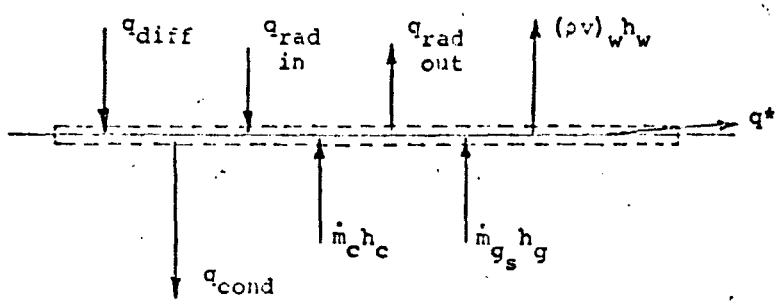

Since the surface control volume is attached to the receding surface, there is an apparent flow of char material into the control volume and an associated energy flux $\dot{m}_c h_c$. The pyrolysis gases flow into the control volume from below, bringing an energy flux $\dot{m}_{g_s} h_g$. There is a diffusional energy flux in from the boundary layer; this is denoted q_{diff}. There is a corrective energy flux away from the surface in the gross motion due to mass injection: $\rho v_w h_w$. An additional important gross motion energy flux is denoted q^* in the sketch; this term represents energy carried away in the removal, through mechanical action, of condensed phase materials. Other terms in the energy balance are the obvious radiation terms and conduction into the material.

In the course of the transient in-depth solution, which essentially is providing the term q_{cond}, it is necessary to evaluate all of the other surface energy balance flux terms. This in turn naturally requires some sort of surface thermochemical state solution. For this purpose it has proved expedient to prepare in advance, using suitable ablation thermochemistry codes, a series of tables which include all the surface mass transfer and chemical relations. The in-depth solution may then be coupled to the surface events through the surface energy balance. For example, when chemical equilibrium is achieved at the ablating surface the development presented in Reference 6 describes the means for obtaining the thermodynamic state of the gas at the ablating surface in terms of the pressure, and char and pyrolysis off-gas rates.

$$\text{Thermodynamic state} = f(B'_g, B'_c, P) \qquad (3)$$

where

$$B'_g = \frac{\dot{m}_g}{\rho_e U_e C_M} \quad \text{(normalized pyrolysis off-gas rate)}$$

$$B'_c = \frac{\dot{m}_c}{\rho_e U_e C_M} \quad \text{(normalized char recession rate)}$$

P = boundary layer edge pressure

The thermodynamic state includes definition of surface temperature and gas molecular composition. This, in turn, enables evaluation of the various quantities appearing in the boundary layer driving potential for heat and mass transfer (References 1 and 6). Tables representing solution to the functional relationship represented by Equation (3) are generated for a complete map covering the range of B'_g B'_c and P, of interest. These tables are usually generated with the Aerotherm ACE program (References 5 and 6). The following section describes the ACE program in more detail.

As an example of the surface energy balance procedure, suppose a table is prepared which, for a parametric array of dimensionless char erosion rates (B'_c), dimensionless pyrolysis off-gas rates (B'_g), and pressure, presents the relevant ablating surface temperature and requisite boundary layer composition and enthalpy quantities. During each time step in the course of the in-depth solution the program generates a pyrolysis gas rate B'_g and computes the rate at which energy is conducted into the material from the surface. With B'_g and the pressure known, the input parametric tables then serve to define that B'_c which yields temperature and enthalpy quantities which provide a balanced, harmonized set of energy fluxes at the surface.

2. The Aerotherm Chemical Equilibrium Program (ACE)

The preceding section has described the surface energy balance performed by the CMA program during the transient solution and indicate that it obtains the necessary enthalpy data from tables of surface thermochemical solutions. These solution tables are prepared in advance by the Aerotherm Chemical Equilibrium Program (ACE). For a given B'_c, B'_g, and P, this program solves the following set of equations

Physics	Number of Equations
Elemental mass balances	K - 1
Thermochemical gas phase equilibrium equations	I - K
Thermochemical surface condensed phase equilibrium equation	1
Fail or melt temperature constraints on candidate surface materials (candidate cannot be surface material above it's input fail temperature)	N
Sum of partial pressures equals input pressure	1
Total	I+N+1

where

I = Number of gasphase species - number of elements

K = Number of elements

N = Number of condensed phase species

and finds the following set of unknowns

Unknown	Number of such Unknowns
Parial pressure of gas phase species at wall	I
Wall temperature	1
Failing rates of fail temperature constrained materials	N
Total	I+N+1

With these unknowns determined, the ACE program can compute secondary unknowns needed for the surface energy balance: the enthalpy of the gas adjacent to the wall and the energy being carried away by the failing or melting species.

With this ACE output information provided as a function of the independent variables B'_c, B'_g, and P, the CMA program can construct the surface energy balance by interpolation, solving by iteration for that B'_c which, for a given P (input) and B'_g (provided at each instant by the in-depth procedure), yields a surface energy balance, thus determining the surface temperature.

APPENDIX B

Derivation of Steady State Response

In this analysis, a reference ablation rate ($B'_{c_{ss}}$) limit is defined by a mass balance analysis of the "steady state" surface off-gas composition. In the analysis it is assumed that the surface recession is controlled by the rate at which the free carbon in the pyrolysis gas and char can be consumed by oxygen diffusing to the surface from the boundary layer edge. "Free carbon" is the carbon in the char and pyrolysis gases, which has not aquired an oxygen molecule from the material decomposition products. Note that it is assumed that the silica (O_2Si) in the char does not dissociate and flows (melts) off of the surface. The amount of free carbon available is defined by assuming that "steady state" material heating and ablation occurs. This corresponds to the situation where the surface, char, and pyrolysis zone recession rates are all equal and constant with time. To conserve mass in-depth, therefore, the composition of material leaving the surface must be identical to that of the virgin material. The "steady state" assumtion is discussed further in Reference 14.

For equal diffusion coefficients the diffusional flux of oxygen to the surface is given by

$$\dot{m}_o = \rho_e U_e C_M \tilde{K}_{o_e}$$

where $\tilde{K}_{o_e}$ is the mass fraction of oxygen in the edge gas

and $\rho_e U_e C_M$ is the mass transfer coefficient

The mass flux of free carbon in the virgin material is defined as follows:

$$\dot{m}_c = \dot{m}_v \tilde{K}_c$$

Where $\tilde{K}_c$ is the mass fraction of free carbon in the virgin material

and $\dot{m}_v$ is the mass flux of virgin material

Since carbon and oxygen combine in a one to one ratio by mole, the ratio of carbon mass to oxygen mass must be $12.011/16.000 \approx 0.75$

for complete carbon consumption.

Therefore,

$$\frac{\dot{m}_c}{\dot{m}_o} = \frac{\dot{m}_v \tilde{K}_c}{\rho_e U_e C_M \tilde{K}_{o_e}} = B'_{total} \frac{\tilde{K}_c}{\tilde{K}_{o_e}} = 0.75$$

where $B'_{total} = \dot{m}_v / \rho_e U_e C_M$

But since,

$$B'_{total} = B'_{char} + B'_{gas} = B'_{char}(1+B'_{gas}/B'_{char})$$

Then

$$B'_{c_{ss}} = \frac{0.75\ \tilde{K}_{o_e}}{(1+B'_{gas}/B'_{char})\ \tilde{K}_c}$$

For steady state ablation the ratio of B'_{gas} to B'_{char} can be found from virgin and char densities as follows

$$\frac{B'_{gas}}{B'_{char}} = \frac{\dot{m}_{gas}}{\dot{m}_{char}} = \frac{\rho_{gas}}{\rho_{char}} = \frac{\rho_{virgin} - \rho_{char}}{\rho_{char}} = \frac{\rho_{virgin}}{\rho_{char}} - 1$$

Therefore, for WBC 2230, silica phenolic $\rho_{virgin} = 85.5$ lb/ft^3

$\rho_{char} = 59.2$ lb/ft^3

$$B'_{gas}/B'_{char} = \frac{85.5}{59.2} - 1 = 0.442$$

The mass fraction of "free carbon" in the virgin material may be evaluated as follows:

Resin Composition	C_6H_6O
Reinforcement Composition	O_2Si
Resin mass fraction	0.31 lb C_6H_6O/lb virgin

The following formula, therefore, represents the virgin material

$$C_6H_6O(O_2Si)_x$$

where x is found as follows:

$$m_{C_6H_6O} = 94.114 \text{ lb } C_6H_6O/\text{lb mole } C_6H_6O$$

$$m_{virgin} = 94.114/0.31 = 303.5 \text{ lb virgin/lb mole } C_6H_6O$$

$$\dot{m}_{O_2Si} = 209.4 \text{ lb } O_2Si/\text{lb mole } C_6H_6O$$

$$x_{O_2Si} = 3.48 \text{ lb mole } O_2Si/\text{lb mole } C_6H_6O$$

Therefore, since the single O in the material will attach itself to one of the C's, we can write schematically

$$C_6H_6O(O_2Si)_{3.48} \longrightarrow C_6 + 3H_2 + CO + 3.84(O_2Si)$$

Thus, the mass fraction of free carbon is

$$\tilde{K}_c = \frac{60.055}{303.5} = 0.198$$

Therefore,

$$B'_{c_{ss}} = 0.75\tilde{K}_{o_e}/(1.442)(0.198) = 2.62\tilde{K}_{o_e}$$

$$B'_{c_{ss}} = 2.62\,\tilde{K}_{o_e}$$

where the following assumptions have been made:

1. Steady state ablation
2. Surface recession controlled by oxygen availability rather than any energy consideration
3. Virgin material composition as defined above
4. All oxygen diffused to the surface is consummed by all of the available carbon to form CO
5. All silica (O_2Si) is melted off the surface
6. No hydrocarbons are formed

APPENDIX F

THRUST CHAMBER PERFORMANCE DATA

Appendix F

The method of determining vacuum specific impulse efficiency was identical to that utilized in the NAS 3-2555 Thrust Chamber Development Program.(14)

Table XXI is a list of symbols while Table XXII is a listing of significant parameters and performance data for all steady-state testing. Figure No. 70 is a plot of specific impulse efficiency versus over-all thrust chamber mixture ratio at the two chamber pressure levels tested. No significant performance difference is evident. These data agree with performance data obtained in the NAS 3-2555 contract. However, it should be noted that the ηIsp 211 is not representative of the efficiencies that can be achieved at high area ratios (i.e., in Contract NAS 3-2555, an ηIsp of approximately 94% was shown for an $\epsilon_E = 40$).

(14) Barsotti, R. J., et al, op. cit.

(15) Ibid

TABLE XXI

LIST OF SYMBOLS, THRUST CHAMBER PERFORMANCE

M.R.	Over-all thrust chamber mixture ratio (Weight flow oxidizer/total weight flow fuel)
$\bar{T}fJ$	Average of two fuel injector temperatures - °R
Isp (measured)	Measured sea level specific impulse - $\frac{\text{lbf-sec}}{\text{lbm}}$
Summary Time	Period through which data is averaged - sec
Pc (face)	Injector face chamber pressure - psia
$\bar{A}_t$	Average throat area during summary time (based on 12 throat diameters - in^2)
ϵ_E	Nozzle expansion ratio (exit area/average throat area)
hIsp	Enthalpy correction factor due to warm hydrogen
Isp (Vac. theo @ ϵ_E)	Theoretical vacuum specific impulse at calculated nozzle expansion ratio and measured over-all thrust chamber mixture ratio - $\frac{\text{lbf-sec}}{\text{lbm}}$
Isp (Vac.theo)(ϵ,h)	Theoretical vacuum specific impulse @ calculated nozzle expansion ratio times enthalpy correction factor - $\frac{\text{lbf-sec}}{\text{lbm}}$
$\eta_{\text{Isp 2:1}}$	Specific impulse efficiency for 2:1 area ratio nozzle (Isp (Vac)/Isp (Vac. theo) (ϵ,h) - %
Geom. Loss	Loss attributed to the loss in thrust caused by the discharge coefficient of the throat and the loss in thrust resulting from non-axial exit momentum - $\frac{\text{lbf-sec}}{\text{lbm}}$

TABLE XXI (cont.)

Isp (Vac) W/O Geom. Loss	Measured sea level specific impulse corrected to altitude plus nozzle geometry loss - $\frac{\text{lbf-sec}}{\text{lbm}}$
$\eta_{\text{Isp 2:1 W/O Geom. Loss}}$	Specific impulse efficiency for 2:1 area ratio nozzle without nozzle geometry loss (Isp (Vac) W/O Geom/Isp (Vac. Theo) (ϵ,h) - %
η_{C^*}	Characteristic exhaust velocity efficiency (measured characteristic exhaust velocity based on nozzle losses/theoretical characteristic exhaust velocity at overall thrust chamber mixture ratio) - %

TABLE XXII

PERFORMANCE DATA

Test No.	Over-All M.R.	$\overline{TfJ}$ °R	$I_{SP(Meas.)}$ (sec)	Summary Time (sec)	Pc(face) (psia)	$\overline{A}_t$ (in^2)	ϵ_E	hI_{SP}	I_{SP} (Vac.Theo @ ϵ) (sec)
001	5.35	100.3	305.7	8.5-17	1047	712.56	2.034	1.0024	353.3
002	5.37	99.3	305.6	10.6-21.3	1041	715.94	2.024	1.0024	352.9
003	5.11	95.8	308.3	11.7-23.5	1058	719.05	2.016	1.0024	354.9
004	5.45	92.6	304.8	11.8-23.6	1063	721.67	2.009	1.0021	351.7
005	5.52	96.3	304.4	11.8-23.7	1064	726.39	1.996	1.0022	351.0
007	5.46	98.5	299.6	4.8-26.0	566	708.70	2.048	1.0023	352.2
007	5.04	87.9	303.7	22.4-44.7	572	710.65	2.040	1.0021	356.0
007	4.87	83.5	305.0	44.2-44.7	583	711.83	2.036	1.0020	357.4
009	5.82	103.5	295.0	4.8-14.9	555	729.53	1.987	1.0024	348.3
009	5.63	97.1	297.8	22.4-44.8	553	733.92	1.975	1.0022	349.7
009	5.46	97.2	300.5	44.3-44.8	557	735.99	1.970	1.0023	351.1

Test No.	I_{SP} (Vac) (sec)	$I_{SP(Vac. Theo)}$ (ϵ,h) (sec)	ηI_{SP} 2:1 (%)	Geom. Loss (sec)	$I_{SP(Vac)}$ W/O Geom. (sec)	ηI_{SP} 2:1 W/O Geom. (%)	η_{c^*} (%)
001	312.7	354.1	88.31	26.1	338.8	95.68	96.5
002	312.6	353.7	88.38	26.1	338.7	95.76	96.5
003	315.3	355.7	88.64	26.3	341.6	96.04	96.8
004	311.7	352.4	88.45	26.0	337.7	95.83	96.5
005	311.2	351.8	88.46	26.0	337.2	95.85	96.4
007	312.3	353.0	88.47	26.0	338.3	95.84	96.4
007	316.5	356.7	88.73	26.3	342.8	96.10	96.8
007	317.8	358.1	88.75	26.5	344.3	96.15	96.9
009	308.0	349.1	88.23	25.8	333.8	95.62	96.3
009	310.9	350.5	88.70	25.9	336.8	96.09	96.4
009	313.6	351.9	89.12	26.0	339.6	96.50	96.5

A_e = 1449.64 in^2

TABLE XXII (cont.)

Test No.	Over-All M.R.	$\overline{T_f J}$ °R	$I_{SP(Meas.)}$ (sec)	Summary Time (sec)	Pc(face) (psia)	$\overline{A}_t$ (in^2)	ϵ_E	hI_{SP}	I_{SP} (Vac.Theo @ ϵ_E) (sec)
010	4.15	85.7	309.9	23.7-47.3	570	736.21	1.969	1.0028	362.0
010	4.04	82.4	310.4	46.8-47.3	572	736.31	1.969	1.0027	362.7
011	5.06	110.3	302.9	23.6-47.2	552	738.60	1.963	1.0031	354.3
012	5.02	110.4	303.0	23.6-47.2	548	743.62	1.949	1.0031	354.4
014	5.75	126.5	299.3	23.7-47.4	544	718.10	2.019	1.0031	349.5
016	5.51	121.6	302.0	22.8-45.6	567	726.42	1.996	1.0031	351.1
017	4.89	111.5	307.2	23.4-46.9	566	728.25	1.991	1.0034	356.3
018	4.90	110.0	306.4	19.2-30.0	569	731.70	1.981	1.0033	356.0
019	5.20	112.7	303.9	22.4-44.9	571	735.68	1.970	1.0030	353.3
020	4.88	107.1	305.7	10.0-20.0	540	739.46	1.960	1.0034	355.8
020	5.26	113.3	299.5	30.0-46.0	567	746.56	1.942	1.0031	352.3

Test No.	I_{SP} (Vac) 2:1 (sec)	$I_{SP(Vac. Theo)}$ (ϵ_E, h) (sec)	ηI_{SP} 2:1 (Vac) (%)	Geom. Loss (sec)	$I_{SP(Vac)}$ 2:1 W/O Geom. (sec)	ηI_{SP} 2:1 Vac (W/O Geom.) (%)	η_{c^*} (%)
010	322.7	363.0	88.90	27.0	349.7	96.34	97.2
010	323.2	363.7	88.86	27.1	350.3	96.32	97.3
011	315.9	355.4	88.89	26.3	342.2	96.29	96.8
012	316.1	355.5	88.92	26.3	342.4	96.32	96.8
014	312.6	350.6	89.16	25.7	338.3	96.49	96.3
016	314.8	352.2	89.38	26.0	340.8	96.76	96.4
017	320.0	357.5	89.51	26.5	346.5	96.92	96.9
018	319.1	357.2	89.33	26.5	345.6	96.75	96.9
019	316.4	354.4	89.28	26.2	342.6	96.67	96.8
020	318.2	357.0	39.13	26.5	344.7	96.55	96.9
020	311.8	353.4	88.23	26.2	338.0	95.64	96.7

A_e = 1449.64 in^2

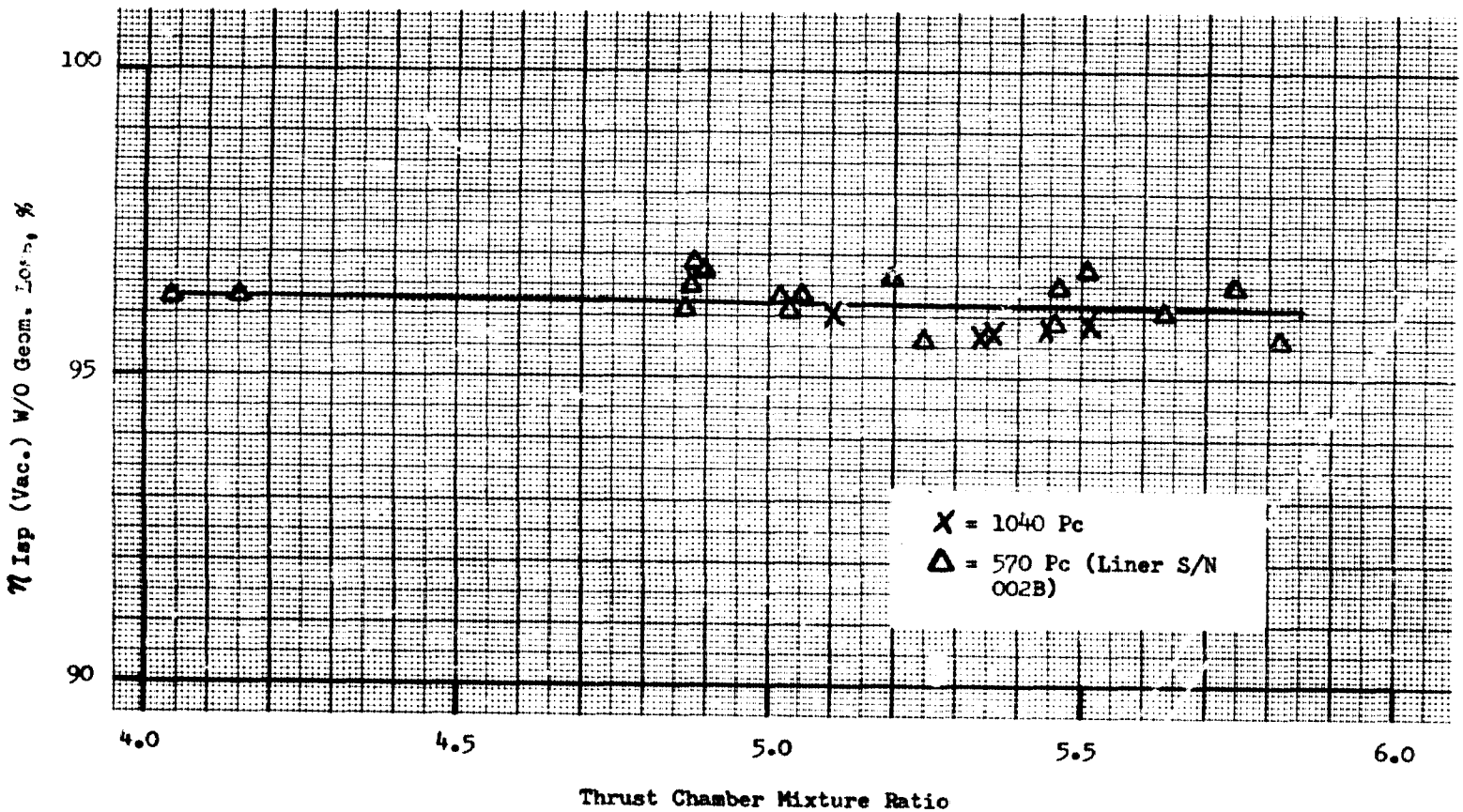

Figure 70. Specific Impulse Efficiency vs Thrust Chamber Mixture Ratio

BIBLIOGRAPHY

Barsotti, R. J., et al, Development of Liquid Oxygen/Liquid Hydrogen Thrust Chamber for the M-1 Engine, NASA CR-54813, 15 May 1968

Bettran, M. R., et al, Liquid Rocket Engine Combustion Instability Studies, Final Report, AFRPL-TR-66-125, 1 July 1966

Elliot, D. G., Bartz, D. R., and Silver, S., Calculation of Turbulent Boundary - Layer Growth and Heat Transfer in Axi-Symmetric Nozzles, JPL TR No. 32-387, 15 February 1963

Kendall, R. M., A General Approach to the Thermochemical Solution of Mixed Equilibrium-Nonequilibrium, Homogenous Systems, NASA CR-1064, June 1968

Moyer, C. B. and Rindal, R. A., Finite Difference Solution for the In-Depth Response of Charring Materials Considering Surface Chemical and Energy Balances, NASA CR-1061, June 1968

Priem, R. J. and Heidman, M. F., Propellant Vaporization as a Design Criterion for Rocket Engine Combustion Chambers, NASA TR-R-67, 1960

Rindal, R. A., Clark, K. J., Moyer, C. B., and Flood, D. T., Experimental and Theoretical Analysis of Ablative Material Response in a Liquid-Propellant Rocket Engine, NASA CR-72301, 1 September 1967

Schaefer, J. W. and Dahm, T. J., Studies of Nozzle Ablative Material Performance for Large Solid Boosters, NASA CR-72080, 15 December 1966

Schaefer, J. W., Dahm, T. J., Rodriguez, D. A., Reese, J. J., Jr., and Wool, M. R., Studies of Ablative Material Performance for Solid Rocket Nozzle Applications, NASA CR-72429, 1 March 1968

Schlichting, H., Boundary Layer Theory, McGraw-Hill, fourth edition, 1960

Leader, J. D., Larsen, J. V., Thompson, R. W., and Chidley, J. D., Catalysis of Internal Endothermic Ablative Reactions Between Char and Reinforcement, AIAA Paper No. 68-505, June 1968

Sykes, G. F., Jr., Decomposition Characteristics of Char-Forming Phenolic Polymer Used for Ablative Composites, NASA TN D-3810, February 1967

Aerotherm Charring Material Ablation Program, Flow Charts, Version 2, Aerotherm Corp., Palo Alto, California, April 1966

Aerotherm Charring Material Ablation Program, Fortran Variable Names, Version 2, Aerotherm Corp., Palo Alto, California, February 1966

Aerotherm Charring Material Ablation Program, Users Manual, Version 2, Aerotherm Corp., Palo Alto, California, January 1966

Bartz, D. R., "A Simple Equation for Rapid Estimation of Rocket Nozzle Convective Heat-Transfer Coefficients," Jet Propulsion, January 1957

Ladacki, M., Hamilton, J. V., and Cohz, S. N., "Heat of Pyrolysis of Resin in Silica-Phenolic Ablation," AIAA Journal, Vol. 4, No. 10, October 1966

Stollery, J. L. and El-Ehwany, A.A.M., "A Note on the Use of Boundary Layer Model for Correlating Film Cooling Data," Heat Mass Transfer, Vol. 8, 1965